ISSN 1997-1397 (Print)
ISSN 2313-6022 (Online)

Журнал Сибирского федерального университета

Математика и физика

Journal of Siberian Federal University

Mathematics & Physics

2025 18 (4)

ISSN 1997-1397
(Print)

ISSN 2313-6022
(Online)

2025 18 (4)

ЖУРНАЛ СИБИРСКОГО ФЕДЕРАЛЬНОГО УНИВЕРСИТЕТА
Математика и Физика

JOURNAL OF SIBERIAN FEDERAL UNIVERSITY
Mathematics & Physics

Издание индексируется Scopus (Elsevier), Emerging Sources Citation Index (WoS, Clarivate Analytics), Российским индексом научного цитирования (НЭБ), представлено в международных и российских информационных базах: Ulrich's periodicals directiory, ProQuest, EBSCO (США), Google Scholar, MathNet.ru, КиберЛенинке.

Включено в список Высшей аттестационной комиссии «Рецензируемые научные издания, входящие в международные реферативные базы данных и системы цитирования».

Все статьи представлены в открытом доступе http://journal.sfu-kras.ru/en/series/mathematics_physics.

Журнал Сибирского федерального университета.
Математика и физика.
Journal of Siberian Federal University. Mathematics & Physics.

Учредитель: Федеральное государственное автономное образовательное учреждение высшего образования "Сибирский федеральный университет"(СФУ)
Главный редактор: А.М. Кытманов. Редакторы: В.Е. Зализняк, А.В. Щуплев.
Компьютерная верстка: Г.В. Хрусталева
№ 4. 26.08.2025. Индекс: 42327. Тираж: 1000 экз. Свободная цена
Адрес редакции и издателя: 660041 г. Красноярск, пр. Свободный, 79, оф. 32-03.
Отпечатано в типографии Издательства БИК СФУ
660041 г. Красноярск, пр. Свободный, 82а.
Свидетельство о регистрации СМИ ПИ № ФС 77-28724 от 29.06.2007 г., выданное Федеральной службой по надзору в сфере массовых коммуникаций, связи и охраны культурного наследия
http://journal.sfu-kras.ru
Подписано в печать 15.08.25. Формат 84×108/16. Усл.печ. л. 12,0.
Уч.-изд. л. 11,8. Бумага тип. Печать офсетная.
Тираж 1000 экз. Заказ 23351
Возрастная маркировка в соответствии с Федеральным законом № 436-ФЗ:16+

CONTENTS

СОДЕРЖАНИЕ

EDN: ALQECJ
УДК 539.2

Moire Patterns in Graphene on Pt(111) Substrate: Computer Simulation

Sergey V. Belim*
Ilya V. Tikhomirov†
Omsk State Technical University
Omsk, Russian Federation

Received 02.12.2024, received in revised form 15.01.2025, accepted 24.03.2025

Abstract. Deformation study for monolayer graphene film on Pt substrate is performed by computer simulation. The surface potential simulates the substrate. Carbon atoms in graphene interact with each other and with the potential of the substrate. The minimum of potential energy determines the position of carbon atoms. Transverse strains of graphene are energetically advantageous due to the strong bond between carbon atoms. Longitudinal deformations in graphene are small. The model uses the Lennard–Jones potential to calculate the substrate potential. The potential parameters are calculated from the equilibrium state of the unperturbed system and experimental data. The surface potential is calculated for one unit cell and translated by parallel transfer to the entire substrate. The interaction between carbon atoms is also described by the Lennard–Jones potential. Moire patterns in graphene have a honeycomb superstructure. The model calculates the dependence of the period for the moire pattern on the angle between the main directions of the crystal lattice on the substrate and graphene. The period of the moire superlattice decreases when the film is rotated according to a nonlinear law. Calculations show a large distance between the substrate and the graphene film. The simulation results are in good agreement with the experimental data.

Keywords: graphene, surface potential, moire pattern, Lennard-Jones potential.

Citation: S.V. Belim, I.V. Tikhomirov, Moire Patterns in Graphene on Pt(111) Substrate: Computer Simulation, J. Sib. Fed. Univ. Math. Phys., 2025, 18(4), 435–445. EDN: ALQECJ.

Inroduction

Moire patterns occur on the surface of monolayer graphene under the substrate action [1, 2, 3]. The cause of moire patterns is the mismatch between the crystal lattice periods of the metal substrate and graphene. The bond between carbon atoms in graphene is stronger than carbon with support atoms. Therefore, vertical strains of graphene are energetically more advantageous than longitudinal strains. These vertical deformations form a periodic superstructure that manifests as a moire pattern. Moire patterns are formed in graphene on various substrates: Ru [4, 5], Ir [6, 7], Rh [8], Pt [9, 10], Cu [11], Pd [12], Co [13], Ni [14]. Crystals with a face-centered crystal lattice serve as a support for the graphene monolayer. As a rule, the surface of the substrate coincides with the plane (111). In this case, the atoms on the substrate surface form a hexogonal structure. The parameters of the moire pattern are determined by the ratio of the periods for

*sbelim@mail.ru
†ivtikhomirov@omgtu.ru

the free graphene lattice and the substrate. The moire superstructure period also depends on the mutual orientation between the crystal lattices of graphene and the substrate. Increasing the angle between the main directions in the lattices reduces the moire pattern period.

The Pt (111) substrate is of particular interest due to the weak interaction between carbon and platinum atoms. Van der Waals forces dominate the interaction between platinum and carbon atoms [15]. The weak interaction between atoms makes it possible to create graphene films oriented at different angles [16]. These capabilities provide a wide variety of moire pattern periods.

The main problem of modeling moire patterns in graphene is the choice of interaction potential. The method of classical molecular dynamics with Tersoff potential [17] demonstrated a wide variety for moire superstructures. The application of the same method with Lennard–Jones potential did not produce interesting results. The density functional method allowed to simulate epitaxial growth of graphene on the Pt (111) surface at angles 0 and 30 [18]. Calculations showed the dependence of the moire patterns period on the location of the graphene monolayer relative to the substrate. Also, the density functional method considers the competition between the interaction energy with the substrate and the energy of elastic strains of graphene [12]. Calculations from the first principles for six different graphene orientation angles [19] confirmed a weak bond between carbon atoms and the substrate. The geometric superposition model of two mismatched hexagonal lattices [20] predicts the appearance of periodic beats that appear as moire patterns. The system of equations in this model has solutions well consistent with the experimental data for Pt (111). Atomistic modeling based on minimizing van der Waals energy [21] is also well consistent with experimental data. Mathematical formalism based on the two-dimensional Fourier transform [22] also leads to the inevitability of the appearance of moire patterns on substrates when there is a mismatch between crystal lattices. However, the authors of this work do not give the results for comparison with the experiment. All of these methods are computationally demanding. Lennard-Jones's potential is one of the easiest to describe van der Waals forces. A computational scheme based on this potential allows simulating systems with a large number of atoms and controlled accuracy.

Previous articles of the authors have shown that the influence of the substrate can be represented as a periodic potential [23, 24]. Deformations of the monoatomic film under the action of the substrate are described by minimizing the total energy for films atoms [25, 26]. Previously, the authors considered longitudinal deformations of thin films. This paper develops a method for calculating the surface potential and behavior of monoatomic films in it for transverse deformations and the formation of moire patterns.

1. Model

Intermolecular forces determine the interaction between carbon atoms and the substrate, since there is a large distance between them. These forces can be approximated by the Lennard–Jones potential [27] in this case.

$$U_{LG}(r) = 4\varepsilon_0 \left(\left(\frac{\sigma}{r} \right)^{12} - \left(\frac{\sigma}{r} \right)^{6} \right). \tag{1}$$

ε_0 is a parameter that determines the depth of the potential pit. σ is a parameter that determines the position of the energy minimum. Both parameters depend on the type of atoms that interact. These parameters can be determined from comparison with experimental data.

We use the surface potential approximation [24, 25] to study the influence of the substrate on graphene. The monolayer film is placed at an external periodic potential in this approach. Substrate atoms create this surface potential with van der Waals forces. The first step in the model determinates parameters for free graphene without a substrate. The second step calculates the potential of the substrate. The third stage consists in placing graphene in the potential of the substrate and finding its equilibrium state.

Monolayer graphene forms a hexagonal lattice of carbon atoms in free-state. The model calculates the interaction energy W_C of one carbon atom with the rest of the atoms to determine the Lennard–Jones potential parameters.

$$W_C = 4\varepsilon_C \sum_{(i,j)} \left(\left(\frac{\sigma_C}{r_{ij}} \right)^{12} - \left(\frac{\sigma_C}{r_{ij}} \right)^{6} \right). \tag{2}$$

r_{ij} is the distance between the selected carbon atom and the carbon atom numbered (i,j). ε_C and σ_C are Lennard-Jones potential parameters for carbon atoms in graphene. There is a KIM repository of Lennard-Jones potential parameter values for various atoms [28]. However, this repository builds on experimental data for the most common crystal lattices. Calculations show that a change in the type of crystal lattice leads to a change in the σ_C parameter in the Lennard-Jones potential [28]. This parameter requires a separate calculation for graphene. The repository contains parameters for graphite. The model calculates the W_C energy for only one atom. The rest of the atoms will have the same energy.

The graphene lattice is two triangular sublattices. The atom with the number (i,j) in the first sublattice has coordinates:

$$\begin{aligned} x_{ij} &= \left(i + \frac{j}{2} - \frac{1}{2} \right) a + \frac{a}{2}, \\ y_{ij} &= \frac{\sqrt{3}}{2} \left(j + \frac{1}{3} \right) a + \frac{a}{2\sqrt{3}}. \end{aligned} \tag{3}$$

The atom with the number (i,j) in the second sublattice has coordinates:

$$\begin{aligned} x_{ij} &= \left(i + \frac{j}{2} - \frac{1}{2} \right) a + \frac{a}{2}, \\ y_{ij} &= \frac{\sqrt{3}}{2} \left(j - \frac{1}{3} \right) a + \frac{a}{2\sqrt{3}}. \end{aligned} \tag{4}$$

The graphene lattice is shifted so that one of the atoms is at the origin. All carbon atoms have the same energy. The energy W_C is calculated for the atom at $(0,0)$. The distance r_{ij} to the atom number (i,j) is directly proportional to the lattice period a. Substituting r_{ij} into the formula (2) gives an expression similar to the Lennard–Jones potential.

$$W_C = 4\varepsilon_C \left(A(n) \left(\frac{\sigma_C}{a} \right)^{12} - B(n) \left(\frac{\sigma_C}{a} \right)^{6} \right). \tag{5}$$

The coefficients $A(n)$ and $B(n)$ depend on the number of atoms considered n. Calculations performed for $n = 20$. Increasing the number of atoms $n > 20$ has little effect on the result.

The calculations determine the σ_C parameter from the requirement to minimize the interaction energy.

$$\frac{\partial W_C}{\partial a}\Big|_{a=a_C} = 0. \tag{6}$$

a is the period of the crystal lattice in graphene. a_C is the experimental value of the lattice period in graphene. Substituting the experimental value $a_C = 2.46$ Å [29] into formula (6) and solving the equation yields a value $\sigma_C = 1.2850$ Å. The calculations use an array with 1000 atoms. The results of the calculations show that you can limit to an array of 400 atoms. A further increase in the number of atoms in the system gives corrections in the fifth sign after the comma. Further calculations use the value from the KIM repository $\varepsilon_C = 6.3695eV$ [28] for the second parameter. This parameter cannot be defined for simple geometric reasons and energy minimization.

The model requires the determination of parameters in the Lennard-Jones potential for the interaction between platinum atoms to calculate the surface potential. Platinum has a face-centered cubic lattice with a period $b_{Pt} = 3.920$ Å. Two types of atoms are distinguished in a unit cell by the number of nearest neighbors. The first type of atoms is located at the top of the cube and has energy W_{Pt1}. The second type of atoms is located in the center of the face and has energy W_{Pt2}. Both energies are calculated using the formula (7).

$$W_{Pti} = 4\varepsilon_{Pt} \sum_{(i,j)} \left(\left(\frac{\sigma_{Pt}}{r_{ij}} \right)^{12} - \left(\frac{\sigma_{Pt}}{r_{ij}} \right)^{6} \right). \quad (i = 1, 2). \tag{7}$$

The distance between the atoms r_{ij} depends on the number of the atom (i, j) and the period of the crystal lattice b.

The average energy per atom accounts for the number of each type atoms per unit cell. One atom of the first type and three atoms of the second type are per unit cell. The average energy per atom is determined by the weighted sum of energies.

$$W_{Pt} = \frac{1}{4} W_{Pt1} + \frac{3}{4} W_{Pt2}. \tag{8}$$

Minimizing energy per atom gives an equation to compute the parameter σ_{Pt}.

$$\frac{\partial W_{Pt}}{\partial b}\Big|_{b=b_{Pt}} = 0. \tag{9}$$

Substituting the experimental value $b_{Pt} = 3.920$ Å into equation (9) gives the value $\sigma_{Pt} = 2.5420$ Å. The calculations use an array of 10000 atoms. The value of the parameter goes to a stable value starting from 8000 atoms in the system. The model uses the second parameter from the KIM repository $\varepsilon_{Pt} = 3.1401eV$ [28].

Surface potential W_{CPt} calculations also use Lennard-Jones potential.

$$W_{CPt} = 4\varepsilon_{CPt} \sum_{j} \left(\left(\frac{\sigma_{CPt}}{r_j} \right)^{12} - \left(\frac{\sigma_{CPt}}{r_j} \right)^{6} \right). \tag{10}$$

r_j is the distance from the atom number j to the point with coordinates (x, y, z).

The model uses combining rules [29] for Lennard-Jones potential parameters when calculating the surface potential.

$$\begin{aligned} \sigma_{CPt} &= \left(\frac{\sigma_{C1}^6 + \sigma_{Pt}^6}{2} \right)^{1/6}, \\ \varepsilon_{CPt} &= \sqrt{\varepsilon_C \varepsilon_{Pt}} \left(\frac{\sqrt{\sigma_C \sigma_{Pt}}}{\sigma_{CPt}} \right)^6. \end{aligned} \tag{11}$$

σ_{C1} is a Lennard-Jones potential parameter for the interaction of carbon atoms with neighboring layers. The parameters in the Lennard-Jones potential for graphene and for the substrate do not match ($\sigma_{C1} \neq \sigma_C$). The model uses a value for σ_{C1} that is characteristic of the interaction between graphite layers. ($\sigma_{C1} = 3.5523$ Å, $\sigma_{CPt} = 3.2319$ Å, $\varepsilon_{CPt} = 2.8896\ eV$).

Surface potential calculations use a 100×100 atom site and three layers of platinum atoms. The model is limited to only three layers, since the Lennard-Jones potential decreases rapidly with distance and the following layers contribute little to the potential value. The surface layer of atoms is located in the $z = 0$ plane. The substrate occupies a half-space $z \leqslant 0$. Surface arrangement of atoms corresponds to plane (111). The following layers of substrate atoms make a small contribution that does not significantly affect the potential value. We calculate a fragment of the potential located in the center of the site and having an area of one unit cell. The potential of an unrestricted substrate consists of combining such fragments produced by parallel transfer. If the height z above the substrate surface is fixed, the potential has the form of a periodic structure with the maxima and minima clearly identified. The height of the extremes depends on the distance from the point of space to the substrate z.

Graphene atoms are located in the external potential $W_{CPt}(x, y, z)$. The model also considers the interaction between carbon atoms in graphene. The total energy per carbon atom near the substrate is the sum of two energies.

$$W_i(x, y, z) = W_{Ci}(x, y, z) + W_{CPti}(x, y, z). \tag{12}$$

i is the number of the carbon atom.

The interaction energy between carbon atoms in graphene significantly exceeds the interaction energy with the substrate. Graphene longitudinal deformations do not exceed 5% [15]. Therefore, the model uses a quadratic approximation for the energy of the interaction forces between graphene atoms.

$$W_{Ci} = \sum_j \frac{K x_{ij}^2}{2} \tag{13}$$

K is the elasticity coefficient, x_{ij} is the distance to the nearest neighboring atom. Calculations used $K = 10$. This elastic coefficient provides the desired longitudinal deformations.

The energy minimum condition determines the coordinates of the carbon atom.

$$\frac{\partial W_i(x, y, z)}{\partial x} = 0, \quad \frac{\partial W_i(x, y, z)}{\partial y} = 0, \quad \frac{\partial W_i(x, y, z)}{\partial z} = 0. \tag{14}$$

The model solves the system of equations (14) for each carbon atom in graphene number i.The central graphene atom is initially placed above the central minimum of the substrate potential. The Monte Carlo method is used to solve this system of equations. The solution is obtained iteratively. Graphene film is flat in initial state. One iteration involves trying to shift the graphene atom by a random vector. If the displacement reduces the energy, then a new position of the atom is accepted, otherwise the atom returns to its original position. The algorithm ends when the next iteration changes the position of all atoms less than 1%.

2. Computer experiment results

Computer simulation is performed for a system having a size 100Å×100Å. The undisturbed graphene film is above this site at the initial stage. The model calculates the equilibrium position

for each graphene atom in the external substrate potential. The calculations vary the positions of the atom by three coordinates. The first computer experiment examines a carbon system with angle $\theta = 0°$ between the main directions of the crystal lattice for the substrate and graphene. Fig. 1 shows the results of the calculations. The figure shows a 50Å×50Å film fragment to zoom in.

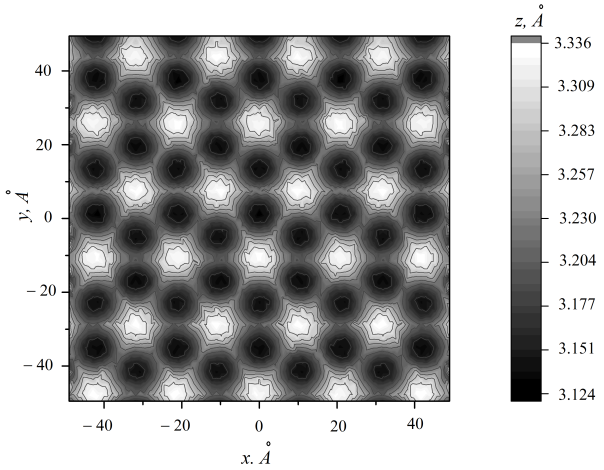

Fig. 1. Arrangement of carbon atoms above Pt substrate for $\theta = 0°$. The height of the atoms above the substrate is shown by the intensity of gray

Fig. 1 shows vertical strains of graphene. Deformations are periodic and form a honeycomb superstructure. The boundaries of the cells for the superstructure are determined by the atoms closest to the substrate. The superstructure period is $d = 25.4$ Å. The lower boundary of the graphene film is located at a distance $z = 2.865$ Å from the substrate. Fig. 2 shows a 3D image of a moire pattern in the graphene.

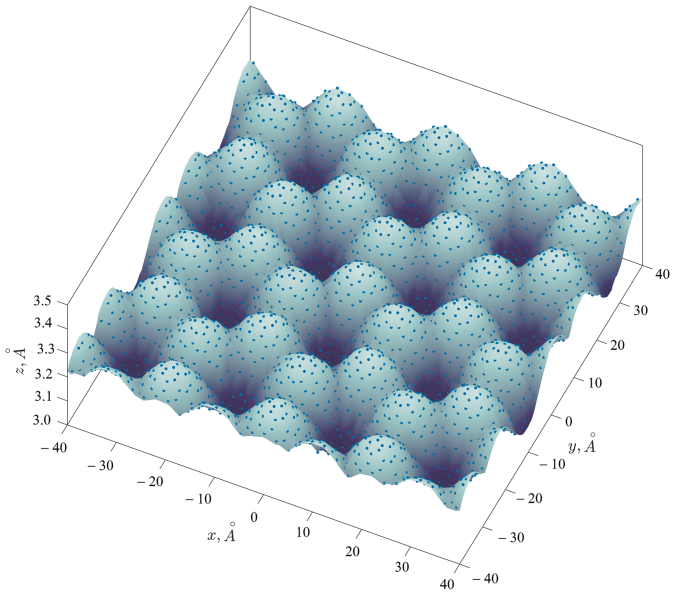

Fig. 2. 3D image of moire pattern in graphene

In the second modeling step, the graphene film is rotated relative to the substrate. The rotation angle θ for the film is measured between the principal directions of the graphene and substrate lattices. The rotation of graphene relative to the crystal lattice main direction in the substrate changes the period of the moire pattern. The rotation angle θ changes the position of the atoms relative to the maxima and minima of the surface potential. Fig. 3 shows the moire pattern at two angles θ.

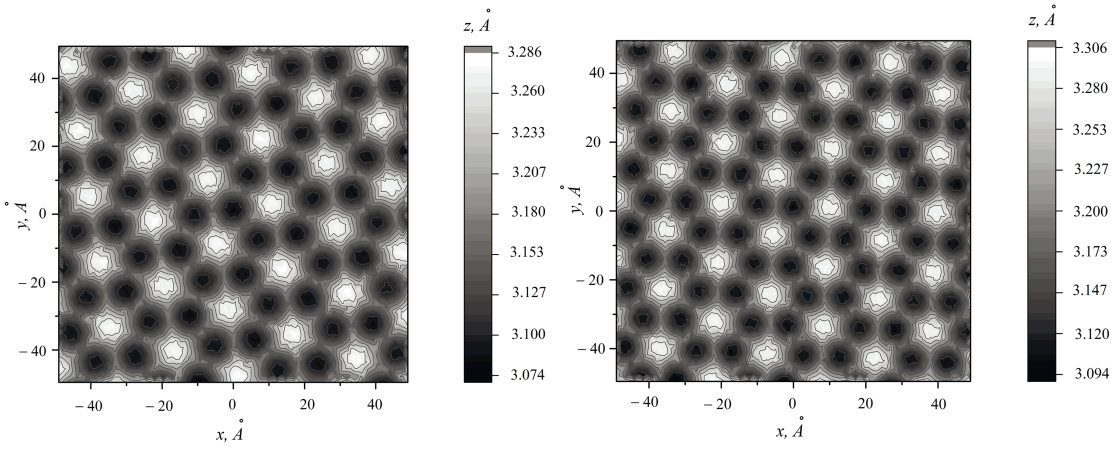

(a) (b)

Fig. 3. Plot for period of moire pattern d versus rotation angle θ of graphene relative to substrate. Moire pattern at two angles of graphene rotation relative to substrate: a) $\theta = 3°$, b) $\theta = 5°$

Calculations show a decrease in the period of moire pattern in graphene with an increase in the angle of rotation relative to the substrate. Calculations are made for angles from $\theta = 0°$ to $\theta = 16°$ with $\Delta\theta = 1°$ increments. Fig. 4 shows the dependence of the moire pattern period d on the rotation angle θ of graphene relative to the substrate.

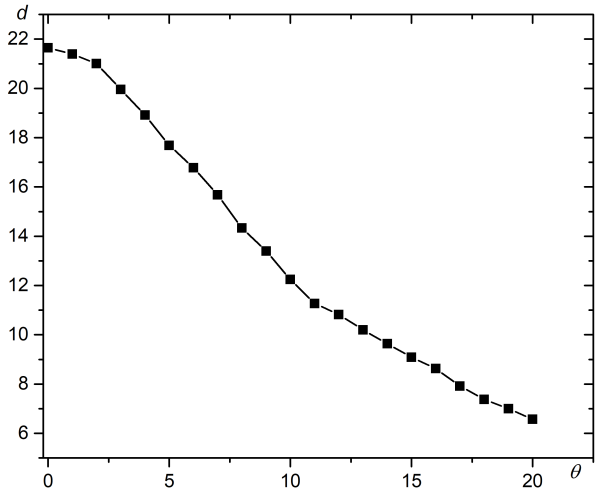

Fig. 4. Plot for period of moire pattern d versus rotation angle θ of graphene relative to substrate

Conclusion

The results of the simulation are in good agreement with the data of other works and experimental data. The experiment shows the distance from the substrate to the graphene film (3.30 ± 0.05) Å [16]. DFT modeling gives a value 3.30 Å [18] for this distance. Our model shows the distance from the substrate to carbon atoms in graphene in the range from 3.23 Å to 3.31 Å. At the same time, our model requires significantly less calculations than the DFT method.

Theoretical values of the moire pattern period are based on the geometric model [20]. This model predicts stable moire patterns only at certain angles between the principal directions of the graphene and platinum crystal lattice. This model allows to calculate the period of moire structures for these angles. DFT modeling [12, 19] performs calculations only for angles predicted by the geometric model. Periods based on DFT modeling and geometric model coincide. Moire pattern periods in our model (OUR) are also consistent with the DFT and geometric model (GM) ($\theta = 0°$, $d(GM) = 22.1$ Å, $d(OUR) = 21.7$ Å; $\theta = 0.8°$, $d(GM) = 21.0$ Å, $d(OUR) = 21.3$ Å; $\theta = 19°$, $d(GM) = 7.4$ Å, $d(OUR) = 7.0$ Å). The experimental value of the moire pattern period at $\theta = 0°$ is $d = 22$ Å. Our model gives the same result.

Our model differs from the geometric model in that it predicts a moire pattern at different angles. A moire pattern exists for any angle between the principal directions of the crystal lattice of the Pt substrate and graphene. The moire pattern has a simple shape for the angles predicted by the geometric model. The moire pattern is more complex for other angles. The highs and lows of this pattern have a more complex shape. In this case, hexagonal symmetry is preserved.

Our model calculates the moire pattern in graphene on the Pt substrate. The model uses a two-step approach. The first step calculates the surface potential of the substrate. The second stage studies the behavior of graphene in the surface potential. The model uses the Lennard–Jones potential to calculate the surface potential. The selection of the two-part potential is based on the large distance from the substrate surface to the graphene film. Van der Waals forces dominate such a system. Lennard-Jones's potential describes these forces well.

This research was funded by Russian Science Foundation, project number 23-29-00108.

References

[1] J.Dong, L.Zhang, B.Wu, et al., Theoretical Study of Chemical Vapor Deposition Synthesis of Graphene and Beyond: Challenges and Perspectives, *J. Phys. Chem. Lett.*, **12**(2021), 7942–7963. DOI: 10.1021/acs.jpclett.1c02316

[2] T.Zhao, J.Guo, T.Li, et al., Substrate engineering for wafer-scale two-dimensional material growth: strategies, mechanisms, and perspectives, *Chem. Soc. Rev.*, **52**(2023), 1650–1671. DOI: 10.1039/d2cs00657j

[3] J.Du, B.Tong, S.Yuan, et al., Advances in Flexible Optoelectronics Based on Chemical Vapor Deposition-Grown Graphene, *Adv. Funct. Mater.*, **32**(2022), 2203115. DOI: 10.1002/adfm.202203115

[4] M.Yang, Y.Liu, T.Fan, et al., Metal-graphene interfaces in epitaxial and bulk systems: A review, *Progress in Materials Science*, **110**(2020), 100652. DOI: 10.1016/j.pmatsci.2020.100652

[5] L.Zhang, J.Dong, Z.Guan, et al., The alignment-dependent properties and applications of graphene moire superstructures on the Ru(0001) surface, *Nanoscale*, **12**(2020), 12831. DOI: 10.1039/d0nr02370a

[6] Q.Shi, K.Tokarska, H.Ta, et al., Substrate Developments for the Chemical Vapor Deposition Synthesis of Graphene, *Advanced Materials Interfaces*, **7**(2020), 1902024. DOI: 10.1002/admi.201902024

[7] S.Kraus, F.Huttmann, J.Fischer, et al., Single-crystal graphene on Ir(110), *Phys. Rev. B*, **105**(2022), 165405. DOI: 10.1103/PhysRevB.105.165405

[8] M.G.Cuxart, D.Perilli, S.Tomekce, et al., Spatial segregation of substitutional B atoms in graphene patterned by the moire superlattice on Ir(111), *Carbon*, **201**(2023), 881. DOI: 10.48550/arXiv.2210.02902

[9] C.Gautam, B.Thakurta, M.Pal, et al., Wafer scale growth of single crystal two-dimensional van der Waals materials, *Nanoscale*, **16**(2024), 5941. DOI: 10.1039/d3nr06678a

[10] Z.Zhang, X.Yang, K.Liu, et al., Epitaxy of 2D Materials toward Single Crystals, *Advanced Science*, **9**(2022), 2105201. DOI: 10.1002/advs.202105201

[11] W.Yao, J.Zhang, J.Ji, et al., Bottom-Up-Etching-Mediated Synthesis of Large-Scale Pure Monolayer Graphene on Cyclic-Polishing-Annealed Cu(111), *Advanced Materials*, **34**(2022), 2108608. DOI: 10.1002/adma.202108608

[12] L.Zhang, F.Ding, Mechanism of Corrugated Graphene Moire Superstructures on Transition-Metal Surfaces, *ACS Appl. Mater. Interfaces*, **13**(2021), 56674–56681. DOI: 10.1021/acsami.1c18512

[13] W.Yue, Q.Guo, Y.Dedkov, et al., Electronic and Magnetic Properties of the Graphene/Y/Co(0001) Interfaces: Insights from the Density Functional Theory Analysis, *ACS omega*, **7**(2022), 7304–7310. DOI: 10.1021/acsomega.1c07136

[14] J.Takahashi, T.Ueyama, K.Kamei, et al., Experimental and theoretical studies on the surface morphology variation of a Ni substrate by graphene growth, *J. Appl. Phys.*, **129**(2021), 024302. DOI:10.1063/5.0036580

[15] C.M.Seah, S.P.Chai, A.R.Mohamed, Mechanisms of graphene growth by chemical vapour deposition on transition metals, *Carbon*, **70**(2014), 1. DOI: 10.1016/j.carbon.2013.12.073

[16] J.I.Martinez, P.Merino, A.L.Pinardi, et al., Role of the Pinning Points in epitaxial Graphene Moire Superstructures on the Pt(111) Surface, *Sci. Rep.*, **6**(2016), 20354. DOI: 10.1038/srep20354

[17] B.Sun, W.Ouyang, J.Gu, et al., Formation of Moire superstructure of epitaxial graphene on Pt(111): A molecular dynamic simulation investigation, *Materials Chemistry and Physics*, **253**(2020), 123126. DOI:10.1016/j.matchemphys.2020.123126

[18] M.S.Christian, A.Otero-de-la-Roza, E.R.Johnson, Adsorption of graphene to metal (111) surfaces using the exchange-hole dipole moment model, *Carbon*, **124**(2017), 531. DOI: 10.1016/j.carbon.2017.08.077

[19] L.Meng, R.Wu, L.Zhang, et al., Multi-oriented moire superstructures of graphene on Ir(111): experimental observations and theoretical models, *J. Phys.: Condens. Matter.*, **24**(2012), 314214. DOI: 10.1088/0953-8984/24/31/314214

[20] P.Zeller, S.Gunther, What are the possible moire patterns of graphene on hexagonally packed surfaces? Universal solution for hexagonal coincidence lattices, derived by a geometric construction, *New J. Phys.*, **16**(2014), 083028. DOI: 10.1088/1367-2630/16/8/083028

[21] M.Neek-Amal, F.M.Peeters, Graphene on boron-nitride: Moire pattern in the van der Waals energy, *Appl. Phys. Lett.*, **104**(2014), 041909. DOI: 10.1063/1.4863661

[22] K.Hermann, Periodic overlayers and moire patterns: theoretical studies of geometric properties, *J. Phys.: Condens. Matter.*, **24**(2012), 314210. DOI: 10.1088/0953-8984/24/31/314210

[23] S.V.Belim, I.V.Tikhomirov, I.V.Bychkov, Simulation of Epitaxial Film-Substrate Interaction Potential, *Coatings*, **12**(2022), 853. DOI: 10.3390/coatings12060853

[24] S.V.Belim, I.V.Tikhomirov, Computer simulation of Fe epitaxial films on a Cu(100) substrate, *Physica Scripta*, **98**(2023), 105973. DOI: 10.1088/1402-4896/acface

[25] S.V.Belim, Investigation of Phase Transitions in Ferromagnetic Nanofilms on a Non-Magnetic Substrate by Computer Simulation, *Materials*, **15**(2022), 2390. DOI: 10.3390/ma15072390

[26] S.V. Belim, I.V. Bychkov, D.A. Kuzmin, Tuning of 2D magnets Curie temperature via substrate, *J. Magn. Magn. Mat.*, **541**(2022), 168553. DOI: 10.1016/j.jmmm.2021.168553

[27] J.E.Lennard-Jones, On the determination of molecular fields. -II. From the equation of state of a gas, *Proceedings of the Royal Society of London A: Mathematical, Physical and Engineering Sciences*, **106**(1924), 463. DOI: 10.1098/RSPA.1924.0082

[28] E.B.Tadmor, R.S.Elliott, J.P.Sethna, et al., The potential of atomistic simulations and the Knowledgebase of Interatomic Models, *JOM*, **63**(2011), 17. DOI: 10.1007/s11837-011-0102-6

[29] D.Boda, D.Henderson, The effects of deviations from Lorentz-Berthelot rules on the properties of a simple mixture, *Molecular Physics*, **106**(2008), 2367. DOI: 10.1080/00268970802471137

Муаровые узоры в графене на подложке Pt(111): компьютерное моделирование

Сергей В. Белим
Илья В. Тихомиров
Омский государственный технический университет
Омск, Российская Федерация

Аннотация. Исследование деформаций монослойной пленки графена на Pt подложке выполнено методом компьютерного моделирования. Влияние подложки моделируется с помощью поверхностного потенциала. Атомы углерода в графене взаимодействуют между собой и с потенциалом

подложки. Минимум потенциальной энергии определяет положение атомов углерода. Поиск равновесного положения атомов углерода выполняется с помощью метода Монте–Карло. Поперечные деформации графена являются энергетически выгодными из-за сильной связи между атомами углерода. Продольные деформации графена являются малыми. Модель использует потенциал Леннард–Джонса для вычисления потенциала подложки. Параметры потенциала вычисляются из равновесного состояния невозмущенной системы. Поверхностный потенциал вычисляется для одной элементарной ячейки и транслируется с помощью параллельного переноса на всю подложку. Взаимодействие между атомами углерода также описывается потенциалом Леннард-Джонса. Муаровые узоры в графене имеют сотовую сверхструктуру. Модель вычисляет зависимость периода муарового узора от угла между главными направлениями кристаллической решетки подложки и графена. Период муаровой сверхрешетки убывает при повороте пленки по нелинейному закону. Расчеты показывают наличие большого расстояния между подложкой и графеновой пленкой. Результаты моделирования находятся в хорошем согласии с экспериментальными данными.

Ключевые слова: графен, поверхностный потенциал, муаровый узор, потенциал Леннард-Джонса.

EDN: AAVDIU
УДК 538.9: 535.37

Synthesis and Spectroscopy of Tm,Ho-codoped Y_2O_3 Transparent Ceramics for 2-μm Lasers

Roman N. Maksimov[*]
Vladislav A. Shitov[†]
Vladimir V. Osipov[‡]
Albert N. Orlov[§]
Institute of Electrophysics UrB RAS
Ekaterinburg, Russian Federation
Ekaterina M. Buzaeva[¶]
Polina A. Ryabochkina[‖]
Aleksandr O. Ariskin[**]
National Research Mordovia State University
Saransk, Russian Federation

Received 02.11.2024, received in revised form 13.12.2024, accepted 24.03.2025

Abstract. In this study, thulium and holmium codoped yttrium sesquioxide (Tm,Ho:Y_2O_3) transparent ceramics were fabricated using solid-state vacuum sintering of nano-sized particles with complex chemical composition synthesized by the laser ablation method. The as-produced powder was in the form of soft aggregates composing of individual spherical particles with a diameter of 16 nm, whose crystal structure underwent conversion from the monoclinic (space group C2/m) to the cubic (space group Ia-3) modification after consolidation into ceramic material. The morphological properties along with their correlation to the optical quality of Tm,Ho:Y_2O_3 ceramics vacuum sintered at 1700–1775 °C were investigated. The sample sintered at 1750 °C featured higher transmittances (81.6% at $\lambda = 600$ nm and 83.0% at $\lambda = 1000$ nm) and lower content of scattering centers of 0.00014 vol.%. The absorption cross-section at 797 nm due to the $^3H_6 \rightarrow {}^3H_4$ transition of Tm^{3+} ions was 4.44×10^{-21} cm^2. The broad luminescence band was observed from 1750 nm to 2100 nm owing to the combination of cross-relaxation of Tm^{3+} ions and nonradiative energy transfer from the $^3F_4$ level (Tm^{3+}) to the $^5I_7$ level (Ho^{3+}). These results suggest that Tm,Ho-codoped Y_2O_3 transparent ceramics are promising gain media for broadly tunable and mode-locked lasers emitting in the 2-μm spectral range.

Keywords: nanopowder, yttrium sesquioxide, optical ceramic, microstructure, codoping, nonradiative energy transfer.

Citation: R.N. Maksimov, V.A. Shitov, V.V. Osipov, A.N. Orlov, E.M. Buzaeva, P.A. Ryabochkina, A.O. Ariskin, Synthesis and Spectroscopy of Tm,Ho-codoped Y_2O_3 Transparent Ceramics for 2-μm Lasers, J. Sib. Fed. Univ. Math. Phys., 2025, 18(4), 446–455. EDN: AAVDIU.

[*]roman.maksimov196@yandex.ru https://orcid.org/0000-0001-5524-9872
[†]vlad@iep.uran.ru https://orcid.org/0000-0001-8761-8329
[‡]osipov@iep.uran.ru
[§]orlov@iep.uran.ru
[¶]katyabuzaeva@yandex.ru https://orcid.org/0000-0001-6906-7623
[‖]ryabochkina@freemail.mrsu.ru https://orcid.org/0000-0001-8503-8486
[**]salex24091999@gmail.com

Introduction

In recent years, solid-state lasers emitting in the 2-μm spectral range have gained significant attention owing to their diverse applications in industry, medicine and fundamental science [1–3]. Trivalent thulium (Tm^{3+}) and holmium (Ho^{3+}) ions possess the most notable optical transitions for laser emission in the 1.9–2.1 μm region. Tm^{3+}-doped active elements can be efficiently pumped at 0.8 μm by commercially available high-power AlGaAs diodes to achieve laser emission due to the $^3F_4 \rightarrow {}^3H_6$ transition. Regarding Ho^{3+} ions, laser operation on the $^5I_7 \rightarrow {}^5I_8$ transition is usually demonstrated under resonant pumping at 1.93 μm using expensive Tm^{3+}-fiber lasers or GaSb (InP) diodes. To address this issue, gain media codoped with Tm^{3+} and Ho^{3+} are currently being actively developed [4–6]. Due to the proximity of the energy levels of Tm^{3+} ($^3F_4$) and Ho^{3+} ($^5I_7$), non-radiative energy transfer from Tm^{3+} to Ho^{3+} occurs enabling laser oscillation based on the $^5I_7 \rightarrow {}^5I_8$ optical transition in Ho^{3+} ions through diode pumping of the $^3H_4$ level of Tm^{3+} at around 0.8 μm. Additionally, this approach is promising for tunable and mode-locked lasers generating ultrashort pulses owing to the broadening of the gain spectrum by combining the individual emission bands of Tm^{3+} and Ho^{3+}.

Yttrium sesquioxide (Y_2O_3) is a promising host material for Tm^{3+}, Ho^{3+}-codoping owing to its excellent optical and thermo-mechanical properties [7]. However, the current Y_2O_3 crystal growth technologies do not enable the synthesis of a material with both high optical quality and large volume. This is due to the fact that melt growth of large-sized single-crystals is practically impossible because of the reversible transition of Y_2O_3 from a cubic to a hexagonal structure near 2300 °C [8], which leads to the destruction of the sample during cooling. In this regard, producing polycrystalline materials based on Y_2O_3 through the sintering of ultrafine powders could serve as an alternative approach to crystal growth, as ceramic technology offers several key advantages, including the possibility to achieve large sizes, composite structures and lower synthesis temperatures [9–11].

Ultrafine powders are crucial as the starting material in the production of optical ceramics. Synthesizing these nanopowders is a particularly challenging and critical stage due to the stringent requirements for high purity, small particle sizes, minimal agglomeration, and complex chemical composition. We employed laser synthesis to produce the nanopowders, a method that effectively meets all these requirements [12]. With respect to Tm^{3+}, Ho^{3+}-codoping, laser ablation synthesis allows for the uniform incorporation of multiple active ions throughout the volume of individual nanoparticles during the vapor condensation process.

In this study, we investigate the properties of Tm^{3+}, Ho^{3+}-codoped Y_2O_3 nanoparticles produced by the laser ablation method, as well as the structural, optical, and spectroscopic properties of transparent ceramics sintered at various temperatures.

1. Materials and methods

Nano-sized particles with a complex chemical composition synthesized by laser evaporation of solid target in an air flow were used as the starting material for the fabrication of Tm,Ho:Y_2O_3 ceramics. A detailed description of the experimental setup based on the LS-07N ytterbium fiber laser (λ=1070 nm, NTO "IRE-Polus", Russia) is presented in [13].The preparation of a solid target was carried out by uniaxial pressing of yttrium, thulium and holmium oxide powders with a purity of at least 99.99 wt.% (LANHIT, Russia) mixed in the proportion $(Tm_{0.03}Ho_{0.003}Y_{0.967})_2O_3$. Next the resulting green body with a diameter of 65 mm and a thick-

ness of 25 mm was annealed in air for 5 h at 1250 °C.

The synthesized nanoparticles were compacted into cylindrical samples with a diameter of 14 mm and a thickness of 3 mm by uniaxial static pressing at 200 MPa. After calcination in air for 3 h at a temperature of 900 °C, the compacts were vacuum sintered for 5 h at 1700 °C, 1725 °C, 1750 °C or 1775 °C under a residual gas pressure of 10^{-3} Pa. The sintered ceramic samples were annealed in air for 2 h at 1400 °C to eliminate oxygen vacancies and then mirror polished on both sides for structural and spectroscopic characterization.

The morphology of the as-synthesized nanopowder was studied using a JEM 2100 (TEM, JEOL Ltd., Japan) transmission electron microscope. The specific surface area of the nanopowder was measured by the Brunauer-Emmett-Teller (BET) method with a TriStar 3000 gas adsorption analyzer (Micromeritics, USA). The crystal structures of the as-obtained nanoparticles and the sintered ceramics were identified by means of X-ray diffraction (XRD) analysis using a D8 Discover diffractometer (Bruker AXS, Germany). The chemical composition of the as-synthesized nanopowder was analyzed by inductively coupled plasma mass spectrometry (ICP MS) using an Optima 2100 DV spectrometer (PerkinElmer, USA).

In order to assess the optical quality of the obtained ceramics, the transmission spectra were measured at room temperature in the wavelength range 200–1100 nm using a UV-1700 double beam spectrophotometer (Shimadzu, Japan). The absorption spectra of the samples were recorded in the interval from 300 to 2200 nm by a Lambda 950 UV-VIS-NIR double beam spectrophotometer (PerkinElmer, USA). The luminescence spectrum was registered in the range 1600–2200 nm under excitation at 811 nm using a FLS980 fluorescence spectrometer (Edinburgh Instruments, UK).

The average content of scattering centers throughout the depth of the samples was estimated by means of the direct count method using an optical microscope BX51TRF (Olympus Corp., Japan).

2. Results and discussion

2.1. Properties of Tm,Ho:Y_2O_3 nanoparticles

To accurately calculate the lattice constant and absorption characteristics of the fabricated ceramics, it is crucial to specify the precise Tm^{3+} and Ho^{3+} contents in the nanopowder. Through ICP-MS analysis, the chemical composition of the synthesized nanoparticles was determined to be $(Tm_{0.032}Ho_{0.003}Y_{0.965})_2O_3$ corresponding to the doping concentrations $N_{Tm} = 6.46\times10^{20}$ at/cm^3 and $N_{Ho} = 0.61\times10^{20}$ at/cm^3. For clarity, this composition will henceforth be referred to as Tm,Ho:Y_2O_3.

Fig. 1 shows a TEM image illustrating the morphology of Tm,Ho:Y_2O_3 nanopowder synthesized using the laser ablation method. The sample primarily consists of ultrafine, loosely aggregated, and weakly faceted particles, with sizes ranging from 10 to 40 nm. The specific surface area of the powder, as measured by the BET method, reached 67 m^2/g corresponding to an average particle diameter of around 16 nm. This small particle size results in a high surface area-to-volume ratio, which increases surface forces such as van der Waals forces. However surface charges from ionization during ablation or from adsorbed molecules create electrostatic repulsion between particles preventing close contact and significant agglomeration. These characteristics are beneficial for fabricating transparent ceramics, as they help reduce density variations in pressed compacts, promoting more uniform densification.

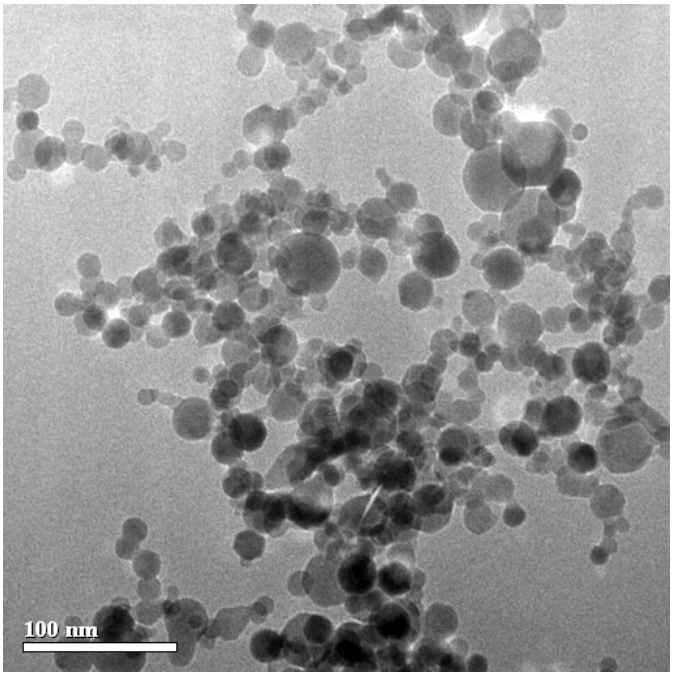

Fig. 1. TEM image of the as-produced Tm,Ho:Y_2O_3 nanoparticles

The crystal structure of the synthesized Tm,Ho:Y_2O_3 nanoparticles was examined through powder X-ray diffraction analysis (Fig. 2a). In addition to the peak broadening attributed to the small crystal size, approximately 14 nm, which aligns with TEM observations, it is apparent that the nanoparticles do not exhibit the equilibrium structure (space group *Ia*-3, No. 206). Instead, the positions and relative intensities of the diffraction peaks correspond to the monoclinic B-type modification of Y_2O_3 (space group $C2/m$), as identified in ICDD PDF No. 00-044-0399 (Fig. 2b). The lattice parameters obtained from crystal structure refinement using the Rietveld method were determined as follows: a = 13.916 Å, b = 3.502 Å, c = 8.634 Å, and $\beta = 100.35°$. However, as discussed in the following section, the nanoparticles underwent a phase transformation to the stable cubic modification of Y_2O_3 after vacuum sintering (Figs. 2c,d).

The presence of the monoclinic phase in the synthesized Tm,Ho:Y_2O_3 nanoparticles can be attributed to several factors including the high-pressure conditions during the laser ablation process and the resulting strain within the crystal structure. The gas-phase synthesis of the Tm_2O_3–Ho_2O_3–Y_2O_3 solid solution may lead to its crystallization in a metastable state, a phenomenon explained by the Gibbs-Thomson effect [14]. Specifically, the pressure difference (Δp) across the curved surface of a spherical particle with a radius (r) is related to the surface tension (γ) by the equation $\Delta p = 2\gamma/r$. For a particle radius of 8 nm and a surface tension of 0.74 N/m near the melting point [15], the calculated pressure difference is approximately 0.185 GPa. In nanoparticles surface tension can be higher than on a flat surface further increasing the internal pressure. Previous research using high-pressure powder and single-crystal X-ray diffraction has demonstrated that Y_2O_3 undergoes a phase transformation from its stable cubic bixbyite-type structure to the monoclinic B-phase at pressures of 11.7 GPa at room temperature or 3 GPa when heated to 900 °C [16,17].

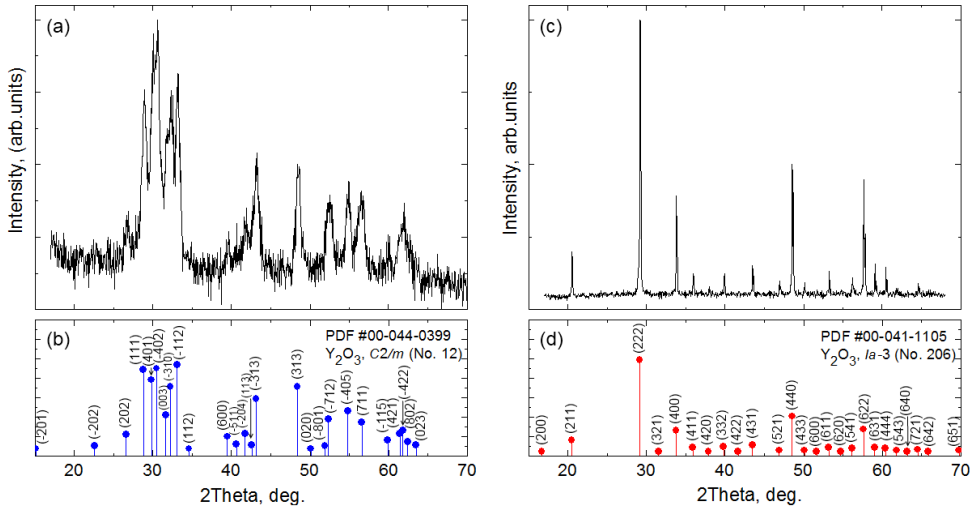

Fig. 2. XRD patterns of the as-synthesized Tm,Ho:Y_2O_3 nanoparticles and sintered ceramics (a, c) and theoretical reflections of monoclinic and cubic Y_2O_3 (b, d)

2.2. Characterization of Tm,Ho:Y_2O_3 transparent ceramics

Fig. 2c shows the XRD pattern of the Tm,Ho:Y_2O_3 ceramic sintered at 1750 °C, revealing diffraction peaks consistent with a single-phase material possessing a cubic bixbyite structure. This pattern aligns with the theoretical reflections of cubic Y_2O_3 (ICDD PDF No. 00-041-1105, as shown in Fig. 2d), indicating the formation of a substitutional solid solution of thulium, holmium, and yttrium sesquioxides. The incorporation of Tm_2O_3 and Ho_2O_3 into the Y_2O_3 lattice results in a slight shift of the diffraction peaks toward larger angles, which suggests a compression of the unit cell. This shift is anticipated given that the ionic radii of Tm^{3+} (0.880 Å) and Ho^{3+} (0.901 Å) for VI-fold oxygen coordination are comparable to or smaller than that of Y^{3+} (0.900 Å) [18]. The lattice parameter of the ceramic was determined to be 10.595 ± 0.005 Å.

Fig. 3 shows the transmission spectra of Tm,Ho:Y_2O_3 ceramics sintered at various temperatures and the theoretical curve for Y_2O_3 (dashed line) calculated using refractive index data [19] and the expression $T = 2n/(n^2+1)$ taking into account Fresnel losses and multiple light reflections from the sample's interfaces. The samples sintered at 1725 °C and 1750 °C exhibit transparency levels that approach the theoretical limit, particularly in the visible and near-IR spectral ranges. However, when the sintering temperature is increased to 1775 °C, the optical transmittance decreases significantly. The higher optical transmittance (81.6% at $\lambda = 600$ nm and 83.0% at $\lambda = 1000$ nm) was observed in the Tm,Ho:Y_2O_3 ceramic sintered at 1750 °C.

The transmission properties of the samples sintered at different temperatures correlate with the content of scattering centers detected using optical microscopy. Spherical pores ranging in size from 2 to 8 μm were relatively uniformly distributed throughout the depth of the samples, as shown in Fig. 4. The average pore volume contents were measured as 0.00153 vol.%, 0.00037 vol.%, 0.00014 vol.%, and 0.01332 vol.% for ceramics sintered at 1700 °C, 1725 °C, 1750 °C, and 1775 °C, respectively. Consequently, the considerable reduction of transparency after sintering at 1775 °C is attributed to the intragranular pores formed as a result of overheating. In turn, the slight decrease in transparency of the sample sintered at 1700 °C, compared to those sintered at 1725 °C and 1750 °C, can be explained by the lower intensity of bulk and surface diffusion processes, as well as insufficient energy to close residual pores at this temperature.

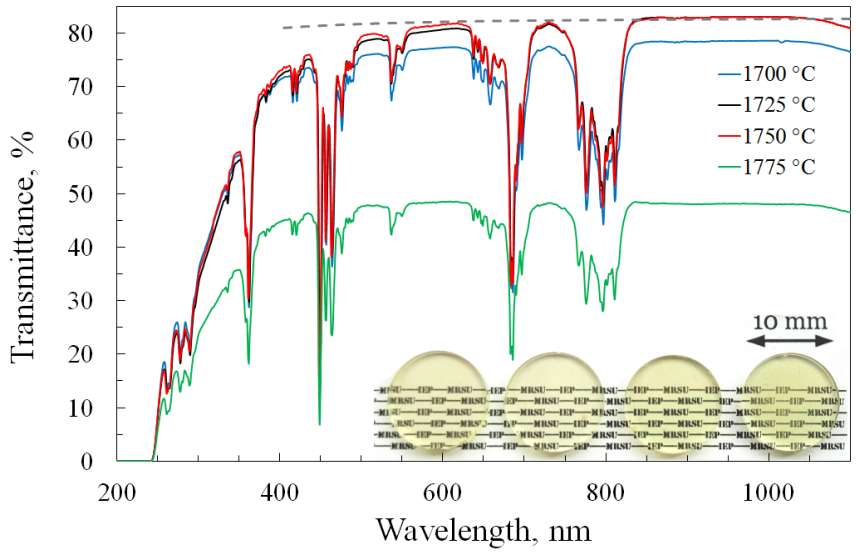

Fig. 3. Transmission spectra of the fabricated Tm,Ho:Y_2O_3 ceramics and the theoretical curve for Y_2O_3 calculated using refractive index data [19]. Inset shows the photograph of samples sintered at various temperatures (from left to right): 1700 °C, 1725 °C, 1750 °C and 1775 °C

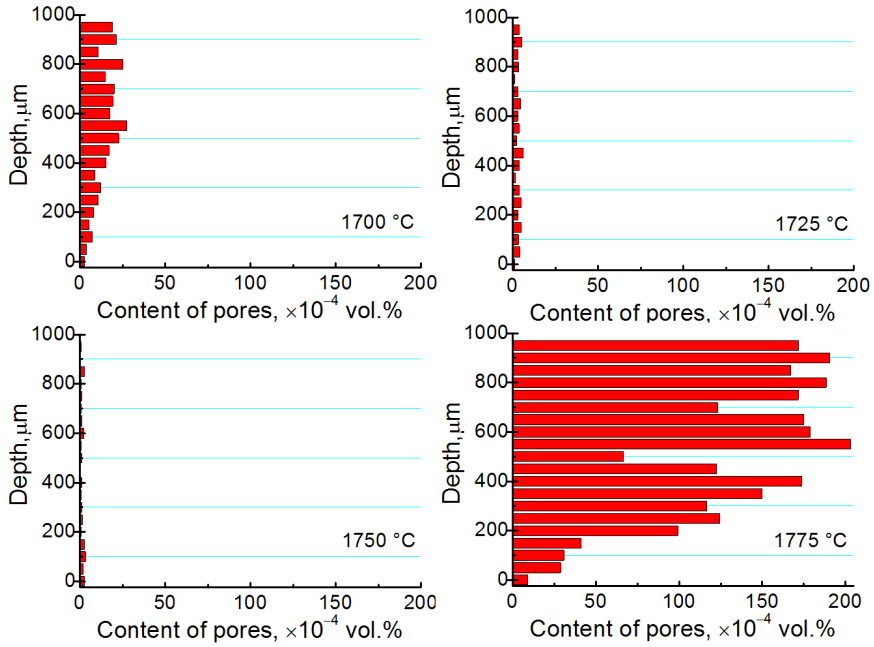

Fig. 4. Distributions of pores through the depth of the samples sintered at various temperatures

Fig. 5 presents the absorption spectrum of Tm,Ho:Y_2O_3 ceramic over the wavelength range of 300–2100 nm. The spectrum reveals six primary absorption peaks located around 362 nm, 477 nm, 684 nm, 797 nm, 1209 nm, and 1630 nm, which correspond to the transitions from the $^3H_6$ level of trivalent thulium ions to $^1D_2$, $^1G_4$, $^3F_{2,3}$, $^3H_4$, $^3H_5$, and $^3F_4$ levels, respectively. Further, seven additional absorption peaks appear near 360 nm, 385 nm, 420 nm, 460 nm,

485 nm, 540 nm, 640 nm, 1140 nm, and 1930 nm, associated with the transitions from the ground state $^5I_8$ of trivalent holmium ions. In addition, the inset of Fig. 5 shows the absorption cross-section spectrum of Tm,Ho:Y_2O_3 ceramic for the $^3H_6 \rightarrow {}^3H_4$ transition of Tm^{3+}. The peak absorption cross-section (σ_{abs}) reached 4.44×10^{-21} cm^2 at 797 nm, with a full width at half maximum (FWHM) of 7.2 nm, which is advantageous for pumping with AlGaAs laser diodes.

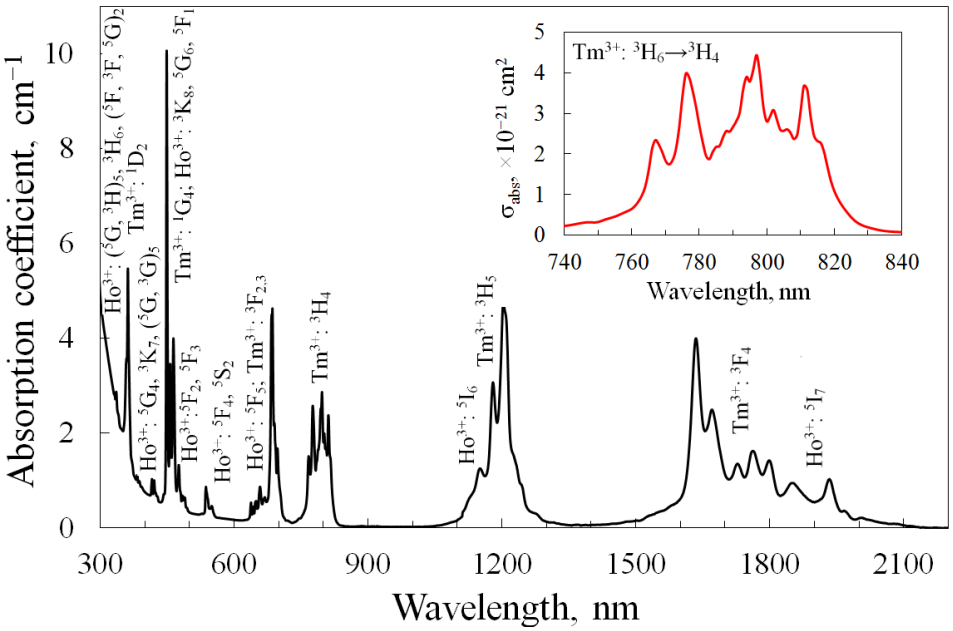

Fig. 5. Room temperature absorption spectrum of Tm,Ho:Y_2O_3 ceramic sintered at 1750 °C. The inset depicts the absorption cross-section spectrum for the $^3H_6 \rightarrow {}^3H_4$ transition of Tm^{3+}

Fig. 6 shows the luminescence spectrum of the obtained Tm,Ho:Y_2O_3 ceramic recorded in the 2-μm region under excitation to the $^3H_4$ level of Tm^{3+} ions at 811 nm. The observed spectrum is a combination of bands corresponding to the $^3F_4 \rightarrow {}^3H_6$ transition of Tm^{3+} (with peaks around 1950 nm) and the $^5I_7 \rightarrow {}^5I_8$ transition of Ho^{3+} ions (with peaks around 2050 nm), extending from 1750 nm to about 2100 nm. This broad spectral range of the emission is well-suited for tunable laser operation. Appearance of two luminescence bands indicates the presence of nonradiative energy transfer (ET) from the $^3F_4$ level of Tm^{3+} ions to the $^5I_7$ level of Ho^{3+} ions. In this case, the primary mechanism responsible for populating the $^3F_4$ energy level of Tm^{3+} ions in Tm,Ho:Y_2O_3 ceramic is the cross-relaxation (CR) process ($^3H_4 \rightarrow {}^3F_4$, $^3H_6 \rightarrow {}^3F_4$) of Tm^{3+} ions. The features of this process in Tm:Y_2O_3 ceramics were studied in detail in [20]. The scheme of the population of the $^5I_7$ level of Ho^{3+} ions considering CR of Tm^{3+} ions and nonradiative energy transfer from the $^3F_4$ level of Tm^{3+} ions to the $^5I_7$ level of Ho^{3+} ions in Tm,Ho:Y_2O_3 ceramics is shown in the inset of Fig. 6.

Conclusion

Transparent Tm,Ho-codoped Y_2O_3 ceramics were successfully fabricated through solid-state vacuum sintering of nano-sized particles with a complex chemical composition synthesized by the laser ablation method. The high sintering activity of the nanoparticles attributed to their small

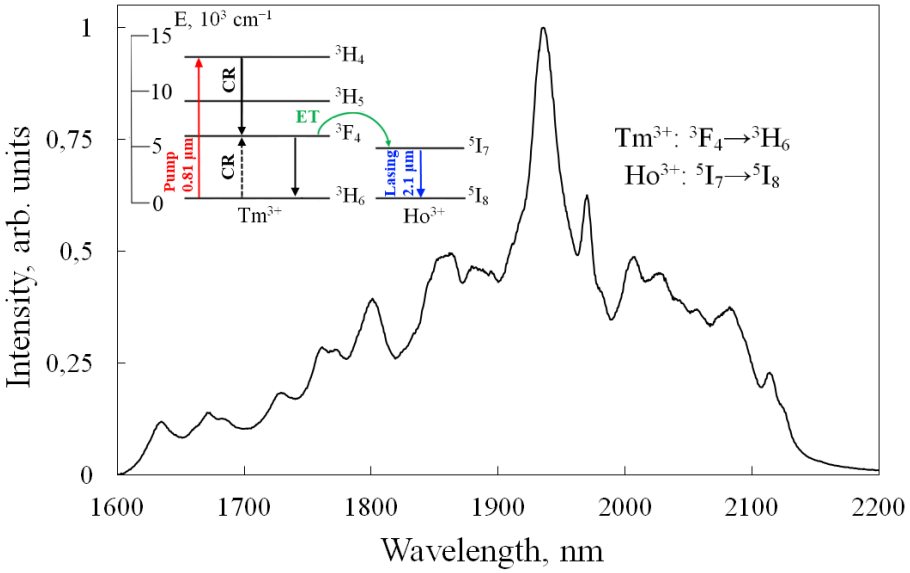

Fig. 6. Luminescence spectrum of Tm,Ho:Y_2O_3 ceramic sintered at 1750 °C under pumping at 811 nm and schematic diagram of population of Ho^{3+}: $^5I_7$ level

size and weak agglomeration, as confirmed by TEM observations, enabled full densification of the ceramics at temperatures approximately 700 °C lower than the melting point of Y_2O_3. The monoclinic phase present in the initial nanopowder was completely transformed into the stable cubic phase of Y_2O_3 after sintering.

The sintering temperature plays a critical role in determining the optical quality and porosity of Tm,Ho-codoped Y_2O_3 ceramics. At a sintering temperature of 1775 °C, the ceramics exhibited the lowest optical quality due to the formation of residual porosity and grain growth. In contrast, at slightly lower temperatures of 1725 °C and 1750 °C, the ceramics achieved the highest and almost identical optical qualities indicating that temperatures near this range are ideal for achieving high transparency and minimal porosity. These results suggest that precise control of the sintering temperature is essential to balance full densification and limit grain growth, which significantly impacts the overall optical performance of the ceramics.

Spectroscopic investigation have shown that non-radiative energy transfer between Tm^{3+} and Ho^{3+} ions in the obtained polycrystalline materials enables intense luminescence around 2.1 μm, specifically on the $^5I_7 \rightarrow {}^5I_8$ transition of Ho^{3+} ions. As a result, Tm,Ho:Y_2O_3 ceramics are promising gain media for compact 2-μm lasers capable of generating broadly tunable emission or ultra-short pulses under diode pumping of the $^3H_4$ level of Tm^{3+} ions at ~800 nm thanks to high absorption cross-section.

The reported study was carried out with the use of grant of the Russian Science Foundation no. 24-23-00460, https://rscf.ru/project/24-23-00460/

References

[1] I.Mingareev, F.Weirauch et al., Welding of polymers using a 2 μm thulium fiber laser, *Opt. Laser Technol.*, **44**(2012), no. 7, 2095–2099. DOI: 10.1016/j.optlastec.2012.03.020

[2] O.Traxer, E.X.Keller, Thulium fiber laser: the new player for kidney stone treatment? A comparison with Holmium:YAG laser, *World J. Urol.*, **38**(2020), no. 8, 1883–1894. DOI: 10.1007/s00345-019-02654-5

[3] F.Silva, S.M.Teichmann et al., Spatiotemporal isolation of attosecond soft X-ray pulses in the water window, *Nature Commun.*, **6**(2015), 6611. DOI: 10.1038/ncomms7611

[4] Z.Pan, P.Loiko et al., Disordered Tm^{3+},Ho^{3+}-codoped CNGG garnet crystal: Towards efficient laser materials for ultrashort pulse generation at ∼2 μm, *J. Alloys Compd.*, **853**(2021), 157100. DOI: 10.1016/j.jallcom.2020.157100

[5] L.Wang, W.Chen et al., Sub-50 fs pulse generation from a SESAM mode-locked Tm,Ho-codoped calcium aluminate laser, *Opt. Lett.*, **46**(2021), no. 11, 2642–2645. DOI: 10.1364/OL.426113

[6] Z.Pan, P.Loiko et al., Tm,Ho:Ca(Gd,Lu)AlO_4 crystals: Polarized spectroscopy and laser operation, *J. Lumin.*, **257**(2023), 119638. DOI: 10.1016/j.jlumin.2022.119638

[7] Z.Liu, A.Ikesue, J.Li, Research progress and prospects of rare-earth doped sesquioxide laser ceramics, *J. Eur. Ceram. Soc.*, **41**(2021), 3895–3910. DOI: 10.1016/j.jeurceramsoc.2021.02.026

[8] M.Zinkevich, Thermodynamics of rare earth sesquioxides, *Prog. Mater. Sci.*, **52**(2007), no. 4, 597–647. DOI: 10.1016/j.pmatsci.2006.09.002

[9] T.Sekine, T.Kurita et al., 253 J at 0.2 Hz, LD pumped cryogenic helium gas cooled Yb:YAG ceramics laser, *Opt. Express*, **30**(2022), no. 25, 44385–44394. DOI: 10.1364/OE.470815

[10] A.Ikesue, Y.L.Aung et al., Composite Laser Ceramics by Advanced Bonding Technology, *Materials*, **11**(2018), no. 2, 271. DOI: 10.3390/ma11020271

[11] R.N.Maksimov, V.A.Shitov et al., Hot isostatic pressing of transparent Yb^{3+}-doped Lu_2O_3 ceramics for laser applications, *Ceram. Int.*, **47**(2021), no. 4, 5168–5176. DOI: 10.1016/j.ceramint.2020.10.094

[12] V.V.Osipov, V.V.Platonov et al., Production of nanopowders of oxides by means of fiber and pulse-periodical CO_2 lasers, *Phys. Status Solidi C*, **10**(2013), no. 6, 926–932. DOI: 10.1002/pssc.201200965

[13] V.V.Osipov, V.V.Platonov et al., Study of nanoparticle production from yttrium oxide by pulse-periodic radiation of ytterbium fibre laser, *Appl. Phys. A*, **124**(2018), 3. DOI: 10.1007/s00339-017-1348-9

[14] D.A.Porter, K.E.Easterling, M.Y. Sherif, Phase transformation in metals and alloys, 3rd edn, Boca Raton, CRC Press, 2009.

[15] J.Paras, O.Takeda et al., The Surface Tension and Density of Molten Sc_2O_3, La_2O_3, Y_2O_3, Al_2O_3, and MgO Measured via a Pendant Droplet Method, *Metall. Mater.Trans. B*, **53**(2022), 2077–2087. DOI: 10.1007/s11663-022-02508-3

[16] S.Jiang, J.Liu et al., High-Pressure Phase Transitions of Cubic Y_2O_3 under High Pressures by In-situ Synchrotron X-Ray Diffraction, *Chin. Phys. Lett.*, **36**(2019), no. 4, 046103. DOI: 10.1088/0256-307X/36/4/046103

[17] X.Li, X.Xia et al., High-temperature high pressure synthesis of monoclinic Y_2O_3, *Mater. Lett.*, **239**(2019), 82–85. DOI: 10.1016/j.matlet.2018.12.068

[18] R.D.Shannon, Revised effective ionic radii and systematic studies of interatomic distances in halides and chalcogenides, *Acta Crystallogr. A*, **A32**(1976), 751–767. DOI: 10.1107/S0567739476001551

[19] A.A.Kaminskii, K.Ueda et al., Lasing and refractive indices of nanocrystalline ceramics of cubic yttrium oxide Y_2O_3 doped with Nd^{3+} and Yb^{3+} ions, *Crystallogr. Rep.*, **48**(2003), 1041–1043. DOI: 10.1134/1.1627445

[20] S.A.Artemov, V.V.Balashov et al., Nonradiative energy transfer of electronic excitation between Tm^{3+} ions in Y_2O_3:Tm laser ceramics, *Opt. Mater.*, **101**(2020), 109762. DOI: 10.1016/j.optmat.2020.109762

Синтез и спектроскопия прозрачных Y_2O_3 керамик, соактивированных Tm и Ho, для 2-мкм лазеров

Роман Н. Максимов
Владислав А. Шитов
Владимир В. Осипов
Альберт Н. Орлов
Институт электрофизики УрО РАН
Екатеринбург, Российская Федерация
Екатерина М. Бузаева
Полина А. Рябочкина
Александр О.Арискин
Национальный исследовательский Мордовский государственный университет им. Н. П. Огарёва
Саранск, Российская Федерация

Аннотация. В данной работе были получены прозрачные керамические материалы на основе оксида иттрия, соактивированного тулием и гольмием ($Tm,Ho:Y_2O_3$), посредством твердофазного вакуумного спекания наноразмерных частиц со сложным химическим составом, синтезированных методом лазерной абляции. Синтезированный порошок представлял собой мягкие агрегаты, состоящие из отдельных сферических частиц диаметром 16 нм, кристаллическая структура которых преобразовывалась из моноклинной (пространственная группа C2/m) в кубическую модификацию (пространственная группа Ia-3) в процессе спекания. Были изучены морфологические свойства и их корреляция с оптическим качеством керамик $Tm,Ho:Y_2O_3$, спечённых при температурах 1700–1775 °C. Образец, спечённый при 1750 °C, обладал более высокой прозрачностью (81.6% при $\lambda = 600$ нм и 83.0% при $\lambda = 1000$ нм) и наименьшим содержанием рассеивающих центров 0.00014 об.%. Сечение поглощения при 797 нм для перехода $^3H_6 \rightarrow {}^3H_4$ ионов Tm^{3+} составляло 4.44×10^{-21} см^2. Широкая полоса люминесценции, наблюдаемая в диапазоне от 1750 нм до 2100 нм, обусловлена комбинацией процессов кросс-релаксации ионов Tm^{3+} и безызлучательного переноса энергии с уровня $^3F_4$ (Tm^{3+}) на уровень $^5I_7$ (Ho^{3+}). Эти результаты указывают на перспективность использований прозрачных $Tm,Ho:Y_2O_3$ керамик в качестве активных сред для лазеров с широким диапазоном плавной перестройки и синхронизацией мод, генерирующих излучение в области 2 мкм.

Ключевые слова: нанопорошок, сесквиоксид иттрия, оптическая керамика, микроструктура, содопирование, безызлучательный перенос энергии.

EDN: HWLOOG
УДК 517.958

Inverse Problem for the Viscoelastic Equation with Additional Information of Special form

Jurabek Sh. Safarov*
Tashkent University of Information Technologies
Tashkent, Uzbekistan
Institute of Mathematics AS of the Republic of Uzbekistan
Tashkent, Uzbekistan

Received 12.12.2024, received in revised form 08.01.2025, accepted 24.03.2025

Abstract. The one-dimensional inverse problem of determining the kernel of the integral term of the integro-differential viscoelasticity equation with constant density and constant Lame coefficients is considered. Firstly, the direct problem is studied and equivalent integral equation for the desired function u(x,t) together with the necessary conditions for this problem are obtained. Secondly, the inverse problem of determining the kernel of the integral term is studied. Using the additional condition, the inverse problem is replaced by an equivalent system of integral equations for unknown functions. The contraction mapping principle is applied to the system of integral equations in the space of continuous functions with weighted norms. Theorem of global unique solvability of the inverse problem is proved.

Keywords: integro-differential equation, inverse problem, integral kernel, Banach theorem.

Citation: J.Sh. Safarov, Inverse Problem for the Viscoelastic Equation with Additional Information of Special form, J. Sib. Fed. Univ. Math. Phys., 2025, 18(4), 456–466.
EDN: HWLOOG.

1. Introduction and problem statement

Problems of mechanics and thermophysics lead to the study of inverse problems for integro-differential equations. Such problems arise in many areas of physics such as electrodynamics, acoustics, quantum scattering theory, geophysics, astronomy, etc.

Problems of propagation of elastic, electromagnetic waves in media where the state of the medium at a given moment in time depends on its state at all previous moments in time are described by integro-differential equations. Mathematically, convolution-type integrals describing the phenomenon of delay are added to the right-hand sides of the corresponding classical wave propagation equations.

One of the fields of science where integro-differential equations arise in the study of medium properties using seismic waves is geophysics. In fact, under the assumption of smoothness the system of equations for the inelastic Boltzmann model [1] (one of the most general for linear inelastic medium) reduces to equation

$$u_{tt}(x,t) = u_{xx}(x,t) + \lambda^{-1}(x)\lambda'(x)u_x(x,t) + \rho(x)\int_0^t h(t-\alpha)\left(u_{xx}(x,\alpha) + \lambda^{-1}(x)\lambda'(x)u_x(x,\alpha)\right)d\alpha.$$

*j.safarov65@mail.ru https://orcid.org/0000-0001-9249-835X

Functions $\lambda(x)$ and $\rho(x)$ in this equation are related to the Lame parameters and the density of the considered viscoelastic medium. Assuming that they are constant ($\lambda = \rho = 1$), this equation can be reduced to the form

$$u_{tt}(x,t) = w_x(x,t).$$

where $u(x,t)$ is the displacement function and w is the stress function that has the following form

$$w(x,t) = u_x(x,t) + \int_0^t h(t-\tau)u_x(x,\tau)d\tau.$$

This relation for a linear inelastic medium describes the relationship between stress and displacement of the medium. The study of inverse problems of determining the kernel of integral operators in these equations with the use of some information about the wave field plays an important role in the study of the structure and properties of the medium.

Various formulations of inverse problems for the viscoelasticity equation can be found [2–11]. In particular, one-dimensional problems of finding the kernel included in an integro-differential equation with the delta function in the right side or in the boundary condition were considered [2–7]. For the inverse problems formulated in these works existence and uniqueness theorems were proved on the basis of the principle of contraction mappings, and estimates of conditional stability were obtained.

For multidimensional inverse problems of finding the kernel in hyperbolic integro-differential equations of the second order unique solvability theorems were proven in the class of functions that are analytic in spatial variables and continuous in time [8–11]. Theorems on the global unique solvability of two-dimensional inverse problems were proved when the kernel of the integral term weakly depends on the horizontal variable [12–17].

The inverse problem of finding the one-dimensional convolution kernel of the integral term of the integro-differential viscoelastic equation is studied in this work on the basis of conditions constituting the initial-boundary (direct) problem and some additional condition.

Let us consider the initial boundary value problem for the string vibration equation with memory in domain $\Omega = \{(x,t) : x > 0, t \in R\}$:

$$u_{tt} - u_{xx} - \int_0^t m(\tau)u_{xx}(x,t-\tau)d\tau = 0, \qquad (x,t) \in \Omega. \tag{1}$$

Initial and boundary conditions are

$$u\,|_{t<0} \equiv 0, \tag{2}$$

$$u\,|_{x=0} = \delta(t), \qquad t \in R, \tag{3}$$

where $\delta(t)$ — is the Dirac delta function. To determine the unknown function $m(t), t > 0$, additional condition is specified in the following special form

$$u_x(0,t) + \int_0^t m(\tau)u_x(0,t-\tau)d\tau = f(t), \tag{4}$$

$f(t)$ — given function for $t > 0$.

Additional information in form (4) was used [18, 19] to determine the memory function of the medium included in the hyperbolic and parabolic equations. The direct problem was the

initial-boundary value problem for equations with distributed sources in bounded domains. A similar problem in a domain bounded in spatial variable was studied [20]. However, problems with concentrated sources localized in the vicinity of a fixed point or on the surface of the region under consideration are important in applications.

2. Study of the direct problem

Let us introduce new function $p(x,t)$ that is defined as

$$p(x,t) := \left[u(x,t) + \int_0^t m(t-\tau)u(x,\tau)d\tau\right] \exp\left(-m(0)t/2\right). \tag{5}$$

The following lemma holds.

Lemma 2.1. *Function $u(x,t)$ is expressed in terms of $p(x,t)$ as*

$$u(x,t) = \exp\left(m(0)t/2\right) p(x,t) + \int_0^t h(t-\tau) \exp\left(m(0)\tau/2\right) p(x,\tau)d\tau, \tag{6}$$

where h is the solution of the Volterra integral equation

$$h(t) = -m(t) - \int_0^t m(t-\tau)h(\tau)\, d\tau, \qquad t > 0. \tag{7}$$

Proof. It follows from 1) that

$$u(x,t) = \exp\left(m(0)t/2\right) p(x,t) - \int_0^t m(\tau)u(x,t-\tau)d\tau = \exp\left(m(0)t/2\right) p(x,t) - I(x,t), \tag{8}$$

where the following designation is introduced

$$I(x,t) = \int_0^t m(\tau)u(x,t-\tau)d\tau.$$

Expressing $m(t)$ from (7) and substituting it into integral $I(x,t)$, one can obtain

$$I(x,t) = \int_0^t m(\tau)u(x,t-\tau)d\tau = -\int_0^t r(\tau)u(x,t-\tau)d\tau - \int_0^t \int_0^\tau m(\tau-\alpha)h(\alpha)u(x,t-\tau)d\alpha d\tau.$$

Changing the order of integration in the second integral, one can obtain

$$I(x,t) = -\int_0^t h(\tau)u(x,t-\tau)d\tau - \int_0^t h(\alpha)\left[\int_\alpha^t m(\tau-\alpha)u(x,t-\tau)d\tau\right] d\alpha.$$

If the roles of the integration variables α and τ is reversed, i.e., $\alpha =: \tau$, $\tau =: \alpha$ in the second integral then I has the form

$$I(x,t) = -\int_0^t h(\tau)u(x,t-\tau)d\tau - \int_0^t h(\tau)\left[\int_\tau^t m(\alpha-\tau)u(x,t-\alpha)d\alpha\right] d\tau.$$

From here

$$I(x,t) = -\int_0^t h(\tau)\left[u(x,t-\tau) + \int_\tau^t m(\alpha-\tau)u(x,t-\alpha)d\alpha\right] d\tau.$$

In the inner integral variable α is replaced with ξ by the formula $\alpha - \tau = \xi$. Then

$$I(x,t) = -\int_0^t h(\tau)\left[u(x,t-\tau) + \int_0^{t-\tau} m(\xi)u(x,t-\tau-\xi)d\xi\right]d\tau.$$

From here, according to formula (1)

$$I(x,t) = -\int_0^t h(\tau)\exp\left(m(0)(t-\tau)/2\right)p(x,t-\tau)d\tau = -\int_0^t h(t-\tau)\exp\left(m(0)\tau/2\right)p(x,\tau)d\tau$$

If found $I(x,t)$ is substituted into equation (8), equality (6) is obtained. □

The following problem for function $p(x,t)$ is obtained from problems (1)–(2)

$$p_{tt} - p_{xx} + h_0 p + \int_0^t H(t-\tau)p(x,\tau)d\tau = 0, \tag{9}$$

$$p\mid_{x=0} = \delta(t) + m(t)\exp\left(h(0)t/2\right)\theta(t), \quad p\mid_{t<0} \equiv 0. \tag{10}$$

Additional condition (3) takes the form

$$p_x(0,t) = f(t)\exp\left(h(0)t/2\right),$$

where the following notations are introduced

$$\begin{aligned} H(t) &= h''(t)\exp\left(h(0)t/2\right), \\ h_0 &= h'(0) - \frac{h^2(0)}{4}. \end{aligned} \tag{11}$$

Suppose that function $f(t)$ has the form

$$f(t) = -\delta'(t) - \frac{h(0)}{2}\delta(t) + \theta(t)f_0(t), \tag{12}$$

where $f_0(t)$ is a regular function.

Let us represent function $p(x,t)$ as $p(x,t) = \delta(t-x) + \theta(t-x)\overline{p}(x,t)$, where $\overline{p}(x,t)$ is a regular function. Using the method of singularity extraction, one can obtain the following equality for the regular part of the solution of the direct problem in the region $t \geqslant x \geqslant 0$ ($p(x,t) = \overline{p}(x,t)$ for $t \geqslant x$)

$$p_{tt} - p_{xx} + h_0 p + H(t-x) + \int_0^{t-x} H(\tau)p(x,t-\tau)d\tau = 0, \tag{13}$$

$$p\big|_{t=x+0} = -h(0) - \frac{h_0}{2}x, \tag{14}$$

$$p(0,t) = m(t)\exp\left(\frac{h(0)t}{2}\right). \tag{15}$$

Taking into account (12), the additional condition for function $p(x,t)$ takes the following form

$$p_x(0,t) = f_0(t)\exp\left(\frac{h(0)t}{2}\right). \tag{16}$$

Equations (13), (15), (16) represent the Cauchy problem for the equation of string vibration with data on the axis $x = 0$. Using Dalember's formula, integral equation for $p(x,t)$ is obtained

$$p(x,t) = \frac{1}{2}\left[\widetilde{m}(t+x) + \widetilde{m}(t-x)\right] + \frac{1}{2}\int_{t-x}^{t+x} \widetilde{f}_0(\tau)d\tau + \\ + \frac{1}{2}\int_0^x \int_{t-x+\xi}^{t+x-\xi} + \left[h_0 p(\xi,\tau) - H(\tau-\xi) + \int_0^{\tau-\xi} H(\alpha)p(\xi,\tau-\alpha)d\alpha\right]d\tau d\xi, t \geqslant x \tag{17}$$

where the following notations are introduced $\widetilde{m}(t) = m(t)\exp\left(h(0)t/2\right)$, $\widetilde{f}_0(t) = f_0(t)\exp\left(h(0)t/2\right)$.

In domain $D = \{(x,t) : 0 \leqslant x \leqslant t \leqslant T - x\}$ equation (17) is a Volterra equation of the second kind. Therefore, the solution of this equation is unique in the class of functions belonging to the space $C(D)$, and it can be obtained by the method of successive approximations. The existence of a solution in this class follows from the fact that $m(t)$ belongs to the class $C^2[0,T]$. Moreover, direct differentiation of equation (17) shows that solution of this equation belongs to the class $C^2(D)$.

3. Reducing the problem to an equivalent system of integral equations

Let us set $t = x + 0$ in equation (17). Taking into account equality (14), one can find that

$$-h(0) - \frac{h_0}{2}x = \frac{1}{2}\left[\widetilde{m}(2x) + \widetilde{m}(0)\right] + \frac{1}{2}\int_0^{2x} \widetilde{f}_0(\tau)d\tau +$$

$$+\frac{1}{2}\int_0^x \int_\xi^{2x-\xi} \left[h_0 p(\xi,\tau) - H(\tau-\xi) + \int_0^{\tau-\xi} H(\alpha)p(\xi,\tau-\alpha)d\alpha\right]d\tau d\xi.$$

Differentiating the last equality with respect to $t(t = 2x)$, the following equation is obtained

$$-\frac{h_0}{4} = \frac{1}{2}\widetilde{m}'(t) + \frac{1}{2}\widetilde{f}_0(t) +$$

$$+\frac{1}{2}\int_0^{\frac{t}{2}} \left[h_0 p(\xi,t-\xi) + \int_0^{t-2\xi} H(\alpha)p(\xi,t-\xi-\alpha)d\alpha\right]d\xi - \frac{1}{2}\int_0^{\frac{t}{2}} H(t-2\xi)d\xi. \tag{18}$$

In the last integral the change of variables $\eta := t - 2\xi$ is made. After this, once again differentiating the last equality, integral equation for function $H(t) is obtained$:

$$H(t) = 2\widetilde{m}''(t) + 2\widetilde{f}_0'(t) - h_0\left(h(0) + \frac{h_0}{4}t\right) + 2\int_0^{\frac{t}{2}} \left[h_0 p_t(\xi,t-\xi) - \right. \\ \left. - \left(h(0) + \frac{h_0}{2}\xi\right)H(t-2\xi) + \int_0^{t-2\xi} H(\alpha)p_t(\xi,t-\xi-\alpha)d\alpha\right]d\xi. \tag{19}$$

The integral equation for function $p_t(x,t)$ is obtained by directly differentiating equation (17) with respect to variable t:

$$\begin{aligned} p_t(x,t) =& \frac{1}{2}\left[\widetilde{m}'(t+x)+\widetilde{m}'(t-x)\right]+\frac{1}{2}\left[\widetilde{f}_0(t+x)-\widetilde{f}_0(t-x)\right]+\frac{x}{2}H(t-x)+ \\ &+\frac{1}{2}\int_0^x \left[h_0\big(p(\xi,t+x-\xi)-p(\xi,t-x+\xi)\big)-H(t+x-2\xi)\right]d\xi+ \\ &+\frac{1}{2}\int_0^x\int_0^{t+x-2\xi} H(\alpha)p(\xi,t+x-\xi-\alpha)d\alpha d\xi-\frac{1}{2}\int_0^x\int_0^{t-x} H(\alpha)p(\xi,t-x+\xi-\alpha)d\alpha d\xi. \end{aligned} \tag{20}$$

Equations (17), (19)–(20) contain unknown functions $\widetilde{m}(t)$, $\widetilde{m}'(t)$, $\widetilde{m}''(t)$. Therefore, to close the system of integral equations (17), (19)–(20), the following obvious equalities are used

$$\widetilde{m}(t) = -h(0)+\left(\frac{h^2(0)}{2}-h'(0)\right)t+\int_0^t (t-\tau)\widetilde{m}''(\tau)d\tau, \tag{21}$$

$$\widetilde{m}'(t) = \frac{h^2(0)}{2}-h'(0)+\int_0^t \widetilde{m}''(\tau)d\tau, \tag{22}$$

$$\widetilde{m}''(t) = -H(t)+\left(\frac{h^2(0)}{4}-h'(0)\right)\widetilde{m}(t)-\int_0^t H(t-\tau)\widetilde{m}(\tau)d\tau. \tag{23}$$

Remark. The equations of system (17), (19)–(23) involve unknown numbers $h(0)$ and $h'(0)$. To determine them one can proceed as follows. First, differentiating equation (7), $m'(0)$ is expressed in terms of $h(0)$ and $h'(0)$:

$$m'(0) = -h'(0)+h^2(0). \tag{24}$$

Further, assuming $t=0$ and taking into account (11) and (24), one can obtain from equalities (14) and (16) that

$$-7h^2(0)-4h'(0) = -8f_0(0).$$

So there is one equation for unknown numbers. To obtain the second equation let us set $t=0$ in equation (18). After simplifications the equation

$$-3h^2(0)-4h'(0) = -8\widetilde{f}_0(0)$$

is obtained. By solving this system of equations, the unknown numbers are found:

$$h(0)=0, \quad h'(0)=2\widetilde{f}_0(0)=2f_0(0).$$

In addition, it follows from (11) that $h_0=h'(0)=2f_0(0)$. In further studies, these numbers will be replaced with the found values.

4. Theorem on the solvability of the inverse problem

The main result of this work is the following theorem on the global unique solvability of the inverse problem.

Theorem 4.1. *Let function $f(t)$ be of form (12) and $f_0(t)\in C^1[0,T]$, $T>0$. Then there exists a single solution to inverse problem (1)–(4), $m(t)\in C^2[0,T]$ for any $T>0$.*

Proof. Let us represent the system of equations (17), (19)–(23) as an operator equation

$$\varphi = A\varphi, \tag{25}$$

where φ is a vector function with components φ_i, $i = \overline{1,6}$

$$\varphi = [\varphi_1(x,t), \varphi_2(x,t), \varphi_3(x,t), \varphi_4(t), \varphi_5(t), \varphi_6(t)] =$$
$$= \Bigg[v(x,t) - \frac{1}{2}\left[\widetilde{m}(t+x) + \widetilde{m}(t-x)\right], v_t(x,t) - \frac{1}{2}\left[\widetilde{m}'(t+x) + \widetilde{m}'(t-x)\right] - \frac{x}{2}H(t-x),$$
$$H(t) - 2\widetilde{m}''(t), \widetilde{m}(t), \widetilde{m}'(t), \widetilde{m}''(t) + H(t) - 2f_0(0)\widetilde{m}(t)\Bigg],$$

and operator A is defined on the set of functions $\varphi \in C[D]$ and according to equations (17), (19)–(23) has the form $A = (A_1, A_2, A_3, A_4, A_5, A_6)$:

$$A_1\varphi = \varphi_{01} + \frac{1}{2}\int_0^x \int_{t-x+\xi}^{t+x-\xi} \Bigg[2f_0(0)\left(\varphi_1(\xi,\tau) + \frac{1}{2}(\varphi_4(\tau-\xi) + \varphi_4(\tau+\xi)\right) -$$
$$-\frac{1}{3}\Big(2\varphi_6(\tau-\xi) + \varphi_3(\tau-\xi) - 2f_0(0)\varphi_4(\tau-\xi)\Big) + \frac{1}{3}\int_0^{\tau-\xi}\big(2\varphi_6(\alpha) + \varphi_3(\alpha) - h_0\varphi_4(\alpha)\big)\times$$
$$\times\left(\varphi_1(\xi,\tau-\alpha) + \frac{1}{2}(\varphi_4(\tau-\alpha-\xi) + \varphi_4(\tau-\alpha+\xi)\right)d\alpha\Bigg]d\tau d\xi,$$

$$A_2\varphi = \varphi_{02} + \frac{1}{2}\int_0^x \Big[2f_0(0)\Big(\varphi_1(\xi,t+x-\xi) - \varphi_1(\xi,t-x+\xi) - \frac{1}{2}\big(\varphi_4(t+x)+$$
$$+\frac{1}{3}\varphi_4(t+x-2\xi) + \varphi_4(t-x) + \varphi_4(t-x+2\xi)\Big) - \frac{1}{3}\big(2\varphi_6(t+x-2\xi) + \varphi_3(t+x-2\xi)\big)\Big]d\xi -$$
$$+\frac{1}{6}\int_0^x\int_0^{t+x-2\xi}\Big(2\varphi_6(\alpha) + \varphi_3(\alpha) - 2f_0(0)\varphi_4(\alpha)\Big)\times$$
$$\times\left(\varphi_1(\xi,t+x-\xi-\alpha) + \frac{1}{2}(\varphi_4(t-x-\alpha) + \varphi_4(t+x-2\xi-\alpha)\right)d\alpha d\xi -$$
$$-\frac{1}{6}\int_0^x\int_0^{t-x}\Big(2\varphi_6(\alpha) + \varphi_3(\alpha) - 2f_0(0)\varphi_4(\alpha)\Big)\times \tag{26}$$
$$\times\left(\varphi_1(\xi,t+x-\xi-\alpha) + \frac{1}{2}(\varphi_4(t-x-\alpha) + \varphi_4(t+x-2\xi-\alpha)\right)d\alpha d\xi,$$

$$A_3\varphi = \varphi_{03} + 2\int_0^{\frac{t}{2}}\Big[2f_0(0)\Big(\varphi_2(\xi,t-\xi) + \frac{1}{2}\left(\varphi_5(t-2\xi) + \varphi_5(t)\right) +$$
$$+\frac{\xi}{3}\big(2\varphi_6(t-2\xi) + \varphi_3(t-2\xi) - 2f_0(0)\varphi_4(t-2\xi)\big)\Big) +$$
$$+\Big(\varphi_2(\xi,t-\xi-\alpha) + \frac{1}{2}\left(\varphi_5(t-2\xi-\alpha) + \varphi_5(t-\alpha)\right) +$$
$$+\frac{\xi}{6}\big(2\varphi_6(t-2\xi-\alpha) + \varphi_3(t-2\xi-\alpha) - 2f_0(0)\varphi_4(t-2\xi-\alpha)\big)\Big)d\alpha\Big]d\xi.$$

$$A_4\varphi = \varphi_{04} + \frac{1}{3}\int_0^t (t-\tau)[\varphi_6(\tau) - \varphi_3(\tau) - 2f_0(0)\varphi_4(\tau)]d\tau,$$

$$A_5\varphi = \varphi_{05} + \frac{1}{3}\int_0^t [\varphi_6(\tau) - \varphi_3(\tau) - 2f_0(0)\varphi_4(\tau)]d\tau,$$

$$A_6\varphi = \varphi_{06} - \frac{1}{3}\int_0^t [\varphi_6(t-\tau) - \varphi_3(t-\tau) - 2f_0(0)\varphi_4(t-\tau)]\varphi_4(\tau)d\tau,$$

where the following notation is introduced

$$\varphi_0(x,t) = (\varphi_{01}, \varphi_{02}, \varphi_{03}, \varphi_{04}, \varphi_{05}, \varphi_{06}, \varphi_{07}) :=$$

$$\left[\frac{1}{2}\int_{t-x}^{t+x} \widetilde{f}_0(\tau)d\tau,\ \frac{1}{2}\left[\widetilde{f}_0(t+x) - \widetilde{f}_0(t-x)\right],\ 2\widetilde{f}_0'(t) - \frac{h_0^2}{4}t, -2f_0(0)t,\ -2f_0(0),\ 0\right].$$

Let C_σ be the Banach space of continuous functions generated by a family of weight norms

$$||\varphi||_\sigma = \max\{\sup_{(x,t)\in D} |\varphi_i(x,t)e^{-\sigma(t+(1+\theta)x)}|, i = \overline{1,2}, \sup_{t\in[0,T]} |\varphi_j(t)e^{-\sigma t}|, j = \overline{3,6}\},$$

where $\sigma \geqslant 0,\ \ 0 < \theta < 1$.

For $\sigma = 0$ this space coincides with the space of continuous functions with the usual norm. This norm is denoted hereafter as $\|\varphi\|$. It follows from the inequality $e^{-\sigma t}\|\varphi\| \leqslant \|\varphi\|_\sigma \leqslant \|\varphi\|$ that norms $\|\varphi\|_\sigma$ and $\|\varphi\|$ are equivalent for any fixed $T \in (0,\infty)$. The number σ will be chosen later. Let $Q_\sigma(\varphi_0, \|\varphi_0\|) =: \{\varphi | \|\varphi - \varphi_0\| \leqslant \|\varphi_0\|\}$ be a ball of radius $\|\varphi_0\|$ with centre at the point φ_0 of some weighted space $C_\sigma(\sigma \geqslant 0)$ in which $\|\varphi_0\| = \max(\|\varphi_{01}\|, \|\varphi_{02}\|, \|\varphi_{03}\|, \|\varphi_{04}\|, \|\varphi_{05}\|, \|\varphi_{06}\|\|)$.

It is easy to see that for $Q_\sigma(\varphi_0, \|\varphi_0\|)$ the estimate

$$\|\varphi\|_\sigma \leqslant \|\varphi_0\|_\sigma + \|\varphi_0\| \leqslant 2\|\varphi_0\|$$

is true. Let $\varphi(x,t) \in Q_\sigma(\varphi_0, \|\varphi_0\|)$. Let us show that with a suitable choice of $\sigma > 0$ operator A takes a ball to a ball, i.e., $A\varphi \in Q_\sigma(\varphi_0, \|\varphi_0\|)$. In fact, using equalities (26) and constructing the norm of differences, one can find for $(x,t) \in D_2$ that

$$\|A_1\varphi - \varphi_{01}\| = \sup_{(x,t)\in D} |(A_1\varphi - \varphi_{01})e^{-\sigma(t+(1+\theta)x)}| =$$

$$= \sup_{(x,t)\in D}\left|\frac{1}{2}\int_0^x \int_{t-x+\xi}^{t+x-\xi}\left[2f_0(0)\Big(\varphi_1(\xi,\tau)e^{-\sigma(\tau+(1+\theta)\xi)}e^{-\sigma(t-\tau+(1+\theta)(x-\xi))} + \right.\right.$$

$$+\frac{1}{2}\big(\varphi_4(\tau-\xi)e^{-\sigma(\tau-\xi)}e^{-\sigma(t-\tau+\xi)} + \varphi_4(\tau+\xi)e^{-\sigma(\tau+\xi)}e^{-\sigma(t-\tau-\xi)}\big)\Big) -$$

$$-\frac{1}{3}\Big(2\varphi_6(\tau-\xi) + \varphi_3(\tau-\xi) - 2f_0(0)\varphi_4(\tau-\xi)\Big)e^{-\sigma(\tau-\xi)}e^{-\sigma(t-\tau+\xi)} +$$

$$-\frac{1}{3}\int_0^{\tau-\xi}\big(2\varphi_6(\alpha) + \varphi_3(\alpha) - h_0\varphi_4(\alpha)\big)e^{-\sigma\alpha}\times$$

$$\times\Big(\varphi_1(\xi,\tau-\alpha)e^{-\sigma(\tau-\alpha+(1+\theta)\xi)}e^{-\sigma(t-\tau+(1+\theta)(x-\xi)-\alpha)} + \frac{1}{2}\big(\varphi_4(\tau-\alpha-\xi)e^{-\sigma(\tau-\alpha-\xi)}e^{-\sigma(t-\tau+\xi)} +$$

$$\left.\left.+\varphi_4(\tau-\alpha+\xi)e^{-\sigma(\tau-\alpha+\xi)}e^{-\sigma(t-\tau-\xi)}\big)\Big)d\alpha\right]d\tau d\xi\right| \leqslant$$

$$\leqslant \frac{\|\varphi_0\|}{\sigma}T\left[\left(\frac{7h_0}{3}+1\right) + 8h_1\|\varphi_0\|T\right] =: \frac{\|\varphi_0\|}{\sigma}\alpha_1,$$

$$\|A_2\varphi - \varphi_{02}\| = \sup_{(x,t)\in D} |(A_2\varphi - \varphi_{02})e^{-\sigma(t+(1+\theta)x)}| \leqslant \frac{\|\varphi_0\|}{\sigma}\left[\frac{11h_0}{3} + 2(3+2f_0(0)))\|\varphi_0\|T\right] =: \frac{1}{\sigma}\alpha_2,$$

$$\|A_3\varphi - \varphi_{03}\| = \sup_{t\in[0;T]} |(A_3\varphi - \varphi_{03})e^{-\sigma t}| \leqslant$$

$$\leqslant \frac{2\|\varphi_0\|}{\sigma}\left[7f_0(0)+h_1T\big(1+2f_0(0)+(4+Th_1)\|\varphi_0\|\big)\right] =: \frac{1}{\sigma}\alpha_3,$$

$$\|A_4\varphi-\varphi_{04}\| = \sup_{t\in[0;T]}|(A_4\varphi-\varphi_{04})e^{-\sigma t}| \leqslant \frac{2\|\varphi_0\|}{\sigma}\frac{(2+2f_0(0))}{3}T =: \frac{\|\varphi_0\|}{\sigma}\alpha_4,$$

$$\|A_5\varphi-\varphi_{05}\| = \sup_{t\in[0;T]}|(A_5\varphi-\varphi_{05})e^{-\sigma t}| \leqslant \frac{2\|\varphi_0\|}{\sigma}\frac{(2+2f_0(0))}{3} =: \frac{\|\varphi_0\|}{\sigma}\alpha_5,$$

$$\|A_6\varphi-\varphi_{06}\| = \sup_{(t\in[0;T]}|(A_6\varphi-\varphi_{06})e^{-\sigma t}| \leqslant$$

$$\frac{2\|\varphi_0\|}{\sigma}\left[2f_0(0)T+\frac{2}{3}\|\varphi_0\|(2+2f_0(0))T^2\right]\frac{(2+2f_0(0))}{3} =: \frac{\|\varphi_0\|}{\sigma}\alpha_6.$$

where $h_1 := 1+\dfrac{2f_0(0)}{3}$. The last inequality is obtained using the fourth and sixth equations of system (26).

Choosing $\sigma \geqslant \alpha_0 = \max(\alpha_1,\alpha_2,\alpha_3,\alpha_4,\alpha_5,\alpha_6)$, one can obtain that A takes ball $Q_\sigma(\varphi_0,\|\varphi_0\|)$ to ball $Q_\sigma(\varphi_0,\|\varphi_0\|)$.

Let now assume that φ^1,φ^2 are any two elements from $Q_\sigma(\varphi_0,\|\varphi_0\|)$. Then, using auxiliary inequalities of the form

$$|\varphi_i^1\varphi_j^1-\varphi_i^2\varphi_j^2|e^{-\sigma t} \leqslant |\varphi_i^1||\varphi_j^1-\varphi_j^2|e^{-\sigma t}+|\varphi_j^2||\varphi_i^1-\varphi_i^2|e^{-\sigma t} \leqslant 4\|\varphi_0\|\|\varphi^1-\varphi^2\|_\sigma,$$

one can find for $(x,t)\in D$, that

$$\|(A\varphi^1-A\varphi^2)_1\|_\sigma = \sup_{(x,t)\in D}|(A\varphi^1-A\varphi^2)_1e^{-\sigma(t+(1+\theta)x)}| \leqslant$$

$$\leqslant\frac{\|\varphi^1-\varphi^2\|_\sigma}{\sigma}T\left[\left(\frac{7f_0(0)}{3}+\frac{1}{2}\right)+8h_1\|\varphi_0\|T\right] =: \frac{\|\varphi^1-\varphi^2\|_\sigma}{\sigma}\beta_1,$$

$$\|(A\varphi^1-A\varphi^2)_2\|_\sigma = \sup_{(x,t)\in D}|(A\varphi^1-A\varphi^2)_1e^{-\sigma(t+(1+\theta)x)}| \leqslant$$

$$\leqslant\frac{\|\varphi^1-\varphi^2\|_\sigma}{\sigma}\left[\frac{11f_0(0)}{3}+2(3+2f_0(0)))\|\varphi_0\|T\right]=: \frac{\|\varphi^1-\varphi^2\|_\sigma}{\sigma}\beta_2,$$

$$\|(A\varphi^1-A\varphi^2)_3\|_\sigma = \sup_{t\in[0;T]}|(A\varphi^1-A\varphi^2)_1e^{-\sigma t}| \leqslant$$

$$\leqslant \frac{\|\varphi^1-\varphi^2\|_\sigma}{\sigma}\left[7f_0(0)+\frac{1}{2}h_1T\big(1+2f_0(0)+2(4+Th_1)\|\varphi_0\|\big)\right] := \frac{\|\varphi^1-\varphi^2\|_\sigma}{\sigma}\beta_3,$$

$$\|(A\varphi^1-A\varphi^2)_4\|_\sigma = \sup_{t\in[0;T]}|(A\varphi^1-A\varphi^2)_1e^{-\sigma t}| \leqslant \frac{\|\varphi^1-\varphi^2\|_\sigma}{\sigma}\frac{(2+2f_0(0))}{3}T := \frac{\|\varphi^1-\varphi^2\|_\sigma}{\sigma}\beta_4,$$

$$\|(A\varphi^1-A\varphi^2)_5\|_\sigma = \sup_{t\in[0;T]}|(A\varphi^1-A\varphi^2)_1e^{-\sigma t}| \leqslant \frac{\|\varphi^1-\varphi^2\|_\sigma}{\sigma}\frac{(2+2f_0(0))}{3} := \frac{\|\varphi^1-\varphi^2\|_\sigma}{\sigma}\beta_5,$$

$$\|(A\varphi^1-A\varphi^2)_6\|_\sigma = \sup_{t\in[0;T]}|(A\varphi^1-A\varphi^2)_1e^{-\sigma t}| \leqslant$$

$$\leqslant \frac{\|\varphi^1-\varphi^2\|_\sigma}{\sigma}\left[(2f_0(0)T+\frac{4}{3}\|\varphi_0\|(2+2f_0(0))T^2\right]\frac{(2+2f_0(0))}{3} := \frac{\|\varphi^1-\varphi^2\|_\sigma}{\sigma}\beta_6,$$

Let us introduce $\beta_0 := \max\limits_{1\leqslant i\leqslant 6}\beta_i$.

It follows from the obtained estimates that if number σ is chosen from the condition $\sigma > \max(\alpha_0, \beta_0)$ then operator A is contractive on $Q_\sigma(\varphi_0, \|\varphi_0\|)$. Then, according to Banach's Theorem [21], there is unique solution of equation (25) in $Q_\sigma(\varphi_0, \|\varphi_0\|)$ for any fixed $T > 0$.

Since $h(0) = 0$ then $m(t) = \widetilde{m}(t)$.

The theorem is proved. □

References

[1] A.S.Alekseev, V.I.Dobrinsky, Some issues of practical use of inverse dynamic seismic problems, Mat. problems of geophysics, Novosibirsk: Computing Center SB AN USSR, Iss. 6, part 2, 1975,7–53 (in Russian).

[2] A.Lorenzi, E.Sinestrari, Stability results for a partial integrodifferential inverse problem, *Pitman Research Notes Math.,* **190**(1989), 271–294.

[3] A.Lorenzi, E.Paparoni, Direct and inverse problems in the theory of materials with memory, *Ren. Sem. Math. Univ*, (1992), no. 87, 105–138.

[4] A.Lorenzi, An identification problem related to a nonlinear hyperbolic integro–differential equation, *Nonlinear Nonlinear Analysis: Theory, Methods & Applications,* **22**(1994), no. 1, 21–44.

[5] J.Sh.Safarov, D.K.Durdiev, Inverse problem for the integro-differential equation of acoustics, *Differ. equat.*, **54**(2018), no. 1, 136–144. DOI: 10.1134/S0374064118010119

[6] J.Sh.Safarov, Global solvability of the one-dimensional inverse problem for the integro-differential equation of acoustics, *J. Sib. Fed. Univ. Math Phys.*, **11**(2018), no. 6, 753–763. DOI: 10.17516/1997-1397-2018-11-6-753-763

[7] V.G.Romanov, On the determination of the coefficients in the viscoelasticity equations, *Siberian Math. J.*, **55**(2014), no. 3, 503–510.

[8] D.K.Durdiev, J.Sh.Safarov, Inverse Problem for an Integro-differential Equation of the Hyperbolic Type protect in a Rectangular Domain, *Math. Notes*, **114**(2023), no. 2, 199–211. DOI: 10.1134/S0001434623070210

[9] A.A.Rahmonov, U.D.Durdiev, Z.R.Bozorov, Problem of determining the speed of sound and the memory of an anisotropic medium, *Theoretical and Mathematical Physics*, **207**(2021), no. 1, 494–513.

[10] D.Guidetti, Reconstruction of a convolution kernel in a parabolic problem with a memory term in the boundary conditions, *Bruno Pini Mathematical Analysis Seminar*, **4**2013, no. 1, 47–55. DOI: 10.6092/issn.2240-2829/4154

[11] C.Cavaterra, D.Guidetti, Identification of a convolution kernel in a control problem for the heat equation with a boundary memory term, *Annali di Matematica*, **193**(2014), 779–816. DOI: 10.1007/s10231-012-0301-y

[12] J.Janno, L.Von Wolfersdorf, Inverse problems for identification of memory kernels in viscoelasticity, *Mathematical methods in the applied sciences*, **20**(1997), no. 4, 291–314.

[13] D.K.Durdiev, A.A.Rakhmonov, The Problem of Determining the 2D Kernel in a System of Integro-Differential Equations of a Viscoelastic Porous Medium, *J. Appl. Ind. Math.*, **14**(2020), 281–295. DOI: 10.1134/S1990478920020076

[14] D.K.Durdiev, Z.Z.Nuriddinov, Determination of a multidimensional kernel in some parabolic integro–differential equation, *J. Sib. Fed. Univ. Math Phys.*, **14**(2021), no. 1, 117–127. DOI: 10.17516/1997-1397-2021-14-1-117-127

[15] J.Sh.Safarov, Two-dimensional Inverse Problem for an Integro-differential Equation of Hyperbolic Type, *J. Sib. Fed. Univ. Math Phys.*, **15**(2022), no. 5, 651–662. DOI: 10.17516/1997-1397-2022-15-5-651-662

[16] D.K.Durdiev, J.S.Safarov, Problem of Determining the Two-Dimensional Kernel of the Viscoelasticity Equation with a Weakly Horizontal Inhomogeneity, *J. Appl. Ind. Math.*, **16**(2022), 22–44. DOI: 10.1134/S1990478922010033

[17] D.K.Durdiev, J.Sh.Safarov, The problem of determining the memory of an environment with weak horizontal heterogeneity, *Vestn. Udmurtsk. Univ. Mat. Mekh. Komp. Nauki*, **32**(2022), no. 3, 383–402. DOI: 10.35634/vm220303

[18] D.K.Durdiev, Z.D.Totieva, About Global Solvability of a Multidimensional Inverse Problem for an Equation with Memory, *Sib. Math. J.*, **62**(2021), 215–229.

[19] J.Janno, L.Von Wolfersdorf, Inverse problems for identification of memory kernels in heat flow, *J. Inv. Ill-Posed Problems*, **4**(1996), no. 1, 39–66.

[20] J.Sh.Safarov, Inverse problem for an integro-differential equation of hyperbolic type with additional information of a special form in a bounded domain, *J. Samara State Tech. Univ., Ser. Phys. Math. Sci.*, **28**(2024), no. 1, 29–44. DOI: 10.14498/vsgtu1997

[21] A.N.Kolmogorov, S.V.Fomin, Elements of Functions Theory and Functional Analysis, Nauka, Moscow, 1968.

Обратная задача для уравнения вязкоупругости с дополнительной информацией, имеющей специальный вид

Журабек Ш. Сафаров
Ташкентский университет информационных технологий
Ташкент, Узбекистан
Институт математики АН Республики Узбекистан
Ташкент, Узбекистан

Аннотация. Рассматривается одномерная обратная задача определения ядра интегрального члена интегро-дифференциального уравнения вязкоупругости с постоянной плотностью и постоянными коэффициентами Ламе. Сначала исследуется прямая задача, при этом мы получаем интегральное уравнение относительно искомой функции $u(x,t)$ и необходимые условия на данные задачи. Далее исследуется обратная задача по определению ядра интегрального члена. Для отыскания его вводится дополнительное условие, заданное в специальном виде при x = 0. Обратная задача заменяется эквивалентной системой интегральных уравнений для неизвестных функций. К последней в пространстве непрерывных функций с весовыми нормами применяется принцип сжатых отображений. Доказана теорема глобальной однозначной разрешимости.

Ключевые слова: интегро-дифференциальное уравнение, обратная задача, ядро интеграла, теорема Банаха.

EDN: IXXNRI
УДК 512.5

A Note on Uniformly Totally Strongly Inert Subgroups of Abelian Groups

Andrey R. Chekhlov*
Faculty of Mathematics and Mechanics
Tomsk State University
Tomsk, Russian Federation
Peter V. Danchev†
Institute of Mathematics and Informatics
Bulgarian Academy of Sciences
Sofia, Bulgaria
Patrick W. Keef‡
Department of Mathematics
Whitman College
Walla Walla, WA, Unites States

Received 11.11.2024, received in revised form 17.01.2025, accepted 24.02.2025

Abstract. We prove in this short note that any uniformly totally inert subgroup of a given group is commensurable with a uniformly fully invariant subgroup of the whole group as well as that any uniformly totally strongly inert subgroup is commensurable with a strongly invariant subgroup, thus somewhat extending results due to Breaz–Călugăreanu in Rend. Sem. Mat. Univ. Padova (2017), Chekhlov–Danchev in Rocky Mount. J. Math. (2025) and Goldsmith–Salce in J. Comm. Algebra (2025).

Keywords: Abelian groups, (characteristically, fully, strongly) invariant subgroups, uniformly (characteristically, fully, totally) inert subgroups.

Citation: A.R. Chekhlov, P.V. Danchev, P.W. Keef, A Note on Uniformly Totally Strongly Inert Subgroups of Abelian Groups, J. Sib. Fed. Univ. Math. Phys., 2025, 18(4), 467–473. EDN: IXXNRI.

(To Brendan Goldsmith on his 75th birthday)

1. Fundamentals

Throughout this brief paper, all groups into consideration are *additively* written and *Abelian*. Our basic notation and terminology will be provided in detail in what follows.

Recall that a subgroup F of an arbitrary group G is said to be *fully invariant* if $\phi(F) \subseteq F$ for any endomorphism ϕ of G as well as that a subgroup C of G is said to be *characteristic* if $\psi(C) \subseteq C$ for any automorphism ψ of G. In the same vein, mimicking [2], a subgroup S of G is said to be *strongly invariant* in G if $f(S) \subseteq S$ for every group homomorphism $f : S \to G$.

It is routine to see that the following (strict) implications for these subgroups are true:

$$\text{strongly invariant} \Rightarrow \text{fully invariant} \Rightarrow \text{characteristic}.$$

On the other hand, imitating [4], a subgroup H of a group G is called *fully inert*, provided $(\phi(H) + H)/H$ is finite for all endomorphisms ϕ of G as well as a subgroup K of G is called

*cheklov@math.tsu.ru https://orcid.org/0000-0002-9078-128X
†danchev@math.bas.bg https://orcid.org/0000-0002-2016-2336
‡keef@whitman.edu https://orcid.org/0000-0003-4983-2273

characteristically inert, provided $(\psi(K)+K)/K$ is finite for all automorphisms ψ of G. This means that the intersections $H\cap\phi(H)$ and $K\cap\psi(K)$ have finite index in $\phi(H)$ and $\psi(K)$, respectively. In the same aspect, refining only the first of these two given notions, in [5] a subgroup T of G is called *totally inert*, provided that the intersection $T\cap\phi(T)$ has finite index both in T and $\phi(T)$ for all non-zero endomorphisms ϕ (notice that the case where this condition is fulfilled for the automorphism ψ is *not* treated there — compare with Problem 2 posed below). Likewise, in [1], a subgroup N of G is called *strongly inert*, provided $(f(N)+N)/N$ is finite for all homomorphisms $f:N\to G$, that is, the intersection $N\cap f(N)$ has finite index in $f(N)$ for all such homomorphisms f. Proceeding in this way, a subgroup S of a group G is named *totally strongly inert*, provided the intersection $S\cap f(S)$ has finite index in both S and $f(S)$ for all non-zero homomorphisms $f:S\to G$.

It is obvious to verify that the following (strict) relationships for these subgroups are valid:

$$\text{strongly inert}\vee\text{totally inert}\Rightarrow\text{fully inert}\Rightarrow\text{characteristically inert}.$$

For simplicity of our exposition, remember also that two subgroups B and C of a group G are called *commensurable*, and thus we write for short that $B\sim C$ or, equivalently, that $C\sim B$ since this is obviously a symmetric relation, whenever both quotients $(B+C)/B$ and $(B+C)/C$ are finite.

Moreover, it is not so difficult to construct concrete examples such that a fully inert subgroup is *not* commensurable with a fully invariant subgroup, such a characteristically inert subgroup is *not* commensurable with a characteristic subgroup, and such that a strongly inert subgroup is *not* commensurable with strongly invariant subgroup (see, e.g., [3] and [1] and compare with Problem 1 arisen below).

Nevertheless, this commensurability is quite possible to hold for the following refinements of the aforementioned group classes: in fact, in [4] a subgroup H of a group G is known to be *uniformly fully inert* requiring the existence of a fixed positive integer m such that the factor-group $(\phi(H)+H)/H$ has at most m elements for every endomorphism ϕ of G, whereas a subgroup K is known to be *uniformly characteristically inert* if the factor-group $(\psi(K)+K)/K$ has at most m elements for every automorphism ψ of G. As demonstrated above, it is evident that any uniformly fully inert subgroup is always uniformly characteristically inert, whereas the reverse implication is wrong in general.

In this direction, imitating the "uniformly" property as presented above, the notions of *uniformly totally inert*, *uniformly totally strongly inert* and *uniformly strongly inert* subgroups can be successfully defined in a way of similarity keeping in mind the listed above relations between them. And so, the subgroup T is uniformly totally inert if it has an intersection $T\cap\phi(T)$ which cardinality is bounded by a fixed positive integer simultaneously in T and $\phi(T)$ for any non-zero endomorphism ϕ of G. However, as it will be emphasized below, the abundance of uniformly totally inert subgroups is rather restricted.

Our pivotal tool here is the following quite more general setting: a subgroup S of a group G is named *uniformly totally strongly inert* if S possesses an intersection $S\cap f(S)$ which power is bounded by a fixed natural number simultaneously in S and $f(S)$ for all non-zero homomorphisms $f:S\to G$.

Besides, we shall say that a fully invariant subgroup S of a group G is *uniformly fully invariant* if the index $[S:\phi(S)]$ is bounded by a fixed natural number for all non-zero endomorphisms ϕ of G.

Since a subgroup commensurable with a totally inert subgroup is always totally inert by [5, Proposition 2.1], one has that the subgroup commensurable with some uniformly fully invariant subgroup must be uniformly totally inert.

On the other hand, it was shown in [4, Corollary 1.9] the important fact that *any uniformly characteristically inert subgroup is commensurable a characteristic subgroup* and, in addition,

in [3, Main Theorem] that *every uniformly fully inert subgroup is commensurable with a fully invariant subgroup.*

Apart from the observation given above for a lack of too many uniformly totally inert subgroups, the objective of the present short article is to show that, based on the idea proposed in [3], each uniformly totally strongly inert subgroup of a given group is commensurable with some strongly invariant subgroup of this group, which fact will be illustrated in the next section. Likewise, it is reasonably natural to ask what is the behavior of uniformly totally strongly inert subgroups defined as above.

2. The chief results

We foremost begin our work with certain preliminaries. So, in what follows, all homomorphisms will be written to the **right** of their arguments.

If G is a group and $A \supseteq B$ are subgroups of G, and C is some other subgroup, then the quotient-group $(A \cap C)/(B \cap C)$ apparently embeds in A/B, so that the inequality

$$[A \cap C : B \cap C] \leqslant [A : B]$$

is fulfilled always.

Even more clearly, if $A \supseteq B \supseteq C$, then the inequality

$$[A : B] \leqslant [A : C]$$

is always fulfilled.

Next, if X and Y are subgroups of G, then $\overline{X} := X/(X \cap Y)$ and $\overline{Y} := Y/(X \cap Y)$ are subgroups of $G/(X \cap Y)$ with $\overline{X} \cap \overline{Y} = \{0\}$ and $\overline{X} + \overline{Y} = (X + Y)/(X \cap Y)$. So, it follows that

$$(X + Y)/(X \cap Y) \cong [X/(X \cap Y)] \oplus [Y/(X \cap Y)].$$

Let us now define

$$q(X, Y) := [X + Y : X \cap Y] = [X : X \cap Y] \cdot [Y : X \cap Y].$$

We, thus, arrive at the following useful claim:

$$X \sim Y \text{ if, and only if, } q(X, Y) \text{ is finite.}$$

Furthermore, the first ingredient of the proof of the basic theorems quoted below is the following one.

Lemma 2.1. *Suppose G is a group, X, Y and Z are subgroups of G, and ϕ is an endomorphism of G.*

(a) If $q(X, Y)$ is finite, then $q(X\phi, Y\phi) \leqslant q(X, Y)$ is also finite.

(b) If $q(X, Y)$ and $q(Y, Z)$ are both finite, then $q(X, Z) \leqslant q(X, Y) \cdot q(Y, Z)$ is also finite.

Proof. Regarding (a), an elementary inspection shows that there is a natural surjection

$$(X + Y)/(X \cap Y) \to (X\phi + Y\phi)/(X\phi \cap Y\phi),$$

which immediately implies the desired result.

Regarding (b), we derive the relations

$$\begin{aligned} q(X, Y) \cdot q(Y, Z) &= [X : X \cap Y] \cdot [Y : X \cap Y] \cdot [Y : Y \cap Z] \cdot [Z : Y \cap Z] \\ &\geqslant [X : X \cap Y] \cdot [Y \cap Z : X \cap Y \cap Z] \cdot [X \cap Y : X \cap Y \cap Z] \cdot [Z : Y \cap Z] \\ &\geqslant [X : X \cap Y \cap Z] \cdot [Z : X \cap Y \cap Z] \end{aligned}$$

$$\geqslant [X : X \cap Z] \cdot [Z : X \cap Z]$$
$$= q(X, Z),$$

as wanted. □

For subgroups X, Y of G, let us now set the distance metric

$$d(X, Y) := \ln(q(X, Y)).$$

So, our next key instrument is the following consequence to the preceding assertion, which technical proof is omitted as we leave it to the interested reader for checking.

Corollary 2.2. *If X, Y and Z are subgroups of G, and ϕ is an endomorphism of G, then the following two inequalities hold:*

(a) $d(X\phi, Y\phi) \leqslant d(X, Y)$;

(b) $d(X, Z) \leqslant d(X, Y) + d(Y, Z)$.

So, one may expect below that, if G is a group and X is a subgroup such that, for every endomorphism ϕ of G, we have $d(X, X\phi) < \infty$, then there will exist a fully invariant subgroup Y such that, for every endomorphism ϕ of G, the inequality $d(Y, Y\phi) < \infty$ holds. However, we will restrict our attention to a more partial case.

Thus, we have now at our disposal all the machinery needed to establish the following main statement.

Theorem 2.3. *Let X be a subgroup of G. Then, X is uniformly totally strongly inert in G if, and only if, one of following three conditions holds:*

(a) $X \cong \mathbb{Q}$ is the entire maximal divisible subgroup of G.

(b) $X \cong \mathbb{Z}(p^\infty)$ is the entire maximal p-torsion divisible subgroup of G.

(c) X is finite.

In particular, every uniformly totally strongly inert subgroup of a given group is commensurable with a strongly invariant subgroup of this group.

Proof. If (a) or (b) holds, then any non-zero homomorphism $X \to G$ must satisfy $X = X\phi$, so that $d(X, X\phi) = 0$.

If (c) holds and X has order k, then, for any homomorphism $\phi : X \to G$, we must have $q(X, X\phi) \leqslant k^2$.

Conversely, suppose X is uniformly totally strongly inert. Suppose $n \in \mathbb{N}$ is given such that $q(X, X\phi) \leqslant n$ for all non-zero homomorphisms $\phi : X \to G$.

If X is not reduced, then one can decompose $X = Y \oplus Z$, where either $Z \cong \mathbb{Q}$ or $Z \cong \mathbb{Z}(p^\infty)$; we want to show that (a) or (b) must hold. We first show that $Y = \{0\}$. If this failed, then the composition of the natural idempotent projection $\phi : X \to Y$ followed by the inclusion $Y \leqslant G$, would not be the zero map. Since the group

$$Z \cong X/Y = X/(X \cap X\phi)$$

is infinite, this would contradict that X is uniformly totally strongly inert in G.

Next, suppose $X \cong \mathbb{Q}$ and D is the maximal divisible subgroup of G; we want to verify that (a) must hold. If $X \neq D$, then one may decompose $D = D' \oplus X' \oplus X$, where X' is isomorphic to either $\mathbb{Q}$ or $\mathbb{Z}(p^\infty)$. There is, clearly, a non-zero homomorphism $\phi : X \to X' \leqslant G$. It thus follows that $X \cap X\phi = \{0\}$, so that $q(X, X\phi)$ is infinite. Therefore, (a) must hold. A similar contradiction can be used to show that, if $X \cong \mathbb{Z}(p^\infty)$, then (b) must hold.

So, we may assume that X is reduced. We will show that the assumption that X is infinite leads to a contradiction, which will establish (c) and complete the entire proof.

To this aim, suppose first that X is not torsion-free but is reduced. Furthermore, for some prime p, if X has non-zero p-torsion, there must be a decomposition $X = Y \oplus Z$, where $Z \cong \mathbb{Z}(p^k)$ for some $k \in \mathbb{N}$. Let $\phi : X \to G$ be the natural idempotent projection onto Z followed by the inclusion $Z \to G$. Apparently, ϕ is not the zero homomorphism; however, the group

$$X/(X \cap X\phi) = X/Z \cong Y$$

is infinite, which contradicts that $q(X, X\phi) \leqslant n$.

Suppose, on the other hand, that X is torsion-free. Since we know it is reduced, it follows that, for some prime p, $pX \neq X$. Let $\phi : X \to G$ be the homomorphism given by $y\phi = p^{n+1}y$. Since X is torsion-free, ϕ is obviously not the zero map. Note that the quotients

$$X/(X \cap X\phi) = X/X\phi = X/p^{n+1}X$$

will have order at least $p^n > n$, which again contradicts that $q(X, X\phi) < n$, as promised. □

We are now also ready to establish the next major statement.

Theorem 2.4. *Let X be a subgroup of G. Then, X is uniformly totally inert in G if, and only if, one of following three conditions holds:*

(a) $X = G \cong \mathbb{Q}$.

(b) $X = G \cong \mathbb{Z}(p^\infty)$.

(c) X is finite.

In particular, every uniformly totally inert subgroup of a given group is commensurable with a uniformly fully invariant subgroup of this group.

Proof. If (a) or (b) holds, then any non-zero homomorphism $X \to X$ is surjective, so that $d(X, X\phi) = 0$.

If (c) holds and X has order k, then, for any endomorphism $\phi : G \to G$, we must have $q(X, X\phi) \leqslant k^2$.

Conversely, suppose X is uniformly totally inert. Suppose $n \in \mathbb{N}$ is given such that $q(X, X\phi) \leqslant n$ for all non-zero endomorphisms $\phi : G \to G$.

If X is not reduced, then one can decompose $X = Y \oplus Z$, where either $Z \cong \mathbb{Q}$ or $Z \cong \mathbb{Z}(p^\infty)$. Suppose $G = G' \oplus Z$, where $Y \leqslant G'$; we want to show $G' = \{0\}$. If this failed, then the natural idempotent projection $\phi : G \to G$ onto G' would not be the zero map. Since the group

$$Z \cong X/Y = X/(X \cap X\phi)$$

is infinite, this would contradict that X is uniformly totally inert in G.

So, we may assume that X is reduced. We will show that the assumption that X is infinite leads to a contradiction, which will establish (c) and complete the whole proof.

To this purpose, suppose first that X is bounded. For some prime p, the group X has a non-zero p-torsion subgroup. Therefore, G also has a non-zero p-torsion subgroup. This implies that there is a decomposition $G = G' \oplus A$, where A is isomorphic to $\mathbb{Z}(p^\infty)$ or $\mathbb{Z}(p^m)$ for some $m \in \mathbb{N}$. Let $\phi : G \to G$ be the natural idempotent projection onto A; obviously, ϕ is non-zero. Since X is bounded, it follows at once that $X\phi \leqslant A$ is also bounded and, consequently, is finite. It follows now that the intersection $X \cap X\phi$ is also finite, and since X is infinite, we can conclude that $q(X, X\phi)$ is infinite too, which contradicts that $q(X, X\phi) \leqslant n$.

Suppose, on the other hand, that X is unbounded. We construct a sequence of primes $p_1, p_2, \ldots$ such that, if μ_m is the product $p_1 p_2 \ldots p_m$, then $\mu_m X \neq \mu_{m+1} X$: having constructed such a finite sequence $p_1, p_2, \ldots, p_n$ and its resulting product μ_n, then since X is unbounded, we must have $\mu_m X \neq 0$. And since X is reduced, there must be a prime, say p_{m+1}, such that $p_{m+1}(\mu_m X) \neq (\mu_m X)$, completing the construction.

Let $\phi : G \to G$ be the endomorphism given by $y\phi = \mu_{n+1}y$. Since X, and hence G, is unbounded, ϕ is easily not the zero map. Note that the factors-groups

$$X/(X \cap X\phi) \cong X/\mu_{n+1}X$$

will have order at least $2^n > n$, which again contradicts the condition $q(X, X\phi) < n$, as expected. □

Remark 1. We now give an independent confirmation that each uniformly totally inert subgroup X of a group G is commensurable with a uniformly fully invariant subgroup Y of G. In fact, suppose we have a fixed finite value δ such that, for every endomorphism $\phi : G \to G$, we write $d(X, X\phi) \leqslant \delta$. It now follows from the previous two assertions listed above that X is totally inert, so employing the main result from [3], there is a fully invariant subgroup Y such that $\gamma := d(X, Y)$ is finite; one easily inspects that Y is, actually, uniformly fully invariant in G.

If we now take $\epsilon = 2\gamma + \delta$, then one finds with the help of Corollary 2.2 that, for every endomorphism ϕ of G, it must be that

$$d(Y, Y\phi) \leqslant d(X, Y) + d(X, X\phi) + d(X\phi, Y\phi) \leqslant \gamma + \delta + d(X, Y) \leqslant \epsilon,$$

as required.

We next proceed with the following commentaries.

Remark 2. To keep a record straight, we should note that the last theorem could be deduced indirectly with some more efforts from results established in [5]; however, we have obtained a rather more conceptual and transparent proof.

Indeed, if $G \cong \mathbb{Z}(p^\infty)$, then all the subgroups of G are uniformly totally inert, while if G is *not* isomorphic to $\mathbb{Z}(p^\infty)$, then only its finite subgroups are uniformly totally inert — indeed, we claim that these are only the rational torsion-free group $\mathbb{Q}$ and the quasi-cyclic p-group $\mathbb{Z}(p^\infty)$. In fact, looking for infinite subgroups H of a group G different from $\mathbb{Q}$ and $\mathbb{Z}(p^\infty)$, respectively, which are uniformly totally inert, from [5, Corollary 2.3] it follows that, in order to admit infinite totally inert subgroups, G must be torsion-free reduced and indecomposable. Furthermore, for such a group G, a subgroup $H \neq \{0\}$ is infinite, but and it cannot be uniformly totally inert, because there is a prime p such that $H/pH \neq \{0\}$ (noticing that H is not divisible), so H/pH has cardinality at least p and, therefore, H/p^nH has cardinality at least p^n, whence H cannot be uniformly totally inert, as suspected.

However, the first theorem is somewhat independent from the corresponding results established in [2] and [1], respectively.

The following principal affirmation, which takes into account the above discussion, is, hopefully, worthy of documentation to stimulate a further research on the subject.

Conjecture. Each uniformly strongly inert subgroup of an arbitrary group is commensurable with a strongly invariant subgroup of the group.

In fact, it was established in [1, Theorem 4.5] that a subgroup of torsion group is strongly inert if, and only if, it is commensurable with a strongly invariant subgroup of the whole group.

We finish our work with the next two questions of interest and importance. The first one states thus:

Problem 1. Decide when a totally inert subgroup is commensurable with a fully invariant subgroup (or, even, with a characteristic subgroup).

We shall say that a subgroup C of a group G is *completely inert*, provided that the intersection $C \cap \psi(C)$ has finite index in both C and $\psi(C)$ for any automorphism ψ of G. In case that this

index is bounded by a fixed positive integer, simultaneously in C and $\psi(C)$, this subgroup is said to be *uniformly completely inert*.

So, we come to our second query.

Problem 2. Explore the structural properties of completely inert and uniformly completely inert subgroups of a given group and provide, if possible, a close transversal with the (uniformly) totally inert subgroups.

The scientific work of the first-named author, A. R. Chekhlov, is supported by the Ministry of Science and Higher Education of Russia under agreement No. 075-02-2024-1437.

References

[1] S.Breaz, G.Calugareanu, Strongly inert subgroups of abelian groups, *Rend. Sem. Mat. Univ. Padova*, **138**(2017), 101–114. DOI: 10.4171/RSMUP/138-5

[2] G.Calugareanu, Strongly invariant subgroups, *Glasgow Math. J.*, **57**(2015), 431–443. DOI 10.1017/S0017089514000391

[3] A.R.Chekhlov, P.V.Danchev, Solution to the uniformly fully inert subgroups problem for Abelian groups, *Rocky Mount. J. Math*, **55**(2025).

[4] U.Dardano, D.Dikranjan, S.Rinauro, Inertial properties in groups, *Int. J. Group Theory*, **7**(2018), 17–62.

[5] B.Goldsmith, L.Salce, Totally inert subgroups of Abelian groups, *J. Comm. Algebra*, **17**(2025).

Заметка о равномерно тотально сильно инертных подгруппах абелевых групп

Андрей Р. Чехлов
Факультет математики и механики
Томский государственный университет
Томск, Российская Федерация
Петр В. Данчев
Институт математики и информатики
Болгарская академия наук
София, Болгария
Патрик У. Кииф
Факультет математики
Колледж Уитмена
Уолла-Уолла, Вашингтон, США

Аннотация. Доказывается, что любая равномерно тотально инертная подгруппа группы соизмерима с равномерно вполне инвариантной подгруппой всей группы, а также что любая равномерно тотально сильно инертная подгруппа соизмерима с сильно инвариантной подгруппой, что несколько обобщает результаты, полученные Breaz–Calugareanu (Rend. Sem. Mat. Univ. Padova, 2017), Chekhlov–Danchev (Rocky Mount. J. Math., 2025) и Goldsmith–Salce (J. Comm. Algebra, 2025).

Ключевые слова: абелевы группы, (характеристически, вполне, сильно) инвариантные подгруппы, равномерно (характеристически, вполне, тотально) инертные подгруппы.

EDN: CQMLLF
УДК 517.54

Analogue of the Carleman's Formula for $A(z)$-analytic Functions

Nasridin M. Zhabborov*
Tashkent State University of Economics
Tashkent, Uzbekistan
Bukhara State University
Bukhara, Uzbekistan

Behzod E. Husenov†
Bukhara State University
Bukhara, Uzbekistan

Received 02.01.2025, received in revised form 28.01.2025, accepted 25.03.2025

Abstract. In this paper, an analogue of the Carleman formula is proved for $A(z)$-analytic functions from the Hardy class. The idea of obtaining the Carleman formulas and the concept of the Carleman function for $A(z)$-analytic functions from the Hardy class belong to M.M. Lavrentiev. In the proof of Carleman's formula, $A(z)$-harmonic functions and the Poisson formula in lemniscates $L(a,r)$, compactly belonging to the domain under consideration $D \subset \mathbb{C}$, are used substantially.

Keywords: $A(z)$-analytic function, Hardy class, $A(z)$-lemniscate, multiple Cauchy integral formula for $A(z)$-analytic functions.

Citation: N.M. Zhabborov, B.E. Husenov, Analogue of the Carleman's Formula for $A(z)$-analytic Functions, J. Sib. Fed. Univ. Math. Phys., 2025, 18(4), 474–483.
EDN: CQMLLF.

One of the major challenges in the classical theory of complex analysis is the integral representation of analytic functions, which allows us to recover a function within a domain from its values along the boundary. Additionally, it is natural to inquire how an analytic function may be reconstructed based on its value at a single point on the boundary of a simply-connected domain. In 1926, T. Carleman achieved a significant breakthrough by solving this issue for certain types of domains. He devised a strategy for constructing a "quenching" function in the context of boundary-value problems. G. M. Goluzin and V. I. Krylov further extended Carleman's findings in 1933, employing a specialized holomorphic function to assist with the process, which relies on a portion of the boundary of the domain. Another method based on the approximation of the kernel of the integral representation was proposed by M. M. Lavrentiev in 1956. It turned out that this method works successfully in the noted cases when the Goluzin-Krylov approach is not applicable [2].

*zhabborovnasridin@gmail.com
†b.e.husenov@buxdu.uz

1. Introduction and preliminaries

1.1. $A(z)$-analytic functions

Let $A(z)$ be an antianalytic function, i.e. $\dfrac{\partial A}{\partial z} = 0$ in the domain $D \subset \mathbb{C}$ and there is a constant $c < 1$ such that $|A(z)| \leqslant c$ for all $z \in D$. The function $f(z)$ is said to be $A(z)$-*analytic* in the domain D if for any $z \in D$, the following equality holds:

$$\frac{\partial f}{\partial \bar{z}} = A(z)\frac{\partial f}{\partial z}. \tag{1}$$

We denote by $O_A(D)$ the class of all $A(z)$-analytic functions defined in the domain D. Since an antianalytic function is smooth, $O_A(D) \subset C^\infty(D)$ (see [1]). In this case, the following takes place:

Theorem 1.1 (see [3], analogue of the Cauchy integral theorem)**.** *If $f \in O_A(D) \cap C\left(\bar{D}\right)$, where $D \subset \mathbb{C}$ is a domain with smooth ∂D, then*

$$\int\limits_{\partial D} f(z)(dz + A(z)d\bar{z}) = 0.$$

Now we assume that the domain $D \subset \mathbb{C}$ is convex and $\xi \in D$ is a fixed point in it. Since the function $\overline{A}(z)$ is analytic, the integral

$$I(z) = \overline{\int\limits_{\gamma(\xi,z)} \overline{A(\tau)}d\tau}$$

is independent of the path of integration; it coincides with the antiderivative $I'(z) = \overline{A}(z)$. Consider the function

$$K(z,\xi) = \frac{1}{2\pi i}\frac{1}{z - \xi + I(z)},$$

where $\gamma(\xi, z)$ is a smooth curve which connects the points $\xi, z \in D$ (see [5]).

Theorem 1.2 (see [5])**.** *$K(z,\xi)$ is an $A(z)$-analytic function outside of the point $z = \xi$, i.e. $K(z,\xi) \in O_A(D\backslash\{\xi\})$. Moreover, at $z = \xi$ the function $K(z,\xi)$ has a simple pole.*

Remark 1.1 (see [5])**.** *If a simply connected domain $D \subset \mathbb{C}$ is not convex, then the function*

$$\psi(\xi, z) = z - \xi + I(z),$$

although well defined in D, may have other isolated zeros except ξ : $\psi(\xi, z) = 0$ for $z \in P\backslash\{\xi, \xi_1, \xi_2, ...\}$. Consequently, $\psi \in O_A(D)$, $\psi(\xi, z) \neq 0$ when $z \notin P$ and $K(z,\xi)$ is an $A(z)$-analytic function only in $D\backslash P$, it has poles at the points of P. Due to this fact we consider the class of $A(z)$-analytic functions only in convex domains.

According to [5], Theorem 1.2, the function $\psi(\xi, z)$ is an $A(z)$-analytic function.

The following set is an open subset of D:

$$L(a, r) = \{z \in D : |\psi(a, z)| < r\}.$$

For suffiently small $r > 0$, this set compactly lies in D (we denote it by $L(a, r) \subset\subset D$) and contains the point a. The set $L(a, r)$ is called an $A(z)$-*lemniscate* centered at the point a. The lemniscate $L(a, r)$ is a simply-connected set (see [5]).

Theorem 1.3 (see [4], Cauchy's integral formula). *Let $D \subset \mathbb{C}$ be a convex domain and $G \subset\subset D$ be an arbitrary subdomain with a smooth or piecewise smooth ∂G. Then for any function $f(z) \in O_A(G) \bigcap C(\bar{G})$, the following formula holds:*

$$f(z) = \int\limits_{\partial G} f(\xi) K(z,\xi) \left(d\xi + A(\xi) d\bar{\xi}\right), \quad z \in G. \tag{2}$$

Note that from formula (2) it follows that if $f(z) \in O_A(L(a,r)) \bigcap C\left(\bar{L}(a,r)\right)$, where $L(a,r) \subset\subset D$ is a fixed $A(z)$-lemniscate, then in $L(a,r)$ the function $f(z)$ is expanded in a Taylor series:

$$f(z) = \sum_{k=0}^{\infty} c_k \psi^k(a,z), \tag{3}$$

where $c_k = \dfrac{1}{2\pi i} \displaystyle\int\limits_{|\psi(a,\xi)|=\rho} \dfrac{f(\xi)}{(\psi(a,\xi))^{k+1}} \left(d\xi + A(\xi) d\bar{\xi}\right), 0 < \rho < r$, $k = 0, 1, 2, \ldots$.

1.2. $A(z)$-harmonic functions

Theorem 1.4 (see [6]). *The real part $u(z)$ of the functions $f(z) \in O_A(D)$ satisfies the equation*

$$\begin{aligned} \Delta_A u := & \frac{\partial}{\partial z}\left(\frac{1}{1-|A|^2}\left(\left(1+|A|^2\right)\frac{\partial u}{\partial \bar{z}} - 2A\frac{\partial u}{\partial z}\right)\right) + \\ & + \frac{\partial}{\partial \bar{z}}\left(\frac{1}{1-|A|^2}\left(\left(1+|A|^2\right)\frac{\partial u}{\partial z} - 2\bar{A}\frac{\partial u}{\partial \bar{z}}\right)\right) = 0 \end{aligned} \tag{4}$$

in the domain D.

Conversely, if D is a simply connected domain, and a function $u \in C^2(D)$ satisfies the differential equation (4), then there is $u(z) = Re f(z)$.

In connection with Theorem 1.4, it is natural to define $A(z)$-harmonic functions as follows.

Definition 1.1 (see [6]). *A function $u \in C^2(D)$, $u : D \to \mathbb{R}$ is called $A(z)$-harmonic if it satisfies in the domain D the differential equation (4).*

The class of $A(z)$-harmonic functions in the domain D is denoted as $h_A(D)$. Thus, the operator $\triangle_A$ in the theory of $A(z)$-harmonic functions plays the same role as Laplace operator $\triangle$ in the theory of harmonic functions. It follows from Theorem 1.4 that the real and imaginary parts of $A(z)$-analytic function $f = u + iv$ in the domain D are $A(z)$-harmonic functions. The function v is called the $A(z)$-conjugate harmonic function to u.

Theorem 1.5 (see [6], analogue of the Poisson formula for $A(z)$-harmonic functions). *If the function $\omega(\zeta)$ is continuous on the boundary of the lemniscate $L(a,r)$, then the function*

$$u(z) = \frac{1}{2\pi r} \int\limits_{|\psi(a,\zeta)|=r} \omega(\zeta) \frac{r^2 - |\psi(a,z)|^2}{|\psi(\zeta,z)|^2} \left|d\zeta + A(\zeta) d\bar{\zeta}\right| \tag{5}$$

is the solution of the Dirichlet problem in $L(a,r)$, i.e. $u(z) \in h_A(L(a,r)) \cap C\left(\bar{L}(a,r)\right)$: $u(z)|_{\partial L(a,r)} = \omega(\zeta)$. Conversely, any function $u(z) \in h_A(L(a,r)) \cap C(\bar{L}(a,r))$ is represented in $L(a,r)$ by the Poisson integral:

$$u(z) = \frac{1}{2\pi r} \int\limits_{|\psi(a,\zeta)|=r} u(\zeta) \frac{r^2 - |\psi(a,z)|^2}{|\psi(\zeta,z)|^2} \left|d\zeta + A(\zeta) d\bar{\zeta}\right|, \quad z \in L(a,r). \tag{6}$$

Formulas (5) and (6) are analogues of the Poisson formula for $A(z)$-harmonic functions. Here, $P(z,\zeta)=\dfrac{r^2-|\psi(a,z)|^2}{|\psi(\zeta,z)|^2}$ is the Poisson kernel.

1.3. Angular limits and Hardy classes for $A(z)$-analytic functions

Let $L(a,r)\subset\subset D$ and $f(z)\in O_A(L(a,r))$. We define the concepts of angular and radial limits of $A(z)$-subharmonic and $A(z)$-analytic functions in lemniscate $L(a,r)$. The radial limits of the function $f(z)$ at some point $\zeta\in\partial L(a,r)$ are denoted as $f^*(\zeta)$ and the angular limits are denoted as $f^*_\sphericalangle(\zeta)$ (see [8]).

In the classical case of the disk $U=\{w\in\mathbb{C}:|w|<1\}\subset\mathbb{C}_w$, the limit by the radius $\tau_\zeta=\{w=t\zeta\},\ 0\leqslant t\leqslant 1,\ \zeta\in\partial U$ of the function $g(w)$,

$$g^*(\zeta)=\lim_{w\to\zeta,w\in\tau_\zeta}g(w)$$

is called the radial limit, and the limit by the angle $\sphericalangle\subset U$, ending at the point $\zeta\in\sphericalangle$, is called the angular limit,

$$g^*_\sphericalangle(\zeta)=\lim_{w\to\zeta,w\in\sphericalangle_\zeta}g(w)\cdot$$

Since lemniscate $L(a,r)$ is a simply connected domain with a real analytic boundary, according to Riemann's theorem there exists a conformal map $\chi(z):U\to L(a,r)$, which is also conformal in some neighborhood of closure $\bar{U}$. Let χ maps the boundary point $\lambda\in\partial U$ to the boundary point $\zeta\in\partial L(a,r)$. Then the curve $\gamma_\zeta=\chi(\tau_\lambda)$ has the property that it connects points a,ζ and is perpendicular to all lines of level $\partial L(a,\rho)=\{|\psi(a,z)|=\rho\}$, $0<\rho\leqslant r$. In the theory of $A(z)$-analytic functions, the curve $\gamma_\zeta=\chi(\tau_\lambda)$ plays the role of the radial direction, and the image of the angle $\chi(\sphericalangle)$ plays the role of the angular set at the point $\zeta\in\partial L(a,r)$. We will denote this angle by $\sphericalangle=\sphericalangle_\zeta$. The limit $f^*(\zeta)=\lim\limits_{z\to\zeta,z\in\gamma_\zeta}f(z)$ is called the radial limit, and $f^*_\sphericalangle(\zeta)=\lim\limits_{z\to\zeta,z\in\sphericalangle_\zeta}f(z)$ is the angular limit of the function $f(z)$ at the point $\zeta\in\partial L(a,r)$ (see [8]).

Now we will show the smoothness of the boundary of lemniscate $L(a,r)$. For this, we take the automorphism $\chi^{-1}(z):\overline{L}(a,r)\to\overline{U}$ by Riemann's theorem. Let there be some neighborhood $V=\{\psi(a,\zeta)=re^{i\theta},|\theta|<\varepsilon\}$ for $\forall\varepsilon>0$. Also has $\chi^{-1}(V)\subset\partial U$ and $\chi^{-1}(\zeta_0)=\lambda_0\in\partial U$. Further, there is a diffeomorphism $\pi=-i\ln\chi^{-1}(\zeta):V\to[-1;1]$. This diffeomorphism represents all boundary points of differentiability of the function $f^*(\zeta)$ and $f^*_\sphericalangle(\zeta)$ (see [8]).

Next we introduce the Hardy class for $A(z)$-analytic functions:

Definition 1.2 (see [8]). *The Hardy class H^p, $p>0$, for $A(z)$-analytic functions is the set of all functions $f(z)$ such that its averages*

$$\frac{1}{2\pi\rho}\int\limits_{|\psi(a,z)|=\rho}|f(z)|^p\big|dz+A(z)d\bar{z}\big| \tag{7}$$

are uniformly bounded for $\rho<r$, i.e. $\sup\limits_{\rho<r}\left\{\dfrac{1}{2\pi\rho}\int\limits_{|\psi(a,z)|=\rho}|f(z)|^p\big|dz+A(z)d\bar{z}\big|\right\}<\infty\cdot$

The Hardy class for $A(z)$-analytic functions in the domain $L(a,r)$ is denoted as $H^p_A(L(a,r))$. The norms in them are defined by the formula (see [8]):

$$\|\ f\ \|_{H^p_A}=\sup_{|\psi(a,z)|<r}\left(\frac{1}{2\pi\rho}\int\limits_{|\psi(a,z)|=\rho}|f(z)|^p\big|dz+A(z)d\bar{z}\big|\right)^{\frac{1}{p}}<\infty\cdot$$

Further, from the inequality $b^q < b^p + 1, \ \ 0 < q < p, \ \ b \geqslant 0$ we conclude that $f \in H_A^p$ follows $f \in H_A^q$, i.e. $H_A^p \subset H_A^q$ for all p and q. Let us define a class of bounded functions

$$H_A^\infty(L(a,r)) = \left\{ f(z) \in O_A(L(a,r)) : \sup_{|\psi(a,z)|<r} \{|f(z)|\} < \infty \right\}.$$

The norm in $H_A^\infty(L(a,r))$ is defined as $\| f(z) \|_{H_A^\infty} = \sup_{z \in L(a,r)} \{|f(z)|\}$ (see [8]).

1.4. The Fatou theorems and Cauchy's integral formula for the Hardy class H_A^1

Now, we will consider the Fatou theorem for the class of functions H_A^1 :

Theorem 1.6 (See [8], the Fatou theorem for the class of functions H_A^1)**.** *If $f(z) \in H_A^1(L(a,r))$, then the angular limit*

$$f_\sphericalangle^*(\zeta) = \lim_{z \to \zeta, z \in \sphericalangle_\zeta} f(z)$$

exists and is finite for almost all $\zeta \in \partial L(a,r)$, except, perhaps, the points of some set E of measure zero.

The following statements follow from Theorem 1.6:

Theorem 1.7 (see [8])**.** *If $f(z) \in H_A^1(L(a,r))$, then $f^*(\zeta) \in L_A^1(\partial L(a,r))$. As $\rho \to r$*

$$\int\limits_{|\psi(a,z)|=\rho} f(z)\big|dz + A(z)d\bar{z}\big| \longrightarrow \int\limits_{|\psi(a,\zeta)|=r} f^*(\zeta)\big|d\zeta + A(\zeta)d\bar{\zeta}\big| \tag{8}$$

and

$$\int\limits_{|\psi(a,z)|=\rho} |f(z) - f^*(\zeta)|\big|dz + A(z)d\bar{z}\big| \longrightarrow 0. \tag{9}$$

According to Cauchy integral formula (2) for lemniscates $L(a,r)$

$$f(z) = \frac{1}{2\pi i} \int\limits_{|\psi(a,\xi)|=\rho} f(\xi)K(\xi,z)\left(d\xi + A(\xi)d\bar{\xi}\right),$$

we conclude that

$$f(z) = \frac{1}{2\pi i} \int\limits_{|\psi(a,\zeta)|=r} f^*(\zeta)K(\zeta,z)\left(d\zeta + A(\zeta)d\bar{\zeta}\right). \tag{10}$$

This is the Cauchy integral formula for functions of H_A^1.

We show a boundary uniqueness theorem for the Hardy class H_A^1:

Theorem 1.8 (see [8])**.** *Let $f(z) \in H_A^1(L(a,r))$. Suppose that for some set $M \subset \partial L(a,r)$ of positive measure $f^*(\zeta) = 0, \ \forall \zeta \in M$. Then $f(z) \equiv 0$.*

2. Carleman's formula for $A(z)$-analytic functions

2.1. $A(z)$-harmonic measure of a boundary set

For a measurable boundary subset of a lemniscate $L(a,r)$, the $A(z)$-harmonic measure $\omega(z, M, L(a,r))$ is defined very simply, according to the Poisson formula. If

$$\aleph_M(\zeta) = \begin{cases} -1, & \zeta \in M, \\ 0, & \zeta \in \partial L(a,r) \backslash M \end{cases}$$

is a characteristic function of the set $M \subset \partial L(a,r)$, then the $A(z)$-harmonic measure is

$$\omega(z, M, L(a,r)) = \frac{1}{2\pi r} \int\limits_{|\psi(a,\zeta)|=r} P(z,\zeta)\aleph_M(\zeta)\big|d\zeta + A(\zeta)d\bar{\zeta}\big|. \tag{11}$$

Note that the $A(z)$-harmonic measure $\omega(z, M, L(a,r))$ is a $A(z)$-harmonic function inside the lemniscate $L(a,r)$ and

$$-1 \leqslant \omega(z, M, L(a,r)) \leqslant 0.$$

Theorem 2.1 (see [9]). *The function $\omega(z, M, L(a,r))$ either does not vanish anywhere, $\omega(z, M, L(a,r)) < 0$, or is identically zero, $\omega(z, M, L(a,r)) \equiv 0$. Moreover, $\omega(z, M, L(a,r)) \equiv 0$ if and only if the bounded set $M \subset \partial L(a,r)$ has measure zero.*

The following theorem is very important in qualitative estimates of $A(z)$-analytic functions.

Theorem 2.2 (see [9]). *Let $M \subset \partial L(a,r)$ be a measurable boundary set of positive measure. Then for almost all points $\zeta^0 \in M$ there exist radial (angular) limits $\omega^*(\zeta^0, M, L(a,r)) = -1$.*

2.2. Construction of a quenching function and the Carleman formula in class H^1_A.

Let $D \subset \mathbb{C}$ be a convex domain, $L(a,r) \subset\subset D$ be some lemniscate, on the boundary of which the set $M \subset \partial L(a,r)$ of positive measure is given. The task is to restore the function $f(z) \in H^1_A(L(a,r))$ to $L(a,r)$ by its boundary values given not over the entire boundary $\partial L(a,r)$, as in (10), but only on M. Applying Carleman's simple idea, we will construct a *"quenching" function* that will allow us to get rid of (10) by integrating over $\partial L(a,r)\backslash M$. For this purpose, it is necessary to construct an auxiliary function $\varphi(z) \in H^\infty_A(L(a,r))$ satisfying two conditions (see [9]):

1. $|\varphi^*(\zeta)| = 1$ almost everywhere on $\partial L(a,r)\backslash M$.
2. $|\varphi(z)| > 1$ at $L(a,r)$.

This can be done by constructing the $A(z)$-harmonic measure $\omega(z, M, L(a,r))$ of the boundary set $M \subset \partial L(a,r)$. According to Theorem 2.2, $\omega(z, M, L(a,r)) \in h_A(L(a,r))$, $-1 \leqslant \omega(z, M, L(a,r)) < 0$ and

$$\omega^*(\zeta, M, L(a,r)) = \lim_{z\to\zeta, z\in\sphericalangle} \omega(z, M, L(a,r)) = -1$$

almost everywhere at M and

$$\omega^*(\zeta, \partial L(a,r)\backslash M, L(a,r)) = \lim_{z\to\zeta, z\in\sphericalangle} \omega(z, \partial L(a,r)\backslash M, L(a,r)) = 0$$

almost everywhere at $\partial L(a,r)\backslash M$ (see [9]).

Since $L(a,r) \subset\subset D$ is simply connected, there is an $A(z)$-harmonic function $v(z)$, conjugated to $\omega(z, M, L(a,r))$. Then $\omega(z, M, L(a,r)) + iv(z) = w(z) \in O_A(L(a,r))$. Consider function $\varphi(z) = e^{-w(z)} \in O_A(L(a,r))$. It satisfies the above conditions:

$$|\varphi(z)| = e^{-\omega(z,M,L(a,r))} \leqslant e$$

everywhere in $L(a,r)$, i.e.

$$\varphi(z) \in H^\infty_A(L(a,r)), \quad |\varphi^*(\zeta)| = e^{-\omega^*(\zeta,M,L(a,r))} = e^0 = 1$$

almost everywhere on $\partial L(a,r)\backslash M$ and

$$|\varphi(z)| = e^{-\omega(z,M,L(a,r))} > 1, \quad \forall z \in L(a,r).$$

This function is called the quenching function with respect to the set M (see [9]).

Now we look at the important formula:

Theorem 2.3 (see [9]). *If $f \in H_A^1(L(a,r))$ and $M \subset \partial L(a,r)$ is the set of positive measure, then the formula*

$$f(z) = \frac{1}{2\pi i} \lim_{m\to\infty} \int_M f^*(\zeta) \left[\frac{\varphi^*(\zeta)}{\varphi(z)}\right]^m K(\zeta,z)\left(d\zeta + A(\zeta)d\bar{\zeta}\right), \tag{12}$$

will be true for any point $z \in L(a,r)$. Moreover, the convergence in (12) will be uniform on compacts from $L(a,r)$.

3. M. M. Lavrentiev's method Carleman's formula for $A(z)$-analytic functions

Let in the set $\partial L(a,r)\backslash M$ with the Cauchy kernel $K(z,\zeta)$ (here $z \in L(a,r)$ is fixed) be approximated by $A(z)$-analytic functions $g_{z,m}(\zeta) \in H_A^\infty(L(a,r))$. These functions are orthogonal to the considered $A(z)$-analytic functions $f \in H_A^1(L(a,r))$ and integration over $\partial L(a,r)$. In addition,

$$\lim_{m\to\infty} \int_{\partial L(a,r)\backslash M} f^*(\zeta)\left(K(z,\zeta) - g_{z,m}(\zeta)\right)\left(d\zeta + A(\zeta)d\bar{\zeta}\right) = 0. \tag{13}$$

We arrive at the following formula:

$$f(z) = \lim_{m\to\infty} \int_M f^*(\zeta)\left(K(z,\zeta) - g_{z,m}(\zeta)\right)\left(d\zeta + A(\zeta)d\bar{\zeta}\right). \tag{14}$$

In formula (14), z is included as a parameter under the integral sign.

Now we construct the Carleman function for $A(z)$-analytic functions. This idea of obtaining the Carleman formula (12) with kernel approximation can be described using the Carleman concept introduced by M. M. Lavrentyev for $A(z)$-analytic functions. A function of two complex ζ, z and a positive variable α, which we denote by $G(z,\zeta,\alpha)$, is called the Carleman function $A(z)$-analytic set M in the domain D if:

1) $G(z,\zeta,\alpha) = \dfrac{1}{\psi(z,\zeta)} + \tilde{G}(z,\zeta,\alpha)$, where $\tilde{G}$ to ζ is a function of class $H_A^\infty(L(a,r))$;

2) $\dfrac{1}{2\pi} \int\limits_{\partial L(a,r)\backslash M} |G(z,\zeta,\alpha)|\left|d\zeta + A(\zeta)d\bar{\zeta}\right| \leqslant |C(z)|\,\alpha$, where the constant $C(z)$ depends on z.

An example of a generalized Carleman function is the kernel in formula (12):

$$G(z,\zeta,\alpha) = \left[\frac{\varphi^*(\zeta)}{\varphi(z)}\right]^{\frac{1}{\alpha}} \frac{1}{\psi(z,\zeta)}.$$

And in general, if the Carleman function is $A(z)$-analytic G, then the Carleman formula for $A(z)$-analytic functions is also true:

$$f(z) = \frac{1}{2\pi i} \lim_{\alpha\to 0} \int_M f^*(\zeta) G(z,\zeta,\alpha)\left(d\zeta + A(\zeta)d\bar{\zeta}\right), \tag{15}$$

It is obvious that generalized formulas (14) and (15) are equivalent.

Let us prove the theorem of M. M. Lavrentiev for the $A(z)$-analytic function:

Theorem 3.1. *Let $L(a,r) \subset\subset D$ be a set whose boundary consists of a finite number of closed piecewise smooth Jordan disjoint curves, and let M be an open subset of $\partial L(a,r)$. Then there is a Carleman formula (14) for function $f(z)$ from class $H_A^1(L(a,r))$:*

$$f(z) = \lim_{m\to\infty} \int\limits_M f^*(\zeta)\left(K(z,\zeta) - g_{z,m}(\zeta)\right)\left(d\zeta + A(\zeta)d\bar{\zeta}\right)$$

which we construct using a chain of integrals and expansions in series.

We first check the limit (13) for uniform convergence by representing $g_{z,m}(\zeta)$, the approximating Cauchy kernel $K(z,\zeta)$, as a series. $\forall z \in L(a,r)$, $\zeta \in \partial L(a,r)$ of

$$2\pi i K(z,\zeta) = \frac{1}{\psi(\zeta,z)} = \frac{1}{\zeta - z + \overline{\int\limits_{\gamma(z,\zeta)} \overline{A(\tau)}d\tau}} = \frac{1}{(\zeta-a) + \overline{\int\limits_{\gamma(a,\zeta)} \overline{A(\tau)}d\tau} - (z-a) - \overline{\int\limits_{\gamma(a,z)} \overline{A(\tau)}d\tau}} =$$

$$= \frac{1}{\psi(a,\zeta)} \frac{1}{1 - \frac{\psi(a,z)}{\psi(a,\zeta)}} = \sum_{k=0}^{\infty} \frac{(\psi(a,z))^k}{(\psi(a,\zeta))^{k+1}}.$$

The Cauchy kernel $K(z,\zeta)$ is extended to $L(a,r)$ lemniscates as indicated above. Now let us check $g_{z,m}(\zeta)$ functions. From the end of subsection 1 we select a function in the form of a finite series:

$$g_{z,m}(\zeta) = \frac{1}{2\pi i} \sum_{k=0}^{m} \frac{(\psi(a,z))^k}{(\psi(a,\zeta))^{k+1}}.$$

Now we move on to limit

$$\lim_{m\to\infty} \int\limits_M f^*(\zeta)\left(K(z,\zeta) - g_{z,m}(\zeta)\right)\left(d\zeta + A(\zeta)d\bar{\zeta}\right) =$$

$$= \lim_{m\to\infty} \int\limits_M f^*(\zeta)\left(\sum_{k=0}^{\infty} \frac{(\psi(a,z))^k}{(\psi(a,\zeta))^{k+1}} - \sum_{k=0}^{m} \frac{(\psi(a,z))^k}{(\psi(a,\zeta))^{k+1}}\right)\left(d\zeta + A(\zeta)d\bar{\zeta}\right).$$

Now let us prove Theorem 3.1:

Proof. From the generalized Runge theorem (see [10], p. 20) it follows that the compact set $\partial L(a,r)\backslash M$ is, for small $\varepsilon > 0$, a compact set $O_A(L(a,r)_\varepsilon)$ — convex. Consider a sequence of compacts $\mathcal{K}_m, m \in \mathbb{N}, \mathcal{K}_m \subset \mathcal{K}_{m+1}$, $\bigcup\limits_{m=1}^{\infty} \mathcal{K}_m = L(a,r)$ each $\mathcal{K}_m$ is $O_A(L(a,r)_\varepsilon)$ — convex. For example, we choose this compact set in this form:

$$\mathcal{K}_m = L\left(a, \left(1 - \frac{1}{m+1}\right) r\right) = L\left(a, \frac{mr}{m+1}\right).$$

Function $K(z,\zeta)$ is $A(z)$-analytic on $(\partial L(a,r)\backslash M) \times \mathcal{K}_m$, and each function from $O_A\left((\partial L(a,r)\backslash M) \times \mathcal{K}_m\right)$ is uniformly approximated on this compact by functions from $O_A\left(L(a,r)_\varepsilon \times L(a,r)_\varepsilon\right)$. We showed uniform convergence above by representing the $g_{z,m}(\zeta)$

functions as a series. Indeed, from $O_A\left(L(a,r)_\varepsilon\right)$ — the convexity of $(\partial L(a,r)\backslash M)$ and $\mathcal{K}_m$ follows $O_A\left(L(a,r)_\varepsilon \times L(a,r)_\varepsilon\right)$ — the convexity of $(\partial L(a,r)\backslash M)\times\mathcal{K}_m$, which is easy to prove using the double integral Cauchy formula (in the special case of space $\mathbb{C}^2$, formula (4) from [7]):

$$f(z)=\frac{1}{(2\pi i)^2}\int\limits_{(\partial L(a,r)\backslash M)\times\mathcal{K}_m}\frac{f_{m,n}(z,\zeta)\left(d\zeta+A(\zeta)d\bar{\zeta}\right)\wedge(dz+A(z)d\bar{z})}{\psi(z,\zeta)\times\psi(a,z)},$$

applied to the neighborhood of $(\partial L(a,r)\backslash M)\times\mathcal{K}_m$, and the fact that the integral is the limit of integral sums. So, evenly on

$$K(z,\zeta)=\lim_{n\to\infty}f_{m,m(n)}(\zeta,z),$$

where

$$f_{m,m(n)}(\zeta,z)\in O_A\left(L(a,r)_\varepsilon\times L(a,r)_\varepsilon\right).$$

Function $g_{z,m}(\zeta)$ is $A(z)$-analytic on $L(a,r)_\varepsilon\times L(a,r)_\varepsilon$ and Carleman's formula (14) is valid. □

In this proof we actually did not use the openness of M, but only the fact that M contains a neighborhood of some point, so we have

Corollary 3.1. *The statement of Theorem 3.1 holds if M contains at least one point from $\partial L(a,r)$ together with its neighborhood on $\partial L(a,r)$.*

Finally, we note that the $A(z)$-analytic kernel $K(z,\zeta)$ in the Carleman formula for $A(z)$-analytic functions from Theorem 3.1 or Corollary 3.1 is constructed as constructively as one can construct an approximation in Runge's theorem (see [10]), i.e. using a chain of integrals and expansions in series.

M. M. Lavrentiev's method has found important applications in the theory of ill-posed problems of analysis and mathematical physics in [11]. And the method of A. M. Kytmanov appeared in relation to homogeneous domains in $\mathbb{C}^n$ (see [12]).

References

[1] I.N.Vekua, Generalized analytical functions, Nauka, Moscow, 1988 (in Russian).

[2] L.A.Aizenberg, Carleman's Formulas in Complex Analysis, Kluwer Academic publishers, Dordrecht/Boston/London, 1993.

[3] N.M.Zhabborov, T.U.Otaboyev, Cauchy's theorem for $A(z)$-analytic functions, *Uzbek Mathematical Journal*, **1**(2014), 15–18 (in Russian).

[4] N.M.Zhabborov, T.U.Otaboyev, An analogue of the Cauchy integral formula for $A(z)$-analytic functions, *Uzbek Mathematical Journal*, **4**(2016), 50–59 (in Russian).

[5] A.Sadullayev, N.M.Jabborov, On a class of A-analytic functions, *Journal of Siberian Federal University. Mathematics-Physics*, **9**(2016), no.3, 374–383.

[6] N.M.Zhabborov, T.U.Otaboyev, Sh.Y.Khursanov, The Schwartz inequality and the Schwartz formula for A-analytic functions, *Journal of Mathematical Sciences*, **264**(2022), no. 6, 703–714. DOI: 10.1007/s10958-022-06031-3

[7] T.U.Otaboyev, On the Hartogs theorem for A-analytic functions in $\mathbb{C}^n$, *Bulleten of NUUz*, **5**(2022), no. 1, 27–38. DOI: 10.56017/2181-1318.1186

[8] N.M.Zhabborov, Sh.Y.Khursanov, B.E.Husenov, Existence of boundary values of Hardy class functions H_A^1, *Bulleten of NUUz*, **5**(2022), no. 2, 79–90. DOI: 10.56017/2181-1318.1218

[9] N.M.Zhabborov, B.E.Husenov, Carleman's formula for $A(z)$-analytic functions, *Lobachevsky Mathematical Journal*, **45**(2024), no. 12, 6541–6549.

[10] L.Hormander, Introduction to the Theory of Functions of Several Variables, Mir, Moscow, 1968 (in Russian).

[11] M.M.Lavrentiev, V.G.Romanov, S.P.Shishatsky, Incorrect Problems of Mathematical Physics and Analysis, Nauka, Moscow, 1980 (in Russian).

[12] A.M.Kytmanov, T.N.Nikitina, Analogues of the Carleman formula for Classical Domains, *Mathematical Notes*, **45**(1989), no. 3, 243–248 (in Russian).

Аналог формулы Карлемана для $A(z)$-аналитических функций

Насридин М. Жабборов
Ташкентский государственный экономический университет
Ташкент, Узбекистан
Бухарский государственный университет
Бухара, Узбекистан
Бехзод Э. Хусенов
Бухарский государственный университет
Бухара, Узбекистан

Аннотация. В работе для $A(z)$-аналитических функций из класса Харди доказывается аналог формулы Карлемана. Идея получения формулы Карлемана и понятие функции Карлемана для $A(z)$-аналитических функций из класса Харди принадлежат М. М. Лаврентьеву. В доказательстве формулы Карлемана существенно используются $A(z)$-гармонические функции и формула Пуассона в лемнискатах $L(a, r)$, компактно принадлежащих в рассматриваемой области $D \subset \mathbb{C}$.

Ключевые слова: $A(z)$-аналитическая функция, класс Харди, $A(z)$-лемниската, кратная интегральная формула Коши для $A(z)$-аналитических функций.

EDN: JFMMFC
УДК 517.953

On Carleman's Formula in $\mathbb{C}^n[m \times m]$

Gulmirza G. Khudayberganov*
National University of Uzbekistan
Tashkent, Uzbekistan
Barlikbay B. Prenov†
Nukus state pedagogical institute named after Ajiniyaz
Nukus, Republic of Karakalpakstan, Uzbekistan
Jonibek Sh. Abdullayev‡
Urgench State University
Urgench, Uzbekistan
Kudrat Sh. Ruzmetov§
Tashkent State Agrarian University
Tashkent, Uzbekistan

Received 12.10.2024, received in revised form 09.12.2024, accepted 24.03.2025

Abstract. This paper considers Carleman's integral formula for a function of matrices in the space $\mathbb{C}^n[m \times m]$. The resulting formula is a general case of G. Khudayberganov's result.

Keywords: Carleman's formulas, holomorphic function, Hardy space, holomorphic continuation, matrix unit disc, automorphism.

Citation: G.G. Khudayberganov, B.B. Prenov, J.Sh. Abdullayev, K.Sh. Ruzmetov, On Carleman's Formula in $\mathbb{C}^n[m \times m]$, J. Sib. Fed. Univ. Math. Phys., 2025, 18(4), 484–490. EDN: JFMMFC.

1. Introduction, preliminaries and problem statement

It is known that Carleman formulas solve the problem of reconstructing a holomorphic function in a domain D (that behaves quite well when approaching the boundary ∂D), from its values on some uniqueness set $M \subset \partial D$ that does not contain the Shilov boundary.

The problem of reconstructing a holomorphic function goes back to the Cauchy integral formula, which is unique in the case of the complex plane. It reconstructs a holomorphic function in a domain using its values on the boundary. Naturally, the question arises whether is it possible to reconstruct a holomorphic function inside a domain using its values not on the entire boundary, but on a part of it. A positive answer to this question first appeared in the works of T. Carleman in 1926 (see [1, 2]) in one particular case, and this explains the name of these formulas after him. He proved a formula that reconstructs a holomorphic function in a sector using its values on the arc of the sector. Later, in 1933, G. M. Goluzin and V. I. Krylov (see [2, 3]) found a method based on the introduction of a damping function, which allows one to solve this problem for an arbitrary simply connected domain of the complex plane.

*gkhudaiberg@mail.ru https://orcid.org/0000-0002-4837-8331
†prenov@doda.uz https://orcid.org/0009-0003-4963-9059
‡j.abdullayev@nuu.uz https://orcid.org/0000-0001-8950-2135
§ruzmetov1967@mail.ru https://orcid.org/0000-0002-2238-0345

He proved the following: If $f \in \mathcal{H}^1(D)$ and a set $M \subset \partial D$ has positive Lebesgue measure, then for any point $z \in D$ the following Carleman formula is true

$$f(z) = \lim_{m\to\infty} \frac{1}{2\pi i} \int_M f(\xi) \left[\frac{\varphi(\xi)}{\varphi(z)}\right]^m \frac{d\xi}{\xi - z}, \tag{1}$$

where $\varphi(z) = \exp(u + iv)$, the function $u(x, y)$ is the solution of the Dirichlet problem for the domain D, and $v(x, y)$ is the conjugate harmonic function to $u(x, y)$.

In 1956, M. M. Lavrentiev (see [2]) proposed a method for obtaining Carleman's formula by approximating the kernel. Further development of this theory in multidimensional complex analysis can be found in the book by L. A. Aizenberg (see [2, 4]). Also in multidimensional complex analysis, this problem was studied in the works of N. N. Tarkhanov [5], Sh. A. Dautov [6], A. M. Kytmanov [7, 8], T. N. Nikitina, G. Khudayberganov [9, 10], S. Kosbergenov [11], B. A. Shaimkulov [12] and others (see [13, 14]).

A. M. Kytmanov proposed a new method for obtaining the Carleman formula for homogeneous domains using automorphisms of these domains: if we can restore a function at one point of the domain, then using automorphisms we can restore it at any point of the domain. And G. Khudaiberganov in his work [9] considered Carleman's formula for matrix functions. We will use G. Khudaiberganov's method to obtain the Carleman formula in our studies.

2. Carleman's formula for matrix functions

Consider $\mathbb{C}^{m^2}$ the space of m^2 complex variables space. In some questions, it is convenient to represent the point Z of this space as $Z = (z_{ij})_{i,j=1}^m$, i.e., as square $[m \times m]$-matrices. With this point of representation, the space $\mathbb{C}^{m^2}$ can be denoted by $\mathbb{C}[m \times m]$. Denote by $\mathbb{C}^n[m \times m]$ the direct product of n copies of $[m \times m]$-matrix spaces: $\underbrace{\mathbb{C}[m \times m] \times \cdots \times \mathbb{C}[m \times m]}_{n}$.

Let $Z = (Z_1, \ldots, Z_n)$ be a vector composed of square matrices Z_j of order m, considered over the field of complex numbers $\mathbb{C}$. Let us write the elements of the vector $Z = (Z_1, \ldots, Z_n)$ as points z of the space $\mathbb{C}^{nm^2}$:

$$z = (z_{11}^{(1)}, \ldots, z_{1m}^{(1)}, \ldots, z_{m1}^{(1)}, \ldots, z_{mm}^{(1)}, \ldots, z_{11}^{(n)}, \ldots, z_{1m}^{(n)}, \ldots, z_{m1}^{(n)}, \ldots, z_{mm}^{(n)}) \in \mathbb{C}^{nm^2}. \tag{2}$$

Hence, we can assume that Z is an element of the space $\mathbb{C}^n[m \times m]$, i.e., we arrive at the isomorphism $\mathbb{C}^n[m \times m] \cong \mathbb{C}^{nm^2}$.

Denote by $D \subset \mathbb{C}^{n^2}$ a bounded set of $[n \times n]$ matrices W. By Gershgorin's theorem (see [15], p. 198) there exists a bounded simply-connected domain $D \subset \mathbb{C}^1$ with piecewise-smooth boundary that contains all eigenvalues of all matrices $W \in D$. Then for every function $f \in \mathcal{O}(D) \cap C(\overline{D})$ is defined $f(W)$, where $W \in D$ (see [15], Sec. 5.8), using the Cauchy formula we have

$$f(W) = \frac{1}{2\pi i} \int_{\partial D} f(z)(zI - W)^{-1} dz, \tag{3}$$

here I is the identity matrix of order n.

Note that the Hardy class $\mathcal{H}^1(D)$ consists of all functions f that are holomorphic in D and for which

$$\|f\|_{H^1} = \sup_{0<r<1} \left(\int_{\partial D} |f(rZ)| \, d\mu \right) < \infty.$$

The definition of (3) can be easily extended to the class $\mathcal{H}^1(D)$. The following is a result of G. Khudaiberganov where a matrix analogue of the classical Carleman formula is obtained (see [9]).

Theorem 2.1. *If $f \in \mathcal{H}^1(D)$ and $M \subset \partial D$ is the set of positive Lebesgue measure, then for any matrix $W \in G$ the Carleman formula is true:*

$$f(W) = \lim_{m\to\infty} \frac{1}{2\pi i} \int_M f(\zeta)(\zeta I - W)^{-1} \left\{ \varphi(\zeta) [\varphi(W)]^{-1} \right\}^m d\zeta, \tag{4}$$

where the function φ is the same as in the one-dimensional Carleman formula.

Note that for $n = 1$ the relation (4) is a generalized Carleman formula (1).

For the matrix unit disc

$$\tau = \{Z \in \mathbb{C}[m \times m] : \ ZZ^* < I\}$$

we can take the usual unit disc

$$U(0,1) = \{z \in \mathbb{C} : |z| < 1\},$$

as D, therefore the next statement is true.

Corollary 2.1. *If $D = \tau$, then the formula (4) is valid, where $M \subset \partial U(0,1)$.*

Corollary 2.2. *If $m_1 = m_2 = \cdots = m_s = 1$, then*

$$f(W) = \lim_{m\to\infty} \frac{1}{2\pi i} \sum_{k=1}^{s} \prod_{\substack{\nu=1 \\ \nu\neq k}}^{s} \frac{W - \lambda_k I}{\lambda_k - \lambda_\nu} \int_M f(\zeta) \left[\frac{\varphi(\zeta)}{\varphi(\lambda_k)} \right]^m \frac{d\zeta}{\zeta - \lambda_k}. \tag{5}$$

where $\lambda_1, \lambda_2, \ldots, \lambda_s$ different eigenvalues of the matrix W with multiplicities $m_1, m_2, \ldots, m_s$ respectively.

The proof of Corollary 3.1 becomes obvious if we take into account that the eigenvalues of the matrices from τ lie in the unit disc [16]. Corollary 3.2 is proved with the use of Theorem 5.5.2 from [15], according to which

$$z_{kj} = \frac{1}{(j-1)!} (\omega - \lambda_k I)^{j-1} \prod_{\nu=1}^{s} \frac{\omega - \lambda_\nu I}{\lambda_k - \lambda_\nu}$$

where $k = 1, 2, \ldots, s$; $j = 1, 2, \ldots, m_k$. We note that from (5), by virtue of equality (1), there follows the Sylvester interpolation formula [17, 18]

$$f(w) = \sum_{k=1}^{s} f(\lambda_k) \prod_{\substack{\nu=1 \\ \nu\neq k}}^{s} \frac{w - \lambda_v I}{\lambda_k - \lambda_v}.$$

This means that these results were used to find the Sylvester interpolation formula in the space $\mathbb{C}[m \times m]$. In this paper, we present an analogue of Theorem 2.1 for $\mathbb{C}^n[m \times m]$, and using the resulting theorem, we write the interpolation formula in the space for the case $\mathbb{C}^n[m \times m]$.

3. Carleman's formula for functions of matrices in $\mathbb{C}^n[m\times m]$

Let $A=(A_1,A_2,\dots,A_n)\in\mathbb{C}^n[m\times m]$ and $\lambda_\nu^{(1)},\dots,\lambda_\nu^{(s_\nu)}$ be different eigenvalues of the matrix with multiplicities $m_1,\dots,m_{s_\nu}$ and $A_\nu\in\mathbb{C}^n[m\times m]$, $\nu=1,\dots,n$, and $D_\nu\subset\mathbb{C}^1$ domain containing $\lambda_\nu^{(1)},\dots,\lambda_\nu^{(s_\nu)}$ and lying in the ν-th coordinate plane of the space $\mathbb{C}^n$, $\nu=1,\dots,n$. According to Gershgorin's theorem such D_ν exist (see e.g. [15]).

Let us assume that the function $f(t)=f(t_1,\dots,t_n)\in\mathcal{H}^1(D)$, where $D=D_1\times D_2\times\cdots\times D_n$.

Let us define a holomorphic function of several matrices variables using the formula:

$$f(A)=\frac{1}{(2\pi i)}\int\limits_{\mathbb{T}^n}f(t)(tI-A)^{-1}dt \tag{6}$$

where $\mathbb{T}^n=\partial D_1\times\partial D_2\times\cdots\times\partial D_n$, $dt=dt_1\dots dt_n$ and

$$(tI-A)^{-1}=(t_1I-A_1)^{-1}\dots(t_nI-A_n)^{-1}.$$

The following spectral expansion theorem holds for $f(A)$.

Theorem 3.1. *If $f\in\mathcal{H}^1(D)$, then there exist matrices*

$$Z_{r_1p_1}^{(1)},\dots,Z_{r_1p_1}^{(1)}\quad r_\nu=1,\dots,s_\nu,\quad p_\nu=1,\dots,m_{r_\nu},\quad \nu=1,\dots,n,$$

independent of f such that

$$f(A)=\sum_{r_1,\dots,r_n=1}^{s_1,\dots,s_n}\ \sum_{p_1,\dots,p_n=1}^{m_{r_1},\dots,m_{r_n}}\left[\frac{\partial^{|p|-n}}{\partial\lambda^{|p|-n}}f(\lambda)\right]_{\lambda=\lambda^{(r_n)}}Z_{r_p}, \tag{7}$$

where

$$r=(r_1,\dots,r_n),\quad p=(p_1,\dots,p_n),$$
$$|p|=p_1+p_2+\cdots+p_n,$$

$Z_{r_p}=Z_{r_1p_1}^{(1)}\dots Z_{r_np_n}^{(n)}$, $\lambda=(\lambda_1\dots\lambda_n)$, where the entry $\lambda=\lambda^{(r)}$ means that $\lambda_1=\lambda_1^{(r_1)},\dots,\lambda_n=\lambda_n^{(r_n)}$. The component $Z_{r_\nu p_\nu}^{(\nu)}$ of the matrix A_ν, $\nu=1,\dots,n$ is determined by the formula:

$$Z_{r_\nu p_\nu}^{(\nu)}=\frac{1}{(p_\nu-1)!}(A_\nu-\lambda_\nu^{r_\nu}I)^{p_\nu-1}\prod_{\substack{j_\nu=1\\ j_\nu\neq r_\nu}}^{S_\nu}\frac{A_\nu-\lambda_\nu^{(j_\nu)}I}{\lambda_\nu^{(r_\nu)}-\lambda_\nu^{(j_\nu)}},\quad \nu=1,\dots,n. \tag{8}$$

Let $D=D_1\times\cdots\times D_n\in\mathbb{C}^n[m\times m]$ be a bounded domain. Then by Gershgorin's theorem (see [15]) there exists a polydisc $U^n(0,R)=\{z\in\mathbb{C}^n:\|z\|<R\}$ containing all eigenvalues of all matrices $W_\nu\in D_\nu$, $\nu=1,\dots,n$. Let Λ_{W_ν} be the spectrum of the matrix W_ν, $\nu=1,\dots,n$, then

$$\Lambda_W=(\Lambda_{W_1},\dots,\Lambda_{W_n})\subset U^n(0,R).$$

Consider the set $E\subset\mathbb{T}^n(0,R)$, $m_nE>0$. For points $\overset{\backprime}{\xi}=(\xi_2,\dots,\xi_n)\in\mathbb{T}^n(0,R)$, $a=(a_1,\dots,a_n)\in\Lambda_W$ and parameter $l\in\mathbb{C}^1$. Let us introduce the set

$$E_{a'\xi}=\{t\in E:t_1=t_1(l),t_j(l,\xi_j),j=2,\dots,n,|l|=R\},$$

where

$$t_1(l)=(a_1-l)(1-\frac{\bar a_1}{R^2}l)^{-1},\quad t_j(l,\xi_j)=\frac{\xi\left(l-\frac{|a_j|^2}{R}l\right)+a_j(1-l)}{\frac{\bar a_j}{R}\xi_j(l-1)+1-\frac{|a_j|^2}{R}l}. \tag{9}$$

By E'_a we denote the set

$$\left\{ {}'\xi \in \mathbb{T}^n(0,R) : m_{n-1}E_{a\,{}'\xi} > 0 \right\}. \tag{10}$$

From Fubini's theorem it follows that $m_{n-1}E'_a > 0$. Let us put

$$\psi_a(t) = \frac{1}{2\pi i} \int\limits_{E_{a,{}'\xi}} \left(\frac{\eta + a_1 - t_1\left(1 + \frac{\bar{a}_1}{R^2}\eta\right)}{t_1\left(1 - \frac{\bar{a}_1}{R^2}\eta\right) + \eta - a_1} \right) \frac{d\eta}{\eta}$$

where t and ${}'\xi$ are related by the relation (9) and (10).

Theorem 3.2. *Let $f(t) \in \mathcal{H}^1(U^n(0,R))$, $E \subset \mathbb{T}^n(0,R)$ and $m_n(E) > 0$, then for an arbitrary $W = (W_1, \ldots, W_n) \in D$ the next formula holds:*

$$f(W) = G(E'_{\Lambda_W})^{-1} \lim_{p\to\infty} \frac{1}{(2\pi i)^n} \int\limits_E f(t) e^{p(\psi_W(t) - \psi_W(W))} (tI - W)^{-1} dt, \tag{11}$$

where

$$G(E'_{\Lambda_W}) = \int\limits_{E'_{\Lambda_W}} P({}'\xi I, {}'W) dm_{n-1},$$

$$\begin{aligned} P({}'\xi I, {}'W) =& \left[(\xi_2 I - W_2)(\xi_2 I - W_2)^*\right]^{-1} (R^2 I - W_2 W_2{}^*) \ldots \\ & \left[(\xi_n I - W_n)(\xi_n I - W_n)^*\right]^{-1} \left(R^2 I - W_n W^*\right), \\ (tI - W)^{-1} =& (t_1 I - W_1)^{-1} \ldots (t_n I - W_n)^{-1}, \\ dt =& dt_1 \wedge dt_2 \wedge \cdots \wedge dt_n, \end{aligned}$$

the set E'_{Λ_W} is defined in the same way as in the formula (10).

Proof. Let $\lambda_1, \ldots, \lambda_s$ be distinct eigenvalues of the matrix W with multiplicities $m_1, m_2, \ldots, m_s$. By virtue of the definition of a holomorphic function of several matrices and by formula (7) we have

$$(2\pi i)^n f(W) = \int\limits_{\mathbb{T}^n} f(t) f(tI - W)^{-1} dt = \int\limits_{\mathbb{T}^n} \prod_{\nu=1}^{S} \sum_{r_\nu=1}^{s_\nu} \sum_{p_\nu=1}^{m_r} \frac{f(t)(p_\nu - 1)!}{\left(t_\nu - \lambda_\nu^{(r_\nu)}\right)^{p_\nu}} dt Z^{(\nu)}_{r_\nu p_\nu} =$$

$$= \sum_{r_1,\ldots,r_n=1}^{s_1,\ldots,s_n} \sum_{p_1,\ldots,p_n=1}^{m_1,\ldots,m_{r_n}} \frac{1}{G(E'_\lambda)} \times$$

$$\times \lim_{p\to\infty} \left[\int\limits_E \left\{ f(t) \frac{\partial^{|p|-n}}{\partial\lambda_1^{p_1-1} \ldots \partial\lambda_1^{p_n-1}} \left(\frac{\psi_\lambda^{-p}(\lambda)}{t-\lambda} \right) \Bigg|_{\lambda_\nu = \lambda_\nu^{(r_\nu)}} \psi_\lambda^p(t) \prod_{\nu=1}^{n} Z^{(\nu)}_{r_\nu p_\nu} \right\} dt \right],$$

where $Z^{(\nu)}_{r_\nu p_\nu}$ components of matrix W_ν. Here we have used the fact that the formula $\lambda_\nu^{(1)}, \ldots, \lambda_\nu^{(S_\nu)}$ can be differentiated and

$$\int\limits_{\mathbb{T}^n} \prod_{\nu=1}^{S} \sum_{r_\nu=1}^{S_\nu} \sum_{p_\nu=1}^{m_{r_\nu}} \frac{f(t)(p_\nu-1)!}{\left(t_\nu - \lambda_\nu^{(r_\nu)}\right)^{p_\nu}} dt = (2\pi i)^n \left[\frac{\partial^{|p|-n}}{\partial\lambda_1^{p_1-1} \ldots \partial\lambda_n^{p_n-1}} \left(f(\lambda_1 \ldots \lambda_n) \right) \right]_{\lambda_\nu = \lambda_\nu^{(r_\nu)}} =$$

$$= G^{-1}(E'_{\Lambda_\lambda}) \lim_{p\to\infty} \int\limits_E f(t) \frac{\partial^{|p|-n}}{\partial\lambda_1^{p_1-1} \ldots \partial\lambda_n^{p_n-1}} \left(\frac{\psi_\lambda^{-p}(\lambda)}{t-\lambda} \right) \Bigg|_{\lambda_\nu = \lambda_\nu^{(r_\nu)}} \psi_\lambda^p(t)\, dt.$$

The proof of Theorem 3.2 completed. □

Note that when $n = m = 1$ the formula (11) turns into the formula of Goluzin and Krylov, and in the case of $n = 1$, when D is matrix unit disc, into the Carleman formula obtained by G. Khudayberganov [9].

References

[1] T.Carleman, Les fonctions quasi-analytiques, Gauthier-Villars, Paris, 1926, 115.

[2] L.A.Aizenberg, *Carleman formulas in complex analysis*, Nauka, Novosibirsk, 1990 (in Russian)

[3] G.M.Goluzin, V.I.Krylov, Verallgemeinerung einer Formel von Carleman und ihre Anwendung auf analytische Fortsetzung, *Mat. Sb.*, **40**(1933), no. 2, 144–149 (in Russian)

[4] L.A.Aizenberg, *Multidimensional analogue of the Carleman formula*, Dokl. Akad. Nauk SSSR, **277**(1984), no. 6, 1289–1291 (in Russian).

[5] N.Tarkhanov, An explicit Carleman formula for the Dolbeault cohomology, *J. Sib. Fed. Univ. Math. Phys.*, **3**(2010), no. 4, 450–460

[6] Sh.A.Dautov, E.S.Mkrtchyan, *Reconstruction of functions from in a polycylinder*, On holomorphic functions of several complex variables: Collection of scientific papers, Krasnoyarsk, 1976, 39–45 (in Russian).

[7] A.M.Kytmanov, T.N.Nikitina, Analogs of Carleman's formula for classical domains, *Math. Notes*, **45**(1989), no. 3, 243–248

[8] A.M.Kytmanov, T.N.Nikitina, Multidimensional Carleman formulas in Siegel domains, *Russian Math. (Iz. VU)*, **34**(1990), no. 3, 50–5.

[9] G.Khudaiberganov, A formula of Carleman for functions of matrices, *Siberian Math. J.*, **29**(1988), no. 1, 159–160.

[10] G.Khudayberganov, A.M.Kytmanov, B.A.Shaimkulov, Analysis in matrix domains, Siberian Federal University, Krasnoyarsk, 2017 (in Russian).

[11] S.Kosbergenov, On the Carleman formula for a matrix ball, *Russian Math. (Iz. VUZ)*, **43**(1999), no. 1, 72–75

[12] B.A.Shoimkhulov, J.T.Bozorov, Carleman's Formula for a Matrix Polydisc, *J. Sib. Fed. Univ. Math. Phys.*, **8**(2015), no. 2, 371–374.

[13] L. N. Znamenskaya, Generalization of the theorem of F. and M. Riesz and the existence of the multidimensional Carleman formula, Siberian Math. J., **29**(1988), no. 4, 573–577.

[14] J.Sh.Abdullayev, K.Sh.Ruzmetov, Z.K.Matyakubov, Carleman's Integral Formula in Cartesian Product of Matrix Upper Half-Plane, *Azerbaijan Journal of Mathematics*, **14**(2024), no. 2, 36–45. DOI: 10.59849/2218-6816.2024.2.36

[15] P.Lancaster, Theory of Matrices, Academic Press, New York, 1969, 45–49.

[16] L.K.Hua, Harmonic Analysis of Functions of Several Complex Variables in Classical Domains, Inostrannaya Literatura, Moscow, 1963 (in Russian)

[17] R.Bellman, *Introduction to Matrix Analysis*, McGraw-Hill, New York, 1970.

[18] J.A.Lappo-Danilevski, Application of functions from matrices to the theory of linear systems of ordinary differential equations, Introduction and editing by academician V. I. Smirnov, State publishing house of technical and theoretical literature, Moscow, 1957 (in Russian]).

Об одной формуле Карлемана в $\mathbb{C}^n\,[m \times m]$

Гулмирза Г. Худайберганов
Национальный университет Узбекистана
Ташкент, Узбекистан
Барлыкбай Б. Пренов
Нукусский государственный педагогический институт имени Ажинияза
Нукус, Республика Каракалпакстан, Узбекистан
Жонибек Ш. Абдуллаев
Ургенчский государственный университет
Ургенч, Узбекистан
Кудрат Ш. Рузметов
Ташкентский государственный аграрный университет
Ташкент, Узбекистан

Аннотация. В работе рассмотрена интегральная формула Карлемана для функции от матриц, в пространстве $\mathbb{C}^n\,[m \times m]$. Полученная формула является обобщением результата Г. Худайберганова.

Ключевые слова: формула Карлемана, голоморфная функция, пространство Харди, голоморфное продолжение, матричный единичный круг, автоморфизм.

EDN: JHXRSH
УДК 543.424

Raman Spectroscopy Method for Assessing the Degree of Demineralisation of Xenomaterials During their Manufacture

Pavel E. Timchenko[*]
Elena V. Timchenko[†]
Institute of Informatics and Cybernetics
Samara University
Samara, Russian Federation
E. V. Pisareva[‡]
Samara University
Samara, Russian Federation
Oleg O. Frolov[§]
Institute of Informatics and Cybernetics
Samara University
Samara, Russian Federation
A. A. Gnedova[¶]
R. T. Samigullin[‖]
Samara University
Samara, Russian Federation
Larisa T. Volova[**]
M. Y. Vlasov[††]
Samara State Medical University
Samara, Russian Federation

Received 02.10.2024, received in revised form 08.11.2024, accepted 24.03.2025

Abstract. This article presents the results of spectral studies of xenomaterials obtained from different sources and at different degrees of demineralisation. Samples of the mineral component of bone were obtained from dental xenomaterials after demineralization in hydrochloric acid with the degree of normality 1.8 n, 2.4 n. All investigations were carried out using Raman spectroscopy. An extended analysis of the xenomaterials during their manufacture was carried out as a result of the investigations. By means of Raman spectroscopy it was established that the yield of mineral components during demineralization occurs more effectively from the Chisels when using hydrochloric acid with concentration of 2.4 n, which allows to optimize the xenomaterials manufacturing process.

Keywords: raman spectroscopy, xenomaterials, bone mineral component, demineralisation, xenomaterial production.

Citation: P.E. Timchenko, E.V. Timchenko, E.V. Pisareva, O.O. Frolov, A.A. Gnedova, R.T. Samigullin, L.T. Volova, M.Y. Vlasov, Raman Spectroscopy Method for Assessing the Degree of Demineralisation of Xenomaterials During their Manufacture, J. Sib. Fed. Univ. Math. Phys., 2025, 18(4), 491–497. EDN: JHXRSH.

[*]timpavel@mail.ru https://orcid.org/0000-0003-3089-7966
[†]lazer-optics.timchenko@mail.ru https://orcid.org/0000-0002-0539-7989
[‡]pisareva@mail.ru https://orcid.org/0000-0003-4995-5839
[§]frolov679@mail.ru https://orcid.org/0000-0002-3225-8511
[¶]gnedova@yandex.ru
[‖]samigullin@yandex.ru
[**]l.t.volova@samsmu.ru https://orcid.org/0000-0002-8510-3118
[††]vlasov@mail.ru https://orcid.org/0000-0002-5867-5727

Introduction

Currently, the problem of obtaining various biomaterials from supporting connective tissues capable of providing conductive and osteoinductive properties of the natural matrix is topical. These materials can be used in various branches of medicine: dentistry, traumatology and orthopaedics, maxillofacial surgery [1]. Dental tissues are promising and accessible sources that can be used to correct disorders of bone metabolism and mineral homeostasis. Bone mineral content (BMC) is obtained by demineralisation of human and animal dental tissues. It is used to fill defects after injuries and traumas, in endoprosthetics in dentistry, to regulate metabolic processes by exogenous introduction into the body, has pronounced osteoinductive properties due to preserved bone morphogenetic proteins. Also this material can be used as a component of toothpastes and various professional dental compositions for prevention of caries and destructive processes of tooth enamel, because the mineral component of dental tissues along with the hexagonal crystalline structure of hydroxyapatite (HAP) contains an amorphous phase, which has the best adhesion to enamel [2]. This raises the need to assess the quality of xenogeneic bone-plastic materials from animal teeth. Optical methods are one of the most common operational methods for evaluating biomaterials for various purposes [3, 4–5]. Among them, Raman spectroscopy [3], IR spectroscopy [4], energy dispersive X-ray fluorescence analysis, atomic adsorption analysis and scanning electron microscopy are widely used to assess the composition of biomaterials [5]. For example, in [3], single crystals of synthetic hydroxyapatite were studied by the method of orientation micro-Raman spectroscopy, as a result, it was found that the crystallites in the studied region have a high orientation. In [4], the analysis using Fourier transform infrared spectroscopy was performed on hydroxyapatite doped with europium, then the antimicrobial activity of nanoparticles of hydroxyapatite doped with europium depends on the concentration of europium. In [5], samples of hydroxyapatite of various species of wild and domestic animal species, as well as humans, were studied using a complex of methods of electron microscopy and atomic adsorption analysis. It was found that bone hydroxyapatite samples contain trace elements, and the mass ratio of calcium and phosphorus corresponds to their ratio in native bone tissue. Images of the microstructure of the surface of hydroxyapatite obtained from the bone tissue of some animals and energy dispersion analysis data reflecting the composition of the samples are presented. Purpose of the work: evaluation of the demineralisation efficiency of xenomaterials of different origin using Raman spectroscopy.

Materials and methods of research

The objects of the study were groups of BMC samples manufactured using the Lioplast® technology from the teeth of Bos taurus cow (TU-9398-001-01963143-2004). The dental material was mechanically cleaned of soft tissues, poured into a 3% hydrogen peroxide solution and left for a day at room temperature, then the solution was drained. The samples were then infused with an alcohol-ether mixture, left for 24 hours at room temperature, then the solution was drained and each tooth was washed with distilled water. The samples were then dried on filter paper. Hydrochloric acid in two concentrations (1.8 n and 2.4 n) was used for demineralisation, with a change once every three days. Teeth for the study were divided into 2 main groups according to the degree of demineralization in hydrochloric acid: group 1 — demineralized in 1.8 n HCl, group 2 — demineralized in 2.4 n HCl. In each group, cow molars and incisors were used to make MCIs. The MIC samples were obtained by sodium hydroxide precipitation followed by washing with distilled water, centrifugation and drying in a drying oven at 180 C for 3 hours. Raman spectroscopy was used as the main method of xenomaterials investigation, implemented by high resolution digital spectrometer AndorShamrockSR-303i with built-in cooled chamber DV420A-OE providing spectral resolution of 0.15 nm and fibre optical probe for Raman spectroscopy RPB785, combined with LuxxMaster LML-785 laser module. 0RB-04 (up to 500 mW,

wavelength 785 nm) [6]. The spectra were taken at three different points and averaged using the Wolframmathematica software package.[7] Linear discriminant analysis in IBM SPSS Statistics software environment was performed for the obtained split CR spectra. A biochemical analysis of the calcium ion concentration in the demineralising solution was performed as an additional method of investigation.

Analysis

Fig. 1 shows the results of the Raman studies of xenomaterial samples. With different degrees of demineralisation depending on the sample types changes in the CD amplitude are observed in the lines 956 cm^{-1} (PO,P-O symmetrical valence), 1071 cm^{-1} (CO_3^{2-},C-O flat valence), 1129–1242 cm^{-1} (Amide III (C-N-H stretching) bending N-H). No significant changes are observed in the other Raman lines. These changes are due to the peculiarities of the enamel structure of molars and incisors.

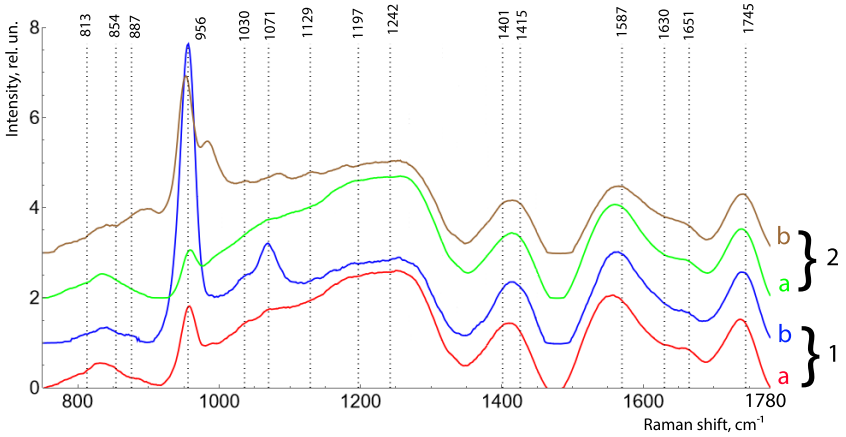

Fig. 1. Averaged Raman spectra of xenomaterials obtained at degree of demineralisation: 1 — 1.8 n and 2 — 2.4 n; by origin a — Molar, b — Chisel

Fig. 1 shows that in xenomaterials derived from molars there is a 956 cm^{-1} decrease in phosphate line intensity (PO_4^{3-}, P-O symmetrical valence) both at 1.8 n acid concentration and at 2.4 n and respectively the line intensity ratio changes at 956 cm^{-1} (PO_4^{3-}, P-O symmetrical valence) and 1071 cm^{-1} (CO_3^{2-}, C-O flat valence), indicating mineral component leaching during demineralisation of xenomaterials. It can be seen that at an acid concentration of 2.4 n, the mineral components are almost completely leached, indicating that the demineralisation process is effective. In contrast, the xenomaterials obtained from incisors show a more saturated content of mineral components. Fig. 1 shows that at acid concentration of 2.4 n the xenomaterials obtained from the incisors are highly mineralized, as evidenced by the CD line intensity at 956 cm^{-1} (PO_4^{3-} (ν_4), P-O symmetric valence). To increase the information content of obtained Raman spectra a non-linear regression analysis of spectra was performed consisting of their decomposition into spectral lines. Fig. 2 shows the result of spectral contour decomposition into the sum of Gauss line distributions. The mean value of the coefficient of determination of the resulting spectrum from the baseline in the range 800-1780 cm^{-1} was R2 = 0.99, the relative error in the intensity of spectral lines a does not exceed 5%, the mean standard deviation of line coordinate x0 is 1 cm^{-1}, the mean standard deviation of line width (HWHM) of Gauss dx is 1 cm^{-1}. In Fig. 3(A), 12 spectra with a degree of demineralisation of 1.8n are analysed. The LD-1 discriminant function describes the variance by 100%. Positive LD-1 values are more common in

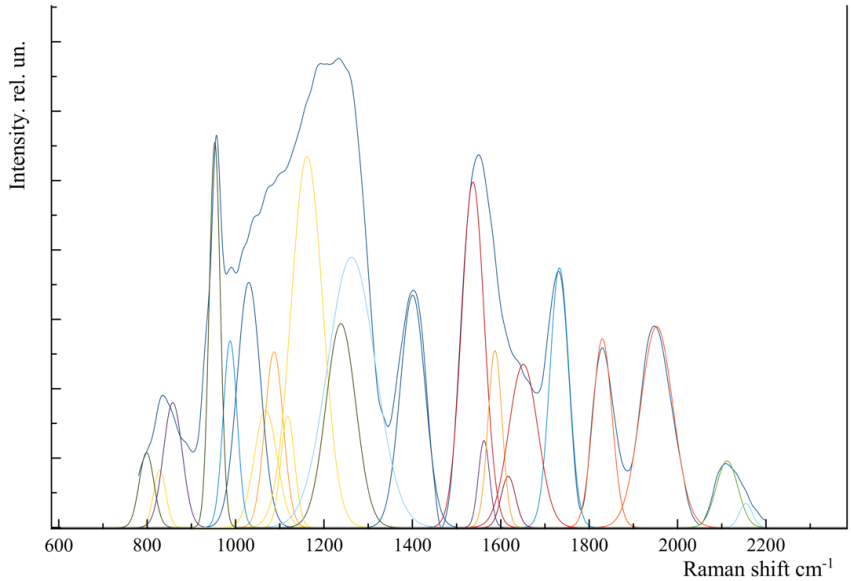

Fig. 2. Spectral contour decomposition of the BMC samples

the CR spectra of incisors. Negative ones for molars. In Fig. 3(B), 18 spectra with a degree of demineralisation of 2.4 n are analysed. The discriminant function LD-1 describes the variance at 100%. Positive LD-1 values are more common in the CR spectra of incisors. Negative values for molars. Fig. 4 shows the coefficients of the factor structure matrix with the physical meaning of the correlation between the variables in the model and the discriminatory function. The higher in modulo the LD-1 value for a variable, the more it determines the difference in the discriminatory model between groups of samples. It is also clear from the extended analysis that xenomaterials from molars are not completely demineralised by grade 2,4 acid. These changes are due to the peculiarities of the enamel structure of molars and incisors. Enamel hydroxyapatite has a highly crystalline calcium phosphate structure, which is less susceptible to degradation, making incisor enamel denser and more saturated with mineral components. In [8], differences in the organic and inorganic composition of enamel and dentin of human, cattle, pigs and sheep teeth were established, which should be taken into account when interpreting the results of studies using xenogenic animal materials as bioimplants. Human and bovine dental tissues were the most similar in composition. An important issue is the selection of the optimum acid concentration for rapid but gentle demineralisation. The rate of demineralisation is also highly dependent on the density and structure of the specimens (it is more convenient to estimate this from the calcium concentration in the solution). A more intensive yield of mineral elements compared to molars is noted from incisors, which is due to the peculiarities of their enamel structure and thickness [9], as well as when using acid with a concentration of 2.4 n relative to the concentration of 1.8 n (Fig. 5). Therefore, when obtaining the mineral component from xenomaterials, incisors and a hydrochloric acid concentration of 2.4 n are preferable for demineralisation.

Conclusions

As a result of this research, an extended analysis of xenomaterial samples during their demineralisation has been carried out. The spectral changes of xenomaterial samples at different degrees of demineralisation have been established. It is shown that full demineralization of xenomaterials occurs at a degree of 2.4 as evidenced by the decrease of CD intensity at 956 cm^{-1}

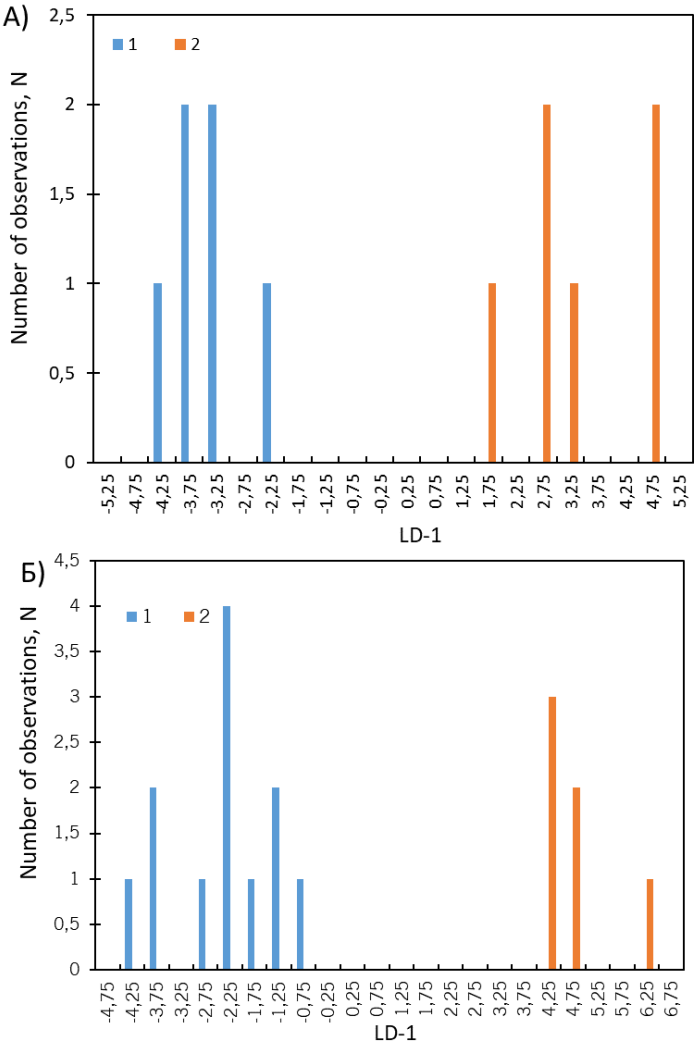

Fig. 3. Graph of values of linear discriminant function of xenomaterials samples: 1 — Molars; 2 — Incisors. A) with degree of demineralisation 1.8 n; B) with degree of demineralisation 2.4 n

(PO_4^{3-},P-O symmetric valence), 1071 cm^{-1} (CO_3^{2-},C-O flat valence) lines. Thus, using Raman spectroscopy, it was found that xenomaterials derived from incisors are preferable for the mineral component because the demineralisation of molars is slower. The results were confirmed by biochemical analysis.

References

[1] S.Chavda, L.Levin, Human studies of vertical and horizontal alveolar ridge augmentation comparing different types of bone graft materials: a systematic review, *J. Oral. Implantol.*, **44**(2018), no. 1, 74–84. DOI: 10.1563/aaid-joi-D-17-00053

[2] A.Agics, I.Gera, A.Sculean, et al., Ten-year results following treatment of intrabony defects with an enamel matrix protein derivative combined with either a natural bone mineral or a

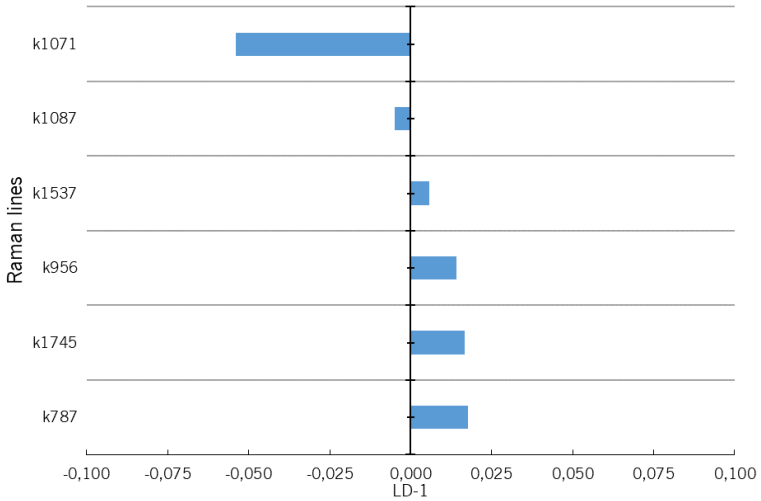

Fig. 4. Factor structure coefficient values

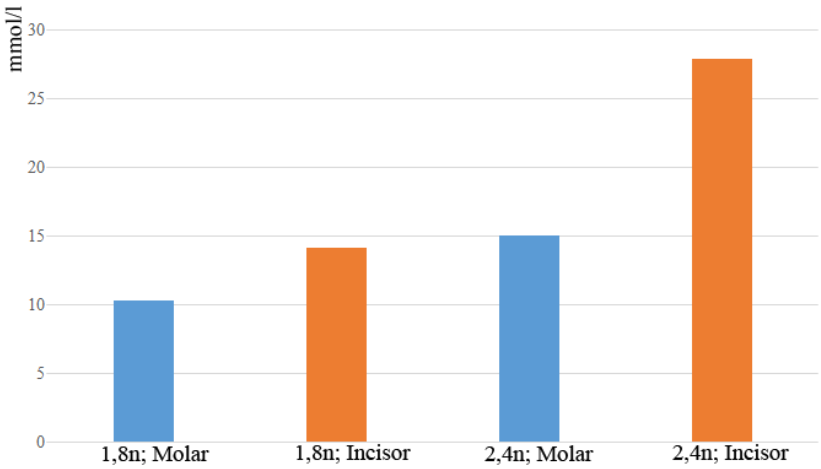

Fig. 5. The concentration of calcium ions in the solution at the end of demineralisation

β-tricalcium phosphate, *J. Periodontol.*, **84**(2013), no. 6, 749–757.
DOI: 10.1902/jop.2012.120238

[3] H.Tsuda, J.Arends, Orientational micro-Raman spectroscopy on hydroxyapatite single crystals and human enamel crystallites, *J. Dent. Res.*, **73**(1994), no. 11, 1703–1710.
DOI: 10.1177/00220345940730110501

[4] Simona-Liliana Iconaru, Mikael Motelica-Heino, Daniela Predoi, Study on Europium-Doped Hydroxyapatite Nanoparticles by Fourier Transform Infrared Spectroscopy and Their Antimicrobial Properties, *Journal of Spectroscopy*, **2013**(2013).

[5] E.V.Pisareva, V M.Y.lasov, L.T.Volova, The structure and properties of biomaterials based on the mineral component of bone tissue, Modern problems of science and education, no. 5, 2015.

[6] E.V.Timchenko, P E.Timchenko, E.V.Pisareva, et al., Spectral Analysis of Rat Bone Tissue During Long Antiorthostostatic Hanging and at Introduction of Allogen Hydroxyapatitis, Optics and Spectroscopy, **128**(2020), no. 7, 989–997. DOI: 10.1134/S0030400X20070243

[7] E.Timchenko, P.Timchenko, L.Volova, O.Frolov, M.Zibin, I.Bazhutova, Raman spectroscopy of changes in the tissues of teeth with periodontitis, *Diagnostics*, **10**(2020), no. 11. DOI: 10.3390/diagnostics10110876

[8] A.J.Ortiz-Ruiz, J.D.Teruel-FernGundez, L.A.Alcolea-Rubio, A.HernGundez-FernGundez, Y.Martínez-Beneyto, F.Gispert-Guirado, Structural differences in enamel and dentin in human, bovine, porcine, and ovine teeth, *Ann. Anat.*, (2018), 7–17. DOI: 10.1016/j.aanat.2017.12.012

[9] K.Elhennawy, D.J.Manton, F.Crombie, et al., Structural, mechanical and chemical evaluation of molar-incisor hypomineralization-affected enamel: a systematic review, *Arch. Oral Biol*, **83**(2017), 272–281. DOI: 10.1016/j.archoralbio.2017.08.008

Метод спектроскопии комбинационного рассеяния для оценки степени деминерализации ксеноматериалов при их изготовлении

Павел Е. Тимченко
Елена В. Тимченко
Институт информатики и кибернетики
Самарский университет
Самара, Российская Федерация
Елена В. Писарева
Самарский университет
Самара, Российская Федерация
Олег О. Фролов
Институт информатики и кибернетики
Самарский университет
Самара, Российская Федерация
Алина А. Гнедова
Равиль Т. Самигуллин
Самарский университет
Самара, Российская Федерация
Лариса Т. Волова
Михаил Ю. Власов
Самарский государственный медицинский университет
Самара, Российская Федерация

Аннотация. В данной статье представлены результаты спектральных исследований ксеноматериалов, полученных из разных источников и при разной степени деминерализации. Образцы минерального компонента кости получены из дентальных ксеноматериалов после деминерализации в соляной кислоте со степенью нормальности 1.8 н, 2.4 н. Все исследования проводились с помощью метода Рамановской спектроскопии. В результате исследований был проведен расширенный анализ ксеноматериалов в процессе их изготовления. С помощью спектроскопии комбинационного рассеяния установлено, что выход минеральных компонентов при деминерализации происходит эффективнее из резцов при использовании соляной кислоты концентрацией 2,4 н, что позволяет оптимизировать процесс изготовления ксеноматериалов.

Ключевые слова: спектроскопия комбинационного рассеяния, ксеноматериалы, минеральный компонент кости, деминерализация, изготовление ксеноматериалов.

EDN: PPDPXM
УДК 512.542, 514

On Regular Polytopes of Rank 3

Bek B. Baktybekov*
Siberian Federal University
Krasnoyarsk, Russian Federation
Marston D. E. Conder†
Department of Matheematics
University of Auckland
Auckland, New Zealand
Yakov N. Nuzhin‡
Anna V. Rezantseva§
Siberian Federal University
Krasnoyarsk, Russian Federation

Received 02.11.2024, received in revised form 18.02.2025, accepted 24.03.2025

Abstract. It is proved that if a finite group G is generated by three involutions α, β and γ, such that α and γ commute, and the orders of the products $\alpha\beta$ and $\beta\gamma$ are greater than 2, then the generating set $\{\alpha, \beta, \gamma\}$ makes G the automorphism group of a regular 3-polytope if and only if the intersection $\langle\alpha\beta\rangle \cap \langle\beta\gamma\rangle$ contains no non-trivial normal subgroup of G, and the intersection $\langle\alpha, \beta\rangle \cap \langle\beta, \gamma\rangle$ is not an elementary abelian subgroup of order 4. This criterion complements a theorem by M. Conder and D. Oliveros (J. Combin. Theory Ser. A, 2013, v. 120, no. 6, pp. 1291–1304

Keywords: regular polytopes, string C-groups, generating triples of involutions.

Citation: B.B. Baktybekov, M.D.E. Conder, Ya.N. Nuzhin, A.V. Rezantseva, On Regular Polytopes of Rank 3, J. Sib. Fed. Univ. Math. Phys., 2025, 18(4), 498–505. EDN: PPDPXM.

Introduction

Groups generated by three involutions, two of which commute, have found various applications in graph theory and discrete geometry, such as Cayley graphs [5] and edge-transitive maps [3]). In considering conditions for the existence of regular polytopes of small ranks, M. Conder and D. Oliveros established the following theorem:

Theorem A [2, Theorem 4.1]. *Let G be a finite group generated by three involutions α, β and γ, such that α and γ commute, and the orders of the products $\alpha\beta$ and $\beta\gamma$ are greater than 2. Then either G is the automorphism group of a regular 3-polytope, or G has a non-trivial cyclic normal subgroup N contained in $\langle\alpha\beta\rangle$ or $\langle\beta\gamma\rangle$.*

Examples show that both of the two possible conclusions of Theorem A can be satisfied simultaneously. More specifically, there exist groups that are automorphism groups of regular

*baktybekovbek04@gmail.com
†m.conder@auckland.ac.nz
‡nuzhin2008@rambler.ru
§annavr042@gmail.com

3-polytopes and yet also contain distinct non-trivial normal subgroups N_1 and N_2 lying respectively in $\langle\alpha\beta\rangle$ and $\langle\beta\gamma\rangle$; see Example 2 in Section 4 below.

We have obtained the following criterion for the existence of a 3-polytope with a given automorphism group, which complements Theorem A:

Theorem B. *Let G be a finite group generated by three involutions α, β and γ, such that α and γ commute, and the orders of the products $\alpha\beta$ and $\beta\gamma$ are greater than 2. Then the generating set $\{\alpha, \beta, \gamma\}$ makes G the automorphism group of a regular 3-polytope if and only if the intersection $\langle\alpha\beta\rangle \cap \langle\beta\gamma\rangle$ contains no non-trivial normal subgroup of G, and the intersection $\langle\alpha, \beta\rangle \cap \langle\beta, \gamma\rangle$ is not elementary abelian of order 4.*

This theorem is proved in Section 3, following some preliminary observations (including background theory) in Section 2, and then some associated examples are presented in Section 4, and some consequences are given in Section 5.

Note that the finiteness condition for G in Theorem B (above) and Corollaries 1 and 2 (in Section 5) can be replaced by the weaker condition that the orders of the products $\alpha\beta$ and $\beta\gamma$ are greater than 2 and finite, since only this weakened finiteness condition is used in the proofs.

1. Preliminary observations

An *abstract n-polytope* $\mathbf{P}$ is a partially ordered set with strictly monotone rank function having range $\{-1, 0, 1, \ldots, n\}$, and satisfying the axioms (P1) to (P4) below.

In this context, an element $F \in \mathbf{P}$ of rank j is called a *j-face* and is often denoted by F_j. Any two faces F_j and G_j of the same rank j are incomparable. A *flag* of $\mathbf{P}$ is a maximal chain in $\mathbf{P}$, and two flags of $\mathbf{P}$ are said to be *adjacent* if they differ in exactly one element. For example, the flags $\Phi = \{F_{-1}, F_0, F_1, F_2\}$ and $\Psi = \{F_{-1}, G_0, F_1, F_2\}$ are adjacent for the polytope in Fig. 1.

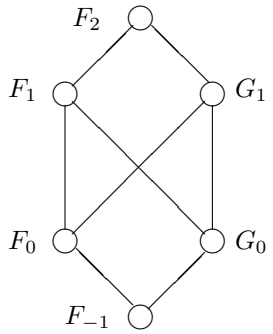

Fig. 1. A polytope of rank 2

The required properties (P1) to (P4) are as follows:

(P1) In $\mathbf{P}$ there exists a least element F_{-1} and a greatest element F_n. These two elements are called *improper* faces, while all other faces are called *proper*.

(P2) Each flag of $\mathbf{P}$ contains exactly $n + 2$ faces, including F_{-1} and F_n.

(P3) If F and H are any two faces of respective ranks $j-1$ and $j+1$ with $F < H$ in $\mathbf{P}$, then there exist exactly two faces G of rank j in $\mathbf{P}$ such that $F < G < H$. This is called the *homogeneity condition*, or *diamond condition*.

(P4) For every two flags Φ and Ψ in $\mathbf{P}$, there exists a sequence $\Phi = \Phi_0, \Phi_1, \ldots, \Phi_k = \Psi$ of flags in $\mathbf{P}$ such that Φ_{i-1} and Φ_i are adjacent for $1 \leqslant i \leqslant k$, and $\Phi \cap \Psi \subseteq \Phi_i$ for $0 \leqslant i \leqslant k$. This condition is called *strong (flag)-connectedness*.

Two abstract polytopes $\mathbf{P}$ and $\mathbf{Q}$ are said to be *isomorphic* if there exists an order-preserving bijection $\theta : \mathbf{P} \to \mathbf{Q}$, and then the automorphism group $Aut(\mathbf{P})$ of the polytope $\mathbf{P}$ is naturally defined as the group of all such bijections from $\mathbf{P}$ to itself. This group permutes the flags of $\mathbf{P}$, and preserves the set of its j-faces, for $0 \leqslant j \leqslant n$.

The number n is called the *rank* of the polytope, and we assume that $n \geqslant 1$. Obviously, up to isomorphism, a polytope of rank 1 is unique, namely as in Fig. 2.

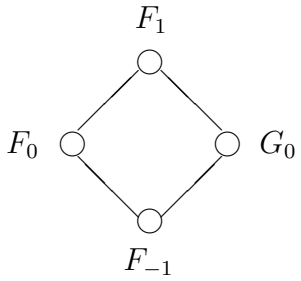

Fig. 2. A polytope of rank 1

The diamond condition (P3) and strong connectedness (P4) imply that every automorphism of $\mathbf{P}$ is uniquely determined by its effect on any given flag, and it follows that the number of automorphisms of $\mathbf{P}$ is bounded above by the number of flags of $\mathbf{P}$. If this upper bound is attained, then $Aut(\mathbf{P})$ acts transitively and hence regularly on flags, and in that case the abstract n-polytope $\mathbf{P}$ is said to be *regular*.

Next, a group G is called a *C-group* if it is generated by a set of involutions $I = \{\rho_0, \ldots \rho_{n-1}\}$ which satisfy the following, known as the *Intersection Condition*:

$$\langle \rho_i \mid i \in J \rangle \cap \langle \rho_i \mid i \in K \rangle = \langle \rho_i \mid i \in J \cap K \rangle \text{ for all subsets } J \text{ and } K \text{ of } \{0, 1, \ldots, n-1\}. \quad (1)$$

Note that taking J and K to be singletons implies that the involutions in I must be distinct. Such a group is called a *string C-group*, or an *n-string group*, or simply a *string group*, if also

$$(\rho_i \rho_j)^2 = 1 \text{ for } |i - j| \geqslant 2, \quad (2)$$

or in other words, if its Coxeter graph is a string (chain). A string group is said to be *irreducible* if every two neighbouring vertices ρ_{i-1} and ρ_i of its Coxeter graph do not commute, that is, if $\rho_{i-1}\rho_i$ has order greater than 2, for $1 \leqslant i < n$.

The following two facts about string groups are obvious:

Lemma 1. *The direct product of two string groups is a string group.*

Lemma 2. *If $I = \{\rho_0, \ldots \rho_{n-1}\}$ is the generating set for the n-string group G, then for $0 \leqslant r < s < n$, the subgroup generated by $\{\rho_r, \rho_{r+1} \ldots, \rho_s\}$ is an $(s - r + 1)$-string group.*

Now let k_i be the order of the product of the involutions ρ_{i-1} and ρ_i, for $1 \leqslant i < n$. Then the ordered set $[k_1, k_2, \ldots, k_{n-1}]$ of natural numbers is called the *type* of the n-string group G.

The following fundamental lemma gives a strong relationship between string groups and regular polytopes, as explained for example in [4, Section 2E].

Lemma 3. *The automorphism group Aut(**P**) of every regular polytope **P** is a string group. Moreover, there is a one-to-one correspondence between regular n-polytopes and n-string groups.*

The correspondence in Lemma 3 can be realised as follows. Let $G = \langle \rho_0, \rho_1, \ldots \rho_{n-1} \rangle$ be an n-string group, so that conditions (1), (2) are satisfied, and define $H_i = \langle \rho_j \mid j \neq i \rangle$ for $0 \leqslant i < n$. We may introduce a partial order on the set of all right cosets of all the subgroups H_i by setting

$$H_i u \leqslant H_j v \quad \text{if and only if} \quad i \leqslant j \ \text{ and } \ H_i u \cap H_j v \neq \emptyset.$$

Adding the identity subgroup $\{1\}$ as a unique minimal element and the group G itself as a unique maximal element, we obtain a regular polytope $\mathbf{P} = \mathbf{P}(G)$, with flags

$$\{1\} \ < \ H_0 g \ < \ H_1 g \ < \ \ldots \ < \ H_{n-1} g \ < \ G$$

as g ranges through all elements of G. The automorphism group of $\mathbf{P}$ is the group G, which acts by right multiplication on the elements of $\mathbf{P}$.

In what follows, we denote by C_m the cyclic group of order m, and by D_m the dihedral group of order $2m$.

Example 1. The dihedral group D_6 is a 2-string group with type [6], and by Lemma 3 is the automorphism group of a regular polytope of rank 2 (namely the regular hexagon). But also D_6 is isomorphic to $D_3 \times C_2$, which is a reducible 3-string group with type $[3, 2]$, and hence is the automorphism group of a regular polytope of rank 3. This shows that a group can be the automorphism group of two non-isomorphic regular polytopes, even two such polytopes with different types and ranks.

Example 1 shows that a dihedral group can be a reducible 3-string group. But also the following holds.

Lemma 4. *A finite dihedral group is not an irreducible n-string group, for any $n \geqslant 3$.*

Proof. By Lemma 2 and the fact that every subgroup of a finite dihedral group is either cyclic or dihedral, it suffices to prove this for $n = 3$. So let G be the dihedral group $D_m = \langle\, u, v \mid u^2 = v^2 = (uv)^m = 1 \,\rangle$, and suppose (in aiming to prove the contrary) that G is an irreducible 3-string group with respect to a triple $T = \{\alpha, \beta, \gamma\}$ of three generating involutions such that α and γ commute. Then m must be even (so that $\alpha\gamma$ has order 2), and furthermore, in order for $\alpha\beta$ and $\beta\gamma$ to have order greater than 2, we see that $m \geqslant 4$, and G has a unique central involution, namely $z = (uv)^{m/2}$, and $z \notin T$.

Now every involution in $G = D_m$ is either equal to $z = (uv)^{m/2}$, or has the form $u(uv)^k$ where $0 \leqslant k < m$. Also it is both well known and easy to prove that the centraliser in D_m of any non-central involution w is the subgroup $\langle w, wz \rangle$, of order 4. As $z \notin T$, we may now suppose without loss of generality that $\alpha = u$ and $\gamma = uz$, and then $\beta = u(uv)^k$ for some k. Clearly the involution u normalises $\langle u, u(uv)^k \rangle = \langle \alpha, \beta \rangle$, and therefore so does $uz = \gamma$. Thus $\langle \alpha, \beta \rangle$ has index 1 or 2 in G, and so must be the unique dihedral subgroup of order m or $2m$ in G. Similarly u centralises $uz = \gamma$, and as $\beta^u = (\beta^u)^z = \beta^\gamma$, we find that u normalises $\langle \beta, \gamma \rangle$, which must also be the unique dihedral subgroup of of order m or $2m$ in G. Hence in particular, $\langle \alpha, \beta \rangle \cap \langle \beta, \gamma \rangle$ contains that dihedral subgroup, contradicting the intersection condition (1).

This completes the proof. □

2. Proof of Theorem B

Let the group G and its involutory generators α, β and γ be as in the statement of Theorem B, with associated Coxeter graph as in Fig. 3, and let $L = \langle \alpha, \beta \rangle$ and $M = \langle \beta, \gamma \rangle$, which are dihedral subgroups of orders $2l$ and $2m$, say.

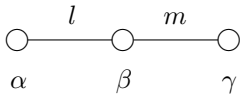

Fig. 3

Here (and for later) we list three conditions that may hold in the formulation of Theorem B:

(a) The generating set $\{\alpha, \beta, \gamma\}$ makes G the automorphism group of a regular 3-polytope.

(b) The intersection $\langle \alpha\beta \rangle \cap \langle \beta\gamma \rangle$ contains a non-trivial normal subgroup of G.

(c) The intersection $\langle \alpha, \beta \rangle \cap \langle \beta, \gamma \rangle$ is an elementary abelian subgroup of order 4.

We can now proceed as follows.

If $L \cap \langle \gamma \rangle = \{1\}$ and $M \cap \langle \alpha \rangle = \{1\}$ and $L \cap M = \langle \beta \rangle$, then G is a 3-string group and so condition (a) holds.

So now suppose that G is not a 3-string group. Then either $L \cap \langle \gamma \rangle \neq \{1\}$, or $M \cap \langle \alpha \rangle \neq \{1\}$, or $L \cap M \neq \langle \beta \rangle$.

In the first case (where $L \cap \langle \gamma \rangle \neq \{1\}$), we find that $\gamma \in L = \langle \alpha, \beta \rangle$ and so $G = \langle \alpha, \beta, \gamma \rangle = L$, and therefore G itself is dihedral of order 2ℓ. Also $M = \langle \beta, \gamma \rangle \leqslant \langle \alpha, \beta \rangle = L = G$, and so $\langle \beta\gamma \rangle$ is not only a cyclic normal subgroup of the dihedral subgroup $\langle \beta, \gamma \rangle = M$, but also a subgroup of the cyclic normal subgroup $\langle \alpha\beta \rangle$ of the dihedral group $L = G$, and so itself is a cyclic normal subgroup of G. Hence the intersection $\langle \alpha\beta \rangle \cap \langle \beta\gamma \rangle$ contains a non-trivial normal subgroup of G, so condition (b) holds. The analogous argument holds in the second case (where $M \cap \langle \alpha \rangle \neq \{1\}$), again showing that condition (b) holds.

This leaves the third case, namely where $L \cap M \neq \langle \beta \rangle$. In this case there exists an element $g \in L \cap M$ distinct from 1 and β, and by the symmetry of occurrences of the involutions α and γ, we have three sub-cases to consider:

(1) $g = (\alpha\beta)^j = (\beta\gamma)^k$,

(2) $g = (\alpha\beta)^j\beta = (\beta\gamma)^k\beta$, or

(3) $g = (\alpha\beta)^j = (\beta\gamma)^k\beta$, where $1 \leqslant j < l = o(\alpha\beta)$ and $1 \leqslant k < m = o(\beta\gamma)$.

In all three sub-cases, let $N = \langle g \rangle$.

In sub-case (1), all three of the involutions α, β, and γ invert g, so $N = \langle g \rangle$ is normal in G, and then since N lies in both $\langle \alpha\beta \rangle$ and $\langle \beta\gamma \rangle$, condition (b) is satisfied.

In sub-case (2), we find that $(\alpha\beta)^j = g\beta = (\beta\gamma)^k$, so $g\beta$ is an element of $L \cap M$ distinct from both 1 and β, and therefore sub-case (1) applies, and again condition (b) is satisfied.

Next, consider sub-case (3). Here $(\alpha\beta)^j = g = (\beta\gamma)^k\beta$ which is an involution, so $l = o(\alpha\beta)$ is even, with $j = l/2$, and g is the central involution $(\alpha\beta)^{l/2}$ of $\langle \alpha, \beta \rangle = L$, as well as being an element of $\langle \beta, \gamma \rangle = M$. Similarly $(\alpha\beta)^j\beta = g\beta = (\beta\gamma)^k$ and therefore $m = o(\beta\gamma)$ is even, with $k = m/2$, and $g\beta$ is the central involution $(\beta\gamma)^{m/2}$ of $\langle \beta, \gamma \rangle = M$, as well as being an element of L. Also $g \neq g\beta$ since β is non-trivial. Hence $L \cap M$ contains the two involutions $g = (\alpha\beta)^{l/2}$ and $g\beta = (\beta\gamma)^{m/2}$, with the former being central in L and the latter being central in M, and therefore the subgroup $E := \langle g, \beta \rangle = \langle g, g\beta \rangle$ is elementary abelian of order 4.

Now if $\langle g, \beta \rangle = L \cap M = \langle \alpha, \beta \rangle \cap \langle \beta, \gamma \rangle$, then the intersection $\langle \alpha, \beta \rangle \cap \langle \beta, \gamma \rangle$ is elementary abelian of order 4, as in condition (c). On the other hand, if $\langle g, \beta \rangle \neq L \cap M$, then $L \cap M$ contains

an element h that is not in E. In this case $h = (\alpha\beta)^r$ or $h = (\alpha\beta)^r\beta$ where $1 \leqslant r < n$, but $r \neq j = l/2$, and since $\beta \in L \cap M$, we find that in both cases, $L \cap M$ contains $(\alpha\beta)^r$, which has order greater than 2. In particular, $N = \langle(\alpha\beta)^r\rangle$ must be a cyclic normal subgroup of each of the dihedral subgroups L and M, and hence must be normal in $\langle L, M\rangle = G$, but also being cyclic of order greater than 2, this normal subgroup is contained in the maximal cyclic normal subgroup of each of L and M, namely $\langle\alpha\beta\rangle$ and $\langle\beta\gamma\rangle$, and hence is contained in their intersection $\langle\alpha\beta\rangle \cap \langle\beta\gamma\rangle$, as in condition (b).

Finally, if either (b) or (c) holds, then $\langle\alpha, \beta\rangle \cap \langle\beta, \gamma\rangle$ cannot be $\langle\beta\rangle$, as the latter has order 2 and is not normal in G, and so (a) cannot hold.

This completes the proof.

3. Some examples associated with Theorems A and B

The following example shows that both conclusions of Theorem A can be satisfied at once.

Example 2. Let $\mathbb{F}_4$ be the field of order 4, with t as one of its primitive elements, and then define three unitriangular matrices α, β and γ over $\mathbb{F}_4$ as follows:

$$\alpha = \begin{pmatrix} 1 & 0 & 0 \\ 0 & 1 & 0 \\ 0 & 1 & 1 \end{pmatrix}, \quad \beta = \begin{pmatrix} 1 & 0 & 0 \\ 1 & 1 & 0 \\ 0 & 0 & 1 \end{pmatrix} \quad \text{and} \quad \gamma = \begin{pmatrix} 1 & 0 & 0 \\ 0 & 1 & 0 \\ 0 & t & 1 \end{pmatrix}.$$

These three matrices are involutions, and α and γ commute, and also

$$(\alpha\beta)^2 = \begin{pmatrix} 1 & 0 & 0 \\ 0 & 1 & 0 \\ 1 & 0 & 1 \end{pmatrix} \quad \text{and} \quad (\beta\gamma)^2 = \begin{pmatrix} 1 & 0 & 0 \\ 0 & 1 & 0 \\ t & 0 & 1 \end{pmatrix},$$

so $\alpha\beta$ and $\beta\gamma$ both have order 4.

Now let $G = \langle\alpha, \beta, \gamma\rangle$. Then it is easy to check (using MAGMA [1] for example) that $|G| = 32$, with $\gamma \notin \langle\alpha, \beta\rangle$ and $\alpha \notin \langle\beta, \gamma\rangle$, and that $\langle\alpha, \beta\rangle \cap \langle\beta, \gamma\rangle = \langle\beta\rangle$. Hence G is a 3-string group of type $[4, 4]$, making it the automorphism group of a regular 3-polytope. On the other hand, $\langle(\alpha\beta)^2\rangle$ and $\langle(\beta\gamma)^2\rangle$ are distinct non-trivial normal subgroups of G lying in $\langle\alpha\beta\rangle$ and $\langle\beta\gamma\rangle$ respectively, and generating the centre of G.

For the rest of this section, let G be a finite group generated by three involutions α, β and γ, such that α and γ commute, and the orders of the products $\alpha\beta$ and $\beta\gamma$ are greater than 2.

Below we give three more examples, in each of which at least one of the conditions (b) and (c) from the proof of Theorem B holds, while condition (a) does not hold.

Our first example shows that condition (c) can hold when conditions (a) and (b) do not. There are many other (and similar) examples like this one, including some where the group G has order 60, 84 and 100.

Example 3. Let G be the group of order 36 with presentation

$$\langle\, \alpha, \beta, \gamma \mid \alpha^2 = \beta^2 = \gamma^2 = (\alpha\gamma)^2 = (\alpha\beta\gamma\beta)^2 = \alpha\beta\alpha\gamma\beta\alpha\gamma\beta\gamma = 1 \,\rangle,$$

which has a faithful permutation representation of degree 6 given by $\alpha \to (1, 2)(3, 4)(5, 6)$, $\beta \to (2, 3)(4, 5)$ and $\gamma \to (1, 3)(2, 4)(5, 6)$.

In the latter representation, $\alpha\beta \to (1,3,5,6,4,2)$ and $\beta\gamma \to (1,3,4,6,5,2)$, so the intersection of the cyclic subgroups of order 6 they generate is trivial, and hence this group does not satisfy condition (b). Also the generating triple $\{\alpha,\beta,\gamma\}$ fails the intersection condition for regular polytopes, because the dihedral subgroups of order 12 generated by $\{\alpha,\beta\}$ and $\{\beta,\gamma\}$ intersect in the elementary abelian subgroup of order 4 generated by β and $(\alpha\beta)^3$, with $(\alpha\beta)^3 = \beta(\beta\gamma)^3 \to (1,6)(2,5)(3,4)$. In particular, the latter subgroup of order 4 is the intersection of $\langle\alpha,\beta\rangle$ and $\langle\beta,\gamma\rangle$, so condition (c) is satisfied, while (a) does not.

Our second example is the following.

Example 4. Let u and v be involutions that generate a dihedral group G of order 8. Then G is also generated by the involutions $\alpha = u$, $\beta = v$ and $\gamma = vuv$, where α and γ commute, $\langle\alpha\beta\rangle \cap \langle\beta\gamma\rangle = \langle\alpha\beta\rangle$ and $\langle\alpha,\beta\rangle \cap \langle\beta,\gamma\rangle = G$. Hence condition (b) holds, but (a) and (c) do not.

Finally, our third example shows that (b) and (c) can both hold when (a) does not.

Example 5. Let $G = \langle\alpha,\beta\rangle \times \langle\delta\rangle$, where α,β,δ are involutions, and the order of the product $\alpha\beta$ is 4. Then $G = \langle\alpha,\beta,\gamma\rangle$ where $\gamma = \alpha\delta$, and $\alpha\gamma = \gamma\alpha$ and $(\beta\gamma)^2 = (\beta\alpha\delta)^2 = (\beta\alpha)^2\delta^2 = (\alpha\beta)^2$. Hence G is generated by three involutions α, β, and γ such that α and γ commute and the orders of the products $\alpha\beta$ and $\beta\gamma$ are greater than 2. Moreover, the subgroup $\langle(\alpha\beta)^2\rangle$ lies in the intersection $\langle\alpha\beta\rangle \cap \langle\beta\gamma\rangle$ and is normal in G. On the other hand, $(\alpha\beta)^2, \beta \in \langle\alpha,\beta\rangle \cap \langle\beta,\gamma\rangle$, so the intersection $\langle\alpha,\beta\rangle \cap \langle\beta,\gamma\rangle$ is an elementary abelian subgroup of order 4, and is not equal to $\langle\beta\rangle$.

4. Some consequences of Theorem B

Corollary 1. *Let G be a finite group generated by three involutions α,β and γ, such that α and γ commute, and the orders of $\alpha\beta$ and $\beta\gamma$ are greater than 2, with at least one of them being an odd prime number p. Then exactly one of the following two conditions holds:*

(a) *The generating set $\{\alpha,\beta,\gamma\}$ makes G the automorphism group of a regular 3-polytope.*

(b) *The group G is dihedral, and the order of one of $\alpha\beta$ and $\beta\gamma$ is even (and the other is p).*

Proof. Without loss of generality, we may assume that the order of $\alpha\beta$ is p, and now suppose that condition (a) does not hold. Then by Theorem B either G contains a non-trivial normal subgroup lying in the intersection $\langle\alpha\beta\rangle \cap \langle\beta\gamma\rangle$, or it contains an elementary abelian subgroup of order 4 lying in the intersection $L \cap M$, where $L = \langle\alpha,\beta\rangle$ and $M = \langle\beta,\gamma\rangle$. The latter case is impossible, since L has twice odd order (namely $2p$), so the former holds. Thus $\langle\beta\gamma\rangle$ contains a non-trivial normal subgroup of $\langle\alpha\beta\rangle$, and then since $\alpha\beta$ has odd prime order p, it follows that M contains L, so $G = \langle L, M\rangle = M$, making G dihedral. But also α and γ are distinct commuting involutions in G, so $M = G$ must have twice even order, and therefore $\beta\gamma$ must have even order.

Finally, if G is a dihedral group, then since we have assumed that the orders of $\alpha\beta$ and $\beta\gamma$ are greater than 2, it follows from Lemma 4 that the generating set $\{\alpha,\beta,\gamma\}$ cannot make G the automorphism group of a regular 3-polytope, and this completes the proof. □

The next corollary is an immediate consequence of the one above.

Corollary 2. *Let G be a finite group generated by three involutions α,β and γ, such that α and γ commute, and the orders of $\alpha\beta$ and $\beta\gamma$ are odd integers greater than 2. If at least one of those orders is prime, then the generating set $\{\alpha,\beta,\gamma\}$ makes G the automorphism group of a regular 3-polytope.*

This work was supported by the Krasnoyarsk Mathematical Center and financed by the Ministry of Science and Higher Education of the Russian Federation (Agreement no. 075-02-2025-1790), and also supported by New Zealand's Marsden Fund (project UOA2320). Also some of the observations were assisted or obtained with help from the Magma *system [1].*

References

[1] W.Bosma, C.Cannon, C.Playoust, The Magma algebra system I: The user language, *J. Symbolic Comput.*, **24**(1997), 235–265.

[2] M.Conder, D.Oliveros, The intersection condition for regular polytopes, *J. Combinatorial Theory Series A*, **120**(2013), no. 6, 1291-1304. DOI: 10.1016/j.jcta.2013.03.009

[3] G.A.Jones, Finite simple automorphism groups of edge-transitive maps, *J. Algebra*, **607**(2022), 454–472.

[4] P.McMullen, E.Schulte, *Abstract Regular Polytopes*, Cambridge University Press, Cambridge, 2002.

[5] I.Pak, R.Radoicic, Hamiltonian paths in Cayley graphs, *Discrete Math.*, **309**(2009), 5501–5508. DOI: 10.1016/j.disc.2009.02.018

О регулярных политопах ранга 3

Бек Б. Бактыбеков
Сибирский федеральный университет
Красноярск, Российская Федерация
Марстон Д.Э. Кондер
Университет Окленда
Окленд, Новая Зеландия
Яков Н. Нужин
Анна В. Резанцева
Сибирский федеральный университет
Красноярск, Российская Федерация

Аннотация. Доказано, что если конечная группа G порождается тремя инволюциями α, β и γ, такими что α и γ перестановочны, а порядки произведений $\alpha\beta$ и $\beta\gamma$ больше 2, тогда порождающее множество $\{\alpha, \beta, \gamma\}$ делает G группой автоморфизмов регулярного 3-политопа тогда и только тогда, когда она не содержит нетривиальных нормальных подгрупп, лежащих в пересечении $\langle\alpha\beta\rangle \cap \langle\beta\gamma\rangle$, и пересечение $\langle\alpha, \beta\rangle \cap \langle\beta, \gamma\rangle$ не является элементарной абелевой подгруппой порядка 4. Данный критерий дополняет один результат М. Кондера и Д. Оливерос (J. Combin. Theory Ser. A, 2013, v. 120, no. 6, pp. 1291–1304).

Ключевые слова: регулярные политопы, струнные C-группы, порождающие тройки инволюций.

EDN: JSJXMY
УДК 519

Almost Complete Convergence of Functional Regression Estimator: a Recursive Nonparametric Approach

Hadjer Djeniba*
Mentouri Brothers University
Constantine 1, Algeria
Sarra Leulmi†
MCA Department of Mathematics.
Mentouri Brothers University
Constantine 1, Algeria

Received 10.02.2025, received in revised form 20.03.2025, accepted 24.04.2025

Abstract. We introduce novel families of recursive kernel estimators for the regression function of a real response variable given a random variable that takes values in a semimetric space. Then, we investigate the rate of the almost complete convergence, which is stronger than almost sure convergence. A simulation study is conducted to illustrate the performance of the proposed recursive estimators.

Keywords: almost complete convergence, functional data, kernel estimator, recursive estimator, regression function.

Citation: H. Djeniba, S. Leulmi, Almost Complete Convergence of Functional Regression Estimator: a Recursive Nonparametric Approach, J. Sib. Fed. Univ. Math. Phys., 2025, 18(4), 506–518. EDN: JSJXMY.

Introduction

The nonparametric estimation of regression function for functional data has garnered significant attention in recent years due to its applications in diverse fields, including finance, biometrics, medicine, econometrics, and environmental science. Functional data encompasses information that can be represented as curves, surfaces, or images, rather than traditional scalar values. This complexity necessitates the development of advanced estimation techniques to study the underlying relationships effectively.

One promising nonparametric approach is the use of kernel methods, which provide a flexible framework for estimating regression function. The pioneer work in the nonparametric setting is found in the monograph of [7], where the authors established pointwise almost-complete (a.co.) convergence for various kernel-type estimators. However, while these classical kernel methods are effective, they can be computationally intensive, particularly when dealing with large datasets. In contrast, recursive estimators, as highlighted by [2] and [8], offer significant advantages in computation time and memory efficiency, particularly for large sequential datasets. Unlike the classical kernel estimator defined in [7], these methods allow for iterative updates without the need for full recalculations, making them both practical and easy to implement. This efficiency makes recursive estimators especially suitable for applications like weather forecasting, where the sample size is not fixed in advance.

*djeniba.hadjer@ensc.dz
†sara.leulmi@umc.edu.dz; math17sara@yahoo.fr https://orcid.org/0009-0003-4338-3734

The first results relating to the recursive kernel estimators of the regression function with functional explanatory variables were obtained by [4], where the author adapted the families of recursive estimators studied in [3] for multivariate data to functional data. These families, in turn, generalized previous research by [1, 9, 10], and [6].

In 2014, [4] investigated the mean square error, almost sure convergence with rates, and a central limit theorem for a family of recursive kernel estimates in functional regression when the observations are independent and identically distributed, while [5] extended these results to dependent functional data.

It is clear from the Borel–Cantelli lemma that almost complete convergence is stronger than almost sure convergence. Therefore, we will focus on studying this mode of convergence, which we believe has not been previously explored. More precisely, we first present novel families of recursive kernel estimators for functional regression in Section 2 of our paper. Then, in Section 3, we establish the rate of their almost complete convergence. Finally, the performance and good behavior of the proposed estimators are illustrated through a simulation study.

1. Novel families recursive kernel regression estimators

Consider n pairs of random variables $(X_i, Y_i)_{1\leqslant i\leqslant n}$ independent and identically distributed as the pair (X, Y) which is valued in $\mathcal{F}\times\mathbb{R}$, where $\mathcal{F}$ is an infinite-dimensional space equipped with a semi-metric d.

Using the same idea as in [4], we construct a family of recursive estimators indexed by a smoothing parameter $\ell\in[0,1]$ defined as follows

$$\widehat{r}_n^{[\ell]}(x)=\frac{\sum\limits_{i=1}^{n}\frac{1}{\psi_x^{\ell}(h_i)}K\left(\frac{d(x,X_i)}{h_i}\right)Y_i}{\sum\limits_{i=1}^{n}\frac{1}{\psi_x^{\ell}(h_i)}K\left(\frac{d(x,X_i)}{h_i}\right)},$$

with

$$\psi_x(h_i)=E\left[K\left(\frac{d(x,X_i)}{h_i}\right)\right],$$

where the function K is a kernel and h_n is a given positive sequence decreasing to 0. Notice that the parameter ℓ is used to obtain a more general recursive estimator.

This family of estimators is a recursive modification of the classical regression estimator introduced by [7] and can be computed recursively through

$$\widehat{r}_{n+1}^{[\ell]}(x)=\frac{\left(\sum\limits_{i=1}^{n}\psi_x^{1-\ell}(h_i)\right)\widehat{r}_{n,1}^{[\ell]}(x)+\left(\sum\limits_{i=1}^{n+1}\psi_x^{1-\ell}(h_i)\right)Y_{n+1}K_{n+1}^{[\ell]}(x)}{\left(\sum\limits_{i=1}^{n}\psi_x^{1-\ell}(h_i)\right)\widehat{r}_{n,0}^{[\ell]}(x)+\left(\sum\limits_{i=1}^{n+1}\psi_x^{1-\ell}(h_i)\right)K_{n+1}^{[\ell]}(x)},$$

with

$$\widehat{r}_{n,s}^{[\ell]}(x)=\frac{1}{\left(\sum\limits_{i=1}^{n}\psi_x^{1-\ell}(h_i)\right)}\sum_{i=1}^{n}\frac{1}{\psi_x^{\ell}(h_i)}K\left(\frac{d(x,X_i)}{h_i}\right)Y_i^s,\quad s\in\{0,1\}$$

and

$$K_i^{[\ell]}(x)=\frac{1}{\psi_x^{\ell}(h_i)\sum\limits_{i=1}^{n}\psi_x^{1-\ell}(h_i)}K\left(\frac{d(x,X_i)}{h_i}\right).$$

2. Main results

In this section, we investigate the almost complete convergence of the estimator $\widehat{r}_n^{[\ell]}(x)$ for a fixed $x \in \mathcal{F}$, under the following assumptions.

(H_1) $\forall r > 0, \Phi_x(r) := P\left(d(x, X_i) \leqslant r\right) > 0.$

(H_2) There exists $\exists b > 0$ such that for all $x' \in B(x, h)$,

$$|r(x) - r(x')| \leqslant C_x d^b\left(x, x'\right),$$

where C_x is a positive constant depending on x.

(H_3) The bandwidth h_n satisfies

$$\lim_{n\to\infty} h_n = 0, \text{ and } \lim_{n\to\infty} \sqrt{\frac{\log n}{n\Phi_x(h_n)}} = 0.$$

(H_4) K is a nonnegative bounded function with compact support $[0, 1]$.

(H_5) $\forall m \geqslant 2$, $\sigma_m : x \to E\left(|Y_i|^m \mid X_i\right)$ is a continuous operator at x.

(H_6) $\mathcal{A}_{n,\ell} := \dfrac{1}{n}\sum_{i=1}^{n}\left(\dfrac{h_i}{h_n}\right)^b \left(\dfrac{\Phi_x(h_i)}{\Phi_x(h_n)}\right)^{1-\ell} \to \mathcal{A}_\ell < \infty, \text{ as } n \to \infty.$

Assumptions (H_1)–(H_5) and are standard in nonparametric regression. The assumptions (H_1)–(H_3) and (H_5) were utilized by [7] and align with those commonly employed in functional settings, while, the assumption (H_4) was used by [4]. Furthermore, the condition (H_6) is specific to the recursive problem and is consistent with those used in functional cases.

If X is a fractal process, then the small ball probabilities are of the form $\Phi_x(h_n) \sim C_x h_n^\kappa$, where C_x and κ are positive constants. The choice of bandwidth $h_n = An^{-\delta}$ with $A > 0$ and $0 < \delta < 1$ implies $\Phi_x(h_n) = C_x n^{-\delta\kappa}$, $C_x > 0$. If $b + \kappa(1-\ell) < 1/\delta$, then $\sum_{i=1}^{n} i^{-\delta(b+\kappa(1-\ell))} \sim \dfrac{n^{1-b+\kappa(1-\ell)}}{1-b+\kappa(1-\ell)}$. Thus, the condition (H_6) holds when $\mathcal{A}_l = \dfrac{1}{1-b+\kappa(1-\ell)}$. This choice of h_n also satisfies the condition (H_3), see [4] for more details.

Theorem 2.1. *Under hypotheses (H_1)–(H_6), we have*

$$\widehat{r}_n^{[\ell]}\left(x\right) - r\left(x\right) = O\left(h_n^b\right) + O_{a.co.}\left(\sqrt{\frac{\log n}{n\Phi_x\left(h_n\right)}}\right). \tag{1}$$

Notice that this rate of convergence is the same as that of [7] (classical kernel estimator) as well as that of [4] (recurssive estimator).

Proof. The proof of this Theorem is based on the following decomposition

$$\widehat{r}_n^{[\ell]}(x) - r(x) = \frac{1}{\widehat{r}_0(x)}\left[\left(\widehat{r}_{n,1}^{[\ell]}(x) - \mathbb{E}\left(\widehat{r}_{n,1}^{[\ell]}(x)\right)\right) - \left(r(x) - \mathbb{E}\left(\widehat{r}_{n,1}^{[\ell]}(x)\right)\right)\right] - \frac{r(x)}{\widehat{r}_{n,0}^{[\ell]}(x)}\left[\widehat{r}_{n,0}^{[\ell]}(x) - 1\right],$$

in addition of the following Lemmas, which study eatch term separately. □

Lemma 2.1. *Assume that hypotheses (H_1)–(H_5) hold, then*

$$\widehat{r}_{n,1}^{[\ell]}\left(x\right) - \mathbb{E}\left(\widehat{r}_{n,1}^{[\ell]}\left(x\right)\right) = O_{a.co.}\left(\sqrt{\frac{\log n}{n\Phi_x(h_n)}}\right).$$

Proof.

$$\begin{aligned}\widehat{r}_1(x)-\mathbb{E}(\widehat{r}_1(x)) &= \frac{1}{\sum_{i=1}^{n}\psi_x^{1-\ell}(h_i)}\sum_{i=1}^{n}\frac{1}{\psi_x^{\ell}(h_i)}\left[K\left(\frac{d(x,X_i)}{h_i}\right)Y_i-E\left(K\left(\frac{d(x,X_i)}{h_i}\right)Y_i\right)\right]\\ &:= \sum_{i=1}^{n}Z_i,\end{aligned}$$

where

$$Z_i=\frac{1}{\psi_x^{\ell}(h_i)\sum_{i=1}^{n}\psi_x^{1-\ell}(h_i)}\left[K\left(\frac{d(x,X_i)}{h_i}\right)Y_i-E\left(K\left(\frac{d(x,X_i)}{h_i}\right)Y_i\right)\right].$$

To apply an exponential inequality, we concentrate on the absolute moments of order m of the random variable Z_i, we have

$$\begin{aligned}|E(Z_i^m)| &= \frac{1}{\psi_x^{m\ell}(h_i)\left(\sum_{i=1}^{n}\psi_x^{1-\ell}(h_i)\right)^m}E\left|\left[K\left(\frac{d(x,X_i)}{h_i}\right)Y_i-E\left(K\left(\frac{d(x,X_i)}{h_i}\right)Y_i\right)\right]^m\right| \leqslant\\ &\leqslant \frac{1}{\psi_x^{m\ell}(h_i)\left(\sum_{i=1}^{n}\psi_x^{1-\ell}(h_i)\right)^m}\sum_{k=0}^{m}C_m^kE\left|K^k\left(\frac{d(x,X_i)}{h_i}\right)Y_i^k\right|E\left|K\left(\frac{d(x,X_i)}{h_i}\right)Y_i\right|^{m-k} \leqslant\\ &\leqslant \frac{1}{\psi_x^{m\ell}(h_i)\left(\sum_{i=1}^{n}\psi_x^{1-\ell}(h_i)\right)^m}\sum_{k=0}^{m}C_m^kE\left|K^k\left(\frac{d(x,X_i)}{h_i}\right)\sigma_k(X_i)\right|E\left|K\left(\frac{d(x,X_i)}{h_i}\right)r(X_i)\right|^{m-k},\end{aligned}$$

the last inequality is derived by conditioning on X_i. Additionally, the condition (H_2) implies that $r(X_i)=r(x)+o(1)$, while $\sigma_k(X_i)=\sigma_k(x)+o(1)$ follows once (H_5) is verified. This, combined with

$$C'\Phi_x(h_i)\leqslant\psi_x(h_i)\leqslant C\Phi_x(h_i), \tag{2}$$

enables us to write

$$\begin{aligned}|E(Z_i^m)| &\leqslant \frac{C}{\Phi_x^{m\ell}(h_i)\left(\sum_{i=1}^{n}\Phi_x^{1-\ell}(h_i)\right)^m}\sum_{k=0}^{m}C_m^k\Phi_x^{1+m-k}(h_i)\leqslant\\ &\leqslant \frac{m!}{2}\frac{\Phi_x(h_i)}{n\Phi_x^2(h_n)}\left(\frac{C}{n\Phi_x(h_n)}\right)^{m-2}.\end{aligned}$$

Finally, it suffices to apply Corollary A.7 in [7] with $a_i^2=\dfrac{\Phi_x(h_i)}{n\Phi_x^2(h_n)}$, $b=\dfrac{C}{n\Phi_x(h_n)}$, $(A_n)^2=\sum_{i=1}^{n}a_i^2$ and $\varepsilon=\varepsilon_0\sqrt{\log n}$, $\varepsilon_0>0$ to obtain

$$\begin{aligned}P\left(\left|\sum_{i=1}^{n}Z_i\right|>\varepsilon A_n\right) &\leqslant 2\exp\left\{\frac{-\varepsilon^2}{2\left(1+\frac{\varepsilon b}{A_n}\right)}\right\}\leqslant\\ &\leqslant 2\exp\left\{\frac{-\varepsilon_0^2\log n}{2\left(1+\varepsilon_0\sqrt{\frac{\log n}{n\Phi_x(h_n)}}\right)}\right\}\leqslant\end{aligned}$$

$$\begin{aligned} &\leqslant 2\exp\left\{-C\varepsilon_0^2\log n\right\}\leqslant \\ &\leqslant 2n^{-C\varepsilon_0^2}, \end{aligned}$$

the last result coming the fact that $(A_n)^2 > \dfrac{1}{n\Phi_x(h_n)}$. Thus, it exists some real number $\xi > 0$ such that

$$P\left(\left|\widehat{r}_{n,1}^{[\ell]}(x) - \mathbb{E}\left(\widehat{r}_{n,1}^{[\ell]}(x)\right)\right| > \varepsilon_0\sqrt{\frac{\log n}{n\Phi_x(h_n)}}\right) \leqslant P\left(\left|\sum_{i=1}^{n} Z_i\right| > \varepsilon A_n\right) \leqslant 2n^{-1-\xi}.$$

□

Lemma 2.2. *Assume that hypotheses* (H_1)*–*(H_4) *hold, then*

$$\widehat{r}_{n,0}^{[\ell]}(x) - \mathbb{E}\left(\widehat{r}_{n,0}^{[\ell]}(x)\right) = O_{a.co.}\left(\sqrt{\frac{\log n}{n\Phi_x(h_n)}}\right).$$

Proof. This result can be derived directly from Lemma 2.1 by taking $Y_i = 1$. □

Lemma 2.3. *If assumptions* (H_1)*–*(H_4) *and* (H_6) *are satisfied, we have*

$$E\left(\widehat{r}_{n,1}^{[\ell]}(x)\right) - r(x) = O\left(h_n^b\right).$$

Proof. We have

$$\begin{aligned} E\left(\widehat{r}_{n,1}^{[\ell]}(x)\right) &= \frac{1}{\left(\sum_{i=1}^{n}\psi_x^{1-\ell}(h_i)\right)}\sum_{i=1}^{n}\frac{1}{\psi_x^{\ell}(h_i)}E\left[K\left(\frac{d(x,X_i)}{h_i}\right)Y_i\right] = \\ &= \frac{1}{\left(\sum_{i=1}^{n}\psi_x^{1-\ell}(h_i)\right)}\sum_{i=1}^{n}\frac{1}{\psi_x^{\ell}(h_i)}E\left[K\left(\frac{d(x,X_i)}{h_i}\right)E\left(Y_i \mid X_i\right)\right] = \\ &= \frac{1}{\left(\sum_{i=1}^{n}\psi_x^{1-\ell}(h_i)\right)}\sum_{i=1}^{n}\frac{1}{\psi_x^{\ell}(h_i)}E\left[K\left(\frac{d(x,X_i)}{h_i}\right)r(X_i)\right]. \end{aligned}$$

The relation (2) and the condition (H_2) give

$$\begin{aligned} \frac{1}{h_n^b}\left|E\left(\widehat{r}_{n,1}^{[\ell]}(x)\right) - r(x)\right| &= \frac{1}{\left(h_n^b\sum_{i=1}^{n}\psi_x^{1-\ell}(h_i)\right)}\sum_{i=1}^{n}\frac{1}{\psi_x^{\ell}(h_i)}E\left[K\left(\frac{d(x,X_i)}{h_i}\right)|r(X_i)-r(x)|\right] \leqslant \\ &\leqslant \frac{C}{h_n^b\left(\sum_{i=1}^{n}\Phi_x^{1-\ell}(h_i)\right)}\sum_{i=1}^{n}\frac{1}{\Phi_x^{\ell}(h_i)}E\left[K\left(\frac{d(x,X_i)}{h_i}\right)|r(X_i)-r(x)|\right] \leqslant \\ &\leqslant C\frac{1}{n}\sum_{i=1}^{n}\left(\frac{h_i}{h_n}\right)^b\left(\frac{\Phi_x(h_i)}{\Phi_x(h_n)}\right)^{1-\ell} \leqslant \\ &\leqslant C\mathcal{A}_{n,\ell}, \end{aligned}$$

the result follows from the condition (H_6). □

3. Simulation study

In this section, we present two examples of simulation to investigate the performance of our studied estimator (RRE) for finite sample.

For the computation of the our estimator (RRE) and the classical kernel regresion estimator (RKE) defined in [7] by

$$\widetilde{r}_n(x) = \frac{\sum_{i=1}^{n} K\left(\frac{d(x,X_i)}{h_n}\right) Y_i}{\sum_{i=1}^{n} K\left(\frac{d(x,X_i)}{h_n}\right)}, \tag{3}$$

we use the quadratic kernel $K(x) = \frac{3}{2}(1-x^2)1_{[0,1]}(x)$ and the smoothing bandwith $h_i = Ci^{-\frac{1}{5}}$, $C > 0$ and $1 \leqslant i \leqslant n$. Take into account of the smoothness of the curves $X_i(t)$, we choose the semi-metric based on the derivative (for the first example in simulation study) and the semi-metric PCA (for the second example in simulation study) described in [7] (see routines "semimetric.pca"), see the website https://www.math.univ-toulouse.fr/∼ferraty/SOFTWARES/NPFDA/npfda-routinesR.txt.

We consider the following nonparametric functional regression model

$$Y = r(X) + \epsilon$$

where X and ϵ are independent. Notice that the conditional mean function on x will coincide and will be equal to $r(x)$.

Example 1. The functional covariate $X(t)$ is defined, for $t \in [0,1]$ by

$$X(t) = A\,(2 - cos(\pi t W)) + (1-A)\,cos(\pi t W),$$

where W is a centered random variable normally distributed with a variance equal to 1 ($W \rightsquigarrow \mathcal{N}(0,1)$) and A is a random variable having a Bernoulli distribution with parameter $p = 0.5$. The curves are discretized on the same grid which is composed of 100-equidistant values in $[0,1]$ in Fig. 1.

The error $\epsilon \rightsquigarrow \mathcal{N}(0, 0.1)$ and

$$r(X) = \frac{1}{4}\int_0^1 \left(X'(t)\right)^2 dt.$$

We present another example to ensure a more effective decision.

Example 2. The functional covariate $X(t)$ is defined, for $t \in [0,1]$ by

$$X(t) = a\sin\left[4\,(b-t)\right] + b + \eta_t,$$

where $a \rightsquigarrow \mathcal{N}(5,2)$, $b \rightsquigarrow \mathcal{N}(0, 0.1)$ and $\eta_t \rightsquigarrow \mathcal{N}(0, 0.2)$. See Fig. 2 for a sample of these curves.

The error $\epsilon \rightsquigarrow \mathcal{N}(0, 0.01)$ and

$$r(X) = \int_0^1 \frac{dt}{1+|X(t)|}.$$

In order to illustrate the performance of our estimator, we proceed with this algorithm.

• Step 1. For a sample sizes, we generate n i.i.d. ϵ_i, the covariable X_i and we compute Y_i.

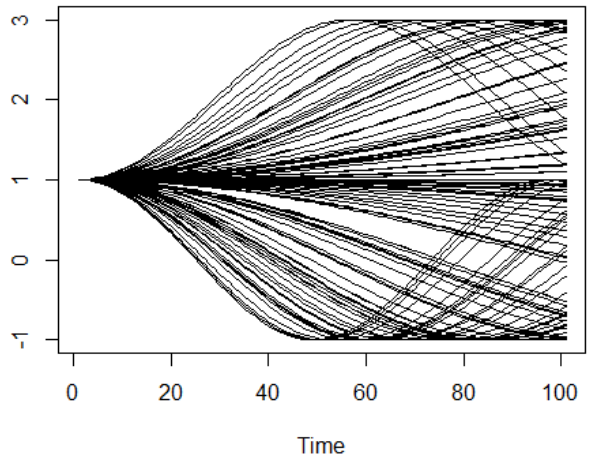

Fig. 1. A sample of 100 curves representing a realization of the functional random variable X for the second example

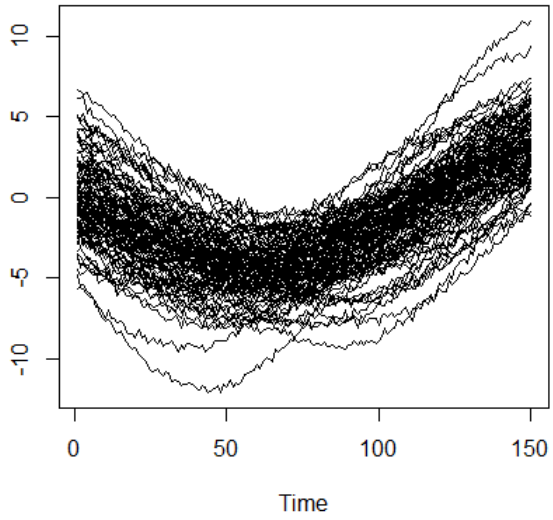

Fig. 2. A sample of 100 curves representing a realization of the functional random variable X for the first example

Furthermore, we split our data into two subsets.
- $(X_i, Y_i)_{1\leqslant i\leqslant n_1}$: The learning sample used to build the estimators, where $n_1 = 2n/3$.
- $(X_i, Y_i)_{n_1+1\leqslant i\leqslant n}$: The testing sample used to make a comparison.

• Step 2. We calculate the RRE estimator $\widehat{r}_n^{[\ell]}(X_i)$ and RKE estimator $\widetilde{r}_n(X_i)$ by using the learning sample.

• Step 3. We evaluate the prediction error given by

$$EMSE := \frac{1}{n-n_1}\sum_{i=n_1+1}^{n}\left(\widehat{Y}_i - r(X_i)\right)^2.$$

where $\widehat{Y}_i$ is the estimated values of both methods (RRE and RKE).

3.1. Effect of the parameter ℓ

We examine the impact of the parameter ℓ while keeping the sample size fixed at $n = 600$. The results are provided in Tab. 1, for both examples.

Table 1. Comparison of $EMSE$ errors computed on 600 simulations for different values of ℓ for both examples

	ℓ	0	0.25	0.5	0.75	1
First example	$EMSE$	0.0449	0.0459	0.047	0.0482	0.0470
Second example	$EMSE$	8.7249	8.7540	8.7780	8.8257	8.8661

We observed that the $EMSE$ values are close, indicating that the parameter ℓ does not significantly affect the quality of the recursive estimator.

3.2. Effect of the sample size

To assess the effect of the sample size n, we first plot the true values $(r(X_i))$ for all i $(n_1+1 \leqslant i \leqslant n)$ against the predicted values from both estimators (RRE and RKE), with each estimator displayed in a separate graph. This is illustrated in Figs. 3–10.

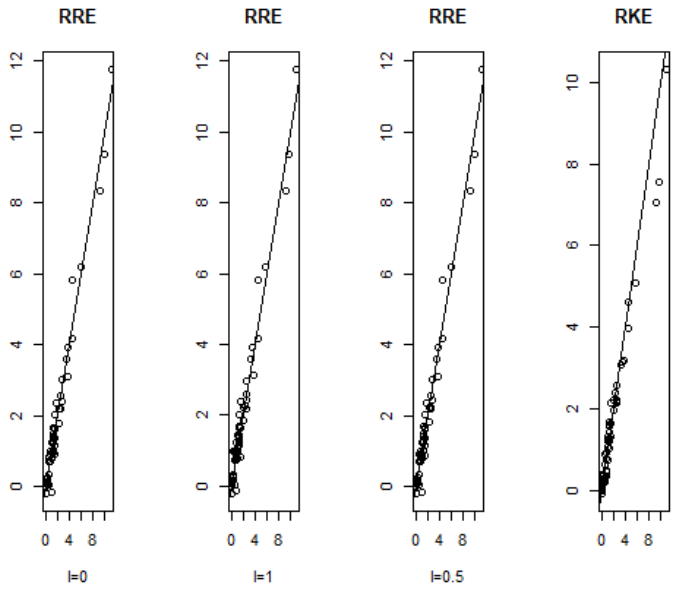

Fig. 3. The RRE and RKE estimators of the regression when $n = 200$ for the first example

Then, for more precisely, we evaluate the prediction error for different values n. The results are presented in Tab. 2, for both examples.

The results indicate that the non-recursive estimator is not significantly better than our estimator in terms of MSE when $\ell = 0$. However, for $\ell = 0.5$ and $\ell = 1$, the MSE values of both the recursive and classical estimators are very close, making it challenging to differentiate between the two. Finally, without surprise, we observe a decrease in MSE values with an increase in sample size n.

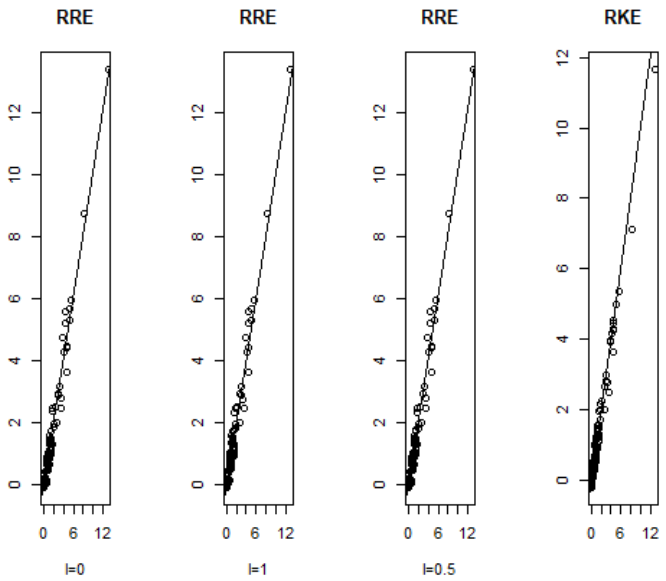

Fig. 4. The RRE and RKE estimators of the regression when $n = 400$ for the first example

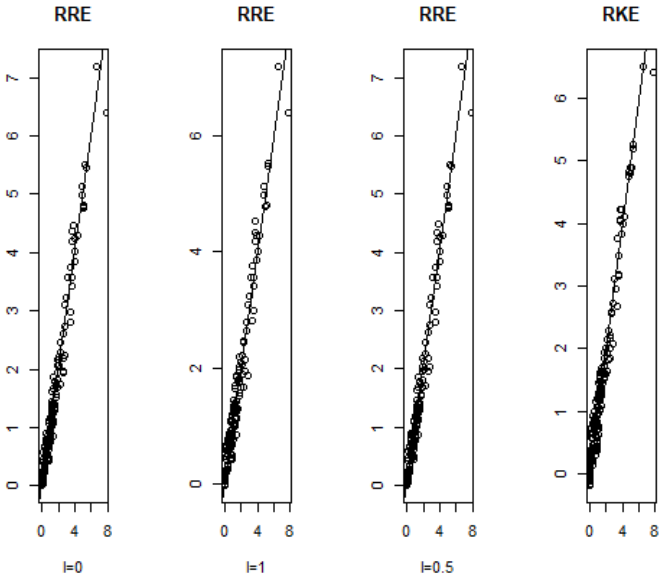

Fig. 5. The RRE and RKE estimators of the regression when $n = 600$ for the first example

3.3. Computational time

This subsection emphasizes a key advantage of the recursive estimator compared to classical one defined by (3) in terms of the computational time required in seconds to make predictions. The obtained results are given in Tab. 3, for both examples.

As anticipated, the computational time increases with the sample size. Furthermore, there are notable differences in computational time between the two estimators. Specifically, the recursive estimator requires significantly less computation time compared to the classical kernel estimator.

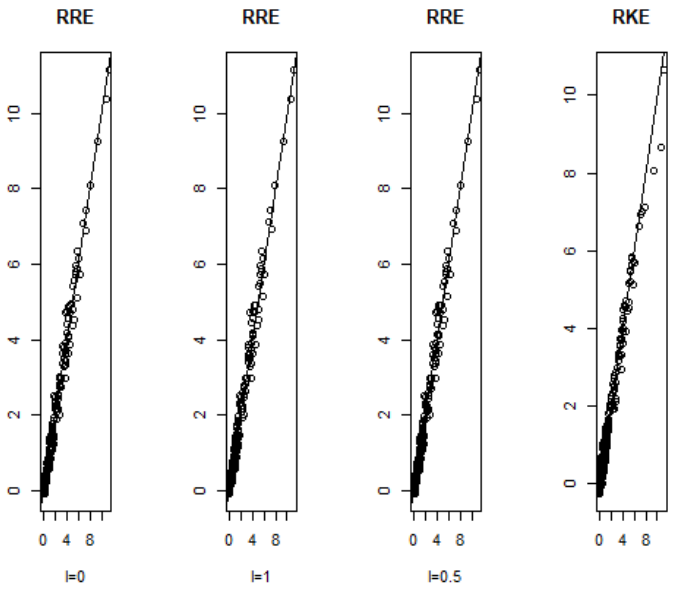

Fig. 6. The RRE and RKE estimators of the regression when $n = 1000$ for the first example

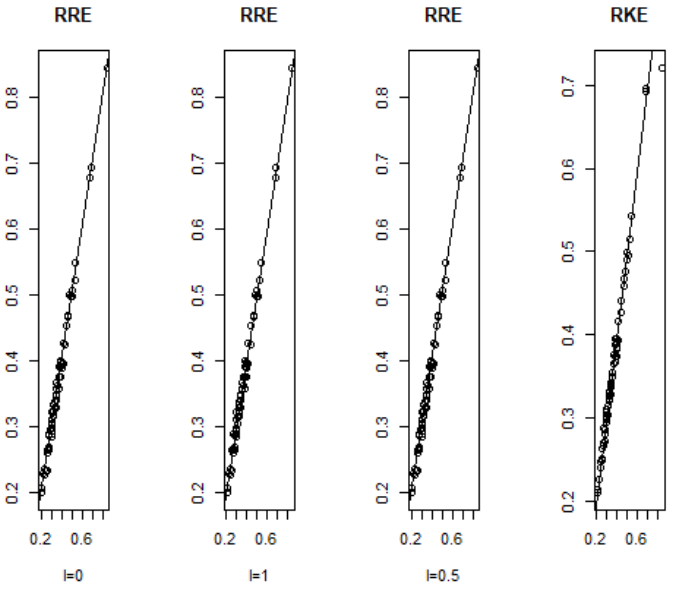

Fig. 7. The RRE and RKE estimators of the regression when $n = 200$ for the second example

Conclusion

In this study, we presented a recursive estimator for the regression function with functional explanatory variables. Our analysis established the almost complete convergence of the proposed estimator.

The simulation study provided numerical support for our theoretical findings, illustrating the estimator's effective performance. The results indicate that the recursive approach not only maintains desirable statistical properties but also offers practical advantages in computational

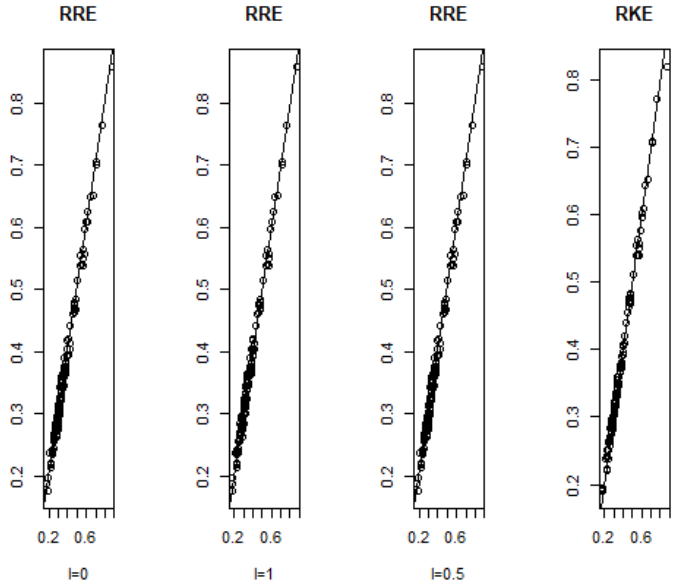

Fig. 8. The RRE and RKE estimators of the regression when $n = 400$ for the second example

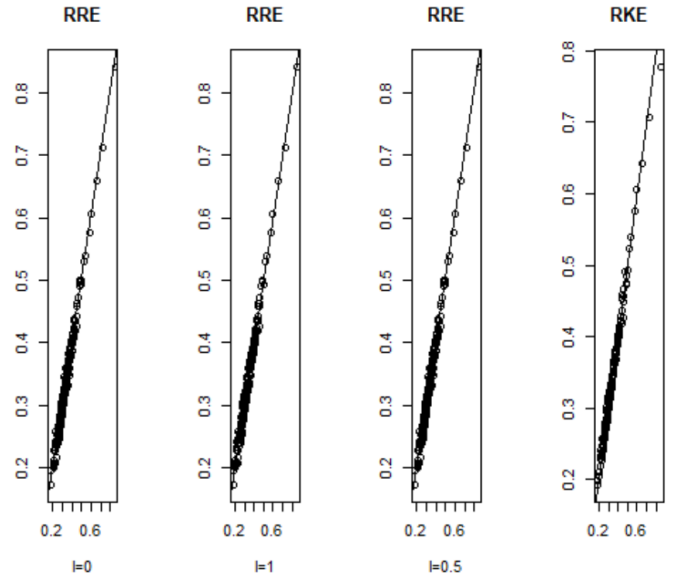

Fig. 9. The RRE and RKE estimators of the regression when $n = 600$ for the second example

efficiency, making it suitable for applications in functional data analysis.

Overall, this work contributes to the growing of literature on nonparametric estimation in functional contexts and opens avenues for further research, including extensions to dependent functional data, exploration of other convergence modes, and extending our results to the case of dependent data.

The authors wish to extend their heartfelt thanks to the editor and reviewers for their insightful suggestions and constructive comments.

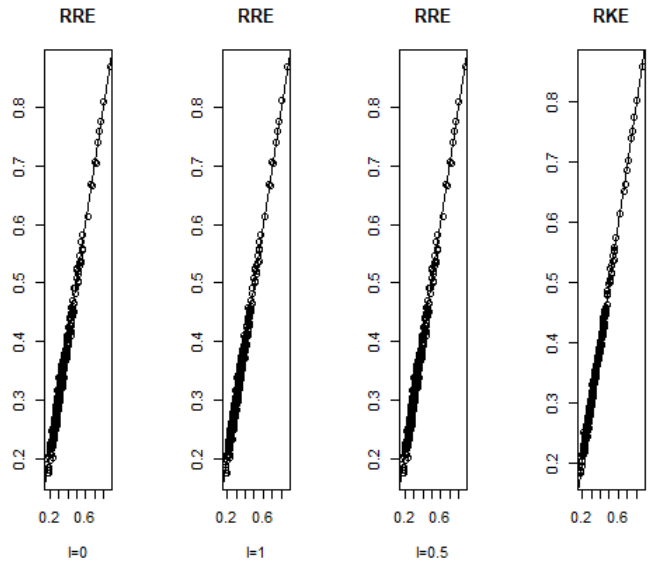

Fig. 10. The RRE and RKE estimators of the regression when $n = 1000$ for the second example

Table 2. Comparison of $EMSE$ errors computed for different values of n for both examples

	n	200	400	600	1000
First exmaple	RRE (l=0)	0.0678	0.0592	0.0431	0.0393
	RRE (l=0.5)	0.0720	0.0596	0.0438	0.0404
	RRE (l=1)	0.0765	0.0603	0.0450	0.0417
	RKE	0.0664	0.0591	0.0430	0.0385
Second exmaple	RRE (l=0)	10.10019	10.0010	8.3191	7.4964
	RRE (l=0.5)	10.1012	10.0005	8.8541	7.3870
	RRE (l=1)	10.1015	10.0007	8.8655	7.4084
	RKE	10.1014	10.0006	8.3091	7.4852

Table 3. Comparison of the time computation of RRE estimator and RKE one according to the different sample size n for both examples

	n	200	400	600	1000
First exmaple	RRE (l=0)	0.6523	0.9206	1.3696	3.4398
	RRE (l=0.5)	0.4639	0.7554	1.0475	3.3003
	RRE (l=1)	0.46116	0.8818	1.0158	3.2272
	RKE	2.8572	9.9402	18.7379	152.7180
Second exmaple	RRE (l=0)	1.7425	3.1703	7.6563	25.1040
	RRE (l=0.5)	1.6280	3.3831	7.5189	25.0967
	RRE (l=1)	1.6347	3.1942	7.5855	25.0803
	RKE	4.8130	5.1873	19.9055	161.8191

References

[1] I.A.Ahmad, P.E.Lin, Nonparametric sequential estimation of a multiple regression function, *Bull. Math. Statis.*, **17**(1976), 63–75.

[2] A.Amiri, Rates of almost sure convergence of families of recursive kernel estimators, *Annales de l'ISUP*, **54**(2010), no. 3, 3–24.

[3] A.Amiri, Recursive regression estimators with application to nonparametric prediction, *Journal of Nonparametric Statistics,* **24**(2012), no. 1, 169–186.

[4] A.Amiri, C.Crambes, B.Thiam, Recursive estimation of nonparametric regression with functional covariate, Computational Statistics & Data Analysis, **69**(2014), 154–172.

[5] A.Amiri, B.Thiam, Consistency of the recursive nonparametric regression estimation for dependent functional data, *Journal of Nonparametric Statistics,* **26**(2014), no. 3, 471–487.

[6] L.P.Devroye, T.J.Wagner, Distribution-free consistency results in nonparametric discrimination and regression function estimation, *The Annals of Statistics,* (1980), 231–239.

[7] F.Ferraty, P.Vieu, Nonparametric functional data analysis. Theory and Practice, Springer Series in Statistics, New York, 2006.

[8] K.A.Mezhoud, Almost sure convergence of recursive kernel estimatiors of the density and the regression under η- weak dependence, *Communications in Statistics-Theory and Methods,* **50**(2021), no. 17, 3913–3927.

[9] E.A.Nadaraya, On Estimating Regression, *Theory of Probability & Its Applications,* **9**(1964), no. 1, 141–142.

[10] G.S.Watson, Smooth regression analysis, *Sankhyā: The Indian Journal of Statistics. Series A,* **26**(1964), no. 4, 359–372.

Почти полная сходимость оценки функциональной регрессии: рекурсивный непараметрический подход

Хаджер Джениба
Университет Фрѐрес Ментури
Константин 1, Алжир
Сарра Леулми
Лаборатория LAMASD
Университет Фрѐрес Ментури
Константин 1, Алжир

Аннотация. Мы вводим новые семейства рекурсивных ядерных оценок для функции регрессии действительной переменной отклика, заданной случайной величиной, которая принимает значения в полуметрическом пространстве. Затем мы исследуем скорость почти полной сходимости, которая сильнее, чем почти надежная сходимость. Проводится имитационное исследование для иллюстрации производительности предлагаемых рекурсивных оценок.

Ключевые слова: почти полная сходимость, функциональные данные, ядерная оценка, рекурсивная оценка, функция регрессии.

EDN: QRNGKM
УДК 524.8

Two Fluid Scenario Dark Energy Cosmological Model with Linearly Varying Deceleration Parameter in Lyra's Geometry

Mandala Krishna*
Raghu Engineering College
Visakhapatnam, AndhraPradesh, India-531162
SobhanBabu Koppala†
University Collage of Engineering Kakinada
Narasaraopeta, AndhraPradesh, India-522616
Santhikumar Rajamahanthi‡
Aditya Institute of Technology and Management
Tekkali, Srikakulam Dist AndhraPradesh, India-532201

Received 09.02.2025, received in revised form 22.04.2025, accepted 30.04.2025

Abstract. In this paper, we explore the evaluation of the dark energy parameter within a spatially homogeneous and anisotropic Bianchi type-VI_0 spacetime, incorporating Lyra geometry. To obtain a determinate solution, we solve the field equations using the linearly varying deceleration parameter proposed by Akarsu and Dereli (2012). We analyze two scenarios involving interacting and non-interacting fluids (barotropic and dark energy) and derive general results for each case. The physical implications of these findings are also discussed.

Keywords: dark energy, two fluid scenario, barotropic, Lyra's geometry.

Citation: M. Krishna, K. SobhanBabu, R. Santhikumar, Two Fluid Scenario Dark Energy Cosmological Model with Linearly Varying Deceleration Parameter in Lyra's Geometry, J. Sib. Fed. Univ. Math. Phys., 2025, 18(4), 519–531. EDN: QRNGKM.

1. Introduction and preliminaries

In recent years, there has been significant interest in cosmological models involving dark energy within the framework of general relativity. This interest is driven by the fact that our observable universe is undergoing accelerated expansion, as confirmed by various cosmological observations such as Type Ia supernovae [1–7], cosmic microwave background (CMB) anisotropy [8, 9], and large-scale structure [10]. These observations strongly suggest that dark energy is the dominant component in the present universe, driving its accelerated expansion. Based on these findings, cosmologists have widely accepted the concept of dark energy as a fluid with negative pressure, comprising approximately 70% of the energy content of the current universe. This negative pressure is thought to be responsible for the observed cosmic acceleration due to its repulsive gravitational effects. To explain the nature of dark energy and fit the observational data, many candidates have been proposed, such as the cosmological constant, tachyon, quintessence, phantom, and others. For instance, quintessence models, which involve scalar fields, lead to a time-dependent equation of state (EoS) parameter, $\omega = \dfrac{p}{\rho}$, where p is the fluid pressure and ρ is the energy density [11]. Unlike the cosmological constant, this parameter in quintessence models is not necessarily constant. Various researchers, including Ray et al. (2010) [12], Akarsu and

*mandala.krishna.phd@gmail.com https://orcid.org/0000-0003-1975-8930
†ksobhanjntu@gmail.com https://orcid.org/0000-0002-2991-7651
‡Corresponding author: skrmahanthi@gmail.com https://orcid.org/0000-0001-5122-3800

Kilinc (2010a, b) [13,14], Yadav et al. (2011) [15], Pradhan et al. (2010) [16], Yadav (2011) [17], and Amirhashchi et al. (2011c) [18], have investigated different aspects of dark energy models in general relativity with a variable EoS parameter.

Several modifications to Riemannian geometry have been proposed in attempts to unify gravitation, the electromagnetic field, and other fundamental interactions in the universe. Weyl(1918) [19] made one such attempt by trying to unify gravitation and electromagnetism within a single spacetime geometry. However, Weyl's theory faced criticism due to its reliance on the non-integrability of length transfer. Later, Lyra (1951) [20] introduced a further modification to Riemannian geometry by incorporating a gauge function into a structureless manifold, thereby eliminating the issue of non-integrability in length transfer. This modification naturally gave rise to a displacement vector. Building on Lyra's work, Sen(1957) [21] and Sen and Dunn(1971) [22] developed a new scalar-tensor theory of gravitation and formulated an analog of the Einstein field equations based on Lyra's geometry. Halford(1970) [23] noted that the constant vector displacement field ϕ_i in Lyra's geometry functions similarly to the cosmological constant Λin conventional general relativity. Furthermore, Halford(1973) [24] demonstrated that the scalar-tensor theory derived from Lyra's geometry yields predictions consistent with observational limits, matching the results of Einstein's theory.

Cosmological observations of the universe's expansion history suggest that the current universe is not only expanding but also undergoing accelerated expansion. This late-time acceleration has been confirmed by high-redshift supernova experiments (Riess et al. (1998); Perlmutter et al. (1999); Bennett et al. (2003) [25–27]. Additionally, observations of the cosmic microwave background radiation (Spergrl, D.N et al. (2003); Oli,S (2012)) [28–29] and large-scale structure [30] offer indirect evidence supporting this late-time acceleration. The simplest model describing the observed universe is well represented by the Friedmann–Robertson–Walker (FRW) models, which are both spatially homogeneous and isotropic. These models provide a good global approximation of the present-day universe. However, on smaller scales, the universe is neither perfectly homogeneous nor isotropic. Theoretical arguments (Chimento,L.P (2004); Misner,C.n (1968) [31,32] and recent experimental data on cosmic microwave background radiation anisotropies suggest the existence of an anisotropic phase that gradually transitions toward isotropy [33]. Bianchi types I–IX cosmological models are significant because they are homogeneous yet anisotropic, allowing the study of the universe's process of isotropization over time. Among these, Bianchi type-VI0 spacetime holds special interest in anisotropic cosmology. [34] highlighted that Bianchi type-VI_0 models provide a better explanation for certain cosmological issues, such as primordial helium abundance, and exhibit isotropization in a unique manner. Santhikumar et al. (2017) [35] discussed an accelerating anisotropic model to explain the universe's expansion, while [36] explored the accelerated expansion of the universe within the framework of Lyra geometry

To determine the scale factor a(t), the Hubble parameter (H) and the dimensionless deceleration parameter (q) are crucial for understanding the universe's dynamic history. The time dependence of the cosmic scale factor a(t) is particularly significant, as both H and q are defined in terms of this scale factor. The study of cosmological models with a time-varying deceleration parameter (DP) has gained significant attention since the discovery of the universe's accelerating expansion, as confirmed by two independent research teams (Perlmutter et al. 1998; Riess et al. 1998, 2001) [37–39]. The variable DP plays a vital role in measuring the universe's expansion rate. In this context, several researchers have explored cosmological models assuming a constant DP law, $q = m - 1$, as suggested by Berman (1983) [40]. Many others have investigated models with a time-dependent DP, following the approach of Akarsu and Dereli (2012) [41] and Misra et al. (2012, 2013a, 2013b, 2016a) [42–45], along with physically suitable relations with the cosmic scale factor. Akarsu and Dereli (2012) [41] proposed a linearly varying deceleration parameter (LVDP) law, $q = -kt + m - 1$ where $k \geqslant 0$ is a constant with the dimension of inverse time, and $m > 1$ is a dimensionless constant. When $k = 0$, the LVDP reduces to Berman's law. This

LVDP law enables the generalization of cosmological solutions. According to this framework, the universe's expansion behaviour can be classified based on the value of q : it exhibits accelerated expansion for $q < -1$, an exponential expansion phase for $-1 \leqslant q < 0$, constant rate expansion for $q = 0$, and a power-law accelerating expansion phase for $1 < q < 0$. It is also noted that the super-exponential expansion represents a rapid expansion rate when $q < -1$ under the LVDP law with a suitable ansatz. This understanding of the deceleration parameter helps to provide a clearer picture of the universe's expansion dynamics over time.

Liang et al. (2000) [46] investigated the cosmological evolution of a two-field dilation model of dark energy. [47] studied viscous dark tachyon cosmology in both interacting and non-interacting scenarios within a non-flat FRW universe. [48] explored a two-fluid scenario for dark energy models, demonstrating that such interactions could help alleviate the coincidence problem. UM [49] examined a Kantowski–Sachs two-fluid radiating cosmological model in Brans–Dicke theory of gravitation. Syed Sabanam et al. (2023) [50] investigated a two-fluid higher-dimensional FRW cosmological model to revisit cosmological tests of Hubble parameter parametrization within Lyra geometry. Praveen Kumar et al. (2022) [51] studied a two-fluid cosmological model in a (2+1)-dimensional Saez–Ballester scalar-tensor theory of gravitation.

Motivated by these studies, we investigate the evolution of the dark energy parameter in an FRW cosmological model filled with two fluids (barotropic fluid and dark energy) within the framework of the scalar-tensor theory of gravitation proposed by Saez and Ballester. We analyze both interacting and non-interacting scenarios and discuss the physical aspects of the two-fluid model. This chapter is organized as follows: Section 2 is dedicated to deriving the field equations using the spatially homogeneous and anisotropic Bianchi type-VI_0 metric in the presence of a barotropic fluid and dark energy within the framework of Lyra geometry. Section 3 focuses on the case of non-interacting two fluids. Section 4 examines the scenario of interacting two fluids. Section 5 provides a detailed discussion of the behaviour of the physical and kinematical parameters in the developed model. Section 6 presents the conclusion.

2. Metric and field equation

We consider spatially homogeneous and anisotropic Bianchi type-VI_0 space time in the form

$$ds^2 = -dt^2 + A^2dx^2 + B^2e^{2x}dy + C^2e^{-2x}dz^2 \tag{1}$$

Einstein modified field equation in normal gauge for Lyra's manifold

$$R_i^j - \frac{1}{2}g_i^j R + \frac{3}{2}\phi_i\phi^j - \frac{3}{4}\phi_k\phi^k g_i^k = -T_i^j \tag{2}$$

Where is the displacement vector defined as $\phi_i = (0, 0, 0, \beta(t))$ and other symbols have their usual meaning as in Riemannian geometry. Also , we have

$$T_{;j}^{ij} = 0 \tag{3}$$

which is a consequence of the field equation (1) and (2). $T_{;j}^{ij}$ is the two fluid energy momentum tensor consisting of dark energy and barotropic fluid and comma and semicolon denote partial and covariant differentiation respectively.

For the metric (1) the field equations (2)–(3) are

$$\frac{\ddot{B}}{B} + \frac{\ddot{C}}{C} + \frac{\dot{B}\dot{C}}{BC} + \frac{1}{A^2} + \frac{3}{4}\beta^2 = -p_{\text{total}} \tag{4}$$

$$\frac{\ddot{A}}{A} + \frac{\ddot{C}}{C} + \frac{\dot{A}\dot{C}}{AC} - \frac{1}{A^2} + \frac{3}{2}\beta^2 = -p_{\text{total}} \tag{5}$$

$$\frac{\ddot{A}}{A}+\frac{\ddot{B}}{B}+\frac{\dot{A}\dot{B}}{AB}-\frac{1}{A^2}+\frac{3}{4}\beta^2=-p_{\text{total}} \tag{6}$$

$$\frac{\dot{A}\dot{B}}{AB}+\frac{\dot{B}\dot{C}}{BC}+\frac{\dot{A}\dot{C}}{AC}-\frac{1}{A^2}-\frac{3}{4}\beta^2=\rho_{\text{total}} \tag{7}$$

$$\frac{\dot{B}}{B}-\frac{\dot{C}}{C}=0 \tag{8}$$

In a co-moving coordinate system the field equations (2)–(3) for the metric (1), in the two fluid scenario, lead to

Eq. (3) leads to

$$\dot{\rho}_{\text{total}}+(\rho_{\text{total}}+p_{\text{total}})\left(\frac{\dot{A}}{A}+\frac{\dot{B}}{B}+\frac{\dot{C}}{C}\right)=\dot{\rho}_{total}+\frac{\dot{a}}{a}(\rho_{total}+p_{total})=0 \tag{9}$$

where $\frac{\dot{A}}{A}+\frac{\dot{B}}{B}+\frac{\dot{C}}{C}=\frac{\dot{a}}{a}=H$ and

$$p_{\text{total}}=p_m+p_d,\quad \rho_{\text{total}}=\rho_m+\rho_d \tag{10}$$

Here $p_m and \rho_m$ are pressure and energy density of barotropic fluid and $p_D and \rho_D$ are pressure and energy density of dark fluid respectively.

Also, The equation of state (EoS) parameters of the barotropic fluid and dark fluid are given by

$$\omega_m=\frac{p_m}{\rho_m}\ \text{ and }\ \omega_D=\frac{p_D}{\rho_D} \tag{11}$$

The Conservation of LHS of equation (2) leads to

$$\left(R_i^j-\frac{1}{2}g_i^jR\right)+\left(\frac{3}{2}\phi_i\phi^j\right)_{;j}-\frac{3}{4}\left(\phi_k\phi^k g_i^j\right)_{;j}=0 \tag{12}$$

$$\frac{3}{2}\beta\dot{\beta}+\frac{3}{2}\beta^2\left(\frac{\dot{A}}{A}+\frac{\dot{B}}{B}+\frac{\dot{C}}{C}\right)=\frac{3}{2}\beta\dot{\beta}+\frac{3}{2}\beta^2\left(\frac{\dot{a}}{a}\right)=0 \tag{13}$$

In the following section we consider two cases: **non − interacting two fluid model** and **interacting fluid model**. Solving the field equations in both the cases we determine $a(t), \rho_m, p_m, \rho_D, p_D, \omega_m and \omega_D$ then study their physical behavior.

3. Non − interactin two − fluid model

Here we consider that two fluid (barotropic fluid and dark energy) which do not interact with each other. Hence the general form of conservation equation (9) leads us to write the conservation equations for the dark fluid and barotropic fluid separately as

$$\dot{\rho}_m+\frac{\dot{a}}{a}(\rho_m+p_m)=0\ \text{ and }\ \dot{\rho}_D+\frac{\dot{a}}{a}(\rho_D+p_D)=0 \tag{14}$$

We can observe that there is a structural difference between equations in Eq. (14). In view of the fact that EoS parameter of barotropic fluid ω_m is constant (Akarsu and Kilinc 2010) [52] while ω_D is allowed to be function of time, integration of equation (14) leads to

$$\rho_m=\rho_0 a^{-3(1+\omega_m)}\quad \text{and}\quad p_m=\omega_m\rho_0 a^{-3(1+\omega_m)} \tag{15}$$

Using equation (14) in the equations (4)–(7), we first obtain $p_D and \rho_D$, in terms of scale factor a(t), as

$$\rho_D = \left(n^2+2n\right)\left(\frac{\dot{A}}{A}\right)^2 - \frac{1}{A^2} - \frac{3}{4}\beta^2 - \rho_m \quad \text{and} \quad p_D = -\left[2\frac{\ddot{B}}{B} + \left(\frac{\dot{B}}{B}\right)^2 + \frac{1}{A^2} + \frac{3}{4}\beta^2\right] + p_m \tag{16}$$

The spatial volume, The average scale factor, The Hubble's parameter, The scalar expansion, The shear scalar for the metric (1) are given by

$$V = ABC \tag{17}$$

$$a = (ABC)^{\frac{1}{3}} \tag{18}$$

$$H = \frac{\dot{a}}{a} = \frac{1}{3}\left(\frac{\dot{A}}{A} + \frac{\dot{B}}{B} + \frac{\dot{C}}{C}\right) \tag{19}$$

$$\theta = 2\frac{\dot{A}}{A} + \frac{\dot{B}}{B} \tag{20}$$

$$\sigma^2 = \frac{1}{3}\left(\frac{\dot{A}}{A} - \frac{\dot{B}}{B}\right)^2 \tag{21}$$

The field equations (4)–(8) are highly non-linear in nature and therefore we require the following plausible physical conditions:

1. By Integrating Es. (8) we have,
$$B = lC \tag{22}$$
Without loss of generality we shall consider $l = 1$
Hence,
$$B = C \tag{23}$$

2. The shear scalar σ is proportional to scalar expansion θ, so that we can take (Collins et al.1980)[53]
$$A = B^n \tag{24}$$
where n≠1 is a constant, it takes care of the anisotropic nature of the model.

3. Akarusu and Dereil(2012) [41] proposed LVDP law given as
$$q = -kt + m - 1 \tag{25}$$

Here $k \geqslant 0$ is constant with the dimension of time inverse and $m \geqslant 0$ is dimension free constant. Solving Equation (25) we have different solutions for the scale factor for LVDP law is given by

$$a = a_1 e^{\frac{2}{m}\tan h^{-1}\left(\frac{k}{m}t-1\right)} \quad for k \geqslant 0 and m > 1 \tag{26}$$

$$a = c(mt+d)^{\frac{1}{m}} \quad for k = 0 and m > 1 \tag{27}$$

$$a = ce^{dt} \quad for k = 0 and m = 0 \tag{28}$$

Therefore, we consider eq. (26) for the scale factor $a = a_1 e^{\frac{2}{m}\tan h^{-1}\left(\frac{k}{m}t-1\right)}$for LVDP law is The Hubble's parameter

$$H = \frac{\dot{a}}{a} = \frac{-2k}{\left[(kt)^2 - 2km\right]} \quad \text{and} \quad \frac{\ddot{a}}{a} = 4k^2 m\left[\frac{2k^2[t+2] - 2km}{\left[(kt)^2 - 2kmt\right]^2}\right] \tag{29}$$

$$A = a^{\frac{3}{2n+1}} = \left[a_1 e^{\frac{2}{m}\tan h^{-1}\left(\frac{k}{m}t-1\right)}\right]^{\frac{3}{2n+1}} = (a_1)^{\frac{3}{2n+1}}\, e^{\frac{6}{m(2n+1)}\tan h^{-1}\left(\frac{k}{m}t-1\right)} \tag{30}$$

$$B = C = A^n = (a_1)^{\frac{3n}{2n+1}}\, e^{\frac{6n}{m(2n+1)}\tan h^{-1}\left(\frac{k}{m}t-1\right)} \tag{31}$$

The form of metric Eq.(1) after substituting A(t), B(t) and C(t) for LVDP model is given by

$$ds^2 = -dt^2 + \left[a_1 e^{\frac{2}{m}\tan h^{-1}\left(\frac{k}{m}t-1\right)}\right]^{\frac{6}{2n+1}} dx^2 + \left[a_1 e^{\frac{2}{m}\tan h^{-1}\left(\frac{k}{m}t-1\right)}\right]^{\frac{6n}{2n+1}} \left[e^{2x}dy + e^{-2x}dz^2\right] \tag{32}$$

Equation (32) represents non-interating two fluid model in Lyra's Geometry with linearly varying decelerating parameter(LVDP) law.

Using equations (29)–(31) in equation (16) we obtain $p_D and \rho_D$ as

$$\rho_D = \frac{9\left(n^2+2n\right)}{\left(2n+1\right)^2}\left(\frac{\dot{a}}{a}\right)^2 + a^{-\frac{6}{2n+1}} - \frac{3}{4}\beta^2 - \rho_0 a^{-(1+\omega_m)} \tag{33}$$

$$\begin{aligned}\rho_D =& \frac{36k^2\left(n^2+2n\right)}{\left(2n+1\right)^2\left(\left(kt\right)^2-2kmt\right)^2} + (a_1)^{-\frac{6}{2n+1}}\, e^{-\frac{12}{m(2n+1)}\tan h^{-1}\left(\frac{k}{m}t-1\right)} - \\ &- \frac{3}{4}\beta_0^2 a_1^{-2} e^{-\frac{4}{m}\tan h^{-1}\left(\frac{k}{m}t-1\right)} - \rho_0\,(a_1)^{-(1+\omega_m)}\, e^{-\frac{-2(1+\omega_m)}{m}\tan h^{-1}\left(\frac{k}{m}t-1\right)}\end{aligned} \tag{34}$$

$$p_D = -\left[\left(\frac{6n}{2n+1}\right)\left(\frac{\ddot{a}}{a}\right) + \frac{3n\left(5n-2\right)}{\left(2n+1\right)^2}\left(\frac{\dot{a}}{a}\right)^2 + a^{-\frac{6}{2n+1}} + \frac{3}{4}\beta^2\right] + \rho_0\omega_m a^{-(1+\omega_m)} \tag{35}$$

$$\begin{aligned}p_D = -\Bigg\{&\left(\frac{24k^2mn}{(2n+1)}\right)\left[\frac{2k^2\left[t+2\right]-2km}{\left[\left(kt\right)^2-2kmt\right]^2}\right] - \frac{12n\left(5n-2\right)k^2}{\left(2n+1\right)^2\left(\left(kt\right)^2-2kmt\right)^2} - \\ &- (a_1)^{-\frac{6}{2n+1}}\, e^{-\frac{12}{m(2n+1)}\tan h^{-1}\left(\frac{k}{m}t-1\right)} - \frac{3}{4}\beta_0^2 a_1^{-2} e^{-\frac{4}{m}\tan h^{-1}\left(\frac{k}{m}t-1\right)}\Bigg\} + \\ &+ \rho_0\omega_m\,(a_1)^{-(1+\omega_m)}\, e^{-\frac{2(1+\omega_m)}{m}\tan h^{-1}\left(\frac{k}{m}t-1\right)}\end{aligned} \tag{36}$$

Using equations (35) and (36) in equation (16) we obtain

$$\begin{aligned}\omega_{\mathbf{D}} = \Bigg[\Bigg\{&-\Bigg\{\left(\frac{\mathbf{24k^2mn}}{\mathbf{(2n+1)}}\right)\left[\frac{\mathbf{2k^2[t+2]-2km}}{\left[\mathbf{(kt)^2-2kmt}\right]^2}\right] - \frac{\mathbf{12n(5n-2)k^2}}{\mathbf{(2n+1)^2\left((kt)^2-2kmt\right)^2}} - \mathbf{(a_1)}^{-\frac{6}{2n+1}}\, \mathbf{e}^{-\frac{12}{m(2n+1)}\tanh^{-1}\left(\frac{k}{m}t-1\right)} \\ &- \tfrac{3}{4}\beta_0^2 a_1^{-2} e^{-\frac{4}{m}\tanh^{-1}\left(\frac{k}{m}t-1\right)}\Bigg\} + \rho_0\omega_m\,(a_1)^{-(1+\omega_m)}\, e^{-\frac{2(1+\omega_m)}{m}\tanh^{-1}\left(\frac{k}{m}t-1\right)}\Bigg\} \div \\ &\div \Bigg\{\Bigg\{\frac{\mathbf{36k^2\left(n^2+2n\right)}}{\mathbf{(2n+1)^2\left((kt)^2-2kmt\right)^2}} + (a_1)^{-\frac{6}{2n+1}}\, e^{-\frac{12}{m(2n+1)}\tanh^{-1}\left(\frac{k}{m}t-1\right)} - \\ &- \tfrac{3}{4}\beta_0^2 a_1^{-2} e^{-\frac{4}{m}\tanh^{-1}\left(\frac{k}{m}t-1\right)} - \rho_0\,(a_1)^{-(1+\omega_m)}\, e^{-\frac{2(1+\omega_m)}{m}\tanh^{-1}\left(\frac{k}{m}t-1\right)}\Bigg\}\Bigg\}\Bigg]\end{aligned} \tag{37}$$

which is the equation of state (EoS) parameter of the dark fluid in terms of the cosmic time t.

It can be observed that for t→0, $\rho_D and p_D$ diverge while for large t they vanish. Equation (37) gives the behavior of EoS in terms of cosmic time t. It is observed that ω_D is increasing function of cosmic time t. The rapidity of their growth at the early stage depends on the type of the universes, while later on they all tend to a constant value.

The expressions of the matter-density Ω_m and dark-energy density Ω_D are given by

$$\Omega_m = \frac{\rho_m}{3H^2} = \left[\frac{\left((kt)^2 - 2kmt\right)^2 \rho_0 \left(a_1\right)^{-(1+\omega_m)} e^{\frac{-2(1+\omega_m)}{m} \tan h^{-1}\left(\frac{k}{m}t-1\right)}}{12k^2}\right] \tag{38}$$

$$\Omega_D = \frac{\rho_D}{3H^2} = \left\{\left(\frac{36k^2\left(n^2+2n\right)}{\left(2n+1\right)^2\left((kt)^2-2kmt\right)^2} + \left(a_1\right)^{-\frac{6}{2n+1}} e^{-\frac{12}{m(2n+1)} \tan h^{-1}\left(\frac{k}{m}t-1\right)} - \right.\right.$$
$$\left.\left. - \frac{3}{4}\beta_0^2 a_1^{-2} e^{-\frac{4}{m} \tan h^{-1}\left(\frac{k}{m}t-1\right)} - \rho_0 \left(a_1\right)^{-(1+\omega_m)} e^{-\frac{-2(1+\omega_m)}{m} \tan h^{-1}\left(\frac{k}{m}t-1\right)}\right)\left((kt)^2-2kmt\right)^2\right\} \div$$
$$\div 12k^2 \tag{39}$$

By adding Eq. (38) and (39) gives us the density parameter

$$\Omega = \Omega_m + \Omega_D = \frac{36\left(n^2+2n\right)}{\left(2n+1\right)^2} +$$
$$+ \frac{\left(\left(a_1\right)^{-\frac{6}{2n+1}} e^{-\frac{12}{m(2n+1)} \tan h^{-1}\left(\frac{k}{m}t-1\right)} - \frac{3}{4}\beta_0^2 a_1^{-2} e^{-\frac{4}{m} \tan h^{-1}\left(\frac{k}{m}t-1\right)}\right)\left((kt)^2-2kmt\right)^2}{12k^2} \tag{40}$$

4. Interacting tow fluid model

Here we consider the interaction between dark energy and barotropic fluid. For this purpose we can write the continuity equation for dark fluid and barotropic fluid as

$$\dot{\rho}_m + 3\frac{\dot{a}}{a}\left(\rho_m + p_m\right) = Q \tag{41}$$

$$\dot{\rho}_D + 3\frac{\dot{a}}{a}\left(\rho_D + p_D\right) = -Q \tag{42}$$

where the quantity Q represents the interaction between dark energy components. Also $Q > 0$ ensure that the second law of thermodynamics is satisfied (Pavon and Wang, 2009) [54]. Following Amendola et al. (2007) [55] and [56], we consider,

$$Q = 3H\sigma\rho_m \tag{43}$$

where σ is a coupling constant.

Using [42] in (42) and integrating we obtain

$$\rho_m = \rho_0 a^{-3(1+a_m-\sigma)} = \rho_0 \left[a_1 e^{\frac{2}{m} \tan h^{-1}\left(\frac{k}{m}t-1\right)}\right]^{-(1+\omega_m-3\sigma)} \tag{44}$$

$$p_m = \omega_m\rho_m = \omega_m\rho_0 a^{-(1+\omega_m-3\sigma)} = \omega_m\rho_0 \left[a_1 e^{\frac{2}{m} \tan h^{-1}\left(\frac{k}{m}t-1\right)}\right]^{-(1+\omega_m-3\sigma)} \tag{45}$$

Now using Eqs. (42)–(44) in [33] and [35] we get (by a straight forward calculation)

$$\rho_D = \left[\frac{36k^2\left(n^2+2n\right)}{\left(2n+1\right)^2\left((kt)^2-2kmt\right)^2} + \left(a_1\right)^{-\frac{6}{2n+1}} e^{-\frac{12}{m(2n+1)} \tan h^{-1}\left(\frac{k}{m}t-1\right)} - \right.$$
$$\left. - \frac{3}{4}\beta_0^2 a_1^{-2} e^{-\frac{4}{m} \tan h^{-1}\left(\frac{k}{m}t-1\right)} - \rho_0 \left(a_1\right)^{-(1+\omega_m-3\sigma)} e^{-\frac{-2(1+\omega_m-3\sigma)}{m} \tan h^{-1}\left(\frac{k}{m}t-1\right)}\right] \tag{46}$$

$$p_D = -\left\{\left(\frac{24k^2mn}{(2n+1)}\right)\left[\frac{2k^2\left[t+2\right]-2km}{\left[\left(kt\right)^2-2kmt\right]^2}\right]-\frac{12n\left(5n-2\right)k^2}{\left(2n+1\right)^2\left(\left(kt\right)^2-2kmt\right)^2}-\right.$$
$$-\left(a_1\right)^{-\frac{6}{2n+1}}e^{-\frac{12}{m(2n+1)}\tan h^{-1}\left(\frac{k}{m}t-1\right)}-\frac{3}{4}\beta_0^2a_1^{-2}e^{-\frac{4}{m}\tan h^{-1}\left(\frac{k}{m}t-1\right)}\Bigg\}+ \tag{47}$$
$$+\rho_0\omega_m\left(a_1\right)^{-(1+\omega_m-3\sigma)}e^{-\frac{2(1+\omega_m-3\sigma)}{m}\tan h^{-1}\left(\frac{k}{m}t-1\right)}$$

$$\omega_{\mathbf{D}}=\Bigg\{-\Bigg\{\left(\frac{\mathbf{24k^2mn}}{\mathbf{(2n+1)}}\right)\left[\frac{\mathbf{2k^2\left[t+2\right]-2km}}{\left[\mathbf{\left(kt\right)^2-2kmt}\right]^2}\right]-\frac{\mathbf{12n\left(5n-2\right)k^2}}{\mathbf{\left(2n+1\right)^2\left(\left(kt\right)^2-2kmt\right)^2}}-$$
$$-\left(\mathbf{a_1}\right)^{-\frac{6}{2n+1}}\mathbf{e}^{-\frac{12}{m(2n+1)}\tanh^{-1}\left(\frac{k}{m}t-1\right)}-\frac{\mathbf{3}}{\mathbf{4}}\beta_0^2\mathbf{a_1^{-2}e}^{-\frac{4}{m}\tanh^{-1}\left(\frac{k}{m}t-1\right)}\Bigg\}+$$
$$+\rho_0\omega_{\mathbf{m}}\left(\mathbf{a_1}\right)^{-(1+\omega_m-3\sigma)}\mathbf{e}^{-\frac{2(1+\omega_m-3\sigma)}{m}\tanh^{-1}\left(\frac{k}{m}t-1\right)}\Bigg\}\div \tag{48}$$
$$\div\left\{\frac{\mathbf{36k^2\left(n^2+2n\right)}}{\mathbf{\left(2n+1\right)^2\left(\left(kt\right)^2-2kmt\right)^2}}+\left(\mathbf{a_1}\right)^{-\frac{6}{2n+1}}\mathbf{e}^{-\frac{12}{m(2n+1)}\tanh^{-1}\left(\frac{k}{m}t-1\right)}\right.$$
$$\left.-\frac{\mathbf{3}}{\mathbf{4}}\beta_0^2\mathbf{a_1^{-2}e}^{-\frac{4}{m}\tanh^{-1}\left(\frac{k}{m}t-1\right)}-\rho_0\left(\mathbf{a_1}\right)^{-(1+\omega_m-3\sigma)}\mathbf{e}^{-\frac{2(1+\omega_m)}{m}\tanh^{-1}\left(\frac{k}{m}t-1\right)}\right\}$$

The model with ρ_D, p_D and ω_D given by equations (46)–(48) represent two fluid interacting dark energy model.

The expressions of the matter-density $\mathbf{\Omega_m}$ and dark-energy density $\mathbf{\Omega_D}$ are given by

$$\Omega_m=\frac{\rho_m}{3H^2}=\left[\frac{\left(\left(kt\right)^2-2kmt\right)^2\rho_0\left(a_1\right)^{-(1+\omega_m-3\sigma)}e^{\frac{-2(1+\omega_m-\sigma)}{m}\tan h^{-1}\left(\frac{k}{m}t-1\right)}}{12k^2}\right] \tag{49}$$

$$\mathbf{\Omega_D}=\frac{\rho_{\mathbf{D}}}{\mathbf{3H^2}}=\left[\left\{\left(\frac{\mathbf{36k^2\left(n^2+2n\right)}}{\mathbf{\left(2n+1\right)^2\left(\left(kt\right)^2-2kmt\right)^2}}+\left(\mathbf{a_1}\right)^{-\frac{6}{2n+1}}\mathbf{e}^{-\frac{12}{m(2n+1)}\tanh^{-1}\left(\frac{k}{m}t-1\right)}-\right.\right.$$
$$-\frac{\mathbf{3}}{\mathbf{4}}\beta_0^2\mathbf{a_1^{-2}e}^{-\frac{4}{m}\tanh^{-1}\left(\frac{k}{m}t-1\right)}-\rho_0\left(\mathbf{a_1}\right)^{-(1+\omega_m-3\sigma)}\mathbf{e}^{-\frac{-2(1+\omega_m-3\sigma)}{m}\tanh^{-1}\left(\frac{k}{m}t-1\right)}\Bigg)\times \tag{50}$$
$$\left.\left.\times\left(\mathbf{\left(kt\right)^2-2kmt}\right)^2\right\}\div\mathbf{12k^2}\right]$$

Using Eq. (49) and [50] gives us the density parameter

$$\Omega=\Omega_m+\Omega_D=\left[\frac{3\left(n^2+2n\right)}{\left(2n+1\right)^2}+\right.$$
$$\left.+\frac{\left(\left(a_1\right)^{-\frac{6}{2n+1}}e^{-\frac{12}{m(2n+1)}\tan h^{-1}\left(\frac{k}{m}t-1\right)}-\frac{3}{4}\beta_0^2a_1^{-2}e^{-\frac{4}{m}\tan h^{-1}\left(\frac{k}{m}t-1\right)}\right)\left(\left(kt\right)^2-2kmt\right)^2}{12k^2}\right] \tag{51}$$

which is same as Eq. (40). Hence the behavior of the density parameter, in this case, is same as that in the non-interacting case.

5. Discussion

Let us now discuss the physics of the universe as described by equation [40]. The universe begins with a Big Bang at t=0 and ends at $t=\frac{2m}{k}$. The increase in spatial volume with cosmic

time indicates the universe's spatial expansion. Key parameters, such as the scale factor, Hubble parameter, energy density, shear scalar, and scalar expansion, diverge at the finite time $t = \frac{2m}{k}$, suggesting a "Big Rip" scenario, as proposed by Caldwell et al. (2003) [57]. Additionally, when $n = 1$ the anisotropy parameter $A_m = 0$ becomes zero, resulting in a shear-free universe ($\sigma^2 = 0$). This implies that the universe initially undergoes deceleration but eventually transitions to late-time acceleration, a process that can occur through "cosmic recollapse," as described by [58]. At late times, the deceleration parameter turns negative, indicating that the universe transitions to an accelerated expansion, consistent with the current understanding of the universe's evolution.

Conclusion

In this study, we have examined a two-fluid scenario within a spatially homogeneous and anisotropic Bianchi type VI_0 spacetime in Lyra geometry. The field equations were solved using the linearly varying deceleration parameter (LVDP) proposed by [41]. The universe begins with a Big Bang at $t = 0$ and ends at $t = \frac{2m}{k}$. The increase in spatial volume with cosmic time indicates the universe's spatial expansion. Key quantities such as the scale factor, Hubble parameter, energy density, shear scalar, and scalar expansion diverge at the finite time $t = \frac{2m}{k}$, indicating a "Big Rip" scenario.

Initially, the universe undergoes deceleration, but it transitions to late-time acceleration, potentially through a process called "cosmic recollapse." At late times, the deceleration parameter becomes negative, leading to accelerated expansion, which aligns with the current understanding of the universe's accelerated expansion.

Moreover, the study of both interacting and non-interacting cases of Bianchi type models with LVDP in Lyra geometry proves significant in relation to the accelerated universe scenario, as it offers solutions to some longstanding issues in standard Big Bang cosmology. The results obtained in this paper contribute to a deeper understanding of the universe's evolution.

References

[1] A.G.Riess, A.V.Filippenko, at al., Observational evidence from supernovae for an accelerating universe and a cosmological constant. The astronomical journal, **116**(1998), no. 3, 1009.

[2] A.G.Riess, at al., The Case for an Accelerating Universe from Supernovac, *Publ; Astron, Soc, Pac.*, **114**(2000), 1248–1299.

[3] A.G.Riess, at al., Evidence for Past Deceleration and Constraints on Dark Energy Evolution *Astrophys. J.*, **607**(2004), 665–687.

[4] S.Perlmutter, et al., Measurements of the Cosmological Parameters Ω and Λ from the First Seven Supernovae at z 0.35, *The astrophysical journal*, **483**(1997), no. 2, 565. DOI:10.1086/304265

[5] S.Perlmutter, et al., Measurements of Ω and Λ from 42 High-Redshift Supernovae, *Astrophys. J*, **517**(1999), 565–586. DOI: 10.1086/307221

[6] S.Perlmutter, et al., Discovery of a supernova explosion at half the age of the Universe, *Nature*, **391**(1998), 51–54. DOI: 10.1038/34124

[7] S.Perlmutter, B.P.Schmidt, Measuring cosmology with supernovae, Supernovae and Gamma-Ray Bursters, 2003, 195–217.

[8] R.R.Caldwell, A phantom menace? Cosmological consequences of a dark energy component with super-negative equation of state, *Phys. Lett. B*, **545**(2002), 23–29.

[9] Zhuo-Yi.Huang, Holographic explanation of wide-angle power correlation suppression in the cosmic microwave background radiation, *Journal of Cosmology and Astroparticle Physics*, **5**(2006).

[10] S.F.Daniel, et al., Large scale structure as a probe of gravitational slip, *Physical Review D—Particles, Fields, Gravitation, and Cosmology*, **77**(2008), no. 10, 103513. DOI: 10.1103/PhysRevD.77.103513

[11] S.M.Carroll, M.Hoffman, M.Trodden, Can the dark energy equation-of-state parameter w be less than? 1?, *Physical Review D*, **68**(2003), no. 2, 023509. DOI: 10.1103/PhysRevD.68.023509

[12] Ray, Saibal, et al, Variable equation of state for generalized dark energy mode, *International Journal of Theoretical Physics*, **50**(2011), no. 9, 2687–2696. DOI: 10.1007/s10773-011-0766-2

[13] Ö.Akarsu, Can Battal Kılınç, LRS Bianchi type I models with anisotropic dark energy and constant deceleration parameter, *General Relativity and Gravitation*, **42**(2010), 119–140. DOI: 10.1007/s10714-009-0821-y

[14] Ö.Akarsu, Can Battal Kılınç, Bianchi type III models with anisotropic dark energy, *General Relativity and Gravitation*, **42**(2010), no. 4, 763–775. DOI: 10.1007/s10714-009-0878-7

[15] A.K.Yadav, L.Yadav, Bianchi type III anisotropic dark energy models with constant deceleration parameter, *International Journal of Theoretical Physics*, **50**(2011), 218–227; Pradhan, et al., *Int. J. Theor. Phys.*, **50**(2011), 2923. DOI: 10.1007/s10773-010-0510-3

[16] A.Pradhan, H.Amirhashchi, Dark energy model in anisotropic Bianchi type-III space-time with variable EoS parameter, *Astrophysics and Space Science*, **332**(2011), no. 2, 441–448. DOI: 10.1007/s10509-010-0539-z

[17] A.K.Yadav, F.Rahaman, S.Ray, Dark energy models with variable equation of state parameter, *International Journal of Theoretical Physics*, **50**(2011), 871–881.

[18] H.Amirhashchi, A.Pradhan, B.Saha, Variable equation of state for Bianchi type-VI 0 dark energy models, *Astrophysics and Space Science*, **333**(2011), 295–303. DOI: 10.1007/s10509-010-0577-6

[19] H.Weyl, Vorlesungen uker Allgemeine relativitotstheorie, Sber. Preuss. Akad. der Wiss., 465 Sitzunbgsberichte, zu Berlin, 1918.

[20] G.Lyra, U" ber eine Modifikation der Riemannschen Geometrie, Math, **54**(1951), no. 3, 52–64 .

[21] D.K.Sen, A static cosmological model, *Zeitschrift für Physik*, **149**(1957), no. 3, 311–323.

[22] D.K.Sen, K.A.Dunn, A scalar-tensor theory of gravitation in a modified Riemannian manifold, *J. Math. Phys.*, **12**(1971), no. 3, 578–586.

[23] W.d.Halford, Cosmological theory based on Lyra's geometry, *Aust. J. Phys.*, **23**(1970), 863–869.

[24] W.d.Halford, Scalar-tensor theory of gravitation in a Lyra manifold, *J. Math. Phys.*, **13**(1972), 1699–1703.

[25] A.G.Riess, A.V.Filippenko, et al., Observational evidence from supernovae for an accelerating universe and a cosmological constant, *The astronomical journal*, **116**(1998), no. 3, 1009–1038.

[26] S.Perlmutter, et al., Measurements of X and K from 42 high- redshift supernovae, *Astrophys. J.*, **517**(1999), 565–585.

[27] C.L.Bennett, et al., First-year Wilkinson microwave anisotropy probe (WMAP) observations: preliminary maps and basic results, *Astrophys. J. Suppl. Ser.*, **148**(2003), 1–27. DOI: 10.1086/377253

[28] D.N.Spergel, et al., First-year Wilkinson microwave anisotropy probe (WMAP) observations: determination of cosmological parameters, *Astrophys. J. Suppl. Ser.*, **148**(2003), 175–194. DOI:10.1086/377226

[29] S.Oli, Interacting and non-interacting two fluid cosmological models in a bianchi type-VI0 space times, *Ind. J. Phys.*, **86**(2012), 755–761. DOI: 10.1007/s12648-012-0123-1

[30] M.Tegmark, et al., Cosmological parameters from SDSS and WMAP, *Phys. Rev. D*, **69**(2004), 103501–103526. DOI: 10.1103/PhysRevD.69.103501

[31] L.P.Chimento, Extended tachyon field, chaplygin gas and solvable k-essence cosmologies, *Phys. Rev. D* , **69**(2004), 123517–10.

[32] C.W.Misner, The isotropy of the universe, *Astrophys*, **151** (1968), 431–457.

[33] K.M.Land, Examination of evidence for a preferred axis in the cosmic radiation anisotropy, *Phys. Rev. Lett.*, **95**(2005), 071301–071304 .

[34] J.D.Barrow, Helium formation in cosmologies with anisotropic curvature, *Mon. Not. R. Astr. Soc.*, **211**(1984), 221–227.

[35] R.Santhikumar, B.Satyannarayana, Accelerating anisotropic cosmological model in f(R,T) theory of gravity, *Indian Journal of Physics*, **91**(2017), no. 10, 1293–1296.

[36] M.Krishna, et al., Accelerating plane symmetric cosmological model with bulk viscous and cosmic strings in Lyra's geometry, *Indian Journal of Physics*, **98**(2024), no. 10, 3733–3740 .

[37] S.Perlmutter, et al., Discovery of a supernova explosion at half the age of the universe. *Nature*, **391**(1998), 51.

[38] A. GRiess, et a., Observational evidence from supernovae for an accelerating universe and a cosmological constant, *Astron*, **116**(1998), 1009.

[39] A.G.Riess, et al., The farthest known supernova: support for an accelerating universe and a glimpse of the epoch of deceleration, *Astrophys. J.*, **560**(2001), 49.

[40] M.S.Berman, F. de Mello Gomide, Cosmological models with constant deceleration parameter, *General Relativity and Gravitation*, **20**(1988), 191–198.

[41] Ö.Akarsu, T.Dereli, Cosmological models with linearly varying deceleration parameter." International Journal of Theoretical Physics, **51**(2012), 612–621. DOI: 10.1007/s10773-011-0941-5

[42] R.K.Mishra, et al., String cosmological models from early deceleration to current acceleration phase with varying G and ?, *Eur. Phys. J. Plus.*, **127**(2012), 137.

[43] R.K.Mishra, et al., Bianchi type-I viscous fluid cosmological models with variable deceleration parameter, *Rom. J. Phys.*, **58**(2013a), 75.

[44] R.K.Mishra, et al., Anisotropic viscous fluid cosmological models from deceleration to acceleration in string cosmology, *Int. J. Theor. Phys.*, **52**(2013b), 2546.

[45] R.K.Mishra, et al, Dark energy models in f (R,T) theory with variable deceleration paramete, *Int. J. Theor. Phys.*, **55**(2016), 1241.

[46] N.M.Liang, et al., A Two-Field Dilaton Model of Dark Energy, *Chin. Phys. Lett.*, **26**(2009), 069501.

[47] M.R.Setare, J.Sadeghi, A.R.Amani, Interacting tachyon dark energy in non-flat universe, *Physics Letters B*, **673**(2009), no. 4-5, 241–246.

[48] D.R.K.Reddy, R.Santhikumar, Two fluid Scenario for Dark Energy Model in a Scalar-Tensor Theory of Gravitation, *Int. J. Theor. Phys.*, **52**(2013), no. 4, 1362–1369.

[49] U.M.Rao, Kantowski-Sachs Two Fluid Radiating Cosmological Model in Brans-Dicke Theory of Gravitation, *Advances in Astrophysics*, **1**(2016), no. 1.

[50] S.Sabanam, et al., Two fluids higher dimensional FRW cosmological model rejuvenating the cosmological tests of parametrization of Hubble Parameter in Lyra geometry, 2023, https://arxiv.org/abs/2312.13297.

[51] Praveen Kumar, G.S.Khadekar, V.J.Dagwal, Two Fluids Cosmological Model in (2+1)-Dimensional Saez-Ballester Scalar-Tensor Theory of Gravitation, *Journal of Dynamical Systems and Geometric Theories*, **20**(2022), no. 1, 91–114.
DOI: 10.1080/1726037X.2022.2079267

[52] Ö.Akarsu, Can Battal Kılınç, LRS Bianchi type I models with anisotropic dark energy and constant deceleration parameter, *General Relativity and Gravitation*, **42**(2010), 119–140.

[53] Collins C.B, Glass E.N, and Wilkinson D.A. : *Exact Spatially Homogeneous Cosmologies. General Relativity and Gravitation* , **12**(1980), 805–823.

[54] D.Pavón, Bin Wang, Le Châtelier–Braun principle in cosmological physics, *General Relativity and Gravitation*, **41**(2009), 1–5.

[55] L.Amendola, G.C.Campos, R.Rosenfeld, Consequences of dark matter-dark energy interaction on cosmological parameters derived from type Ia supernova data, *Physical Review D—Particles, Fields, Gravitation, and Cosmology*, **75**(2007), no. 8, 083506.

[56] Z.-K.Guo, N.Ohta, S.Tsujikawa, Probing the coupling between dark components of the universe, *Physical Review D—Particles, Fields, Gravitation, and Cosmology*, **76**(2007), no. 2, 023508.

[57] CR.R.aldwell, et.al., Phantom Energy: Dark Energy with. 1 Causes a Cosmic Doomsday, *Phys. Rev.Lett.*, **91**(2003).

[58] S.Nojiri, S.D.Odintsov, Modified gravity with negative and positive powers of curvature: Unification of inflation and cosmic acceleration, *Phys. Rev.D*, **68**(2003).

Двухжидкостный сценарий космологической модели темной энергии с линейно изменяющимся параметром замедления в геометрии Лиры

М. Кришна
Инженерный колледж Рагху
Вишакхапатнам, Андхра-Прадеш, Индия
К. СобханБабу
Университетский колледж инженерии
Нарасараопета, Андхра-Прадеш, Индия
Р. Сантикумар
Институт технологий и менеджмента Адитьи
Теккали, Шрикакулам, Андхра-Прадеш, Индия

Аннотация. В этой статье мы исследуем оценку параметра темной энергии в пространственно однородном и анизотропном пространстве-времени типа Бианки-VI_0, включающем геометрию Лиры. Чтобы получить определенное решение, мы решаем уравнения поля, используя линейно изменяющийся параметр замедления, предложенный Акарсу и Дерели (2012). Мы анализируем два сценария, включающих взаимодействующие и невзаимодействующие жидкости (баротропную и темную энергию), и выводим общие результаты для каждого случая. Также обсуждаются физические последствия этих результатов.

Ключевые слова: темная энергия, двухжидкостный сценарий, баротропный, геометрия Лиры.

EDN: PNAGOD
УДК 517.9

The Spectrum of the Boundary Value Problem Describing a Two-dimensional Flat Stationary Thermocapillary Flow in a Channel

Elena N. Lemeshkova*
Institute of Computational Modelling SB RAS
Krasnoyarsk, Russian Federation

Received 10.11.2024, received in revised form 21.01.2025, accepted 11.04.2025

Abstract. The problem of two-dimensional thermocapillary fluid flow in a channel with heated bottom is considered. Condition of thermal contact is set on the upper free boundary. The velocity field is linear with respect to the longitudinal coordinate, and the temperature and pressure fields are quadratic functions of the same coordinate. The analysis of the compatibility of the Navier-Stokes equations and the equation of heat transfer leads to a non-linear eigenvalue problem for finding the flow field in the layer. The spectrum of this problem is studied analytically for small Marangoni numbers (second approximation) and numerically for abitrary Marangoni numbers. The non-uniqueness of the solution is established. It is typical for problems of this kind.

Keywords: thermocapillary convection, equations of viscous heat-conducting liquid, inverse problem, spectrum of boundary value problem.

Citation: E.N. Lemeshkova, The Spectrum of the Boundary Value Problem Describing a Two-dimensional Flat Stationary Thermocapillary Flow in a Channel, J. Sib. Fed. Univ. Math. Phys., 2025, 18(4), 532–541. EDN: PNAGOD.

Introduction

Capillary forces associated with the existence of surface tension at the interface between two liquids (or liquid and gas) play a noticeable and in many cases decisive role in reduced gravity conditions. The temperature dependence of the surface tension coefficient is one of the important factors that determines dynamics of the interfacial surface in the presence of inhomogeneous temperature field in the system.

The thermocapillary flow problem of a liquid in the weightless state with a parabolic dependence of surface tension on temperature was studied in [1, 2]. The considered problem admits self-similar solutions within the framework of the Navier-Stokes equations, and it is reduced to an ordinary differential equation similar to the Faulkner-Skene equation in boundary layer theory. It was established that problem can have from one to three solutions. It depends on the values of the defining parameters.

The two-dimensional stationary motion problem of a liquid in a flat channel with free boundary along which the surface tension linearly depends on temperature was considered in [3,4]. The application of the tau method showed that problem has three different solutions. The problem has one solution in the case of thermally insulated free boundary. Characteristic flow structures were constructed for each of the solutions.

*elena_cher@icm.krasn.ru https://orcid.org/0000-0002-9059-2876

One of the characteristic features of the non-linear problem discussed in [1–4] (and in this paper) is the non-uniqueness of the solution. The motion of a viscous liquid in a layer enclosed between two parallel flat surfaces experiencing linear tension at a constant velocity was studied in [5]. It was established that from one to three values of the pressure coefficient can correspond to a fixed value of the Reynolds number. There is no solution at all in a certain range of Reynolds numbers in the axisymmetric case.

In this paper, unlike [3, 4], the solution spectrum of the problem for arbitrary Marangoni number is constructed numerically. The evolution of the spectrum is also traced for non-zero values of the dimensionless heat flux and the Prandtl number. The non-uniqueness of the solution is established. It is typical for problems of this kind

1. Statement of problem

The viscous incompressible fluid flow in a layer of constant thickness l on a flat solid unevenly heated surface is considered. A thermal contact condition is set on the free surface $y = l$ and the surface tension σ depends linearly on temperature: $\sigma(\theta) = \sigma_0 - æ(\theta - \theta_0)$, σ^0, æ and θ_0 are positive constants. The temperature in the fluid is distributed quadratically: $\theta(x, y) = a(y)x^2 + b(y)$, where $|x| < \infty$, $0 \leqslant y \leqslant l$. Such temperature distribution means that at the beginning of the Cartesian coordinate system, the temperature has maximum value for $a(0) < 0$ and minimum value for $a(0) > 0$. Let $u_1(x, y) = w(y)x$, $u_2(x, y) = v(y)$ are components of the velocity vector and $p(x, y)$ is pressure. The stationary flow in the layer that corresponds to the establishment of balance of tangential thermocapillary and viscous stresses on the free surface of the fluid is described by the following system of equations and boundary conditions

$$\begin{gathered} vw_y + w^2 = f + \nu w_{yy}, \quad w + v_y = 0, \\ 2wa + va_y = \chi a_{yy}, \quad vb_y = \chi b_{yy} + 2\chi a, \quad 0 < y < l, \end{gathered} \tag{1}$$

$$y = 0: \quad w = v = 0, \quad a = a_0, \quad b = b_0, \tag{2}$$

$$y = l: \quad v = 0, \quad \rho\nu w_y = -2æa, \quad k\theta_y + \gamma(\theta - \theta_{gas}) = q. \tag{3}$$

In equations (1) parameters $\nu > 0$, $\chi > 0$ are the constant kinematic viscosity and thermal conductivity of the fluid, respectively. The pressure is represented as

$$\frac{1}{\rho}p = d - \frac{f}{2}x^2, \quad d(y) = \nu v_y - \frac{1}{2}v^2 + d_0, \quad d_0 = \text{const},$$

where $\rho > 0$ is fluid density, and f is an arbitrary constant. Parameters a_0, b_0 in equalities (2) are known constants. The first two conditions in (3) are consequences of kinematic and dynamic conditions. In the last equation (3) (thermal contact condition) $k > 0$ is the coefficient of thermal conductivity, $q(x)$ is preset heat flow, $\gamma \geqslant 0$ is the coefficient of heat exchange for fluid-gas interface. It follows from the condition for normal stresses that free surface remains flat. This assumption can be fulfilled, for example, under the action of sufficiently high capillary pressure (value $\sigma_0 \gg 1$) [6]. In accordance with the representation of temperature in the thermal contact condition it is necessary to assume in the general case that

$$\theta_{gas} = a_1x^2 + b_1, \quad q = a_2x^2 + b_2$$

with the specified constants a_k, b_k, $k = 1, 2$. Therefore, the thermal contact condition provides two more relations for $a(y)$, $b(y)$

$$y = l: \quad ka_y + \gamma a = a_2 + a_1\gamma, \quad kb_y + \gamma b = b_2 + b_1\gamma. \tag{4}$$

Remark 1. *The considered problem is non-linear and inverse since constant f is unknown. Indeed, if $v(y)$ is excluded from the mass conservation equation (the second equation (1)) then problem for functions $w(y)$, $a(y)$ is obtained. The problem for function $b(y)$ is separated for known $v(y)$ and $a(y)$, it is considered here.*

Let us introduce dimensionless variables and parameters:

$$\xi = \frac{y}{l}, \quad W = \frac{l^2}{\nu}w, \quad V = \frac{l}{\nu}v, \quad F = \frac{l^4}{\nu^2}f, \quad A = \frac{a}{a_0},$$

$$\mathrm{Pr} = \frac{\nu}{\chi}, \quad \mathrm{Ma} = \frac{a_0 æ l^3}{\rho\nu^2}, \quad \mathrm{Bi} = \frac{\gamma l}{k}.$$

Here Pr is the Prandtl number, Ma is the Marangoni number and Bi is the Bio number.

To define new unknown functions $V(\xi)$, $A(\xi)$ and constant F which is the eigenvalue of the problem the following two-point boundary value problem for non-linear system of ordinary differential equations is obtained from (1)-(4):

$$V''' + V'^2 - VV'' - F = 0, \tag{5}$$

$$A'' + \mathrm{Pr}(2V'A - VA') = 0, \tag{6}$$

$$\xi = 0: \quad V = 0, \quad V' = 0, \quad A = 1, \tag{7}$$

$$\xi = 1: \quad V = 0, \quad V'' = 2\mathrm{Ma}A, \quad A' + \mathrm{Bi}A = Q, \tag{8}$$

where $Q = l(a_2 + a_1\gamma)/k$ is the specified constant.

Remark 2. *For* Ma=0 *problem* (5)-(8) *has a solution: a) for* Q = Bi = 0 *(or* Q = Bi*)* $V^{(0)} = 0$, $F^{(0)} = 0$, $A^{(0)} = 1$*; b) for* Q $\neq 0$ *and* Bi $\neq 0$ $V^{(0)} = 0$, $F^{(0)} = 0$, $A^{(0)} = \delta\xi + 1$, $\delta = (Q - \mathrm{Bi})(1 + \mathrm{Bi})^{-1}$.*For* $|Ma| < 1$ *solution is taken in the form*

$$V = \mathrm{Ma}V^{(1)}, \quad F = \mathrm{Ma}F^{(1)}, \quad A = A^{(0)} + \mathrm{Ma}A^{(1)}, \tag{9}$$

where the order of magnitude of $V^{(1)}, F^{(1)}, A^{(1)}$ is equal to one. After substituting (9) *in system* (5)-(8) *and neglecting the quadratic Marangoni terms, linear problem for $V^{(1)}$, $F^{(1)}$ and $A^{(1)}$ is obtained. After solving the resulting problem with an accuracy of $O(Ma^2)$ for functions V, A and constant F, one can obtain*

$$\begin{gathered} V = \mathrm{Ma}(\delta + 1)\xi^2(\xi - 1), \quad F = 3\mathrm{Ma}(\delta + 1), \\ A = -\frac{\mathrm{MaPr}(\delta + 1)}{60}\left[2\delta\xi^6 - 3(\delta - 1)\xi^5 - 5\xi^4 + \frac{5 + 3\delta + \mathrm{Bi}(2 + \delta)}{1 + \mathrm{Bi}}\xi\right] + A^{(0)}. \end{gathered} \tag{10}$$

2. The second approximation with respect to the Marangoni number

Decompositions of functions W, A and eigenvalue F into series with respect to Marangoni number Ma up to the terms $O(\mathrm{Ma}^3)$ have the form

$$V = \mathrm{Ma}V^{(1)} + \mathrm{Ma}^2V^{(2)}, \quad F = \mathrm{Ma}F^{(1)} + \mathrm{Ma}^2F^{(2)}, \quad A = A^{(0)} + \mathrm{Ma}A^{(1)} + \mathrm{Ma}^2A^{(2)},$$

where functions $V^{(1)}, A^{(1)}$ and constant $F^{(1)}$ are already known (see (9), (10)). Let us write the boundary value problem for the second approximation

$$V^{(2)\prime\prime\prime} + \left(V^{(1)\prime}\right)^2 - V^{(1)}V^{(1)\prime\prime} - F^{(2)} = 0, \tag{11}$$

$$A^{(2)\prime\prime} + \mathrm{Pr}\left(2(V^{(1)\prime}A^{(1)} + V^{(2)\prime}A^{(0)}) - V^{(1)}A^{(1)\prime} - V^{(2)}A^{(0)\prime}\right) = 0, \tag{12}$$

$$\xi = 0: \quad V^{(2)} = 0, \quad V^{(2)\prime} = 0, \quad A^{(2)} = 0, \tag{13}$$

$$\xi = 1: \quad V^{(2)} = 0, \quad V^{(2)\prime\prime} = 2A^{(1)}, \quad A^{(2)\prime} + \mathrm{Bi}A^{(2)} = 0. \tag{14}$$

Using relations (10) and taking into account conditions (13), one can find from (11), (12) that

$$V^{(2)} = -\frac{(\delta+1)^2}{840}(3\xi^2 - 7\xi^6 + 7\xi^5) + \frac{F^{(2)}\xi^3}{6} + \frac{C_1\xi^2}{2},$$

$$A^{(2)} = \frac{\mathrm{Pr}(\delta+1)^2}{20}\left[\frac{\delta}{45}x^{10} - \left(\frac{\delta}{54} + \frac{\delta-1}{24}\right)x^9 + \left(\frac{\delta-1}{28} - \frac{5}{56}\right)x^8 + \frac{5}{63}x^7 + \frac{\delta_1}{20}x^5 - \frac{\delta_1}{20}x^4\right] +$$

$$+\frac{\mathrm{Pr}(\delta+1)^2}{24}\left[\frac{13\delta}{840}x^9 - \left(\frac{11\delta}{280} - \frac{3}{140}\right)x^8 + \frac{1}{70}(3\delta-4)x^7 + \frac{1}{15}x^6 - F^{(2)}\delta x^5 - (3C_1\delta + 2F_2)x^4\right] -$$

$$-\frac{1}{3}\mathrm{Pr}C_1x^3 + C_2x, \qquad \delta_1 = \frac{5 + 3\delta + \mathrm{Bi}(2+\delta)}{1+\mathrm{Bi}}. \tag{15}$$

There is linear system for unknown coefficients C_1, C_2 and eigenvalue $F^{(2)}$ that follows from three boundary conditions (14). The solution of this system is

$$C_1 = -\frac{\mathrm{Pr}(\delta+1)}{60}(\delta - \delta_1 + 2) - \frac{19}{840}(\delta+1)^2,$$

$$C_2 = \frac{\mathrm{Pr}(\mathrm{Bi}+1)^{-1}}{151200}\Big[315\delta(\delta+1)^2 + \mathrm{PrBi}(17\delta^3 + 42\delta^2\delta_1 - 146\delta^2 + 294\delta\delta_1 - 553\delta + 252\delta_1) +$$

$$+\mathrm{Pr}(570\delta^3 - 525\delta^2\delta_1 + 1980\delta^2 - 735\delta\delta_1 + 1935\delta - 210\delta_1 + 525) + 15\mathrm{Bi}(\delta^3 - 36\delta^2 - 27\delta - 14)\Big],$$

$$F^{(2)} = \frac{5}{56}(\delta+1)^2 + \frac{\mathrm{Pr}}{20}(\delta+1)(\delta - \delta_1 + 2).$$

Then

$$F = 3\mathrm{Ma}(\delta+1) + \mathrm{Ma}^2\left[\frac{5}{56}(\delta+1)^2 + \frac{\mathrm{Pr}}{20}(\delta+1)(\delta - \delta_1 + 2)\right] + O(\mathrm{Ma}^3).$$

As can be seen, pressure coefficient F here depends on the Prandtl number. It means that thermal and hydrodynamic fields in the layer become interconnected.

3. Numerical integration

An algorithm for numerical analysis of system (5)–(8) is proposed below for arbitrary values of the Marangoni number (Ma). Boundary value problem (5)–(8) is reduced the to the Cauchy problem. Let us subject the differential equations in (5), (6) to the action of a linear transformation group [7]

$$\xi = D_1\overline{\xi}, \quad V = D_2\overline{V}, \quad A = \overline{A}, \tag{16}$$

where $D_1 \neq 0, D_2 \neq 0$ are parameters to be determined. The transformed equations have the form

$$\overline{V}''' + D_1D_2\overline{V}'^2 - D_1D_2\overline{V}\,\overline{V}'' - D_1^{-3}D_2^{-1}F = 0, \quad \overline{A}'' + D_1D_2\mathrm{P}(2\overline{V}'\overline{A} - \overline{V}\,\overline{A}') = 0, \tag{17}$$

It can be seen that resulting equations is invariant with respect to the transformation parameters if

$$D_1D_2 = 1. \tag{18}$$

Then system (17) takes the form

$$\overline{V}''' + \overline{V}'^2 - \overline{V}\,\overline{V}'' - \overline{F} = 0, \quad \overline{A}'' + \mathrm{P}(2\overline{V}'\overline{A} - \overline{V}\,\overline{A}') = 0, \tag{19}$$

where

$$\overline{F} = D_1^4F. \tag{20}$$

The boundary conditions at the point $\xi = 0$ is not changed:

$$\overline{\xi} = 0: \quad \overline{V} = 0, \quad \overline{V}' = 0, \quad \overline{A} = 1. \tag{21}$$

The missing conditions for $\overline{\xi} = 0$ are obviously conditions for the second and first derivatives: $\overline{V}''$, $\overline{A}'$. To obtain these conditions it is required that after the transformation they do not depend on D_1: $V''(0) = D_1^{-3}, A'(0) = D^{-1}$. Then, after converting (16), one can obtain

$$\overline{V}''(0) = 1, \quad \overline{A}'(0) = 1. \tag{22}$$

These two conditions together with conditions (21) allows one to solve system of equations (19) as Cauchy problem.

The first condition of (14) at the point $\xi = 1$ after the transformation of (16) takes the form

$$\overline{V}(D_1^{-1}) = 0. \tag{23}$$

This allows one to determine conversion parameter D_1 and hence D_2 from (18).

The described actions allow one to develop the following scheme for constructing spectra $F = F(\mathrm{Ma}, \mathrm{Pr})$ and $F = F(Q, \mathrm{Pr})$ of boundary value problem (5)-(8). The value of $\overline{F} \in (-\infty, \infty)$ is set, and Cauchy problem (19), (21), (22) is integrated until condition $\overline{V} = 0$ is satisfied. Let this happen for a certain value $\overline{\xi} = \overline{\xi}_0$. In accordance with conditions (18), (23), the values of the transformation parameters are obtained: $D_2 = D_1^{-1} = \overline{\xi}_0$. The values of the Marangoni number and parameter Q are found using the last two conditions (8), namely, taking into account (16), $\mathrm{Ma} = \overline{\xi}_0^3\overline{V}''(\overline{\xi}_0)/2\overline{A}(\overline{\xi}_0)$, $Q = \overline{\xi}_0\overline{A}'(\overline{\xi}_0) + \mathrm{Bi}\overline{A}\,\overline{\xi}_0$. Finally, the eigenvalue of original problem (5)–(8) is obtained in the form $F = D_1^{-4}\overline{F} = \overline{\xi}_0^4\overline{F}$.

Note that during the implementation of the described algorithm the possibility of non-uniqueness of the root $\overline{\xi}_0$ of the equation $\overline{V}(\overline{\xi}_0) = 0$ is taken into account. In addition, since

parameters D_1, D_2 (16) can have any sign the integration of problem (19), (21), (22) should be performed separately in intervals $\overline{\xi}_0 \in (-\infty, 0]$ and $\overline{\xi}_0 \in [0, +\infty)$.

Fig. 1a schematically shows the behaviour of function $\overline{V}(\overline{\xi})$ at $\overline{\xi} \in (-\infty, 0]$ in relation to the value of the modified pressure gradient $\overline{F}$. It can be seen that in the interval $\overline{F} \in (\overline{F}_*, +\infty)$ ($\overline{F}_* \approx 0.755$) there are two non-zero roots $\overline{\xi}_{01}$ and $\overline{\xi}_{02}$ of equation $\overline{V}(\overline{\xi}) = 0$. In the interval $\overline{F} \in (-\infty, \overline{F}_*]$ the function $\overline{V}(\overline{\xi})$ has no zeros, when $\overline{\xi} \in (-\infty, 0]$. For $\overline{\xi} \in [0, +\infty)$ equation $\overline{V}(\overline{\xi}) = 0$ has single root $\overline{\xi}_0$ for any value of the modified pressure gradient $\overline{F} \in (-\infty, +\infty)$ (Fig. 1b).

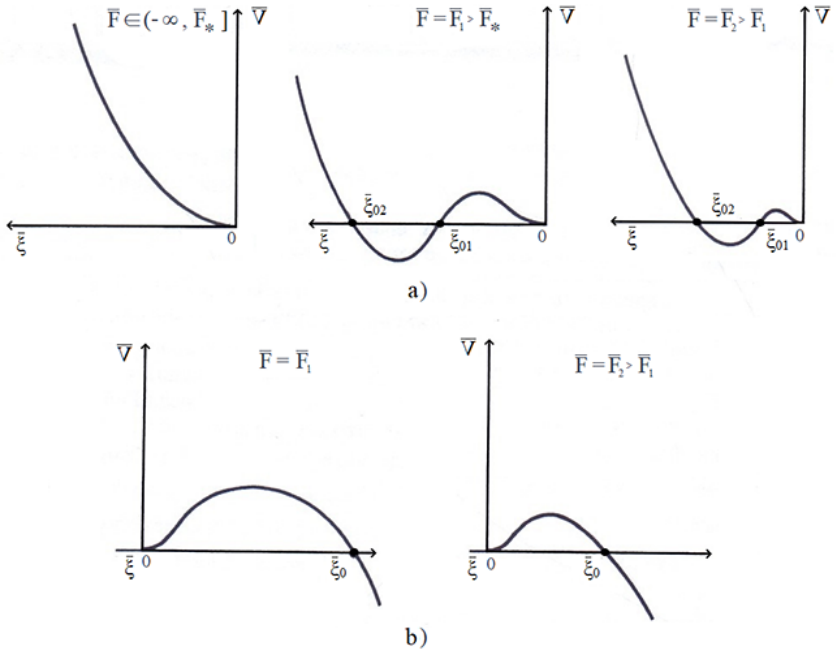

Fig. 1. Behavior of function $\overline{V}(\overline{\xi})$

Fig. 2 shows numerical spectrum of $F = F(\mathrm{Ma}, 0)$ ($\mathrm{Bi} = 0, Q = 0$ and $A = 1$). The root $\overline{\xi}_{01}$ (see above) generates spectrum for positive Marangoni numbers (branch 1). The root $\overline{\xi}_0$ together with the root $\overline{\xi}_{01}$ give branch 2 that corresponds to the negative Marangoni numbers. The values of the root $\overline{\xi}_0$ generate branch 3 of the spectrum ($\mathrm{Ma} < 0$), one of the ends of which corresponds to asymptote (10), and the other tends when $\overline{F} \to 0 - 0$ to a vertical asymptote common to branch 2 for $\lg |\mathrm{Ma}| \approx 2.758$. Only branch 3 corresponds to negative values of $\overline{F}$.

It is established that there are non-unique solutions with spectrum $F = F(\mathrm{Ma}, 0)$. In particular, there are at most two solutions in the considered range of the modified pressure gradient $\overline{F} \in (0.756; 10^4)$ on branch 1 ($\mathrm{Ma} > 0$). Branches 2 and 3 ($\mathrm{Ma} < 0$) have from one to three eigenvalues F corresponding to fixed value of the Marangoni number (branch 3 has one solution). The section of branch 2 with non-unique solution is shown in the insert in Fig. 2. One should note that there are at least two solutions with zero eigenvalue: one solution corresponds to asymptote (10), $\mathrm{Ma} = 0$, and the second solution corresponds to $\mathrm{Ma} = -572.426$ (the vertical asymptote of branches 2 and 3).

Characteristics of the fluid flow that occurs in the layer as a result of heating of the lower solid wall are shown in Fig. 3. The profiles of the horizontal velocity in the region $x > 0$ are depicted for a number of points in spectrum $F = F(\mathrm{Ma}, 0)$ ($\mathrm{Bi} = 0, Q = 0$ and $A = 1$).

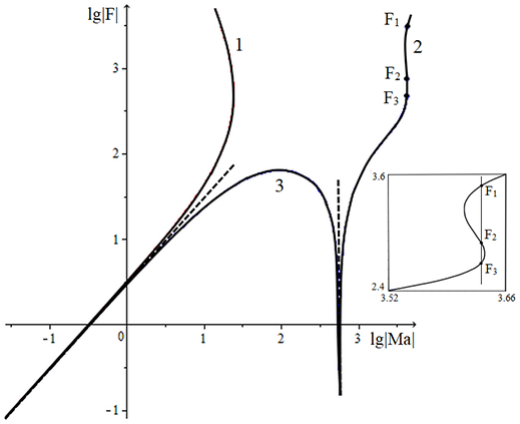

Fig. 2. Spectrum $F = F(\mathrm{Ma}, 0)$ of problem (5)-(8) for $\mathrm{Bi} = 0, Q = 0$

Functions $W(\xi) = l^2\nu^{-1}w$, $W = -V_\xi$ are plotted along the abscissa axis. Curves 1-3 correspond to $F_1 = 2783.857, F_2 = 887.843$ and $F_3 = 421.954$, respectively (see Fig. 2, branch 2). In these cases, the direction of fluid flow is changed twice, that is, a two-vortex flow occurs in the layer (see Fig. 4a). Curve 4 corresponds to the solution for zero eigenvalue: $F = 0$, $\mathrm{Ma} = -572.426$. In this case, there is one return flow zone which makes up almost $2/3$ of the layer (see Fig. 4b). All points of the spectrum forming branches 1 and 3 correspond to a single-vortex flow (one zone of return flow, see Fig. 4b). Moreover, for all points of branch 1 ($\mathrm{Ma} > 0$, $F > 0$) the return flow zone is located near the free boundary.

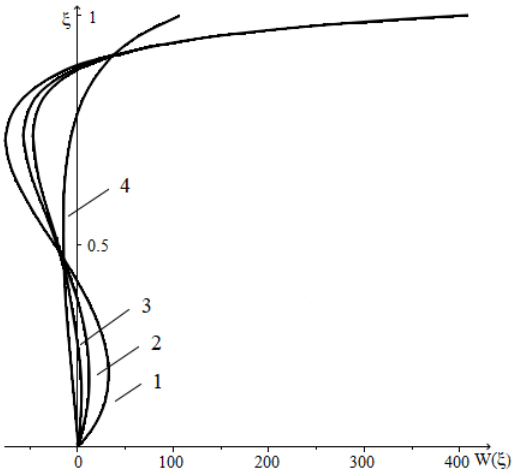

Fig. 3. The profile of the horizontal velocity for $x > 0$

Fig. 5 shows spectra $F = F(\mathrm{Ma}, 0)$ for $\mathrm{Bi} = 0$, $Q = 1$ (a) and $Q = 5$(b) (the heat flux is set at the free boundary). For $Q = 1$, branch 1 corresponds to a positive value of the Marangoni number, and branches 2, 3 correspond to a negative value of the Marangoni number. It can be seen that there is no more than one solution on all branches. For $Q = 5$, the positive values of the Marangoni number correspond to branches 1, 2, and the negative values of the Marangoni number correspond to branches 3, 4, 5. It can be seen that there are up to four solutions on

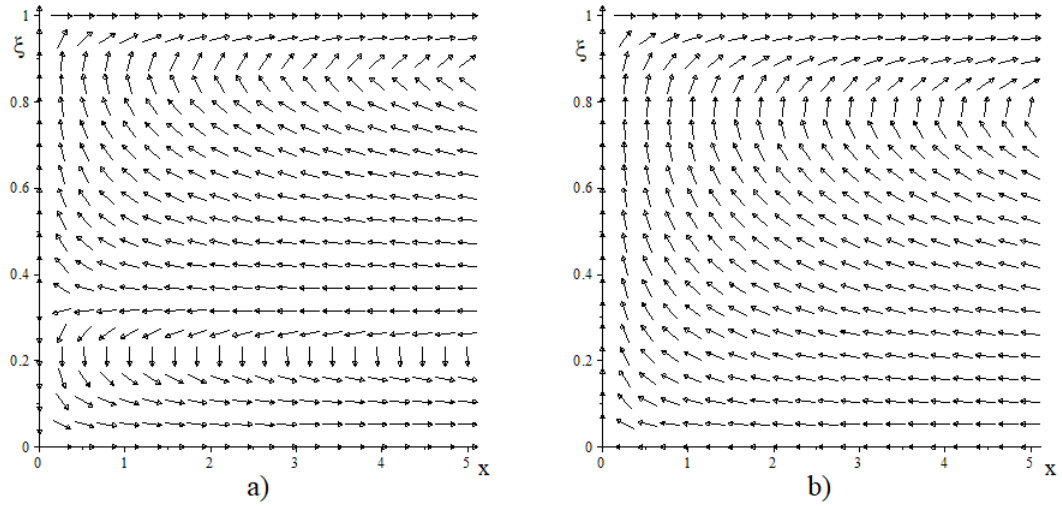

Fig. 4. Streamlines in the layer for $F = 421.954$ (a) and $F = 0$ (b)

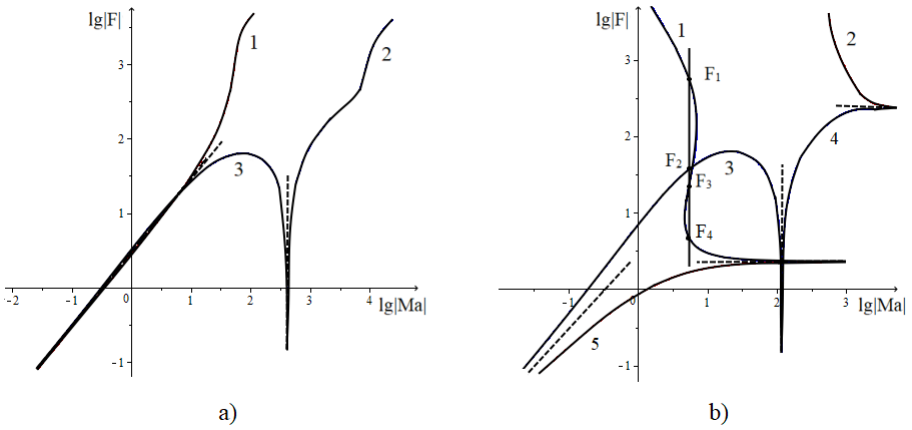

Fig. 5. Spectrum $F = F(\mathrm{Ma}, 0)$ of problem (5)-(8) for $\mathrm{Bi} = 0, Q = 1$ (a) and $Q = 5$ (b)

branch 1 ($\mathrm{Ma} > 0$).

Fig. 6, 7 show spectra $F = F(\mathrm{Ma}, \mathrm{Pr})$(a) and $F = F(Q, \mathrm{Pr})$(b) for the Prandtl numbers $\mathrm{Pr} = 5$ and $\mathrm{Pr} = 50$. The positive values of the Marangoni number and the dimensionless parameter Q correspond to branches 2, 4 (Fig. 6a) and branch 3 (Fig. 6b). Branches 1 and 4 in Fig. 6a (and branch 1 in Fig. 6b) correspond to positive eigenvalues F. The result can be interpreted as follows: the value of the dimensionless pressure gradient F_1 can be obtained by setting two different combinations of the Marangoni number Ma and the dimensionless heat flow Q (Ma_1, Q_1 и Ma_2, Q_2). Variation in the Bio number (Bi) does not provide qualitative changes in the spectrum of solutions of boundary value problem (5)-(8). Therefore, it is assumed to be zero in all calculations.

In conclusion, one should emphasize the importance of the proposed method. In most thermocapillary convection problems containing parameters, the total number of solutions for the entire range of parameter values is of interest rather than particular solution for a specific set of

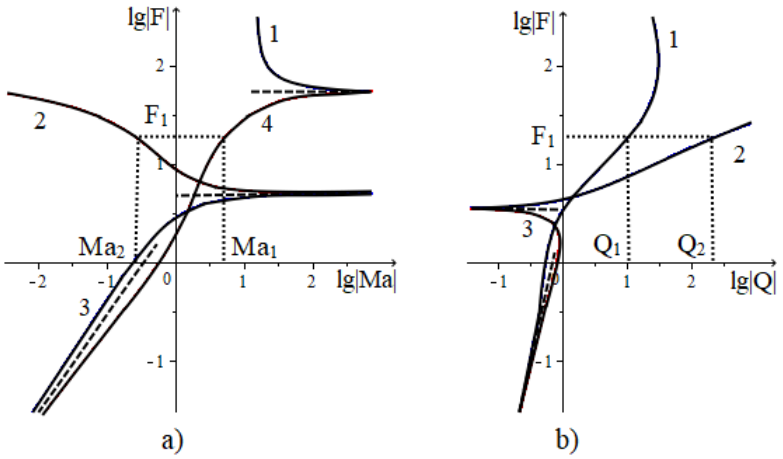

Fig. 6. Spectra $F = F(\mathrm{Ma}, 5)$ (a) and $F = F(Q, 5)$ (b) of problem (5)-(8) for $\mathrm{Bi} = 0$

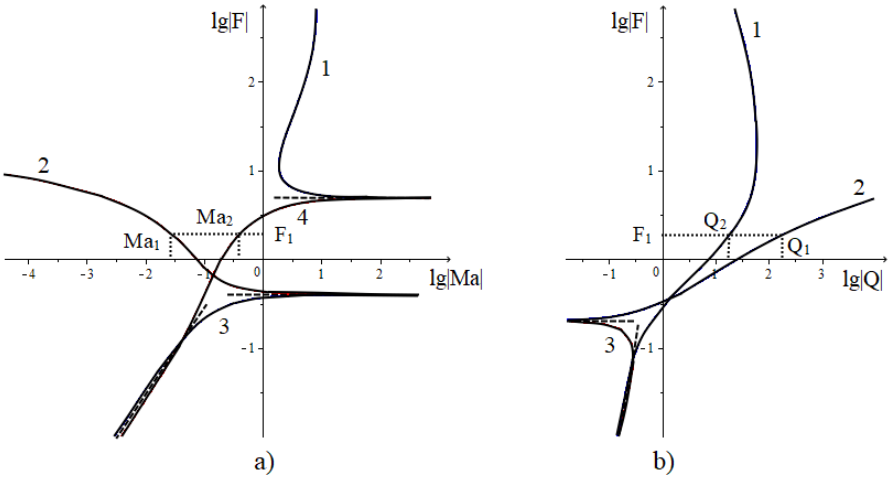

Fig. 7. Spectra $F = F(\mathrm{Ma}, 50)$ (a) and $F = F(Q, 50)$ (b) of problem (5)-(8) for $\mathrm{Bi} = 0$

parameter values.

This work is supported by the Krasnoyarsk Mathematical Center and financed by the Ministry of Science and Higher Education of the Russian Federation in the framework of the establishment and development of regional Centers for Mathematics Research and Education (Agreement no. 075-02-2024-1378).

References

[1] N.N.Bobkov, Yu.P.Gupalo, The flow pattern in a liquid layer and the spectrum of the boundary-value problem when the surface tension depends non-linearly on the temperature, *Journal of Applied Mathematics and Mechanics*, **60**(1996), no. 6, 999–1005.
DOI: 10.1016/S0021-8928(96)00122-0

[2] Y.P.Gupalo, Y.S.Ryazantsev, Thermocapillary motion of a liquid with a free surface with nonlinear dependence of the surface tension on the temperature, *Fluid Dynamics*, **23**(1988), 752–757. DOI: 10.1007/BF01051714

[3] E.N.Lemeshkova, Two-dimensional thermocapillary motion of a liquid in an open channel, *The Bulletin of Irkutsk State University. Mathematics Series*, **41**(2022), 121–130 (in Russian). DOI: 10.26516/1997-7670.2022.41.121

[4] E.N.Lemeshkova, Two-Dimensional Plane Steady-State Thermocapillary Flow, *Fluid Dynamics*, **54**(2019), 33–41. DOI: 10.1134/S0015462819010087

[5] J.F.Brady, A.Acrivos, Steady flow in a channel or tube with an accelerating surface velocity. An exact solution to the Navier – Stokes equations with reverse flow, *J. Fluid Mech.*, **112**(1981), 127–150. DOI: 10.1017/S0022112081000323

[6] R.H.Zeytunyan, The problem of thermocapillary instability of Benard – Marangoni, *UFN*, **168**(1998), 259–286 (in Russian). DOI: 10.1070/PU1998v041n03ABEH000374

[7] C.Na, Computational methods for solving applied boundary value problems, Moscow, Mir, 1982 (in Russian).

Спектр краевой задачи, описывающей двумерное плоское стационарное термокапиллярное течение в канале

Елена Н. Лемешкова
Институт вычислительного моделирования СО РАН
Красноярск, Российская Федерация

Аннотация. Исследуется задача о двумерном термокапиллярном течении жидкости в канале с подогреваемым нижним дном. На верхней свободной границе задано условие теплового контакта. Поле скоростей линейно по продольной координате, поля температуры и давления — квадратичные функции той же координаты. Анализ совместности уравнений Навье–Стокса и теплопроводности приводит к нелинейной задаче на собственные значения для нахождения поля течения в слое. Спектр этой задачи исследуется аналитически при малых числах Марангони (второе приближение) и численно при любых числах Марангони. Установлена неединственность решения, характерная для задач подобного рода.

Ключевые слова: термокапиллярная конвекция, уравнения вязкой теплопроводной жидкости, обратная задача, спектр краевой задачи.

EDN: RPFJEL
УДК 517.9

Enhancing Secure Communication Using a Robust Synchronization Scheme of Fractional-order Hyperchaotic Systems

Nabil Haneche*
Applied Mathematics and Modeling Laboratory
Department of Mathematics
University of Mentouri Brothers
Constantine 25000, Algeria
Tayeb Hamaizia†
Mathematical Modeling and Simulation Laboratory
Department of Mathematics
University of Mentouri Brothers
Constantine 25000, Algeria

Received 19.11.2024, received in revised form 13.01.2025, accepted 14.05.2025

Abstract. In recent years, there has been great interest shown in the literature in the study of chaotic dynamical systems. In this paper, an adaptive control scheme has been introduced to achieve synchronization between two different fractional-order hyperchaotic systems with unknown parameters. By using rigorous techniques of fractional calculus, the controller has been designed based on Lyapunov stability theory. The adaptive hybrid synchronization between fractional-order hyperchaotic Lorenz and Chen systems has evolved to illustrate the constructed synchronization scheme. In order to create high security for signal transmission, an application of synchronization in secure communication has been performed. Computer simulations were carried out to validate the theoretical results derived from this study.

Keywords: fractional-order, hyperchaotic system, synchronization, secure communication.

Citation: N. Haneche, T. Hamaizia, Enhancing Secure Communication Using a Robust Synchronization Scheme of Fractional-order Hyperchaotic Systems, J. Sib. Fed. Univ. Math. Phys., 2025, 18(4), 542–554. EDN: RPFJEL.

Introduction

In recent years, the topic of chaotic systems has received great attention from a number of researchers in chaos theory. The main reason for this interest is due to the many applications of chaotic systems in sciences and engineering. Biology, neural networks, cryptography, physics, chemistry, and secure communication are most fields were the chaotic systems are frequently applied in practice [1]. A hyperchaotic system is defined as chaotic system has more than one positive Lyapunov exponent, in which the minimal dimension for a continuous-time hyperchaotic system is four [2].

Recently, fractional calculus has become an important topic in mathematics and physics. Due to the hereditary and nonlocal distributed behaviors in dynamic phenomena, modeling

*nabil.haneche@doc.umc.edu.dz https://orcid.org/0009-0005-2866-6853
†el.tayyeb@umc.edu.dz

of dynamical systems in sciences and engineering using fractional differential equations is more suitable than integer-order equations [3]. Since the works of Leibniz in 1695, the idea of fractional derivative of continuous function has been explored [4]. In recent decades, several fractional differential and integral operators have been defined. Since the works of Carroll and Pecora (1990) [5], the field of synchronization of systems using chaos theory has become very popular in the literature. Nowadays, control and synchronization of chaos phenomena in fractional-order chaotic systems have significant interest, due to their important applications in cryptography and signal transmission. In the chaos control problem, the desired goal is to construct an efficient control law to stabilize the state trajectories of the chaotic system. On the other side, a pair of dynamical chaotic systems called master and slave systems are said to be synchronized when the trajectories of the slave system asymptotically track the trajectories of the master system in infinite time. Many control schemes have been reported to control fractional-order chaotic systems, such as adaptive control [6], active control [7], passive control [8], sliding mode control [9], and many others. Furthermore, various types of synchronization of chaotic systems have been introduced, such as complete synchronization [10], anti-synchronization [11], projective synchronization [12], lag synchronization [13], etc. Recently, a new type of chaotic synchronization has developed called function projective synchronization, where the master and response systems could be synchronized up to a scaling function [14].

In the literature, several fractional-order chaotic systems have been employed in the construction of secure communication schemes using the techniques of chaos synchronization [15, 16]. To our knowledge, the general idea for transmitting a message signal via chaotic systems is that an original information signal is injected in the transmitter system, which produces a chaotic signal. The chaotic signal is then transmitted to the receiver via a public channel. Finally, after the transmitter and receiver systems are synchronized, the encrypted information signal can be successfully recovered at the receiver. In this work, our aim is to synchronize two nonidentical fractional-order hyperchaotic systems by performing a suitable adaptive controller. Based on the Lyapunov theory of fractional-order systems, the theoretical results in this paper have been demonstrated. Computer simulations were performed to validate the feasibility and effectiveness of the proposed method.

The remainder of this paper is organized as follows. In Section 2, basic notions of fractional calculus are introduced. In Section 3, the general idea of the proposed synchronization method based on fractional-order hyperchaotic systems is discussed. In Section 4, based on the stability theory of fractional-order systems, an adaptive hybrid synchronization between two nonidentical fractional-order hyperchaotic systems is achieved. In Section 5, a secure communication scheme based on adaptive hybrid synchronization of fractional-order hyperchaotic systems is constructed. Finally, we draw conclusions in Section 6.

1. Mathematical background

In this section, we provide some notions of fractional calculus that help us build this paper.

Definition 1. *The Riemann-Liouville fractional integral of order $q \in \mathbb{R}^+$ of a continuous function $u : \mathbb{R}^+ \to \mathbb{R}$ is defined as [17]*

$$J_{t_0}^q u(t) = \frac{1}{\Gamma(q)} \int_{t_0}^{t} (t-s)^{q-1} u(s) ds, \tag{1}$$

where $t > t_0$, $\Gamma(.)$ is the Gamma function.

Definition 2. *The Caputo fractional derivative of order $q \in \mathbb{R}^+$ of a continuous function $u : [t_0, +\infty[\to \mathbb{R}$ is defined as [18]*

$$ {}^cD^q_{t_0} u(t) = \frac{1}{\Gamma(m-q)} \int_{t_0}^{t} \frac{u^{(m)}(s)}{(t-s)^{q+1-m}} ds \tag{2} $$

where $t > t_0$, $m-1 < q \leqslant m$ with $m = \lceil q \rceil$.

We have the following fundamental properties of the differential operator ${}^cD^q_{t_0}$ [19]

1. If $p > q \geqslant 0$ where $0 \leqslant m-1 \leqslant p < m$ and $0 \leqslant n-1 \leqslant q < n$ such that m and n are two integers, then
$$ {}^cD^p_{t_0} \left({}^cD^{-q}_{t_0} u(t) \right) = {}^cD^{p-q}_{t_0} u(t) \tag{3} $$
2. If $p, q \geqslant 0$ where $0 \leqslant m-1 \leqslant p < m$ and $0 \leqslant n-1 \leqslant q < n$ such that m and n are two integers, then
$$ {}^cD^p_{t_0} \left({}^cD^q_{t_0} u(t) \right) = {}^cD^{p+q}_{t_0} u(t) - \sum_{j=1}^{n} \left[{}^cD^{q-j}_{t_0} u(t) \right]_{t=t_0} \frac{(t-t_0)^{-p-j}}{\Gamma(1-p-j)}. \tag{4} $$
3. For $p, q > 0$, we assume that there exists some $n \in \mathbb{N}$ such that $p, p+q \in [n-1, n]$, then
$$ D^p D^q u(t) = D^{p+q} u(t). \tag{5} $$
4. Let $n-1 < q < n$, $n \in \mathbb{N}$. We assume that both ${}^cD^q_{t_0} u(t)$ and ${}^cD^q_{t_0} v(t)$ exist, the Caputo fractional derivative is a linear operator
$$ {}^cD^q_{t_0} \left(u(t) + v(t) \right) = {}^cD^q_{t_0} u(t) + {}^cD^q_{t_0} v(t). \tag{6} $$

Lemma 1 ([20]). *Let $u(t) \in \mathbb{R}^n$ be a continuous and derivable function. Then for any time instant $t \geqslant t_0$*

$$ \frac{1}{2} {}^cD^q_{t_0} \left(u^T(t) u(t) \right) \leqslant u^T(t) \times {}^cD^q_{t_0} u(t), \ \forall\, q \in (0,1) \tag{7} $$

The following theorem establishes the stability of equilibrium point of the following fractional-order system by extending the Lyapunov direct method to a fractional-order systems.

$$ {}^cD^q_{t_0} x(t) = f(t, x(t)), \tag{8} $$

where $q \in (0,1)$, $x \in \mathbb{R}^n$ and t represents the time.

Theorem 1.1 ([21]). *If there exists a positive definite Lyapunov function $V(t, x(t))$ such that*

$$ {}^cD^q_{t_0} V(t, x(t)) \leqslant 0, \quad \forall\, t \geqslant t_0, \tag{9} $$

then the trivial solution of system (8) is asymptotically stable.

2. Problem description

In order to construct the desired adaptive hybrid synchronization between the master and slave systems with unknown parameters, we take the master hyperchaotic system in the form of

$$ {}^cD^q_{t_0} x = f(x) + F(x)\alpha \tag{10} $$

and the slave hyperchaotic system in the form of

$$ {}^{c}D_{t_0}^{q} y = g(y) + G(y)\beta + u, \tag{11} $$

where $x, y \in \mathbb{R}^n$ are the state vectors, $u \in \mathbb{R}^n$ is the adaptive controller, $\alpha \in \mathbb{R}^m$, $\beta \in \mathbb{R}^r$ are unknown parameter vectors, $f(x), g(y) \in \mathbb{R}^n$, $F(x) \in \mathbb{R}^{n\times m}$, $G(y) \in \mathbb{R}^{n\times r}$. Next, we divide the master and slave systems into two parts, then system (10) can be expressed as

$$ \begin{aligned} {}^{c}D_{t_0}^{q} x_i &= f_i(x) + F_i(x)\alpha_i, \\ {}^{c}D_{t_0}^{q} x_j &= f_j(x) + F_j(x)\alpha_j, \end{aligned} \tag{12} $$

and the slave system can be described as

$$ \begin{aligned} {}^{c}D_{t_0}^{q} y_i &= g_i(y) + G_i(y)\beta_i + u, \\ {}^{c}D_{t_0}^{q} y_j &= g_j(y) + G_j(y)\beta_j + u. \end{aligned} \tag{13} $$

Next, we define the synchronization error between the master and slave systems as

$$ e_i = y_i - x_i, \tag{14} $$

and the anti-synchronization error between the master and slave systems as

$$ e_j = y_j + x_j. \tag{15} $$

From the definition of complete synchronization, if $\lim_{t\to\infty} \|e_i\| = \lim_{t\to\infty} \|y_i(t, y_0) - x_i(t, x_0)\| = 0$, where $x_0 = (x_i(0), x_j(0))$ and $y_0 = (y_i(0), y_j(0))$ are the initial conditions of the master and slave systems, respectively, the complete synchronization between the master and slave systems is achieved. Also, if $\lim_{t\to\infty} \|e_j\| = \lim_{t\to\infty} \|y_j(t, y_0) + x_j(t, x_0)\| = 0$, we get the anti-synchronization between the master and slave systems where $\|.\|$ is the Euclidean norm. Our objective is to construct an effective adaptive controller to achieve the synchronization between systems (12) and (13).

Theorem 2.2. *If the controller $u(t, x, y)$ is selected as*

$$ u(t,x,y) = \begin{cases} f_i(t,x) + F_i(t,x)\hat{\alpha}_i - G_i(t,y)\hat{\beta}_i - g_i(t,y) - e_i, \\ -f_j(t,x) - F_j(t,x)\hat{\alpha}_j - G_j(t,y)\hat{\beta}_j - g_j(t,y) - e_j, \end{cases} \tag{16} $$

and adaptive law of parameters is chosen as

$$ \begin{aligned} {}^{c}D_{t_0}^{q}\hat{\alpha}_i &= -[F_i(t,x)]^T e_i, \qquad {}^{c}D_{t_0}^{q}\hat{\beta}_i = [G_i(t,y)]^T e_i \\ {}^{c}D_{t_0}^{q}\hat{\alpha}_j &= -[F_j(t,x)]^T e_j, \qquad {}^{c}D_{t_0}^{q}\hat{\beta}_j = [G_j(t,y)]^T e_j, \end{aligned} \tag{17} $$

then the sychronization and anti-synchronization between the master system (12) *and slave system* (13) *are achieved, in which the estimations of the unknown parameters α_i, β_i, α_j, and β_j are $\hat{\alpha}_i$, $\hat{\beta}_i$, $\hat{\alpha}_j$, and $\hat{\beta}_j$, respectively.*

Proof. From equations (12), (13) and (16), the fractional-order error system can be expressed as

$$ {}^{c}D_{t_0}^{q} e = F_i(x)\left(\alpha_i - \hat{\alpha}_i\right) - G_i(y)\left(\beta_i - \hat{\beta}_i\right) + F_j(x)\left(\alpha_j - \hat{\alpha}_j\right) + G_j(y)\left(\beta_j - \hat{\beta}_j\right) - e \tag{18} $$

where $e = (e_i, e_j)^T$. Now, we define the quadratic Lyapunov function by

$$ V\left(e_i, e_j, \tilde{\alpha}_i, \tilde{\alpha}_j, \tilde{\beta}_i, \tilde{\beta}_j\right) = \frac{1}{2}\left(e_i^T e_i + e_j^T e_j + \tilde{\alpha}_i^T\tilde{\alpha}_i + \tilde{\alpha}_j^T\tilde{\alpha}_j + \tilde{\beta}_i^T\tilde{\beta}_i + \tilde{\beta}_j^T\tilde{\beta}_j\right), \tag{19} $$

where $\tilde{\alpha}_i = \alpha_i - \hat{\alpha}_i$, $\tilde{\alpha}_j = \alpha_j - \hat{\alpha}_j$, $\tilde{\beta}_i = \beta_i - \hat{\beta}_i$, $\tilde{\beta}_j = \beta_j - \hat{\beta}_j$. Obviously, V is a positive definite function on $\mathbb{R}^n$. Taking the fractional derivative of the Lyapunov function V and using Lemma 1, we obtain

$$\begin{aligned} {}^cD^q_{t_0}V &\leqslant e_i^T\,{}^cD^q_{t_0}e_i + e_j^T\,{}^cD^q_{t_0}e_j + \tilde{\alpha}_i^T\,{}^cD^q_{t_0}\tilde{\alpha}_i + \tilde{\alpha}_j^T\,{}^cD^q_{t_0}\tilde{\alpha}_j + \tilde{\beta}_i^T\,{}^cD^q_{t_0}\tilde{\beta}_i + \tilde{\beta}_j^T\,{}^cD^q_{t_0}\tilde{\beta}_j = \\ &= [-G_i(y)\tilde{\beta}_i + F_i(x)\tilde{\alpha}_i - e_i]^T e_i - \tilde{\alpha_i}^T[F_i(x)]^T e_i + \tilde{\beta_i}^T[G_i(y)]^T e_i + \\ &+ [G_j(y)\tilde{\beta}_j + F_j(x)\tilde{\alpha_j} - e_j]^T e_j - \tilde{\alpha_j}^T[F_j(x)]^T e_j - \tilde{\beta_j}^T[G_j(y)]^T e_j = \\ &= -\left(\|e_i\|^2 + \|e_j\|^2\right) \leqslant 0 \end{aligned} \tag{20}$$

Hence, ${}^cD^q_{t_0}V$ is a negative definite function on $\mathbb{R}^n$. According to theorem 1.1, the error system is globally asymptotically stable, i.e, $\lim\limits_{t\to\infty}\|e\| = \lim\limits_{t\to\infty}\|y(t,y_0) \pm x(t,x_0)\| = 0$. Therefore, the fractional-order slave system (13) can synchronize and anti-synchronize the fractional-order master system (12). This completes the proof. □

3. Adaptive hybrid synchronization between two different fractional-order hyperchaotic systems

3.1. ABM algorithm

In this paper, the numerical solution of a fractional-order system will be derived using the Adams–Bashforth–Moulton method (ABM), which is as follows [22].
Consider a fractional-order nonlinear equation

$$\begin{cases} {}^cD^q_{t_0}x(t) = f(t,x(t)), \quad 0 \leqslant t \leqslant T \\ x^k(0) = x_0^{(k)}, \quad k = 0,1,\ldots,m-1 \end{cases} \tag{21}$$

where $x(t) = [x_1(t), x_2(t), \ldots, x_n(t)]^T$ is the state variables, $x^{(k)}(t_0^+) = b_k, k = 0,1,\ldots,m-1$ is the initial condition, $q \in (0,1)$ is the fractional order. The fractional differential equation (21) is equivalent to the Volterra integral equation

$$x(t) = \sum_{k=0}^{n-1} x_0^{(k)}\frac{t^k}{k!} + \frac{1}{\Gamma(q)}\int_0^t (t-s)^{q-1}f(s,x(t))ds. \tag{22}$$

Let $h = T/N$, $t_j = jh\ (j = 0,1,\ldots,n)$, then the correction formula is defined as

$$x_h(t_{n+1}) = \sum_{k=0}^{m-1} x_0^{(k)}\frac{t_{n+1}^k}{k!} + \frac{h^q}{\Gamma(q+2)}f(t_{n+1}, x_h^p(t_{n+1})) + \frac{h^q}{\Gamma(q+2)}\sum_{j=0}^{n}\alpha_{j,n+1}f(t_j, x_h(t_j)). \tag{23}$$

where

$$\alpha_{j,n+1} = \begin{cases} n^{q+1} - (n-q)(n+1)^q \quad \text{for} \quad j = 0, \\ (n-j-2)^{q+1} + (n-j)^{q+1} - 2(n-j+1)^{q+1} \quad \text{for} \quad 0 \leqslant j \leqslant n. \end{cases} \tag{24}$$

Adopting the Adams-Bashforth rule, the prediction formula is given by

$$x_h^p(t_{n+1}) = \sum_{k=0}^{n-1} x_0^{(k)}\frac{t_{n+1}^k}{k!} + \frac{1}{\Gamma(q)}\sum_{j=0}^{n} b_{j,n+1}f(t_j, x_h(t_j)), \tag{25}$$

where

$$b_{j,n+1} = \frac{h^q}{q}\left((n-j+1)^q - (n-j)^q\right), \quad 0 \leqslant j \leqslant n. \tag{26}$$

It should be noted that the error of this numerical method can be calculated as

$$e = \max_{i=0,1,\ldots,N} |x(t_j) - x_h(t_j)| = o\left(h^p\right), \tag{27}$$

where $p = \min(2, 1+q)$.

3.2. Application

In order to simulate the proposed synchronization method, we consider two different fractional-order hyperchaotic systems where the Lorenz 4-D hyperchaotic systems is taken as the master system, whereas the Chen 4-D hyperchaotic system is taken as the slave system. Furthermore, the ABM algorithm has been employed to solve numerically the fractional-order hyperchaotic systems.

The fractional-order Lorenz hyperchaotic system is described as [23]

$$\begin{cases} {}^cD^q_{t_0} x_1 = a_1(y_1 - x_1) + w_1, \\ {}^cD^q_{t_0} y_1 = c_1 x_1 + y_1 - x_1 z_1, \\ {}^cD^q_{t_0} z_1 = x_1 y_1 - b_1 z_1, \\ {}^cD^q_{t_0} w_1 = -y_1 z_1 + r_1 w_1, \end{cases} \tag{28}$$

where $(x_1, y_1, z_1, w_1)^T$ is the state vector of the system, a_1, b_1, c_1, and r_1 are constant parameters. When the system parameters are selected as $a_1 = 10$, $b_1 = 8/3$, $c_1 = 28$, $r_1 = -1$, and the fractional order as $q = 0.98$ with the initial conditions $(x_1(0), y_1(0), z_1(0), w_1(0)) = (1, 1, 1, 1)$, the system (28) exhibits hyperchaotic attractor as shown in Fig. 1. The fractional-order Chen

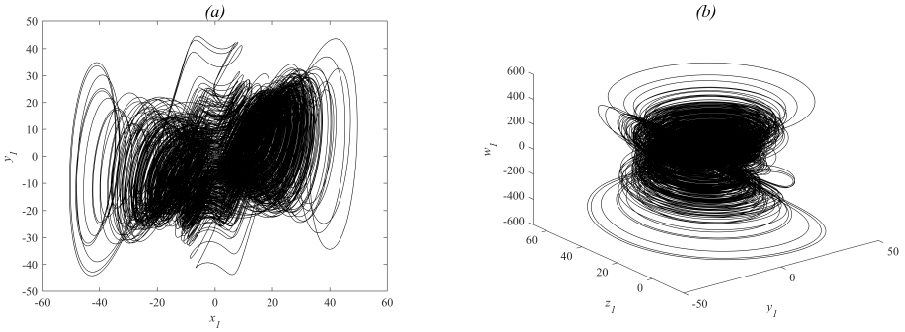

Fig. 1. Hyperchaotic attractor of the Lorenz fractional-order system: (a) in (x_1, y_1)-plane; (b) in (x_1, y_1, z_1)-space

hyperchaotic system with controller is expressed as [24]

$$\begin{cases} {}^cD^q_{t_0} x_2 = a_2(y_2 - x_2) + w_2 + u_1, \\ {}^cD^q_{t_0} y_2 = c_2 x_2 + k y_2 - x_2 z_2 + u_2, \\ {}^cD^q_{t_0} z_2 = x_2 y_2 - b_2 z_2 + u_3, \\ {}^cD^q_{t_0} w_2 = y_2 z_2 + r_2 w_2 + u_4, \end{cases} \tag{29}$$

where $(x_2, y_2, z_2, w_2)^T$ is the state vector of the system, a_2, b_2, c_2, k, and r_2 are constant parameters, $u = (u_1, u_2, u_3, u_4)^T$ is the controller. When the system parameters are selected as $a_2 = 35$, $b_2 = 3$, $k = 12$, $c_2 = 7$, $r_2 = 0.5$, and the fractional order as $q = 0.98$ with the initial conditions $(x_2(0), y_2(0), z_2(0), w_2(0)) = (5, 8, -1, -3)$, the system (29) without controller $(u_i = 0,\ i = 1, 2, 3, 4)$ exhibits hyperchaotic attractor as shown in Fig. 2. We define the state

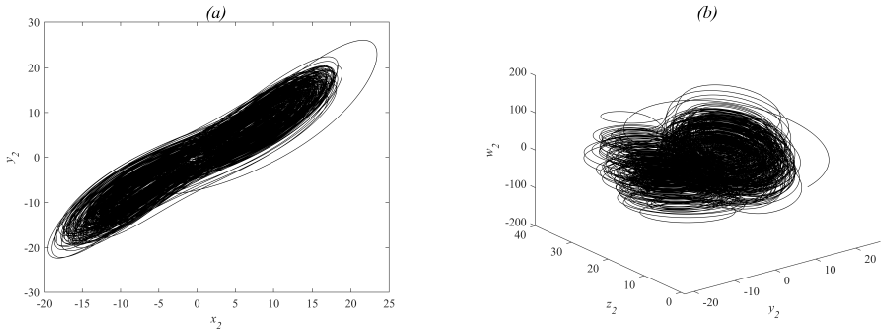

Fig. 2. Hyperchaotic attractor of the Chen fractional-order system: (a) in (x_2, y_2)-plane; (b) in (x_2, y_2, w_2)-space

errors between the systems (28) and (29) as $e_1 = x_2 - x_1$, $e_2 = y_2 + y_1$, $e_3 = z_2 - z_1$, $e_4 = w_2 + w_1$. Thus, the error dynamics of the fractional-order systems can be determined as

$$\begin{cases} {}^cD^q_{t_0} e_1 = a_2(y_2 - x_2) + w_2 - a_1(y_1 - x_1) - w_1 + u_1, \\ {}^cD^q_{t_0} e_2 = c_2 x_2 + c_1 x_1 + k y_2 + y_1 - x_2 z_2 - x_1 z_1 + u_2, \\ {}^cD^q_{t_0} e_3 = x_2 y_2 - x_1 y_1 - b_2 z_2 + b_1 z_1 + u_3, \\ {}^cD^q_{t_0} e_4 = y_2 z_2 - y_1 z_1 + r_2 w_2 + r_1 w_1 + u_4. \end{cases} \tag{30}$$

Our goal is to achieve adaptive hybrid synchronization between the master system (28) and the slave system (29) by constructing a suitable controller u and parameter update law in which $\lim_{t\to\infty} \|e(t)\| = 0$ with $e(t) = [e_1(t), e_2(t), e_3(t), e_4(t)]^T$. Next, we select the adaptive control law as

$$\begin{cases} u_1 = -\hat{a}_2(y_2 - x_2) - w_2 + \hat{a}_1(y_1 - x_1) + w_1 - e_1, \\ u_2 = -\hat{c}_2 x_2 - \hat{c}_1 x_1 - \hat{k} y_2 - y_1 + x_2 z_2 + x_1 z_1 - e_2, \\ u_3 = -x_2 y_2 + x_1 y_1 + \hat{b}_2 z_2 - \hat{b}_1 z_1 - e_3, \\ u_4 = -y_2 z_2 + y_1 z_1 - \hat{r}_2 w_2 - \hat{r}_1 w_1 - e_4, \end{cases} \tag{31}$$

and we take the parameter adaptive law as

$$\begin{aligned} &\dot{\hat{a}}_1 = -(y_1 - x_1)e_1, \quad && \dot{\hat{b}}_1 = z_1 e_3, \quad && \dot{\hat{c}}_1 = -x_1 e_2, \quad && \dot{\hat{r}}_1 = -w_1 e_4, \quad && \dot{\hat{k}} = y_2 e_2 \\ &\dot{\hat{a}}_2 = (y_2 - x_2)e_1, && \dot{\hat{b}}_2 = -z_2 e_3, && \dot{\hat{c}}_2 = x_2 e_2, && \dot{\hat{r}}_2 = w_2 e_4, \end{aligned} \tag{32}$$

where $\hat{a}_1$, $\hat{b}_1$, $\hat{c}_1$, $\hat{r}_1$, $\hat{k}$, $\hat{a}_2$, $\hat{b}_2$, $\hat{c}_2$, and $\hat{r}_2$ are the estimations of the unknown parameters a_1, b_1, c_1, r_1, k, a_2, b_2, c_2, and r_2, respectively. Combining (30) and (31), we obtain

$$\begin{cases} {}^cD^q_{t_0} e_1 = \tilde{a}_2(y_2 - x_2) - \tilde{a}_1(y_1 - x_1) - e_1, \\ {}^cD^q_{t_0} e_2 = \tilde{c}_2 x_2 + \tilde{c}_1 x_1 + \tilde{k} y_2 - e_2, \\ {}^cD^q_{t_0} e_3 = -\tilde{b}_2 z_2 + \tilde{b}_1 z_1 - e_3, \\ {}^cD^q_{t_0} e_4 = \tilde{r}_2 w_2 + \tilde{r}_1 w_1 - e_4, \end{cases} \tag{33}$$

where $\tilde{a}_1 = a_1 - \hat{a}_1$, $\tilde{b}_1 = b_1 - \hat{b}_1$, $\tilde{c}_1 = c_1 - \hat{c}_1$, $\tilde{r}_1 = r_1 - \hat{r}_1$, $\tilde{k} = k - \hat{k}$, $\tilde{a}_2 = a_2 - \hat{a}_2$, $\tilde{b}_2 = b_2 - \hat{b}_2$, $\tilde{c}_2 = c_2 - \hat{c}_2$, $\tilde{r}_2 = r_2 - \hat{r}_2$.

Theorem 3.3. *The fractional-order hyperchaotic systems* (28) *and* (29) *are globally asymptotically synchronized and anti-synchronized using the adaptive control law* (31) *and parameter update law* (32) *for all initial conditions.*

Proof. We define the quadratic Lyapunov function as

$$V = \frac{1}{2}\left(e^T e + \tilde{a}_1^2 + \tilde{b}_1^2 + \tilde{c}_1^2 + \tilde{r}_1^2 + \tilde{k}^2 + \tilde{a}_2^2 + \tilde{b}_2^2 + \tilde{c}_2^2 + \tilde{r}_2^2\right). \tag{34}$$

Taking the fractional derivative of (34) and using Lemma 1, we obtain

$$\begin{aligned} {}^cD_{t_0}^q V \leqslant e^T\, {}^cD_{t_0}^q e + \tilde{a}_1\, {}^cD_{t_0}^q \tilde{a}_1 + \tilde{b}_1\, {}^cD_{t_0}^q \tilde{b}_1 + \tilde{c}_1\, {}^cD_{t_0}^q \tilde{c}_1 + \tilde{r}_1\, {}^cD_{t_0}^q \tilde{r}_1 + \tilde{k}\, {}^cD_{t_0}^q \tilde{k} + \\ + \tilde{a}_2\, {}^cD_{t_0}^q \tilde{a}_2 + \tilde{b}_2\, {}^cD_{t_0}^q \tilde{b}_2 + \tilde{c}_2\, {}^cD_{t_0}^q \tilde{c}_2 + \tilde{r}_2\, {}^cD_{t_0}^q \tilde{r}_2. \end{aligned} \tag{35}$$

From (32) and (33), the inequality in (35) can be simplified as

$$\begin{aligned} &{}^cD_{t_0}^q V \leqslant e_1[\tilde{a}_2(y_2 - x_2) - \tilde{a}_1(y_1 - x_1) - e_1] + e_2[\tilde{c}_2 x_2 + \tilde{c}_1 x_1 + \tilde{k} y_2 - e_2] + \\ &+ e_3[-\tilde{b}_2 z_2 + \tilde{b}_1 z_1 - e_3] + e_4[\tilde{r}_2 w_2 + \tilde{r}_1 w_1 - e_4] + \tilde{a}_1[(y_1 - x_1)e_1] + \tilde{b}_1[-z_1 e_3] + \tilde{c}_1[-x_1 e_2] + \\ &+ \tilde{r}_1[-w_1 e_4] + \tilde{k}[-y_2 e_2] + \tilde{a}_2[-(y_2 - x_2)e_1] + \tilde{b}_2[z_2 e_3] + \tilde{c}_2[-x_2 e_2] + \tilde{r}_2[-w_2 e_4] = \\ &\qquad = -\|e\|^2 \leqslant 0, \end{aligned} \tag{36}$$

then ${}^cD_{t_0}^q V$ is a negative definite function. Based on the stability result of Theorem 1.1, the error system is globally asymptotically stable. Hence, the adaptive hybrid synchronization between the systems (28) and (29) is achieved. This completes the proof. □

3.3. Numerical simulations

For the numerical simulations, the ABM algorithm has been used to solve numerically the fractional-order hyperchaotic systems. The parameter values and initial conditions of the fractional-order systems (28) and (29) are selected as in the hyperchaotic case, and the fractional order as $q = 0.98$. Also, the initial values of the parameter estimates are arbitrarily taken as $\hat{a}_1(0) = 12$, $\hat{b}_1(0) = 2.6$, $\hat{c}_1(0) = 30$, $\hat{r}_1(0) = -1.2$, $\hat{k}(0) = 10$, $\hat{a}_2(0) = 34$, $\hat{b}_2(0) = 4$, $\hat{c}_2(0) = 6$, and $\hat{r}_2(0) = 0.4$. Fig. 3 displays the state trajectories of the drive system (28) and the slave system (29), whereas Fig. 4 shows the adaptive hybrid synchronization errors between the systems (28) and (29). As can be observed, the adaptive hybrid synchronization error $e(t) = [e_1(t), e_2(t), e_3(t), e_4(t)]^T$ converges asymptotically towards zero in infinite time, then the synchronization objective is gained.

4. Application to secure communication

Secure communication is one significant area in which chaotic synchronization may be applied in recent years. Three strategies of chaotic communication have been used: chaos masking [25], chaos modulation [26], and chaos shift keying [27]. In the current paper, we adopt the chaotic masking strategy.

We apply the proposed adaptive hybrid synchronization to secure communication. Fig. 5 displays the block diagram for our communication scheme. An information sinusoidal signal $m(t) = 4\sin(3\pi t)$ is added to the variable x_1 at the transmitter end, termed the transmitted

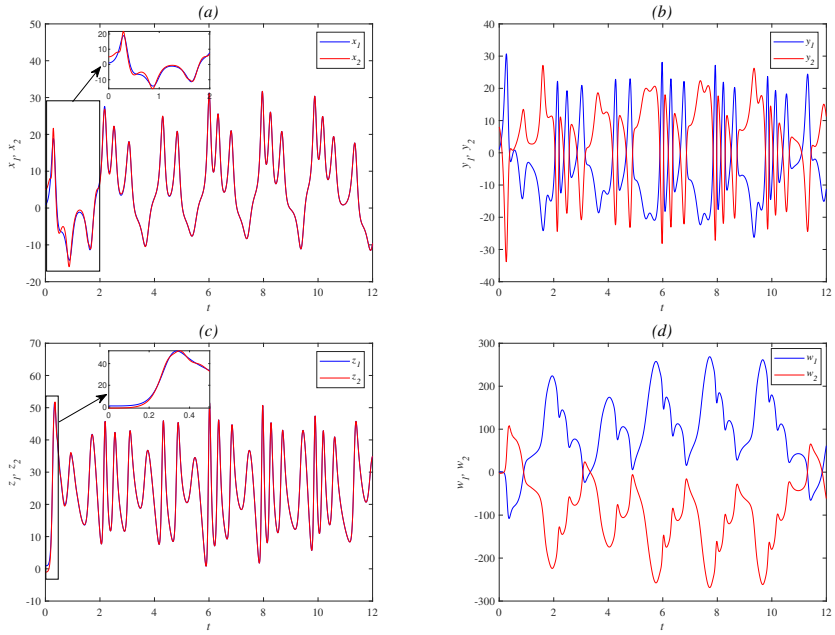

Fig. 3. State trajectories of the synchronized hyperchaotic fractional-order systems (28) and (29) with $q = 0.98$

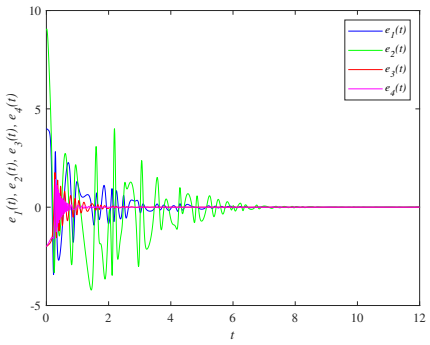

Fig. 4. Time evolutions of the adaptive hybrid synchronization errors $e_1(t)$, $e_2(t)$, $e_3(t)$, and $e_4(t)$

signal, and encrypted as $s(t) = x_1 + m(t)$. At the receiver end, the received information signal is recovered as $\hat{m}(t) = s(t) - x_2$ by employing the desired adaptive hybrid synchronization. Figure 6(a) shows the decrypted signal $s(t)$, whereas Fig. 6(b) shows the original information and recovered signals. From Fig. 6(b), it is easy to see that the recovered message signal $\hat{m}(t)$ coincides with good precision with the original information signal $m(t)$ after a short transient. Thus, the original information signal $m(t)$ is recovered accurately.

In addition, the original information signal can be selected as an impulse signal. Then, we add the original information signal $m(t)$ to the variable w_1 at the transmitter end, termed the transmitted signal, and encrypted as $s(t) = w_1 + m(t)$. At the receiver end, the received information signal is recovered as $\hat{m}(t) = s(t) + w_2$ by performing the desired adaptive hybrid synchronization. The decrypted signal $s(t)$ is depicted in Fig. 7(a), whereas Fig. 7(b) shows the

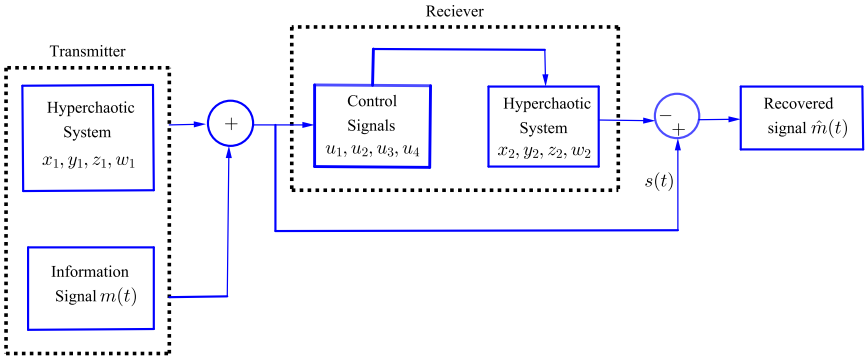

Fig. 5. The block diagram of secure communication based on hyperchaotic synchronization

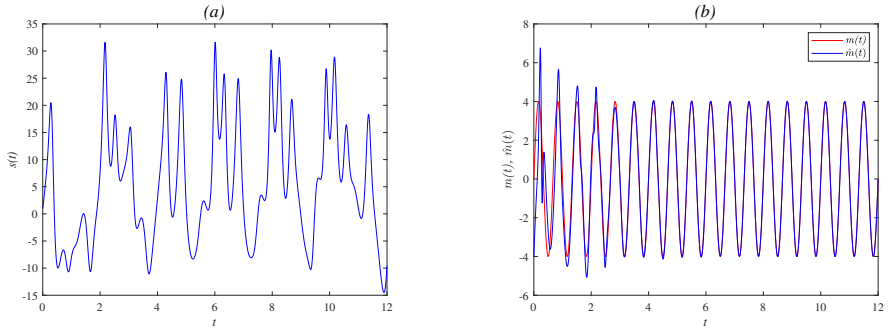

Fig. 6. Results of secure communication based on adaptive hybrid synchronization. Case of sinusoidal information signal: (a) The encrypted signal $s(t)$; (b) The original and recovered information signals $m(t)$ and $\hat{m}(t)$

original and decrypted signals. One can observe that the recovered message signal $\hat{m}(t)$ coincides well with the original information signal $m(t)$ in sufficient time. This shows the accuracy and effectiveness of the constructed secure communication scheme.

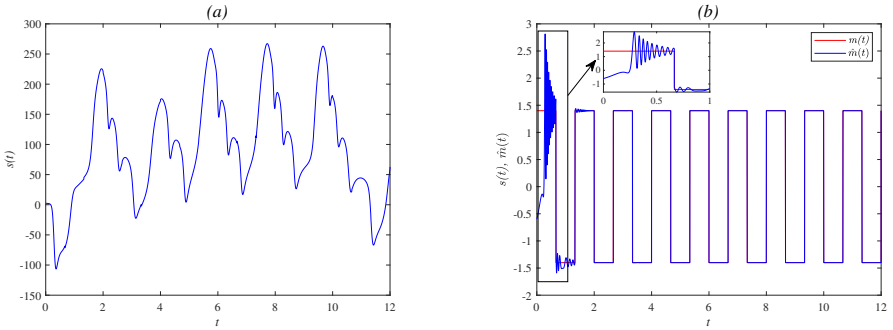

Fig. 7. Results of secure communication based on adaptive hybrid synchronization. Case of impulse information signal: (a) The encrypted signal $s(t)$; (b) The original and recovered information signals $m(t)$ and $\hat{m}(t)$

5. Conclusion

In this paper, we present a robust method of synchronization of fractional-order systems. Using the techniques of fractional calculus and Lyapunov stability theory, an effecient adaptive controller has been designed. Our synchronization process has been illustrated via two non-identical hyperchaotic fractional-order systems, where the 4-D Lorenz and Chen systems have employed. In addition, the application of chaotic synchronization in secure communication has been presented, where the information message signal can be encrypted and successfully recovered at the receiver. Computer simulations in MATLAB were provided to validate the theoretical results.

It is believed that the proposed robust synchronization scheme will contribute to the development of the theoretical study of fractional-order hyperchaotic systems. Furthermore, the proposed robust synchronization scheme holds potential applications in various scientific and engineering fields such as medical image encryption, signal processing, and data analysis.

Funding

This research received no external funding.

Conflicts of Interest

The authors declare no conflict of interest.

References

[1] N.Haneche, T.Hamaizia, A secure communication scheme based on generalized modified projective synchronization of a new 4-D fractional-order hyperchaotic system, *Phys. Scr.*, **99**(2024), no. 1, 095203. DOI: 10.1088/1402-4896/ad6515.

[2] K.U.Shahna, Novel chaos based cryptosystem using four-dimensional hyper chaotic map with efficient permutation and substitution techniques, *Chaos Solit. Fractals*, **170**(2023), 113383. DOI: 10.1016/j.chaos.2023.113383.

[3] P.A.Naik, K.M.Owolabi, M.Yavuz, J.Zu, Chaotic dynamics of a fractional order HIV-1 model involving AIDS-related cancer cells, *Chaos Solit. Fractals*, **140**(2020), 110272. DOI: 10.1016/j.chaos.2020.110272.

[4] A.A.Khennaoui, A.Ouannas, S.Bendoukha, X.Wang, V.T.Pham, On chaos in the fractional-order discrete-time unified system and its control synchronization, *Entropy*, **20**(2018), no. 7, 530. DOI: 10.3390/e20070530.

[5] L.M.Pecora, T.L.Carroll, Synchronization in chaotic systems, *Phys. Rev. Lett.*, **64**(1990), no. 8, 821. DOI: 10.1103/PhysRevLett.64.821.

[6] Y.P.Dousseh, A.V.Monwanou, A.A.Koukpйmиdji, C.H.Miwadinou, J.B.Chabi Orou, Dynamics analysis, adaptive control, synchronization and anti-synchronization of a novel modified chaotic financial system, *Int. J. Dyn. Contr.*, **11**(2023), no. 2, 862–876. DOI: 10.1007/s40435-022-01003-6.

[7] A.O.Adelakun, S.T.Ogunjo, Active control and electronic simulation of a novel fractional order chaotic jerk system, *Commun. Nonlinear Sci. Numer. Simul.*, **130**(2024), 107734. DOI: 10.1016/j.cnsns.2023.107734

[8] H.Su, R.Luo, J.Fu, M.Huang, Fixed time control and synchronization of a class of uncertain chaotic systems with disturbances via passive control method, *Math. Comput. Simul.*, **198**(2022), 474–493. DOI: 10.1016/j.matcom.2022.03.010.

[9] A.Karami-Mollaee, O.Barambones, Sliding observer in sliding mode control of multi-inputs fractional-order chaotic systems, *Pramana*, **96**(2022), no. 4, 180. DOI: 10.1007/s12043-022-02423-x.

[10] T.L.Carroll, L.M.Pecora, Synchronizing chaotic circuits, Nonlinear dynamics in circuits, World Scientific, 1995, 215–248.

[11] M.M.Al-Sawalha, M.S.M.Noorani, M.M.Al-Dlalah, Adaptive anti-synchronization of chaotic systems with fully unknown parameters, *Comput. Math. Appl.*, **59**(2010), no. 10, 3234–3244. DOI: 10.1016/j.camwa.2010.03.010.

[12] M.A.Khan, S.Poria, Projective synchronization of chaotic systems with bidirectional nonlinear coupling, *Pramana*, **81**(2013), 395–406. DOI: 10.1007/s12043-013-0592-6.

[13] J.Huang, P.Wei, Lag synchronization in coupled chaotic systems via intermittent control, *Procedia Eng.*, **15**(2011), 568–572. DOI: 10.1016/j.proeng.2011.08.107.

[14] H.Du, Q.Zeng, C.Wang, M.Ling, Function projective synchronization in coupled chaotic systems, *Nonlinear Anal. Real World Appl.*, **11**(2010), no. 2, 705–712. DOI: 10.1016/j.nonrwa.2009.01.016.

[15] M.Bettayeb, U.M.Al-Saggaf, S.Djennoune, Single channel secure communication scheme based on synchronization of fractional-order chaotic Chua's systems, *Trans. Inst. Meas. Control.*, **40**(2018), no. 13, 3651–3664. DOI: 10.1177/0142331217729425.

[16] B.Nail, M.A.Atoussi, S.Saadi, I.E.Tibermacine, C.Napoli, Real-time synchronisation of multiple fractional-order chaotic systems: an application study in secure communication, *Fractal Fract.*, **8**(2024), no. 2, 104. DOI: 10.3390/fractalfract8020104.

[17] D.Cafagna, G.Grassi, Fractional-order systems without equilibria: the first example of hyperchaos and its application to synchronization, *Chin. Phys. B*, **24**(2015), no. 8, 080502. DOI: 10.1088/1674-1056/24/8/080502.

[18] Y.Xu, K.Sun, S.He, L.Zhang, Dynamics of a fractional-order simplified unified system based on the Adomian decomposition method, *Eur. Phys. J. Plus*, **131**(2016), 1–12. DOI: 10.1140/epjp/i2016-16186-3.

[19] I.Podlubny, Fractional differential equations, NewYork: Academic, 1999.

[20] K.Rajagopal, A.Karthikeyan, Chaos suppression of fractional order willamowski-rössler chemical system and its synchronization using sliding mode control, *Nonlinear Eng.*, **5**(2026), no. 3, 177–183. DOI: 10.1515/nleng-2016-0027.

[21] N.Aguila-Camacho, M.A.Duarte-Mermoud, J.A.Gallegos, Lyapunov functions for fractional order systems, *Commun. Nonlinear Sci. Numer. Simul.*, **19**(2014), no. 9, 2951–2957. DOI: 10.1016/j.cnsns.2014.01.022.

[22] D.Peng, K.Sun, S.He, A.O.Alamodi, What is the lowest order of the fractional-order chaotic systems to behave chaotically?, *Chaos Solit. Fractals*, **119**(2019), 163–170. DOI: 10.1016/j.chaos.2018.12.022.

[23] L.Chen, Y.Chai, R.Wu, Lag projective synchronization in fractional-order chaotic (hyperchaotic) systems, *Phys. Lett. A*, **375**(2011), no. 21, 2099–2110. DOI: 10.1016/j.physleta.2011.04.015.

[24] A.E.Matouk, A.A.Elsadany, Achieving synchronization between the fractional-order hyperchaotic Novel and Chen systems via a new nonlinear control technique, *Appl. Math. Lett.*, **29**(2014), 30–35. DOI: 10.1016/j.aml.2013.10.010.

[25] A.Ouannas, A.Karouma, G.Grassi, V.T.Pham, A novel secure communications scheme based on chaotic modulation, recursive encryption and chaotic masking, *Alex. Eng. J.*, **60**(2021), no. 1, 1873–1884. DOI: 10.1016/j.aej.2020.11.035.

[26] X.J.Wu, H.Wang, H.T.Lu, Hyperchaotic secure communication via generalized function projective synchronization, *Nonlinear Anal. Real World Appl.*, **12**(2011), no. 2, 1288–1299. DOI: 10.1016/j.nonrwa.2010.09.026.

[27] Y.Y.Hou, H.C.Chen, J.F.Chang, J.J.Yan , T.L.Liao, Design and implementation of the Sprott chaotic secure digital communication systems, *Appl Math Comput.*, **218**(2012), no. 24, 11799–11805. DOI: 10.1016/j.amc.2012.04.076.

Улучшение безопасной связи с использованием надежной схемы синхронизации гиперхаотических систем дробного порядка

Набил Ханече
Лаборатория прикладной математики и моделирования
Университет братьев Ментури
Константина 25000, Алжир
Тайеб Хамаизи
Лаборатория математического моделирования и имитации
Кафедра математики
Университет братьев Ментури
Константина 25000, Алжир

Аннотация. В последние годы в литературе проявляется большой интерес к изучению хаотических динамических систем. В данной статье представлена схема адаптивного управления для достижения синхронизации между двумя различными гиперхаотическими системами дробного порядка с неизвестными параметрами. Используя строгие методы дробного исчисления, был разработан контроллер на основе теории устойчивости Ляпунова. Адаптивная гибридная синхронизация между гиперхаотическими системами Лоренца и Чена дробного порядка была разработана для иллюстрации построенной схемы синхронизации. Для создания высокой безопасности передачи сигналов было выполнено применение синхронизации в защищенной связи. Было проведено компьютерное моделирование для проверки теоретических результатов, полученных в этом исследовании.

Ключевые слова: дробный порядок, гиперхаотическая система, синхронизация, безопасная связь.

EDN: WHIXNK
УДК 517.984

Four-electron First Singlet State in the Impurity Hubbard Model

Sadulla M. Tashpulatov*
Institute of Nuclear Physics of Academy of Science of Republic of Uzbekistan
Tashkent, Uzbekistan
Rukhsat T. Parmanova†
Institute of Nuclear Physics of Academy of Science of Republic of Uzbekistan
Tashkent, Uzbekistan
Institute of Fundamental and Applied Research
National Research University TIIAME
Tashkent, Uzbekistan

Received 06.11.2024, received in revised form 20.01.2025, accepted 07.05.2025

Abstract. We consider the energy operator of four-electron systems in the impurity Hubbard model and investigate the structure of essential spectra and discrete spectrum of the system in the first singlet state of the system. The investigations show that there are such situation: 1) the essential spectrum of the system in the first singlet states consists of the union of ten segments, and the discrete spectrum of the system consists of six eigenvalues; 2) the essential spectrum of the system in the first singlet states consists of the union of sixteen segments, and the discrete spectrum of the system consists of ten eigenvalues; 3) the essential spectrum of the system in the first singlet states consists of the union of nineteen segments, and the discrete spectrum of the system consists of sixteen eigenvalues; 4) the essential spectrum of the system in the first singlet states consists of the union of four segments, and the discrete spectrum of the system consists of two eigenvalues.

Keywords: four-electron system, impurity Hubbard model, singlet state, quintet state, triplet state, essential spectra, discrete spectra.

Citation: S.M. Tashpulatov, R.T. Parmanova, Four-electron First Singlet State in the Impurity Hubbard Model, J. Sib. Fed. Univ. Math. Phys., 2025, 18(4), 555–567.
EDN: WHIXNK.

Introduction

The spectrum and wave functions of the system of four electrons in a crystal described by the Hubbard Hamiltonian were studied in [1, 2]. In the four-electron systems are exists a six states: quintet state, three type triplet state, and two type singlet states. In the work [1] investigated the spectrum and wave functions of four-electron systems in a Hubbard model in triplet states. In the work [2] considered the spectrum and wave functions of four-electron systems in a Hubbard model in a quintet and singlet states.

In the work [2] proved that the essential spectrum of the system in a quintet state purely continuous and consists of the segment $[4A - 8B\nu, 4A + 8B\nu]$, and the four-electron bound state or four-electron antibound state is absent.

Naturally, the question arises, if we consider four-electron system in the Impurity Hubbard model, then how can the spectrum of the system change? And actually this, led us to consider the following task. In addition, the intense development of the physics of the film state and also the

*sadullatashpulatov@yandex.com https://orcid.org/0000-0002-7744-0085
†togaymurodota@gmail.com

use of films in different areas of physics and technology underlie the great interest in studying local impurity states magnets. Therefore, it is important to study the spectral properties of electron systems in the impurity Hubbard model. The structure of essential spectra and discrete spectrum of two-electron systems in the impurity Hubbard model in the singlet state were studied in the work S. Tashpulatov [3, 4].

1. Four-electron systems in the impurity Hubbard model. First singlet state

Here, we consider the energy operator of four-electron systems in the Impurity Hubbard model and investigate the structure of the essential spectrum and discrete spectra of the system for first singlet state. The Hamiltonian of the chosen model has the form

$$H = A\sum_{m,\gamma} a^+_{m,\gamma}a_{m,\gamma} + B\sum_{m,\tau,\gamma} a^+_{m,\gamma}a_{m+\tau,\gamma} + U\sum_{m} a^+_{m,\uparrow}a_{m,\uparrow}a^+_{m,\downarrow}a_{m,\downarrow} + \\ +(A_0-A)\sum_{\gamma} a^+_{0,\gamma}a_{0,\gamma} + (B_0-B)\sum_{\tau,\gamma}(a^+_{0,\gamma}a_{\tau,\gamma} + a^+_{\tau,\gamma}a_{0,\gamma}) + (U_0-U)a^+_{0,\uparrow}a_{0,\uparrow}a^+_{0,\downarrow}a_{0,\downarrow}. \tag{1}$$

Here, A (A_0) is the electron energy at a regular (impurity) lattice site; B (B_0) is the transfer integral between electrons (between electron and impurity) in a neighboring sites (for convenience, we assume that $B > 0$ and $B_0 > 0$), $\tau = \pm e_j$ for $j = 1, 2, \ldots, \nu$, where e_j are unit mutually orthogonal vectors, i.e. the summation is over the nearest neighbors, U (U_0) is the parameter of the on-site Coulomb interaction of two electrons, correspondingly in the regular (impurity) lattice site; γ is the spin index,$\gamma =\uparrow$ or $\gamma =\downarrow$, $\uparrow$ or $\downarrow$ denote the spin values $\frac{1}{2}$ or $-\frac{1}{2}$, and $a^+_{m,\gamma}$ and $a_{m,\gamma}$ are the respective electron creation and annihilation operators at a site $m \in Z^\nu$.

The four-electron first singlet state corresponds four electron bound states (or antibound states) to the basis functions: ${}^1s^0_{p,q,r,t} = a^+_{p,\uparrow}a^+_{q,\uparrow}a^+_{r,\downarrow}a^+_{t,\downarrow}\varphi_0$. The subspace ${}^1\widetilde{\mathcal{H}}^0_s$, corresponding to the four-electron first singlet state is the set of all vector's of the form:
${}^1\psi^0_s = \sum\limits_{p,q,r,t\in Z^\nu} f(p,q,r,t)\,{}^1s^0_{p,q,r,t}, f \in l^{as}_2$, where l^{as}_2 is the subspace of antisymmetric functions in $l_2((Z^\nu)^4)$.

In the four-electron systems exists quintet state, two type singlet states, and three type triplet states.

Hamiltonian (1) commutes with all components of the total spin operator $S = (S^+, S^-, S^z)$, and the structure of eigenfunctions and eigenvalues of the system therefore depends on S.

The Hamiltonian H acts in the antisymmetric Fock space $\widetilde{\mathcal{H}}_{as}$. Let φ_0 be the vacuum vector in the space $\widetilde{\mathcal{H}}_{as}$. The four-electron first singlet state corresponds to the free motion of four electrons over the lattice, and their interactions.

We denote by ${}^1H^0_s$ the restriction of the operator H to the subspace ${}^1\widetilde{\mathcal{H}}^0_s$. We call the operator ${}^1H^0_s$ the four-electron first singlet state operator.

Theorem 1. *The subspace ${}^1\widetilde{\mathcal{H}}^0_s$ is invariant under the operator H, and the operator ${}^1H^0_s$ is a bounded self-adjoint operator. It generates a bounded self-adjoint operator ${}^1\overline{H}^0_s$, acting in the space l^{as}_2 as*

$$ {}^1\overline{H}^0_s\ {}^1\psi^0_s = 4Af(p,q,r,t) + B\sum_{\tau}\big[f(p+\tau,q,r,t) + f(p,q+\tau,r,t) + f(p,q,r+\tau,t) + \\ + f(p,q,r,t+\tau)\big] + U(\delta_{p,r}+\delta_{p,t}+\delta_{q,r}+\delta_{q,t})f(p,q,r,t) + (A_0-A)(\delta_{p,0}+\delta_{q,0}+\delta_{r,0}+\delta_{t,0})\times \\ \times f(p,q,r,t) + (B_0-B)\sum_{\tau}\big[\delta_{p,0}f(\tau,q,r,t) + \delta_{q,0}f(p,\tau,r,t) + \delta_{r,0}f(p,q,\tau,t) + \delta_{t,0}f(p,q,r,\tau) + \\ + \delta_{p,\tau}f(0,q,r,t) + \delta_{q,\tau}f(p,0,r,t) + \delta_{r,\tau}f(p,q,0,t) + \delta_{t,\tau}f(p,q,r,0)\big] +$$

$$+ (U_0 - U)[\delta_{p,r}\delta_{p,0} + \delta_{q,r}\delta_{q,0} + \delta_{p,t}\delta_{p,0} + \delta_{q,t}\delta_{q,0}]f(p,q,r,t), \quad (2)$$

where $\delta_{k,j}$ is the Kronecker symbol. The operator ${}^1H_s^0$, acts on a vector ${}^1\psi_s^0 \in {}^1\widetilde{\mathcal{H}}_s^0$ as

$${}^1H_s^0 \ {}^1\psi_s^0 = \sum_{p,q,r,t} ({}^1\overline{H}_s^0 f)(p,q,r,t) \ {}^1s_{p,q,r,t}^0. \quad (3)$$

Proof. We act with the Hamiltonian H on vectors $\psi \in {}^1\widetilde{\mathcal{H}}_s^0$ using the standard anti-commutation relations between electron creation and annihilation operators at lattice sites, $\{a_{m,\gamma}, a_{n,\beta}^+\} = \delta_{m,n}\delta_{\gamma,\beta}$, $\{a_{m,\gamma}, a_{n,\beta}\} = \{a_{m,\gamma}^+, a_{n,\beta}^+\} = \theta$, and also take into account that $a_{m,\gamma}\varphi_0 = \theta$, where θ is the zero element of ${}^1\widetilde{\mathcal{H}}_s^0$. This yields the statement of the theorem. □

Lemma 1. *The spectra of the operators ${}^1H_s^0$ and ${}^1\overline{H}_s^0$ coincide.*

Proof. The proof follows by using the Weyl criterion (see [5], chapter VII, pp. 262–263).

We let $\mathcal{F}$ denote the Fourier transform: $\mathcal{F} : l_2((Z^\nu)^4) \to L_2((T^\nu)^4) \equiv {}^1\widetilde{\mathcal{H}}_s^0$, where T^ν is the ν-dimensional torus endowed with the normalized Lebesgue measure $d\lambda$, $\lambda(T^\nu) = 1$.

We set ${}^1\widetilde{H}_s^0 = \mathcal{F}\ {}^1\overline{H}_s^0 \mathcal{F}^{-1}$. In the quasimomentum representation, the operator ${}^1\overline{H}_s^0$ acts in the Hilbert space $L_2^{as}((T^\nu)^4)$, where L_2^{as} is the subspace of antisymmetric functions in $L_2((T^\nu)^4)$. □

Theorem 2. *The Fourier transform of operator ${}^1\overline{H}_s^0$ is an bounded self-adjoint operator ${}^1\widetilde{H}_s^0 = \mathcal{F}\ {}^1\overline{H}_s^0\ \mathcal{F}^{-1}$, acting in the space ${}^1\widetilde{\mathcal{H}}_s^0$ by the formula*

$$\begin{aligned}
({}^1\widetilde{H}_s^0\widetilde{f})(\lambda,\mu,\gamma,\theta) &= \Big\{4A + 2B\sum_{i=1}^{\nu}[\cos\lambda_i + \cos\mu_i + \cos\gamma_i + \cos\theta_i]\Big\}\times \\
&\times \widetilde{f}(\lambda,\mu,\gamma,\theta) + U\int_{T^\nu}\widetilde{f}(s,\mu,\lambda+\gamma-s,\eta)ds + U\int_{T^\nu}\widetilde{f}(t,\mu,\gamma,\lambda+\theta-t)dt + \\
&+ U\int_{T^\nu}\widetilde{f}(\lambda,\xi,\mu+\gamma-\xi,\theta)d\xi + U\int_{T^\nu}\widetilde{f}(\lambda,\eta,\gamma,\mu+\theta-\eta)d\eta + \varepsilon_1\Big[\int_{T^\nu}f(s,\mu,\gamma,\theta)ds + \\
&+ \int_{T^\nu}f(\lambda,t,\gamma,\theta)dt + \int_{T^\nu}f(\lambda,\mu,\xi,\theta)d\xi + \int_{T^\nu}f(\lambda,\mu,\gamma,\eta)d\eta\Big] + 2\varepsilon_2\int_{T^\nu}\sum_{i=1}^{\nu}[\cos\lambda_i + \cos s_i]\times \\
&\times \widetilde{f}(s,\mu,\gamma,\theta)ds + 2\varepsilon_2\int_{T^\nu}\sum_{i=1}^{\nu}[\cos\mu_i + \cos t_i]\widetilde{f}(\lambda,t,\gamma,\theta)dt + 2\varepsilon_2\int_{T^\nu}\sum_{i=1}^{\nu}[\cos\gamma_i + \cos\xi_i]\times \\
&\times \widetilde{f}(\lambda,\mu,\xi,\theta)d\xi + 2\varepsilon_2\int_{T^\nu}\sum_{i=1}^{\nu}[\cos\theta_i + \cos\eta_i]\widetilde{f}(\lambda,\mu,\gamma,\eta)d\eta + \varepsilon_3\Big[\int_{T^\nu}\int_{T^\nu}f(s,\mu,\xi,\theta)dsd\xi + \\
&+ \int_{T^\nu}\int_{T^\nu}f(\lambda,t,\xi,\theta)dtd\xi + \int_{T^\nu}\int_{T^\nu}f(s,\mu,\gamma,\eta)dsd\eta + \int_{T^\nu}\int_{T^\nu}f(\lambda,t,\xi,\theta)dtd\xi\Big], \quad (4)
\end{aligned}$$

where $\varepsilon_1 = A_0 - A$, $\varepsilon_2 = B_0 - B$ and $\varepsilon_3 = U_0 - U$.

The prove Theorem 2, the Fourier transform of (2) should be considered directly.

Using tensor products of Hilbert spaces and tensor products of operators in Hilbert spaces [6], we can verify that the operator ${}^1\widetilde{H}_0^s$ can be represented in the form

$$\begin{aligned}
{}^1\widetilde{H}_0^s &= \Big\{\widetilde{H}_1 \bigotimes I + I \bigotimes \widetilde{H}_1 - 2U\int_{T^\nu}\widetilde{f}(s,\lambda+\gamma-s)ds\Big\} \bigotimes I \bigotimes I + \\
&+ I \bigotimes I \bigotimes \Big\{\widetilde{H}_1 \bigotimes I + I \bigotimes \widetilde{H}_1 + 2U\int_{T^\nu}\widetilde{f}(t,\lambda+\theta-t)dt + 2\varepsilon_2\int_{T^\nu}\int_{T^\nu}\widetilde{f}(t,\xi)dtd\xi.\Big\} \quad (5)
\end{aligned}$$

where

$$\left(\widetilde{H}_1\widetilde{f}\right)(\lambda)=\left\{A+2B\sum_{i=1}^{\nu}[\cos\lambda_i]\right\}\widetilde{f}(\lambda)+\varepsilon_1\int_{T^\nu}\widetilde{f}(s)ds+2\varepsilon_2\sum_{i=1}^{\nu}\int_{T^\nu}[\cos\lambda_i+\cos s_i]f(s)ds$$

is the energy operator of one-electron systems in the impurity Hubbard model.

It can be seen from formula (5) that the spectral properties of four-electron systems in the impurity Hubbard model in the first singlet state are closely related to those of its one-electron subsystems in the impurity Hubbard model. Therefore, we first study the spectrum and localized impurity states of one-electron systems.

The use films in various areas of physics and technology arouses great interest in studying a localized impurity state (LIS) of magnet. Therefore, it is important to study the spectral properties of electron systems in the impurity Hubbard model.

2. One-electron systems in the impurity Hubbard Model.

The Hamiltonian of one-electron systems in the impurity Hubbard model has the form:

$$\begin{gathered}H=A\sum_{m,\gamma}a^+_{m,\gamma}a_{m,\gamma}+B\sum_{m,\tau,\gamma}a^+_{m,\gamma}a_{m+\tau,\gamma}+\\+(A_0-A)\sum_{\gamma}a^+_{0,\gamma}a_{0,\gamma}+(B_0-B)\sum_{\tau,\gamma}(a^+_{0,\gamma}a_{\tau,\gamma}+a^+_{\tau,\gamma}a_{0,\gamma}),\end{gathered}\tag{6}$$

here A (A_0) is the electron energy at a regular (impurity) lattice site; $B>0$ ($B_0>0$) is the transfer integral between electrons (between electron and impurity) in a neighboring sites, $\tau=\pm e_j$, $j=1,2,\ldots,\nu$, where e_j are unit mutually orthogonal vectors, which means that summation is taken over the nearest neighbors; γ is the spin index, $\gamma=\uparrow$ or $\gamma=\downarrow$, $\uparrow$ and $\downarrow$ denote the spin values $\frac{1}{2}$ and $-\frac{1}{2}$, and $a^+_{m,\gamma}$ and $a_{m,\gamma}$ are the respective electron creation and annihilation operators at a site $m\in Z^\nu$.

We let $\mathcal{H}_1$ denote the Hilbert space spanned by the vectors in the form $\chi=\sum\limits_p a^+_{p,\uparrow}\varphi_0$. It is called the space of one-electron states of the operator H. The space $\mathcal{H}_1$ is invariant with respect to action of the operator H. Denote by $H_1=H|_{\mathcal{H}_1}$ the restriction of H to the subspace $\mathcal{H}_1$.

As in the proof of Theorem 1, using the standard anticommutation relations between electron creation and annihilation operators at lattice sites, we get the following

Theorem 3. *The subspace $\mathcal{H}_1$ is invariant with respect to the action of the operator H, and the restriction H_1 is a linear bounded self-adjoint operator, acting in $\mathcal{H}_1$ as*

$$H_1\chi=\sum_p(\overline{H}_1f)(p)a^+_{p,\uparrow}\varphi_0,\ \chi\in\mathcal{H}_1,\tag{7}$$

where $\overline{H}_1$ is a linear bounded self-adjoint operator acting in the space l_2 as

$$(\overline{H}_1f)(p)=Af(p)+B\sum_\tau f(p+\tau)+\varepsilon_1\delta_{p,0}f(p)+\varepsilon_2\sum_\tau(\delta_{p,\tau}f(0)+\delta_{p,0}f(\tau)),\tag{8}$$

where $\varepsilon_1=A_0-A$, $\varepsilon_2=B_0-B$ and $\varepsilon_3=U_0-U$.

Lemma 2. *The spectra of the operators $\overline{H}_1$ and H_1 coincide.*

The proof of Lemma 2 is the same as the proof of the Lemma 1.

As in Section 1 denote by $\mathcal{F}:l_2(Z^\nu)\to L_2(T^\nu)\equiv\widetilde{\mathcal{H}}_1$ the Fourier transform. Setting $\widetilde{H}_1=\mathcal{F}\overline{H}_1\mathcal{F}^{-1}$ we get that the operator $\overline{H}_1$ acts in the Hilbert space $L_2(T^\nu)$.

Using the equality (11) and properties of the Fourier transform we have the following

Theorem 4. *The operator $\widetilde{H}_1$ acting in the space $\widetilde{\mathcal{H}}_1$ as*

$$\begin{aligned}\big(\widetilde{H}_1 f\big)(\mu) = \Big[A + 2B\sum_{i=1}^{\nu}\cos\mu_i\Big] f(\mu) + \varepsilon_1 \int_{T^\nu} f(s)ds + \\ +2\varepsilon_2 \int_{T^\nu} \sum_{i=1}^{\nu} [\cos\mu_i + \cos s_i] f(s)ds, \quad \mu = (\mu_1, \ldots, \mu_n),\ s = (s_1, \ldots, s_n) \in T^\nu.\end{aligned} \tag{9}$$

In these formula $\varepsilon_1 = A_0 - A$, $\varepsilon_2 = B_0 - B$ and $\varepsilon_3 = U_0 - U$.

It is clear that the continuous spectrum of operator $\widetilde{H}_1$ is independent of the numbers ε_1 and ε_2, and is equal to segment $[m_\nu, M_\nu] = [A - 2B\nu, A + 2B\nu]$, where $m_\nu = \min\limits_{x\in T^\nu} h(x)$, $M_\nu = \max\limits_{x\in T^\nu} h(x)$ $\big($here $h(x) = A + 2B\sum\limits_{i=1}^{\nu}\cos x_i\big)$.

Denote via

$$\begin{aligned}\Delta_\nu(z) = \left(1 + \int_{T^\nu} \frac{\varepsilon_1 + 2\varepsilon_2\sum_{i=1}^{\nu}\cos s_i}{A + 2B\sum_{i=1}^{\nu}\cos s_i - z} ds_1 \ldots ds_\nu\right)\left(1 + \nu\int_{T^\nu} \frac{\cos s_i ds_1 \ldots ds_\nu}{A + 2B\sum_{i=1}^{\nu}\cos s_i - z}\right) - \\ -2\varepsilon_2\nu \int_{T^\nu} \frac{\cos s_i[\varepsilon_1 + 2\varepsilon_2\sum_{i=1}^{\nu}\cos s_i]}{A + 2B\sum_{i=1}^{\nu}\cos s_i - z} ds_1 \ldots ds_\nu \int_{T^\nu} \frac{ds_1 \ldots ds_\nu}{A + 2B\sum_{i=1}^{\nu}\cos s_i - z}.\end{aligned}$$

Lemma 3. *If a real number $z \notin [m_\nu, M_\nu]$ then z is an eigenvalue of the operator $\widetilde{H}_1$ if and only if $\Delta_\nu(z) = 0$.*

Proof. The equation for eigenvalues is an integral equation with a degenerate kernel. Therefore, it is equivalent to a system of linear homogeneous algebraic equations. It is known that a system of linear homogeneous algebraic equations has a nontrivial solutions if and only if the determinant of the system is equal to zero. Taking into account that the function $h(s_1, s_2, \ldots, s_\nu)$ is symmetric with respect to s_i and s_j and performing the corresponding transformations, we find that the determinant of the system has the form $\Delta_\nu(z) = 0$. □

In the work's [3,4] well described of the exchange of the spectrum of operator $\widetilde{H}_1$ in the cases $\nu = 1$ and $\nu = 3$. Here we use the results of these theorems.

In the three-dimensional case, the integral

$$\int_{T^3} \frac{ds_1 ds_2 ds_3}{3 + \cos s_1 + \cos s_2 + \cos s_2} = \int_{T^3} \frac{ds_1 ds_2 ds_3}{3 - \cos s_1 - \cos s_2 - \cos s_2}$$

have the finite value, equal to $\dfrac{W}{3}$. Expressing these integral via Watson integral [7]

$W = \dfrac{1}{\pi^3}\displaystyle\int_{-\pi}^{\pi}\int_{-\pi}^{\pi}\int_{-\pi}^{\pi} \frac{3dxdydz}{3 - \cos x - \cos y - \cos z} \simeq 1.516$, and taking into account, what the measure is normalized, we have, that $J(z) = \displaystyle\int_{T^3} \frac{ds_1 ds_2 ds_3}{A + 2B\sum_{i=1}^{\nu}\cos s_i - z} = \frac{W}{6B}$.

From obtaining results is obviously, that the spectrum of operator $\widetilde{H}_1$ is consists from continuous spectrum and no more than two eigenvalues.

The spectrum of the operator $A\bigotimes I + I\bigotimes B$, where A and B are densely defined bounded linear operators, was studied in [8,9]. Explicit formulas were given there that express the essential spectrum $\sigma_{ess}(A\bigotimes I + I\bigotimes B)$ and discrete spectrum $\sigma_{disc}(A\bigotimes I + I\bigotimes B)$ of operator $A\bigotimes I + I\bigotimes B$ in terms of the spectrum $\sigma(A)$ and the discrete spectrum $\sigma_{disc}(A)$ of A and in terms of the spectrum $\sigma(B)$ and the discrete spectrum $\sigma_{disc}(B)$ of B :

$$\begin{aligned}\sigma_{disc}(A\bigotimes I + I\bigotimes B) = \{\sigma(A)\backslash\sigma_{ess}(A) + \sigma(B)\backslash\sigma_{ess}(B)\}\backslash\{(\sigma_{ess}(A) + \\ + \sigma(B)) \cup (\sigma(A) + \sigma_{ess}(B))\},\end{aligned} \tag{10}$$

and

$$\sigma_{ess}(A\bigotimes I + I\bigotimes B) = (\sigma_{ess}(A) + \sigma(B)) \cup (\sigma(A) + \sigma_{ess}(B)). \tag{11}$$

It is clear that $\sigma(A\bigotimes I + I\bigotimes B) = \{\lambda + \mu : \lambda \in \sigma(A), \mu \in \sigma(B)\}$.

It can be seen from representation (5) that we must first investigate the spectra of operators $\widetilde{H}_2 = \widetilde{H}_1\bigotimes I + I\bigotimes \widetilde{H}_1 - 2U\int\limits_{T^\nu} \widetilde{f}(s, \lambda+\mu-s)ds$ and $\widetilde{H}_3 = \widetilde{H}_1\bigotimes I + I\bigotimes \widetilde{H}_1 + 2U\int\limits_{T^\nu} \widetilde{f}(s, \lambda+\mu-s)ds + 2\varepsilon_3\int\limits_{T^\nu}\int\limits_{T^\nu} \widetilde{f}(s,t)dsdt$.

3. Structure of the essential spectrum and discrete spectrum of operator ${}^1\widetilde{H}_s^0$

Consequently, the operator represented of the form

$${}^1\widetilde{H}_s^0 = \widetilde{H}_2\bigotimes I\bigotimes I + I\bigotimes I\bigotimes \widetilde{H}_3. \tag{12}$$

From the beginning, we consider the operator $\widetilde{H}(U) = \widetilde{H}_1\bigotimes I + I\bigotimes \widetilde{H}_1 - 2U\int\limits_{T^\nu} f(s, \lambda+\mu-s)ds$.

Since, the family of the operators $\widetilde{H}(U)$ are the family of bounded operators, that the $\widetilde{H}(U)$ are the family of bounded operator valued analytical functions. Therefore, in these family, one can the apply the Kato–Rellix theorem.

Theorem 5 (Kato–Rellix theorem [6]). *Let $T(\beta)$ is the analytical family in the terms of Kato. Let E_0 is a nondegenerate eigenvalue of $T(\beta_0)$. Then as β, near to β_0, the exist exactly one point $E(\beta) \in \sigma(T(\beta))$ the near E_0 and this point is isolated and nondegenerated. $E(\beta)$ is an analytical function of β as β, the near to β_0, and exist the analytical eigenvector $\Omega(\beta)$ as β the near to β_0. If the as real $\beta - \beta_0$ the operator $T(\beta)$ is a self-adjoint operator, then $\Omega(\beta)$ can selected thus, that it will be normalized of real $\beta - \beta_0$.*

Since, the operator $\widetilde{H}_1\bigotimes I + I\bigotimes \widetilde{H}_1$ has a nondegenerate eigenvalue, such as, the near of eigenvalue $2z_1$ of the operator $\widetilde{H}_1\bigotimes I + I\bigotimes \widetilde{H}_1$, the operator $\widetilde{H}(U)$ as U, near $U_0 = 0$, has a exactly one eigenvalue $E(U) \in \sigma(\widetilde{H}(U))$ the near $2z_1$ and this point is isolated and nondegenerated. The $E(U)$ is a analytical function of U as U, the near to $U_0 = 0$.

As the large values the existence no more one additional eigenvalue of the operator $\widetilde{H}(U)$ is following from the same, what the perturbation $(K_1\widetilde{f})(\lambda,\mu) = -2U\int\limits_{T^\nu} f(s, \lambda+\mu-s)ds$ is the one-dimensional operator, for a fixed value of the total quasimomentum of two electrons. This additional eigenvalue of operator $\widetilde{H}_2$ we will denote by z_3.

A new we consider the family of operators $\widetilde{H}(\varepsilon_3) = \widetilde{H}(U) + 2U\int\limits_{T^\nu} \widetilde{f}(s, \lambda+\mu-s)ds + 2\varepsilon_3\int\limits_{T^\nu}\int\limits_{T^\nu} \widetilde{f}(s,t)dsdt$.

As, the operator $\widetilde{H}(U)$ has a nondegenerate eigenvalue, consequently, the near of eigenvalue $E(U)$ the operator $\widetilde{H}(U)$, operator $\widetilde{H}(\varepsilon_3)$ as ε_3, the near of $\varepsilon_3 = 0$, has a exactly one eigenvalue $E(\varepsilon_3) \in \sigma(\widetilde{H}(\varepsilon_3))$ the near $E(U)$ and this point is the isolated and nondegenerated. The $E(\varepsilon_3)$ is a analytical function of ε_3, as ε_3, the near to $\varepsilon_3 = 0$.

Later on via z_4, and z_5 we denote the additional eigenvalues of operator $\widetilde{H}_3$.

Now, using the obtained results (Theorem 8 and 9 in the work [3]) and representation (5) and (12), we describe the structure of the essential spectrum and discrete spectrum of the operator ${}^1\widetilde{H}_s^0$.

Theorem 6. *Let $\nu = 1$. Then*

A) If $\varepsilon_2 = -B$ and $\varepsilon_1 < -2B$ (respectively, $\varepsilon_2 = -B$ and $\varepsilon_1 > 2B$), then the essential spectrum of the operator ${}^1\widetilde{H}_s^0$ consists of the union of ten segments: $\sigma_{ess}({}^1\widetilde{H}_s^0) = [4A-8B, 4A+8B] \cup [3A-6B+z, 3A+6B+z] \cup [2A-4B+2z, 2A+4B+2z] \cup [A-2B+3z, A+2B+3z] \cup [2A-4B+z_3, 2A+4B+z_3] \cup [A-2B+z+z_3, A+2B+z+z_3] \cup [2A-4B+z_4, 2A+4B+z_4] \cup [A-2B+z+z_4, A+2B+z+z_4] \cup [2A-4B+z_5, 2A+4B+z_5] \cup [A-2B+z+z_5, A+2B+z+z_5]$ and the discrete spectrum of the operator ${}^1\widetilde{H}_s^0$ consists of six eigenvalues: $\sigma_{disc}({}^1\widetilde{H}_s^0) = \{4z, 2z+z_3, 2z+z_4, 2z+z_5, z_3+z_4, z_3+z_5\}$, where $z = A+\varepsilon_1$ and z_3 and z_4 and z_5 are the additional eigenvalues of the operator $\widetilde{H}_2$ and $\widetilde{H}_3$, respectively.

B) If $\varepsilon_2 = -2B$ or $\varepsilon_2 = 0$ and $\varepsilon_1 < 0$ (respectively, $\varepsilon_2 = -2B$ or $\varepsilon_2 = 0$ and $\varepsilon_1 > 0$), then the essential spectrum of the operator ${}^1\widetilde{H}_s^0$ consists of the union of ten segments: $\sigma_{ess}({}^1\widetilde{H}_s^0) = [4A-8B, 4A+8B] \cup [3A-6B+z, 3A+6B+z] \cup [2A-4B+2z, 2A+4B+2z] \cup [A-2B+3z, A+2B+3z] \cup [2A-4B+z_3, 2A+4B+z_3] \cup [A-2B+z+z_3, A+2B+z+z_3] \cup [2A-4B+z_4, 2A+4B+z_4] \cup [A-2B+z+z_4, A+2B+z+z_4] \cup [2A-4B+z_5, 2A+4B+z_5] \cup [2A-4B+z+z_5, 2A+4B+z+z_5]$ and discrete spectrum of the operator ${}^1\widetilde{H}_s^0$ consists of six eigenvalues: $\sigma_{disc}({}^1\widetilde{H}_s^0) = \{4z, 2z+z_3, 2z+z_4, 2z+z_5, z_3+z_4, z_3+z_5\}$, where $z = A-\sqrt{4B^2+\varepsilon_1^2}$ (respectively, $z = A+\sqrt{4B^2+\varepsilon_1^2}$).

C) If $\varepsilon_1 = 0$ and $\varepsilon_2 > 0$ or $\varepsilon_1 = 0$ and $\varepsilon_2 < -2B$, then the essential spectrum of the operator ${}^1\widetilde{H}_s^0$ consists of the union of sixteen segments: $\sigma_{ess}({}^1\widetilde{H}_s^0) = [4A-8B, 4A+8B] \cup [3A-6B+z_1, 3A+6B+z_1] \cup [3A-6B+z_2, 3A+6B+z_2] \cup [2A-4B+2z_1, 2A+4B+2z_1] \cup [2A-4B+2z_2, 2A+4B+2z_2] \cup [A-2B+3z_1, A+2B+3z_1] \cup [A-2B+3z_2, A+2B+3z_2] \cup [2A-4B+z_4, 2A+4B+z_4] \cup [2A-4B+z_5, 2A+4B+z_5] \cup [A-2B+z_1+z_4, A+2B+z_1+z_4] \cup [A-2B+z_1+z_5, A+2B+z_1+z_5] \cup [A-2B+z_2+z_4, A+2B+z_2+z_4] \cup [A-2B+z_2+z_5, A+2B+z_2+z_5] \cup [2A-4B+z_3, 2A+4B+z_3] \cup [A-2B+z_1+z_3, A+2B+z_1+z_3] \cup [A-2B+z_2+z_3, A+2B+z_2+z_3]$, and discrete spectrum of the operator ${}^1\widetilde{H}_s^0$ consists of ten eigenvalues: $\sigma_{disc}({}^1\widetilde{H}_s^0) = \{4z_1, 2z_1+z_4, 2z_1+z_5, 4z_2, 2z_2+z_4, 2z_2+z_5, 2z_1+z_3, 2z_2+z_3, z_3+z_4, z_3+z_5\}$, where $z_1 = A-\frac{2BE}{\sqrt{E^2-1}}$ and $z_2 = A+\frac{2BE}{\sqrt{E^2-1}}$ and $E = \frac{(B+\varepsilon_2)^2}{\varepsilon_2^2+2B\varepsilon_2}$.

D) If $\varepsilon_1 = \frac{2(\varepsilon_2^2+2B\varepsilon_2)}{B}$ (respectively, $\varepsilon_1 = -\frac{2(\varepsilon_2^2+2B\varepsilon_2)}{B}$), then the essential spectrum of the operator ${}^1\widetilde{H}_s^0$ consists of the union of ten segments: $\sigma_{ess}({}^1\widetilde{H}_s^0) = [4A-8B, 4A+8B] \cup [3A-6B+z, 3A+6B+z] \cup [2A-4B+2z, 2A+4B+2z] \cup [2A-4B+z_4, 2A+4B+z_4] \cup [2A-4B+z_5, 2A+4B+z_5] \cup [A-2B+3z, A+2B+3z] \cup [2A-4B+z_3, 2A+4B+z_3] \cup [A-2B+z+z_3, A+2B+z+z_3] \cup [2A-4B+z_4, 2A+4B+z_4] \cup [A-2B+z+z_4, A+2B+z+z_4]$, and discrete spectrum of the operator ${}^1\widetilde{H}_s^0$ consists of six eigenvalues: $\sigma_{disc}({}^1\widetilde{H}_s^0) = \{4z, 2z+z_3, 2z+z_4, 2z+z_5, z_3+z_4, z_3+z_5\}$, where $z = A+\frac{2B(E^2+1)}{E^2-1}$ (respectively, $z = A-\frac{2B(E^2+1)}{E^2-1}$) and $E = \frac{(B+\varepsilon_2)^2}{\varepsilon_2^2+2B\varepsilon_2}$.

E) If $\varepsilon_2 > 0$ and $\varepsilon_1 > \frac{2(\varepsilon_2^2+2B\varepsilon_2)}{B}$ (respectively, $\varepsilon_2 < -2B$ and $\varepsilon_1 > \frac{2(\varepsilon_2^2+2B\varepsilon_2)}{B}$), then the essential spectrum of the operator ${}^1\widetilde{H}_s^0$ consists of the union of ten segments: $\sigma_{ess}({}^1\widetilde{H}_s^0) = [4A-8B, 4A+8B] \cup [3A-6B+z, 3A+6B+z] \cup [2A-4B+2z, 2A+4B+2z] \cup [2A-4B+z_4, 2A+4B+z_4] \cup [2A-4B+z_5, 2A+4B+z_5] \cup [A-2B+3z, A+2B+3z] \cup [2A-4B+z+z_4, 2A+4B+z+z_4] \cup [2A-4B+z+z_5, 2A+4B+z+z_5] \cup [2A-4B+z_3, 2A+4B+z_3] \cup [A-2B+z+z_3, A+2B+z+z_3]$, and discrete spectrum of the operator ${}^1\widetilde{H}_s^0$ consists of six eigenvalues: $\sigma_{disc}({}^1\widetilde{H}_s^0) = \{4z, 2z+z_4, 2z+z_5, 2z+z_3, z_3+z_4, z_3+z_5\}$, where $z = A+\frac{2B(\alpha+E\sqrt{E^2-1+\alpha^2})}{E^2-1}$ and $E = \frac{(B+\varepsilon_2)^2}{\varepsilon_2^2+2B\varepsilon_2}$ and the real number $\alpha > 1$.

F) If $\varepsilon_2 > 0$ and $\varepsilon_1 < -\frac{2(\varepsilon_2^2+2B\varepsilon_2)}{B}$ (respectively, $\varepsilon_2 < -2B$ and $\varepsilon_1 < -\frac{2(\varepsilon_2^2+2B\varepsilon_2)}{B}$), then

the essential spectrum of the operator ${}^1\widetilde{H}_s^0$ *consists of the union of ten segments:* $\sigma_{ess}({}^1\widetilde{H}_s^0) = [4A-8B, 4A+8B] \cup [3A-6B+z, 3A+6B+z] \cup [2A-4B+2z, 2A+4B+2z] \cup [2A-4B+z_4, 2A+4B+z_4] \cup [2A-4B+z_5, 2A+4B+z_5] \cup [A-2B+3z, A+2B+3z] \cup [2A-4B+z+z_4, 2A+4B+z+z_4] \cup [2A-4B+z+z_5, 2A+4B+z+z_5] \cup [2A-4B+z_3, 2A+4B+z_3] \cup [A-2B+z+z_3, A+2B+z+z_3]$, *and discrete spectrum of the operator* ${}^1\widetilde{H}_s^0$ *consists of six eigenvalues:* $\sigma_{disc}({}^1\widetilde{H}_s^0) = \{4z, 2z+z_4, 2z+z_5, 2z+z_3, z_3+z_4, z_3+z_5\}$, *where* $z = A - \frac{2B(\alpha + E\sqrt{E^2-1+\alpha^2})}{E^2-1}$ *and* $E = \frac{(B+\varepsilon_2)^2}{\varepsilon_2^2+2B\varepsilon_2}$ *and the real number* $\alpha > 1$.

K) If $\varepsilon_2 > 0$ *and* $0 < \varepsilon_1 < \frac{2(\varepsilon_2^2+2B\varepsilon_2)}{B}$ *(respectively,* $\varepsilon_2 < -2B$ *and* $0 < \varepsilon_1 < \frac{2(\varepsilon_2^2+2B\varepsilon_2)}{B}$, *then the essential spectrum of the operator* ${}^1\widetilde{H}_s^0$ *consists of the union of nineteen segments:* $\sigma_{ess}({}^1\widetilde{H}_s^0) = [4A-8B, 4A+8B] \cup [3A-6B+z_1, 3A+6B+z_1] \cup [3A-6B+z_2, 3A+6B+z_2] \cup [2A-4B+2z_1, 2A+4B+2z_1] \cup [2A-4B+2z_2, 2A+4B+2z_2] \cup [2A-4B+z_1+z_2, 2A+4B+z_1+z_2] \cup [A-2B+3z_1, A+2B+3z_1] \cup [A-2B+3z_2, A+2B+3z_2] \cup [A-2B+2z_1+z_2, A+2B+2z_1+z_2] \cup [A-2B+z_1+2z_2, A+2B+z_1+2z_2] \cup [2A-4B+z_3, 2A+4B+z_3] \cup [2A-4B+z_4, 2A+4B+z_4] \cup [A-2B+z_1+z_3, A+2B+z_1+z_3] \cup [A-2B+z_1+z_4, A+2B+z_1+z_4] \cup [A-2B+z_2+z_3, A+2B+z_2+z_3] \cup [A-2B+z_2+z_4, A+2B+z_2+z_4] \cup [2A-4B+z_5, 2A+4B+z_5] \cup [A-2B+z_1+z_5, A+2B+z_1+z_5] \cup [A-2B+z_2+z_5, A+2B+z_2+z_5]$, *and discrete spectrum of the operator* ${}^1\widetilde{H}_s^0$ *consists of sixteen eigenvalues:* $\sigma_{disc}({}^1\widetilde{H}_s^0) = \{4z_1, 3z_1+z_2, 2z_1+2z_2, z_1+3z_2, 4z_2, 2z_1+z_3, z_1+z_2+z_3, 2z_2+z_3, 2z_1+z_4, 2z_2+z_4, z_1+z_2+z_4, 2z_1+z_5, z_1+z_2+z_5, 2z_2+z_5, z_3+z_4, z_3+z_5\}$, *where* $z_1 = A + \frac{2B(\alpha + E\sqrt{E^2-1+\alpha^2})}{E^2-1}$ *and* $z_2 = A + \frac{2B(\alpha - E\sqrt{E^2-1+\alpha^2})}{E^2-1}$ *and* $E = \frac{(B+\varepsilon_2)^2}{\varepsilon_2^2+2B\varepsilon_2}$ *and the real number* $0 < \alpha < 1$.

M) If $\varepsilon_2 > 0$ *and* $-\frac{2(\varepsilon_2^2+2B\varepsilon_2)}{B} < \varepsilon_1 < 0$ *(respectively,* $\varepsilon_2 < -2B$ *and* $-\frac{2(\varepsilon_2^2+2B\varepsilon_2)}{B} < \varepsilon_1 < 0$*), then the essential spectrum of the operator* ${}^1\widetilde{H}_s^0$ *consists of the union of nineteen segments:* $\sigma_{ess}({}^1\widetilde{H}_s^0) = [4A-8B, 4A+8B] \cup [3A-6B+z_1, 3A+6B+z_1] \cup [3A-6B+z_2, 3A+6B+z_2] \cup [2A-4B+2z_1, 2A+4B+2z_1] \cup [2A-4B+2z_2, 2A+4B+2z_2] \cup [2A-4B+z_1+z_2, 2A+4B+z_1+z_2] \cup [A-2B+3z_1, A+2B+3z_1] \cup [A-2B+3z_2, A+2B+3z_2] \cup [A-2B+2z_1+z_2, A+2B+2z_1+z_2] \cup [A-2B+z_1+2z_2, A+2B+z_1+2z_2] \cup [2A-4B+z_3, 2A+4B+z_3] \cup [2A-4B+z_4, 2A+4B+z_4] \cup [A-2B+z_1+z_3, A+2B+z_1+z_3] \cup [A-2B+z_1+z_4, A+2B+z_1+z_4] \cup [A-2B+z_2+z_3, A+2B+z_2+z_3] \cup [A-2B+z_2+z_4, A+2B+z_2+z_4] \cup [2A-4B+z_5, 2A+4B+z_5] \cup [A-2B+z_1+z_5, A+2B+z_1+z_5] \cup [A-2B+z_2+z_5, A+2B+z_2+z_5]$, *and discrete spectrum of the operator* ${}^1\widetilde{H}_s^0$ *consists of sixteen eigenvalues:* $\sigma_{disc}({}^1\widetilde{H}_s^0) = \{4z_1, 3z_1+z_2, 2z_1+2z_2, z_1+3z_2, 4z_2, 2z_1+z_3, z_1+z_2+z_3, 2z_2+z_3, 2z_1+z_4, 2z_2+z_4, z_1+z_2+z_4, 2z_1+z_5, z_1+z_2+z_5, 2z_2+z_5, z_3+z_4, z_3+z_5\}$, *where* $z_1 = A + \frac{2B(\alpha + E\sqrt{E^2-1+\alpha^2})}{E^2-1}$ *and* $z_2 = A + \frac{2B(\alpha - E\sqrt{E^2-1+\alpha^2})}{E^2-1}$ *and* $E = \frac{(B+\varepsilon_2)^2}{\varepsilon_2^2+2B\varepsilon_2}$ *and the real number* $0 < \alpha < 1$.

N) If $-2B < \varepsilon_2 < 0$, *then the essential spectrum of the operator* ${}^1\widetilde{H}_s^0$ *consists of the union of four segments:* $\sigma_{ess}({}^1\widetilde{H}_s^0) = [4A-8B, 4A+8B] \cup [2A-4B+z_3, 2A+4B+z_3] \cup [2A-4B+z_4, 2A+4B+z_4] \cup [2A-4B+z_5, 2A+4B+z_5]$, *and discrete spectrum of the operator* ${}^1\widetilde{H}_s^0$ *consists of two eigenvalues:* $\sigma_{disc}({}^1\widetilde{H}_s^0) = \{z_3+z_4, z_3+z_5\}$.

Proof. A). From the representation (5), (12) and the formulas (10) and (11), and the Theorem 8 in the work [3], follow the in one-dimensional case, the continuous spectrum of the operator $\widetilde{H}_1$ consists $\sigma_{cont}(\widetilde{H}_1) = [A-2B, A+2B]$, and the discrete spectrum of the operator $\widetilde{H}_1$ consists of unique eigenvalue $z = A+\varepsilon_1$. Therefore, the essential spectrum of the operators $\widetilde{H}_1 \bigotimes I + I \bigotimes \widetilde{H}_1$ consists from segments $[2A-4B, 2A+4B]$, and $[A-2B+z, A+2B+z]$. Discrete spectrum of operator $\widetilde{H}_1 \bigotimes I + I \bigotimes \widetilde{H}_1$ is consists of eigenvalue $2z$. The operator $\widetilde{H}_2 = \widetilde{H}_1 \bigotimes I + I \bigotimes \widetilde{H}_1 - 2U \int\limits_{T^\nu} \widetilde{f}(s, \Lambda - s)ds$, where $\Lambda = \lambda + \mu$, has additional eigenvalue z_3, and operator $\widetilde{H}_3 = \widetilde{H}_1 \bigotimes I +$

$I \bigotimes \widetilde{H}_1 + 2U \int\limits_{T^\nu} \widetilde{f}(s, \Lambda - s)ds + 2\varepsilon_2 \int\limits_{T^\nu} \int\limits_{T^\nu} \widetilde{f}(s,t)dsdt$ has additional eigenvalues z_4 and z_5. It follows that the essential spectrum of operator ${}^1\widetilde{H}_s^0$ consists of the union of ten segments and discrete spectrum of operator ${}^1\widetilde{H}_s^0$ consists of six eigenvalues. These give the proof statement A) of the Theorem 6.

B) In this case the operator $\widetilde{H}_1$ has a one eigenvalue z_1, lying the outside of the continuous spectrum of operator $\widetilde{H}_1$. Therefore, the essential spectrum of the operators $\widetilde{H}_1 \bigotimes I + I \bigotimes \widetilde{H}_1$ consists of the union of two segments and discrete spectrum of the operator $\widetilde{H}_1 \bigotimes I + I \bigotimes \widetilde{H}_1$ consists of single point. These give the statement B) of the Theorem 6. These give the proof statement B) of the Theorem 6. □

The next theorems is described the structure of essential spectrum of the operator ${}^1\widetilde{H}_s^0$ in the three-dimensional case.

Theorem 7. *Let $\nu = 3$. Then*

A) 1. If $\varepsilon_2 = -B$ and $\varepsilon_1 < -6B$ (respectively, $\varepsilon_2 = -B$ and $\varepsilon_1 > 6B$), then the essential spectrum of the operator ${}^1\widetilde{H}_s^0$ consists of the union of ten segments: $\sigma_{ess}({}^1\widetilde{H}_s^0) = [4A-24B, 4A+24B] \cup [3A-18B+z, 3A+18B+z] \cup [2A-12B+2z, 2A+12B+2z] \cup [A-6B+3z, A+6B+3z] \cup [2A-12B+z_3, 2A+12B+z_3] \cup [A-6B+z+z_3, A+6B+z+z_3] \cup [2A-12B+z_4, 2A+12B+z_4] \cup [2A-12B+z_5, 2A+12B+z_5] \cup [A-6B+z+z_4, A+6B+z+z_4] \cup [A-6B+z+z_5, A+6B+z+z_5]$, and discrete spectrum of the operator ${}^1\widetilde{H}_s^0$ consists of six eigenvalues: $\sigma_{disc}({}^1\widetilde{H}_s^0) = \{4z, 2z+z_3, 2z+z_4, 2z+z_5, z_3+z_4, z_3+z_5\}$, where $z = A+\varepsilon_1$, z_3 and z_4 and z_5 are the eigenvalues of the operators $\widetilde{H}_2$ and $\widetilde{H}_3$.

2. If $\varepsilon_2 = -B$ and $-6B \leqslant \varepsilon_1 < -2B$ (respectively, $\varepsilon_2 = -B$ and $2B < \varepsilon_1 \leqslant 6B$), then the essential spectrum of the operator ${}^1\widetilde{H}_s^0$ consists of the union of four segments: $\sigma_{ess}({}^1\widetilde{H}_s^0) = [4A-24B, 4A+24B] \cup [2A-12B+z_3, 2A+12B+z_3] \cup [2A-12B+z_4, 2A+12B+z_4] \cup [2A-12B+z_5, 2A+12B+z_5]$, and discrete spectrum of the operator ${}^1\widetilde{H}_s^0$ consists of two eigenvalues: $\sigma_{disc}({}^1\widetilde{H}_s^0) = \{z_3+z_4, z_3+z_5\}$.

B) If $\varepsilon_2 = -2B$ or $\varepsilon_2 = 0$, and $\varepsilon_1 < 0$, $\varepsilon_1 \leqslant -\dfrac{6B}{W}$ (respectively, $\varepsilon_2 = -2B$ or $\varepsilon_2 = 0$, and $\varepsilon_1 > 0$, $\varepsilon_1 \geqslant \dfrac{6B}{W}$), then the essential spectrum of the operator ${}^1\widetilde{H}_s^0$ consists of the union of ten segments: $\sigma_{ess}({}^1\widetilde{H}_s^0) = [4A-24B, 4A+24B] \cup [3A-18B+z_1, 3A+18B+z_1] \cup [2A-12B+2z_1, 2A+12B+2z_1] \cup [A-6B+3z_1, A+6B+3z_1] \cup [2A-12B+z_3, 2A+12B+z_3] \cup [A-6B+z_1+z_3, A+6B+z_1+z_3] \cup [2A-12B+z_4, 2A+12B+z_4] \cup [2A-12B+z_5, 2A+12B+z_5] \cup [A-6B+z_1+z_4, A+6B+z_1+z_4] \cup [A-6B+z_1+z_5, A+6B+z_1+z_5]$ (respectively, $\sigma_{ess}({}^1\widetilde{H}_s^0) = [4A-24B, 4A+24B] \cup [3A-18B+z_2, 3A+18B+z_2] \cup [2A-12B+2z_2, 2A+12B+2z_2] \cup [A-6B+3z_2, A+6B+3z_2] \cup [2A-12B+z_3, 2A+12B+z_3] \cup [A-6B+z_2+z_3, A+6B+z_2+z_3] \cup [2A-12B+z_4, 2A+12B+z_4] \cup [2A-12B+z_5, 2A+12B+z_5] \cup [A-6B+z_2+z_4, A+6B+z_2+z_4] \cup [A-6B+z_2+z_5, A+6B+z_2+z_5]$), and discrete spectrum of the operator ${}^1\widetilde{H}_s^0$ consists of six eigenvalues: $\sigma_{disc}({}^1\widetilde{H}_s^0) = \{4z_1, 2z_1+z_3, 2z_1+z_4, 2z_1+z_5, z_3+z_4, z_3+z_5\}$ (respectively, $\sigma_{disc}({}^1\widetilde{H}_s^0) = \{4z_2, 2z_2+z_3, 2z_2+z_4, 2z_2+z_5, z_3+z_4, z_3+z_5\}$), where z_1 (respectively, z_2) are the eigenvalue of operator $\widetilde{H}_1$.

If $-\dfrac{6B}{W} \leqslant \varepsilon_1 < 0$ (respectively, $0 < \varepsilon_1 \leqslant \dfrac{6B}{W}$), then the essential spectrum of the operator ${}^1\widetilde{H}_s^0$ consists of the union of four segments: $\sigma_{ess}({}^1\widetilde{H}_s^0) = [4A-24B, 4A+24B] \cup [2A-12B+z_3, 2A+12B+z_3] \cup [2A-12B+z_4, 2A+12B+z_4] \cup [2A-12B+z_5, 2A+12B+z_5]$, and discrete spectrum of the operator ${}^1\widetilde{H}_s^0$ consists of two eigenvalue: $\sigma_{disc}({}^1\widetilde{H}_s^0) = \{z_3+z_4, z_3+z_5\}$.

*C) If $\varepsilon_1 = 0$ and $\varepsilon_2 > 0, E < W$ (respectively, $\varepsilon_1 = 0$ and $\varepsilon_2 < -2B, E < W$), then the essential spectrum of the operator ${}^1\widetilde{H}_s^0$ consists of the union of ten segments: $\sigma_{ess}({}^1\widetilde{H}_s^0) = [4A-24B, 4A+24B] \cup [3A-18B+z, 3A+18B+z] \cup [2A-12B+2z, 2A+12B+2z] \cup [A-6B+3z, A+$

$6B+3z]\cup[2A-12B+z_3, 2A+12B+z_3]\cup[A-6B+z+z_3, A+6B+z+z_3]\cup[2A-12B+z_4, 2A+12B+z_4]\cup[2A-12B+z_5, 2A+12B+z_5]\cup[A-6B+z+z_4, A+6B+z+z_4]\cup[A-6B+z+z_5, A+6B+z+z_5]$ *(respectively,* $\sigma_{ess}({}^1\widetilde{H}_s^0) = [4A-24B, 4A+24B]\cup[3A-18B+\widetilde{z}, 3A+18B+\widetilde{z}]\cup[2A-12B+2\widetilde{z}, 2A+12B+2\widetilde{z}]\cup[A-6B+3\widetilde{z}, A+6B+3\widetilde{z}]\cup[2A-12B+z_3, 2A+12B+z_3]\cup[A-6B+\widetilde{z}+z_3, A+6B+\widetilde{z}+z_3]\cup[2A-12B+z_4, 2A+12B+z_4]\cup[2A-12B+z_5, 2A+12B+z_5]\cup[A-6B+\widetilde{z}+z_4, A+6B+\widetilde{z}+z_4]\cup[A-6B+\widetilde{z}+z_5, A+6B+\widetilde{z}+z_5]$*), and discrete spectrum of the operator* ${}^1\widetilde{H}_s^0$ *consists of six eigenvalues:* $\sigma_{disc}({}^1\widetilde{H}_s^0) = \{4z, 2z+z_3, 2z+z_4, 2z+z_5, z_3+z_4, z_3+z_5\}$ *(respectively,* $\sigma_{disc}({}^1\widetilde{H}_s^0) = \{4\widetilde{z}, 2\widetilde{z}+z_3, 2\widetilde{z}+z_4, 2\widetilde{z}+z_5, z_3+z_4, z_3+z_5\}$*), where z (respectively,* $\widetilde{z}$*), is the eigenvalue of operator* $\widetilde{H}_1$*, and* $E = \frac{(B+\varepsilon_2)^2}{\varepsilon_2^2+2B\varepsilon_2}$*. If* $\varepsilon_1 = 0$ *and* $\varepsilon_2 > 0, E > W$ *(respectively,* $\varepsilon_1 = 0$ *and* $\varepsilon_2 < -2B, E > W$*), then the essential spectrum of the operator* ${}^1\widetilde{H}_s^0$ *consists of a union of four segments:* $\sigma_{ess}({}^1\widetilde{H}_s^0) = [4A-24B, 4A+24B]\cup[2A-12B+z_3, 2A+12B+z_3]\cup[2A-12B+z_4, 2A+12B+z_4]\cup[2A-12B+z_5, 2A+12B+z_5]$ *and discrete spectrum of the operator* ${}^2\widetilde{H}_t^1$ *consists of two eigenvalues:* $\sigma_{disc}({}^1\widetilde{H}_s^0) = \{z_3+z_4, z_3+z_5\}$.

D) If $\varepsilon_1 = \frac{2(\varepsilon_2^2+2B\varepsilon_2)}{B}$ *and* $E < \frac{4}{3}W$ *(respectively,* $\varepsilon_1 = -\frac{2(\varepsilon_2^2+2B\varepsilon_2)}{B}$ *and* $E < \frac{4}{3}W$*), then the essential spectrum of the operator* ${}^1\widetilde{H}_s^0$ *consists of the union of ten segments:* $\sigma_{ess}({}^1\widetilde{H}_s^0) = [4A-24B, 4A+24B]\cup[3A-18B+z, 3A+18B+z]\cup[2A-12B+2z, 2A+12B+2z]\cup[A-6B+3z, A+6B+3z]\cup[2A-12B+z_3, 2A+12B+z_3]\cup[A-6B+z+z_3, A+6B+z+z_3]\cup[2A-12B+z_4, 2A+12B+z_4]\cup[A-6B+z+z_4, A+6B+z+z_4]\cup[2A-12B+z_5, 2A+12B+z_5]\cup[A-6B+z+z_5, A+6B+z+z_5]$ *(respectively,* $\sigma_{ess}({}^1\widetilde{H}_s^0) = [4A-24B, 4A+24B]\cup[3A-18B+\widetilde{z}, 3A+18B+\widetilde{z}]\cup[2A-12B+2\widetilde{z}, 2A+12B+2\widetilde{z}]\cup[A-6B+3\widetilde{z}, A+6B+3\widetilde{z}]\cup[2A-12B+z_3, 2A+12B+z_3]\cup[A-6B+\widetilde{z}+z_3, A+6B+\widetilde{z}+z_3]\cup[2A-12B+z_4, 2A+12B+z_4]\cup[2A-12B+z_5, 2A+12B+z_5]\cup[A-6B+\widetilde{z}+z_4, A+6B+\widetilde{z}+z_4]\cup[2A-12B+\widetilde{z}+z_5, 2A+12B+\widetilde{z}+z_5]$*), and discrete spectrum of the operator* ${}^1\widetilde{H}_s^0$ *consists of six eigenvalues:* $\sigma_{disc}({}^1\widetilde{H}_s^0) = \{4z, 2z+z_3, 2z+z_4, 2z+z_5, z_3+z_4, z_3+z_5\}$ *(respectively,* $\sigma_{disc}({}^1\widetilde{H}_s^0) = \{4\widetilde{z}, 2\widetilde{z}+z_3, 2\widetilde{z}+z_4, 2\widetilde{z}+z_5, z_3+z_4, z_3+z_5\}$*), where z (respectively,* $\widetilde{z}$*) is the eigenvalue of operator* $\widetilde{H}_1$.

E) If $\varepsilon_2 > 0$ *and* $\varepsilon_1 > \frac{2(\varepsilon_2^2+2B\varepsilon_2)}{B}$ *and* $E < \left(1+\frac{\alpha}{3}\right)W$ *(respectively,* $\varepsilon_2 < -2B$ *and* $\varepsilon_1 > \frac{2(\varepsilon_2^2+2B\varepsilon_2)}{B}$ *and* $E < \left(1+\frac{\alpha}{3}\right)W$*), then the essential spectrum of the operator* ${}^1\widetilde{H}_s^0$ *consists of the union of ten segments:* $\sigma_{ess}({}^1\widetilde{H}_s^0) = [4A-24B, 4A+24B]\cup[3A-18B+z_1, 3A+18B+z_1]\cup[2A-12B+2z_1, 2A+12B+2z_1]\cup[A-6B+3z_1, A+6B+3z_1]\cup[2A-12B+z_3, 2A+12B+z_3]\cup[A-6B+z_1+z_3, A+6B+z_1+z_3]\cup[2A-12B+z_4, 2A+12B+z_4]\cup[A-6B+z_1+z_4, A+6B+z_1+z_4]\cup[2A-12B+z_5, 2A+12B+z_5]\cup[A-6B+z_1+z_5, A+6B+z_1+z_5]$, *and discrete spectrum of the operator* ${}^1\widetilde{H}_s^0$ *consists of six eigenvalues:* $\sigma_{disc}({}^1\widetilde{H}_s^0) = \{4z_1, 2z_1+z_3, 2z_1+z_4, 2z_1+z_5, z_3+z_4, z_3+z_5\}$, *where* z_1 *is the eigenvalue of operator* $\widetilde{H}_1$.

F) If $\varepsilon_2 > 0$ *and* $\varepsilon_1 < -\frac{2(\varepsilon_2^2+2B\varepsilon_2)}{B}$ *and* $E < \left(1+\frac{\alpha}{3}\right)W$ *(respectively,* $\varepsilon_2 < -2B$ *and* $\varepsilon_1 < -\frac{2(\varepsilon_2^2+2B\varepsilon_2)}{B}$ *and* $E < \left(1+\frac{\alpha}{3}\right)W$*), then the essential spectrum of the operator* ${}^1\widetilde{H}_s^0$ *consists of the union of ten segments:* $\sigma_{ess}({}^1\widetilde{H}_s^0) = [4A-24B, 4A+24B]\cup[3A-18B+z_1, 3A+18B+z_1]\cup[2A-12B+2z_1, 2A+12B+2z_1]\cup[A-6B+3z_1, A+6B+3z_1]\cup[2A-12B+z_3, 2A+12B+z_3]\cup[A-6B+z_1+z_3, A+6B+z_1+z_3]\cup[2A-12B+z_4, 2A+12B+z_4]\cup[A-6B+z_1+z_4, A+6B+z_1+z_4]\cup[2A-12B+z_5, 2A+12B+z_5]\cup[A-6B+z_1+z_5, A+6B+z_1+z_5]$, *and discrete spectrum of the operator* ${}^1\widetilde{H}_s^0$ *consists of six eigenvalues:* $\sigma_{disc}({}^1\widetilde{H}_s^0) = \{4z_1, 2z_1+z_3, 2z_1+z_4, 2z_1+z_5, z_3+z_4, z_3+z_5\}$, *where* z_1 *is the eigenvalue of operator* $\widetilde{H}_1$.

K) If $\varepsilon_2 > 0$ *and* $0 < \varepsilon_1 < \frac{2(\varepsilon_2^2+2B\varepsilon_2)}{B}$ *and* $\left(1-\frac{\alpha}{3}\right)W < E < \left(1+\frac{\alpha}{3}\right)W$ *(respectively,* $\varepsilon_2 < -2B$ *and* $0 < \varepsilon_1 < \frac{2(\varepsilon_2^2+2B\varepsilon_2)}{B}$ *and* $\left(1-\frac{\alpha}{3}\right)W < E < \left(1+\frac{\alpha}{3}\right)W$*), then the essential*

spectrum of the operator ${}^1\widetilde{H}_s^0$ *consists of the union of nineteen segments:* $\sigma_{ess}({}^1\widetilde{H}_s^0) = [4A - 24B, 4A + 24B] \cup [3A - 18B + z_1, 3A + 18B + z_1] \cup [3A - 18B + z_2, 3A + 18B + z_2] \cup [2A - 12B + 2z_1, 2A + 12B + 2z_1] \cup [2A - 12B + z_1 + z_2, 2A + 12B + z_1 + z_2] \cup [2A - 12B + 2z_2, 2A + 12B + 2z_2] \cup [2A - 12B + z_4, 2A + 12B + z_4] \cup [2A - 12B + z_5, 2A + 12B + z_5] \cup [A - 6B + 3z_1, A + 6B + 3z_1] \cup [A - 6B + 2z_1 + z_2, A + 6B + 2z_1 + z_2] \cup [A - 6B + z_1 + 2z_2, A + 6B + z_1 + 2z_2] \cup [A - 6B + z_1 + z_4, A + 6B + z_1 + z_4] \cup [A - 6B + z_1 + z_5, A + 6B + z_1 + z_5] \cup [A - 6B + 3z_2, A + 6B + 3z_2] \cup [A - 6B + z_2 + z_4, A + 6B + z_2 + z_4] \cup [A - 6B + z_2 + z_5, A + 6B + z_2 + z_5] \cup [2A - 12B + z_3, 2A + 12B + z_3] \cup [A - 6B + z_1 + z_3, A + 6B + z_1 + z_3] \cup [A - 6B + z_2 + z_3, A + 6B + z_2 + z_3]$, *and discrete spectrum of the operator* ${}^1\widetilde{H}_s^0$ *consists of sixteen eigenvalues* $\sigma_{disc}({}^1\widetilde{H}_s^0) = \{4z_1, 2z_1 + z_3, 2z_1 + z_4, 2z_1 + z_5, z_3 + z_4, z_3 + z_5, 3z_1 + z_2, 2z_1 + 2z_2, z_1 + 3z_2, z_1 + z_2 + z_4, z_1 + z_2 + z_5, 4z_2, 2z_2 + z_4, 2z_2 + z_5, z_1 + z_2 + z_3, 2z_2 + z_3\}$, *where* z_1 *and* z_2 *is the eigenvalue of operator* $\widetilde{H}_1$.

M) If $\varepsilon_2 > 0$ *and* $-\dfrac{2(\varepsilon_2^2 + 2B\varepsilon_2)}{B} < \varepsilon_1 < 0$ *and* $\Big(1 - \dfrac{\alpha}{3}\Big)W < E < \Big(1 + \dfrac{\alpha}{3}\Big)W$ *(respectively,* $\varepsilon_2 < -2B$ *and* $-\dfrac{2(\varepsilon_2^2 + 2B\varepsilon_2)}{B} < \varepsilon_1 < 0$ *and* $\Big(1 - \dfrac{\alpha}{3}\Big)W < E < \Big(1 + \dfrac{\alpha}{3}\Big)W$*), then the essential spectrum of the operator* ${}^1\widetilde{H}_s^0$ *consists of the union of nineteen segments:* $\sigma_{ess}({}^1\widetilde{H}_s^0) = [4A - 24B, 4A + 24B] \cup [3A - 18B + z_1, 3A + 18B + z_1] \cup [3A - 18B + z_2, 3A + 18B + z_2] \cup [2A - 12B + 2z_1, 2A + 12B + 2z_1] \cup [2A - 12B + z_1 + z_2, 2A + 12B + z_1 + z_2] \cup [2A - 12B + 2z_2, 2A + 12B + 2z_2] \cup [2A - 12B + z_4, 2A + 12B + z_4] \cup [2A - 12B + z_5, 2A + 12B + z_5] \cup [A - 6B + 3z_1, A + 6B + 3z_1] \cup [A - 6B + 2z_1 + z_2, A + 6B + 2z_1 + z_2] \cup [A - 6B + z_1 + 2z_2, A + 6B + z_1 + 2z_2] \cup [A - 6B + z_1 + z_4, A + 6B + z_1 + z_4] \cup [A - 6B + z_1 + z_5, A + 6B + z_1 + z_5] \cup [A - 6B + 3z_2, A + 6B + 3z_2] \cup [A - 6B + z_2 + z_4, A + 6B + z_2 + z_4] \cup [A - 6B + z_2 + z_5, A + 6B + z_2 + z_5] \cup [2A - 12B + z_3, 2A + 12B + z_3] \cup [A - 6B + z_1 + z_3, A + 6B + z_1 + z_3] \cup [A - 6B + z_2 + z_3, A + 6B + z_2 + z_3]$, *and discrete spectrum of the operator* ${}^1\widetilde{H}_s^0$ *consists of sixteen eigenvalues* $\sigma_{disc}({}^1\widetilde{H}_s^0) = \{4z_1, 2z_1 + z_3, 2z_1 + z_4, 2z_1 + z_5, z_3 + z_4, z_3 + z_5, 3z_1 + z_2, 2z_1 + 2z_2, z_1 + 3z_2, z_1 + z_2 + z_4, z_1 + z_2 + z_5, 4z_2, 2z_2 + z_4, 2z_2 + z_5, z_1 + z_2 + z_3, 2z_2 + z_3\}$, *where* z_1 *and* z_2 *is the eigenvalue of operator* $\widetilde{H}_1$.

N) If $-2B < \varepsilon_2 < 0$*, then the essential spectrum of the operator* ${}^1\widetilde{H}_s^0$ *consists of the union of four segments:* $\sigma_{ess}({}^1\widetilde{H}_s^0) = [4A - 24B, 4A + 24B] \cup [2A - 12B + z_4, 2A + 12B + z_4] \cup [2A - 12B + z_5, 2A + 12B + z_5] \cup [2A - 12B + z_3, 2A + 12B + z_3]$, *and discrete spectrum of the operator* ${}^1\widetilde{H}_s^0$ *consists of two eigenvalues* $\sigma_{disc}({}^1\widetilde{H}_s^0) = \{z_3 + z_4, z_3 + z_5\}$.

Proof. A). From the representation (5), (12) and the formulas (10),(11) and Theorem 9 in the work [3], follow the in three-dimensional case, the continuous spectrum of the operator $\widetilde{H}_1$ consists $\sigma_{cont}(\widetilde{H}_1) = [A - 6B, A + 6B]$, and the discrete spectrum of the operator $\widetilde{H}_1$ consists of unique eigenvalue $z = A + \varepsilon_1$. Therefore, the essential spectrum of the operator $\widetilde{H}_1 \bigotimes I + I \bigotimes \widetilde{H}_1$ consists from segments $[2A - 12B, 2A + 12B]$ and $[A - 6B + z, A + 6B + z]$. Discrete spectrum of operator $\widetilde{H}_1 \bigotimes I + I \bigotimes \widetilde{H}_1$ consists of eigenvalue $2z$. The operator $\widetilde{H}_2 = \widetilde{H}_1 \bigotimes I + I \bigotimes \widetilde{H}_1 - 2U \int\limits_{T^\nu} \widetilde{f}(s, \Lambda - s)ds$, where $\Lambda = \lambda + \mu$, has additional eigenvalue z_3, and operator $\widetilde{H}_3 = \widetilde{H}_1 \bigotimes I + I \bigotimes \widetilde{H}_1 + 2U \int\limits_{T^\nu} \widetilde{f}(s, \Lambda - s)ds + 2\varepsilon_2 \int\limits_{T^\nu} \int\limits_{T^\nu} \widetilde{f}(s, t)dsdt$ has additional eigenvalues z_4 and z_5. It follows that the essential spectrum of operator ${}^1\widetilde{H}_s^0$ consists of the union of ten segments and discrete spectrum of operator ${}^1\widetilde{H}_s^0$ consists of six eigenvalues. These give the proof statement B) of the Theorem 7.

K) From the representation (5), (12) and the formulas (10) and (11), and Theorem 9 in the work [3], follow the in three-dimensional case, the continuous spectrum of the operator $\widetilde{H}_1$ consists $\sigma_{cont}(\widetilde{H}_1) = [A - 6B, A + 6B]$, and the discrete spectrum of the operator $\widetilde{H}_1$ consists of exactly two eigenvalues z_1 and z_2. Therefore, the essential spectrum of the operator $\widetilde{H}_1 \bigotimes I + I \bigotimes \widetilde{H}_1$ consists from segments $[2A - 12B, 2A + 12B]$ and $[A - 6B + z_1, A + 6B + z_1]$ and $[A - 6B + z_2, A + 6B + z_2]$. Discrete spectrum of operator $\widetilde{H}_1 \bigotimes I + I \bigotimes \widetilde{H}_1$ consists of eigenvalues $2z_1$, $z_1 + z_2$, and $2z_2$.

The operator $\widetilde{H}_2 = \widetilde{H}_1 \bigotimes I + I \bigotimes \widetilde{H}_1 - 2U \int\limits_{T^\nu} \widetilde{f}(s, \Lambda - s)ds$, where $\Lambda = \lambda + \mu$, has additional eigenvalue z_3, and operator $\widetilde{H}_3 = \widetilde{H}_1 \bigotimes I + I \bigotimes \widetilde{H}_1 + 2U \int_{T^\nu} \widetilde{f}(s, \Lambda - s)ds + 2\varepsilon_2 \int\limits_{T^\nu} \int\limits_{T^\nu} \widetilde{f}(s, t)dsdt$ has additional eigenvalues z_4 and z_5. It follows that the essential spectrum of operator ${}^1\widetilde{H}_s^0$ consists of the union of nineteen segments and discrete spectrum of operator ${}^1\widetilde{H}_s^0$ consists of sixteen eigenvalues. These give the proof statement K) of the Theorem 7.

The other statements of the Theorem 7 the analogously is proved. □

Conclusion

In this paper, we consider four-electron systems in the impurity Hubbard model and investigated the structure of essential spectrum and discrete spectra of the system in the first singlet state of the system. We proved in the first singlet state the essential spectrum of the system consists of the union of nineteen or sixteen or ten of four segments, and the discrete spectrum of the system consists of sixteen or ten or six or two eigenvalues. The obtaining results can be applied in the field of magnetic semiconductors and other fields of science and technology.

They can also be the basis for further research in the field of spectral theory of multiparticle systems.

References

[1] S.M.Tashpulatov, Spectra of the energy operator of four-electron systems in the triplet state in the Hubbard Model, *Journal of Physics: Conference Series*, **697**(2016), 012025. DOI: 10.1088/1742-6596/697/1/012025.

[2] S.M.Tashpulatov, The structure of essential spectra and discrete spectrum of four-electron systems in the Hubbard model in a singlet state, *Lobachevskii Journal of Mathematics*, **38**(2017), no. 3, 530–541. DOI: 10.1134/S1995080217030246

[3] S.M.Tashpulatov, Spectra of the energy operator of two-electron system in the impurity hubbard model, *Journal of Applied Mathematics and Physics*, **10**(2022), 2743–2779. DOI: 10.4236/jamp.2022.109184

[4] S.M.Tashpulatov, Monography. Spectra of the two-electron System in the Impurity Hubbard Model, LAP LAMBERT Academic Publishing, 2022.

[5] M.Reed, B.Simon, Methods of Modern Mathetical Physics, New York, Acad. Press., Vol. 1, Functional Analysis, 1972.

[6] M.Reed, B.Simon, Methods of Modern Mathetical Physics, New York, Acad. Press., Vol. 4, Operator Analysis, 1978.

[7] V.V.Val'kov, S.G.Ovchinnikov, O.P.Petrakovskii, "The excitation spectra of two-magnon systems in easy-axis quasidimensional ferromagnets, *Sov. Phys. Solid. State.*, **30**(1988), 3044–3047.

[8] T.Ichinose, Spectral properties of tensor products of linear operators, 1, *Trans. Am. Math. Soc.*, **235**(1978), 75–113.

[9] T.Ichinose, Spectral properties of tensor products of linear operators, 2: The approximate point spectrum and Kato essential spectrum, *Trans. Am. Math. Soc.*, **237**(1978), 223–254.

Четырехэлектронный первый синглет в примесной модели Хаббарда

Садулла М. Ташпулатов
Институт ядерной физики Академии наук республики Узбекистан
Ташкент, Узбекистан
Рухсат Т. Парманова
Институт ядерной физики Академии наук республики Узбекистан
Ташкент, Узбекистан
Институт фундаментальных и прикладных исследований
Национальный исследовательский университет "ТИИИМСХ"
Ташкент, Узбекистан

Аннотация. Рассматривается оператор энергии четырехэлектронных систем в примесной модели Хаббарда и исследуются структура существенного спектра и дискретный спектр системы для первого синглетного состояния системы. Исследование показывает, что в случае первого синглетного состояния имеют место нижеследующие ситуации: 1) в первом синглетном состоянии существенный спектр системы есть объединение десяти отрезков, а дискретный спектр системы состоит из шести собственных значений; 2) в первом синглетном состоянии существенный спектр системы есть объединение шестнадцати отрезков, а дискретный спектр системы состоит из десяти собственных значений; 3) в первом синглетном состоянии существенный спектр системы есть объединение девятнадцати отрезков, а дискретный спектр системы состоит из шестнадцати собственных значений; 4) в первом синглетном состоянии существенный спектр системы есть объединение четырех отрезков, а дискретный спектр системы состоит из двух собственных значений.

Ключевые слова: четырехэлектронная система, примесная модель Хаббарда, синглетное состояние, квинтетное состояние, триплетное состояние, существенный спектр, дискретный спектр.

EDN: XFNSTE
УДК 517.9

On Certain New Eulerian, Laplace and Edwards-type Integrals Comprising Generalised Hypergeometric Functions

Ambika Narayana*
Research Center, Department of Mathematics
A J Institute of Engineering and Technology
(Visvesvaraya Technological University (VTU), Belagavi)
Mangaluru-575006, Karnataka, India
Department of Mathematics
NMAM Institute of Technology, Nitte (Deemed to be University)
Nitte, 574110, Karnataka, India
Shantha Kumari Kurumujji†
Department of Mathematics
A J Institute of Engineering and Technology
(Visvesvaraya Technological University (VTU), Belagavi)
Mangaluru-575006, Karnataka, India

Received 04.11.2024, received in revised form 07.03.2025, accepted 24.04.2025

Abstract. In 2018, Masjed–Jamei & Koepf [12] established some summation theorems for the generalized hypergeometric functions. In 2021, Awad et al. [3] investigated extensions of these classical summation theorems for the series ${}_3F_2$ and ${}_4F_3$, with applications in Eulerian-type and Laplace-type Integrals. In this study, new Eulerian, Laplace, and Edwards-type integrals are established using extensions of the classical summation theorems provided by Awad et al. [3]. As special instances of our primary findings, the findings from previous studies by Awad et al. [3], Koepf et al. [9] and Kim et al. [7] are also demonstrated.

Keywords: generalized hypergeometric function, classical summation theorems, Eulerian-type integral, Laplace-type integral, Edwards-type integral.

Citation: A. Narayana, S.K. Kurumujji, On Certain new Eulerian, Laplace and Edwards-type Integrals Comprising Generalised Hypergeometric Functions, J. Sib. Fed. Univ. Math. Phys., 2025, 18(4), 568–579. EDN: XFNSTE.

1. Introduction and preliminaries

The generalised hypergeometric function ${}_pF_q$ where $p, q \in \mathbb{N}_0$, as defined by [1, 6], is an eminently evident generalisation of the Gauss's hypergeometric function ${}_2F_1$ and is given by

$$ {}_pF_q\left[\begin{array}{c} a_1,\ \ldots,\ a_p \\ b_1,\ \ldots,\ b_q \end{array};\ z\right] = \sum_{m=0}^{\infty} \frac{(a_1)_m \ldots (a_p)_m}{(b_1)_m \ldots (b_q)_m} \frac{z^m}{m!} \tag{1} $$

where $b_i \neq 0, -1, -2, \cdots$, $(\lambda)_m$ is the well known Pochhammer symbol (or the raised factorial or the shifted factorial since $(1)_m = m!$) defined for any complex $a \in \mathbb{C}$ by

$$ \begin{aligned} (\lambda)_m &= \frac{\Gamma(\lambda + m)}{\Gamma(\lambda)}, \quad \left(\lambda \in \mathbb{C}\backslash\mathbb{Z}_0^-\right) \\ &= \begin{cases} \lambda(\lambda+1)\ldots(\lambda+n-1), & (n \in \mathbb{N}) \\ 1, & (n = 0) \end{cases} \end{aligned} \tag{2} $$

*ambika.1921@nitte.edu.in https://orcid.org/0009-0004-5849-424X
†shanthakk99@gmail.com https://orcid.org/0000-0002-2153-0524

where Γ is the well known Gamma function.

It can be easily verified by the ratio test [1, 2] that the series is convergent for all $p \leqslant q$. Additionally, it converges in $|z| < 1$ for $p = q + 1$, converges everywhere for $p < q + 1$ and converges nowhere $(z \neq 0)$ for $p > q + 1$.
Further, if $p = q + 1$, it converges absolutely for $|z| = 1$ provided

$$\delta = \mathrm{Re}\left(\sum_{j=1}^{q} b_j - \sum_{j=1}^{p} a_j\right) > 0$$

holds and is conditionally convergent for $|z| = 1$ and $z \neq 1$ if $-1 < \delta \leqslant 0$ and diverges for $|z| = 1$ and $z \neq 1$ if $\delta \leqslant -1$. For more details we refer [4, 15].
When $p = 2$ and $q = 1$, the above series (1) take the form

$${}_2F_1\left[\begin{array}{c} a, \quad b \\ c \end{array}; z\right] = \sum_{n=0}^{\infty} \frac{(a)_n (b)_n}{(c)_n} \frac{z^n}{n!}$$

which converges for $|z| \leqslant 1$ and popularly known as Gauss's hypergeometric function.
When $p = 1, q = 1$, the series (1) takes the form:

$${}_1F_1\left[\begin{array}{c} a \\ c \end{array}; z\right] = \sum_{n=0}^{\infty} \frac{(a)_n}{(c)_n} \frac{z^n}{n!}$$

which converges everywhere and is also referred to as Kummer's function or the Confluent hypergeometric function in the literature. There are numerous physical problems where the hypergeometric functions of Kummers and Gauss are used [13, 14, 17].
In the theory of hypergeometric series, the following classical summation theorems play a key role.

Gauss summation theorem [8]

$${}_2F_1\left[\begin{array}{c} a, \ b \\ c \end{array}; 1\right] = \frac{\Gamma(c)\,\Gamma(c-a-b)}{\Gamma(c-a)\,\Gamma(c-b)} \tag{3}$$

provided $Re(c - a - b) > 0$.

Gauss second summation theorem [8]

$${}_2F_1\left[\begin{array}{c} a, \ b \\ \frac{1}{2}(a+b+1) \end{array}; \frac{1}{2}\right] = \frac{\Gamma\left(\frac{1}{2}\right)\Gamma\left(\frac{1}{2}a + \frac{1}{2}b + \frac{1}{2}\right)}{\Gamma\left(\frac{1}{2}a + \frac{1}{2}\right)\Gamma\left(\frac{1}{2}b + \frac{1}{2}\right)}. \tag{4}$$

Kummer summation theorem [8]

$${}_2F_1\left[\begin{array}{c} a, \ b \\ 1+a-b \end{array}; -1\right] = \frac{\Gamma\left(1 + \frac{1}{2}a\right)\Gamma(1+a-b)}{\Gamma(1+a)\,\Gamma\left(1 + \frac{1}{2}a - b\right)}. \tag{5}$$

Bailey summation theorem [8]

$${}_2F_1\left[\begin{array}{c} a, \ 1-a \\ b \end{array}; \frac{1}{2}\right] = \frac{\Gamma\left(\frac{1}{2}b\right)\Gamma\left(\frac{1}{2}b + \frac{1}{2}\right)}{\Gamma\left(\frac{1}{2}b + \frac{1}{2}a\right)\Gamma\left(\frac{1}{2}b - \frac{1}{2}a + \frac{1}{2}\right)}. \tag{6}$$

In 2010, Kim et al. [10] extended the classical summation theorems described above in the following form:

Extended Gauss summation theorem :

$$
\begin{aligned}
&{}_3F_2\left[\begin{array}{c} a,\ b,\ d+1 \\ c+1,\ d \end{array};1\right] = \\
&\quad = \frac{\Gamma(c+1)\,\Gamma(c-a-b)}{\Gamma(c-a+1)\,\Gamma(c-b+1)}\left[(c-a-b)+\frac{ab}{d}\right]
\end{aligned}
\tag{7}
$$

provided $Re(c-a-b)>0$.
For $d=c$, it reduces to Gauss summation Theorem (3).

Extended Gauss second summation theorem :

$$
\begin{aligned}
{}_3F_2\left[\begin{array}{c} a,\ b,\ d+1 \\ \frac{1}{2}(a+b+3),\ d \end{array};\frac{1}{2}\right] &= \frac{\Gamma\left(\frac{1}{2}\right)\Gamma\left(\frac{1}{2}a+\frac{1}{2}b+\frac{3}{2}\right)\Gamma\left(\frac{1}{2}a-\frac{1}{2}b-\frac{1}{2}\right)}{\Gamma\left(\frac{1}{2}a-\frac{1}{2}b+\frac{3}{2}\right)} \times \\
&\times\left\{\frac{\left(\frac{1}{2}(a+b-1)-\frac{ab}{d}\right)}{\Gamma\left(\frac{1}{2}a+\frac{1}{2}\right)\Gamma\left(\frac{1}{2}b+\frac{1}{2}\right)}+\frac{\left(\frac{1}{d}(a+b+1)-2\right)}{\Gamma\left(\frac{1}{2}a\right)\Gamma\left(\frac{1}{2}b\right)}\right\}.
\end{aligned}
\tag{8}
$$

For $d=\dfrac{1}{2}(a+b+1)$, it reduces to Gauss second summation Theorem (4).

Extended Kummer summation theorem :

$$
\begin{aligned}
{}_3F_2\left[\begin{array}{c} a,\ b,\ d+1 \\ 2+a-b,\ d \end{array};-1\right] &= \frac{\Gamma\left(\frac{1}{2}\right)\Gamma(2+a-b)}{2^a(1-b)} \times \\
&\times\left\{\frac{\left(\frac{1}{d}(1+a-b)-1\right)}{\Gamma\left(\frac{1}{2}a\right)\Gamma\left(\frac{1}{2}a-b+\frac{3}{2}\right)}+\frac{\left(1-\frac{a}{d}\right)}{\Gamma\left(\frac{1}{2}a+\frac{1}{2}\right)\Gamma\left(1+\frac{1}{2}a-b\right)}\right\}.
\end{aligned}
\tag{9}
$$

For $d=1+a-b$, it reduces to Kummer summation Theorem (5).

Extended Bailey summation theorem :

$$
\begin{aligned}
&{}_3F_2\left[\begin{array}{c} a,\ 1-a,\ d+1 \\ b+1,\ d \end{array};\frac{1}{2}\right] = \\
&= \frac{\Gamma\left(\frac{1}{2}\right)\Gamma(b+1)}{2^b} \times \\
&\times\left\{\frac{\left(\frac{2}{d}\right)}{\Gamma\left(\frac{1}{2}b+\frac{1}{2}a\right)\Gamma\left(\frac{1}{2}b-\frac{1}{2}a+\frac{1}{2}\right)}+\frac{\left(1-\frac{b}{d}\right)}{\Gamma\left(\frac{1}{2}b+\frac{1}{2}a+\frac{1}{2}\right)\Gamma\left(\frac{1}{2}b-\frac{1}{2}a+1\right)}\right\}.
\end{aligned}
\tag{10}
$$

For $d=b$, it reduces to Bailey summation Theorem (6).

2. Results required

In order to establish some new results in this paper, we shall need the following known result recorded in [11]

$$
\begin{aligned}
&{}_pF_q\left[\begin{array}{c} a_1,\ \ldots,\ a_{p-1},1 \\ b_1,\ \ldots,b_{q-1},\ m \end{array};z\right] = \\
&\quad = \frac{\Gamma(b_1)\ldots\Gamma(b_{q-1})}{\Gamma(a_1)\ldots\Gamma(a_{p-1})}\frac{\Gamma(1+a_1-m)\ldots\Gamma(1+a_{p-1}-m)}{\Gamma(1+b_1-m)\ldots\Gamma(1+b_{q-1}-m)}\frac{(m-1)!}{z^{m-1}} \times \\
&\qquad \times\left\{{}_{p-1}F_{q-1}\left[\begin{array}{c} 1+a_1-m,\ \ldots,\ 1+a_{p-1}-m, \\ 1+b_1-m,\ \ldots,\ 1+b_{q-1}-m, \end{array};z\right]-\right. \\
&\qquad\quad \left.-\ {}^{(m-2)}_{p-1}F_{q-1}\left[\begin{array}{c} 1+a_1-m,\ \ldots,\ 1+a_{p-1}-m, \\ 1+b_1-m,\ \ldots,\ 1+b_{q-1}-m, \end{array};z\right]\right\}
\end{aligned}
\tag{11}
$$

where ${}^{(m)}_{p}F_{q}$ is the finite sum of the hypergeometric series defined by

$$ {}^{(m)}_{p}F_{q}\left[\begin{array}{c} a_1,\ldots,a_p, \\ b_1,\ldots,b_q, \end{array};z\right]=\sum_{n=0}^{m}\frac{(a_1)_n\ldots(a_p)_n}{(b_1)_n\ldots(b_q)_n}\frac{z^n}{n!}, \tag{12} $$

where for instance,

$$ {}^{(-1)}_{p}F_{q}[z]=0,\ {}^{(0)}_{p}F_{q}[z]=1,\ {}^{(1)}_{p}F_{q}[z]=1+\frac{a_1\ldots a_p}{b_1\ldots b_q}z. $$

In 2018, Masjed–Jamei and Koepf [12] generalized the classical summation theorems (3) to (10) and in 2021, extensions of these results are established by Awad et al. [3] in the following form :

Extension of Gauss's Summation Theorem:

$$ \begin{aligned} {}_4F_3\left[\begin{array}{c} a,\ b,\ d+1,\ 1 \\ c+1,\ d,\ m \end{array};1\right] &= \frac{\Gamma(m)\Gamma(c+1)\Gamma(d)\Gamma(1+a-m)\Gamma(1+b-m)\Gamma(d-m+2)}{\Gamma(a)\Gamma(b)\Gamma(d+1)\Gamma(c-m+2)\Gamma(d-m+1)}\times \\ &\times\left\{\frac{\Gamma(c-m+2)\Gamma(c-a-b-1+m)}{\Gamma(c-a+1)\Gamma(c-b+1)}\ \times\right. \\ &\times\left[(c-a-b-1+m)+\frac{(a-m+1)(b-m+1)}{(d-m+1)}\right]- \\ &\left.-\ {}^{(m-2)}_{3}F_{2}\left[\begin{array}{c} a-m+1,\ b-m+1,\ d-m+2 \\ c-m+2,\ d-m+1 \end{array};1\right]\right\}= \\ &=\Omega_1, \end{aligned} \tag{13} $$

provided $m\in\mathbb{N}$ and $Re(c-a-b+m-1)>0$

Extension of Gauss's Second Summation Theorem :

$$ \begin{aligned} &{}_4F_3\left[\begin{array}{c} a,\ b,\ d+1,\ 1 \\ \frac{1}{2}(a+b+3),\ d,\ m \end{array};\frac{1}{2}\right]= \\ &=\frac{2^{m-1}\Gamma(m)\Gamma(d)\Gamma(1+a-m)\Gamma(1+b-m)\Gamma(d-m+2)\Gamma\left(\frac{1}{2}(a+b+3)\right)}{\Gamma(a)\Gamma(b)\Gamma(d+1)\Gamma\left(\frac{1}{2}(a+b+5)-m\right)\Gamma(d-m+1)}\times \\ &\times\left\{k-\ {}^{(m-2)}_{3}F_{2}\left[\begin{array}{c} a-m+1,\ b-m+1,\ d-m+2 \\ \frac{1}{2}(a+b+5)-m,\ d-m+1 \end{array};\frac{1}{2}\right]\right\}= \\ &=\Omega_2, \end{aligned} \tag{14} $$

where $m\in\mathbb{N}$ and

$$ k=\frac{\Gamma\left(\frac{1}{2}\right)\Gamma\left(\frac{1}{2}(a+b+5)-m\right)\Gamma\left(\frac{1}{2}(a-b-1)\right)}{\Gamma\left(\frac{1}{2}(a-b+3)\right)}\left\{\frac{\left[\frac{1}{2}(a+b-2m+1)-\frac{(a-m+1)(b-m+1)}{(d-m+1)}\right]}{\Gamma\left(\frac{1}{2}a+1-\frac{1}{2}m\right)\Gamma\left(\frac{1}{2}b+1-\frac{1}{2}m\right)}+\right. $$

$$ \left.+\frac{\left[\frac{(a+b-2m+3)}{(d-m+1)}-2\right]}{\Gamma\left(\frac{1}{2}a+\frac{1}{2}-\frac{1}{2}m\right)\Gamma\left(\frac{1}{2}b+\frac{1}{2}-\frac{1}{2}m\right)}\right\}. $$

Extension of Kummer's Summation Theorem :

$$
\begin{aligned}
&{}_4F_3\left[\begin{matrix} a,\ b,\ d+1,\ 1 \\ 1+a-b+m,\ d,\ m \end{matrix};-1\right] = \\
&= \frac{(-1)^{m-1}\Gamma(m)\Gamma(d)\Gamma(1+a-m)\Gamma(1+b-m)\Gamma(d-m+2)\Gamma\left(1+a-b+m\right)}{\Gamma(a)\Gamma(b)\Gamma(d+1)\Gamma\left(2+a-b\right)\Gamma(d-m+1)} \times \\
&\times \left\{k - {}^{(m-2)}_{\ 3}F_2\left[\begin{matrix} a-m+1,\ b-m+1,\ d-m+2 \\ 2+a-b,\ d-m+1 \end{matrix};-1\right]\right\} = \\
&= \Omega_3,
\end{aligned}
\tag{15}
$$

where $m \in \mathbb{N}$ and

$$
k = \frac{\Gamma\left(\frac{1}{2}\right)\Gamma\left(2+a-b\right)}{2^{a-m+1}(m-b)}\left[\frac{\left(\frac{a-b-d+m}{1+d-m}\right)}{\Gamma\left(\frac{1}{2}a+\frac{1}{2}-\frac{1}{2}m\right)\Gamma\left(\frac{1}{2}a-b+\frac{1}{2}m+1\right)} + \right.
$$

$$
\left. + \frac{\left(\frac{d-a}{1+d-m}\right)}{\Gamma\left(\frac{1}{2}a+1-\frac{1}{2}m\right)\Gamma\left(\frac{1}{2}a-b+\frac{1}{2}m+\frac{1}{2}\right)}\right].
$$

Extension of Bailey's Summation Theorem :

$$
\begin{aligned}
&{}_4F_3\left[\begin{matrix} a,\ 2m-a-1,\ d+1,\ 1 \\ b+1,\ d,\ m \end{matrix};\frac{1}{2}\right] = \\
&= \frac{2^{m-1}\Gamma(m)\Gamma(b+1)\Gamma(d)\Gamma(m-a)\Gamma(1+a-m)\Gamma(d-m+2)}{\Gamma(a)\Gamma(d+1)\Gamma\left(2m-a-1\right)\Gamma(2+b-m)\Gamma(1+d-m)} \times \\
&\times \left\{k - {}^{(m-2)}_{\ 3}F_2\left[\begin{matrix} a-m+1,\ m-a,\ 2+d-m \\ 2+b-m,\ 1+d-m \end{matrix};\frac{1}{2}\right]\right\} = \\
&= \Omega_4,
\end{aligned}
\tag{16}
$$

where $m \in \mathbb{N}$ and

$$
k = \frac{\Gamma\left(\frac{1}{2}\right)\Gamma\left(2+b-m\right)}{2^{b-m+1}}\left[\frac{\left(\frac{2}{1+d-m}\right)}{\Gamma\left(\frac{1}{2}b+\frac{1}{2}a-m+1\right)\Gamma\left(\frac{1}{2}b-\frac{1}{2}a+\frac{1}{2}\right)} + \right.
$$

$$
\left. + \frac{\left(1-\frac{1+b-m}{1+d-m}\right)}{\Gamma\left(\frac{1}{2}b+\frac{1}{2}a-m+\frac{3}{2}\right)\Gamma\left(\frac{1}{2}b-\frac{1}{2}a+1\right)}\right].
$$

As an application of the results (13) to (16), Awad et. al. [3] evaluated new class of Eulerian-type integrals and Laplace-type integrals involving generalized hypergeometric functions.

Edward's double integral : The following double integral is attributed to Edwards [5], and we intend to produce eight double integrals involving generalised hypergeometric functions by utilising this result.

$$
\int_0^1 \int_0^1 y^{\alpha}(1-x)^{\alpha-1}(1-y)^{\beta-1}(1-xy)^{1-\alpha-\beta}dxdy = \frac{\Gamma(\alpha)\Gamma(\beta)}{\Gamma(\alpha+\beta)} \tag{17}
$$

provided $Re(\alpha) > 0, Re(\beta) > 0$.

The goal of this study is to evaluate four new integrals of Eulerian-type in Section 3, four integrals of Laplace-type in Section 4, and eight integrals of Edwards-type in Section 5 that use generalised hypergeometric functions, utilising the extended summation Theorems (13)–(16) recorded in [3]. The same will be given in the next section.

3. Eulerian-type single integrals

In this section, we shall establish the following four integrals asserted in the following theorems.

Theorem 3.1. *For $m \in \mathbb{N}$, $Re(e) > 0$, $Re(f-e) > -1$ and $Re(c-a-b+m) > -1$, the following result holds true.*

$$\int_0^1 x^{e-1}(1-x)^{f-e}{}_5F_4\left[\begin{array}{c} a,\ b,\ f+1,\ d+1,\ 1 \\ c+1,\ d,\ e,\ m \end{array};x\right]dx = \\ = \frac{\Gamma(e)\Gamma(f-e+1)}{\Gamma(f+1)}\Omega_1, \tag{18}$$

where Ω_1 is same as given in (13).

Theorem 3.2. *For $m \in \mathbb{N}$, $Re(e) > 0$ and $Re(f-e+3) > 0$ the following result holds true.*

$$\int_0^1 x^{e-1}(1-x)^{\frac{1}{2}(f-e+1)}{}_5F_4\left[\begin{array}{c} a,\ b,\ \frac{1}{2}(f+e+3),\ d+1,\ 1 \\ \frac{1}{2}(a+b+3),\ d,\ e,\ m \end{array};\frac{x}{2}\right]dx = \\ = \frac{\Gamma(e)\Gamma(\frac{1}{2}(f-e+3))}{\Gamma(\frac{1}{2}(f+e+3))}\Omega_2, \tag{19}$$

where Ω_2 is the same as given in (14).

Theorem 3.3. *For $m \in \mathbb{N}$, $Re(e) > 0$ and $Re(a-2e+m) > -1$ the following result holds true.*

$$\int_0^1 x^{e-1}(1-x)^{a-2e+m}{}_5F_4\left[\begin{array}{c} a,\ b,\ a-e+m+1,\ d+1,\ 1 \\ 1+a-b+m,\ d,\ e,\ m \end{array};-x\right]dx = \\ = \frac{\Gamma(e)\Gamma(a-2e+m+1)}{\Gamma(a-e+m+1)}\Omega_3, \tag{20}$$

where Ω_3 is the same as given in (15).

Theorem 3.4. *For $m \in \mathbb{N}$, $Re(e) > 0$ and $Re(f-e) > -1$ the following result holds true.*

$$\int_0^1 x^{e-1}(1-x)^{f-e}{}_5F_4\left[\begin{array}{c} a,\ 2m-a-1,\ f+1,\ d+1,\ 1 \\ b+1,\ e,\ d,\ m \end{array};\frac{x}{2}\right]dx = \\ = \frac{\Gamma(e)\Gamma(f-e+1)}{\Gamma(f+1)}\Omega_4, \tag{21}$$

where Ω_4 is the same as given in (16).

Proof. The derivations of the four Eulerian-type integrals asserted in the above mentioned theorems are quite straight forward. Therefore in order to evaluate the integral (18) we proceed as follows. Denoting the left-hand side of (18) by I, we have

$$I = \int_0^1 x^{e-1}(1-x)^{f-e}{}_5F_4\left[\begin{array}{c} a,\ b,\ f+1,\ d+1,\ 1 \\ c+1,\ d,\ e,\ m \end{array};x\right]dx.$$

Now, by expressing ${}_5F_4$ as a series and altering the sequence of integration and summation, which is easily seen to be justified due to the uniform convergence of the series involved in the process, we have

$$I = \sum_{n=0}^{\infty} \frac{(a)_n\ (b)_n\ (f+1)_n\ (d+1)_n\ (1)_n}{(c+1)_n\ (d)_n(e)_n\ (m)_n\ n!} \int_0^1 x^{n+e-1}(1-x)^{f-e}dx.$$

Evaluating the beta integral and using the result (2) we get, after some simplification

$$I = \frac{\Gamma(e)\Gamma(f-e+1)}{\Gamma(f+1)} \sum_{n=0}^{\infty} \frac{(a)_n\,(b)_n\,(d+1)_n\,(1)_n}{(c+1)_n\,(d)_n\,(m)_n\,n!}.$$

Summing up the series, we have

$$I = \frac{\Gamma(e)\Gamma(f-e+1)}{\Gamma(f+1)} {}_4F_3\left[\begin{array}{c} a,\ b,\ d+1,\ 1 \\ c+1,\ d,\ m \end{array};1\right],$$

Finally, using the summation theorem (13), we easily arrive at the right-hand side of (18). This completes the proof of (18). □

In a similar way, the summation theorems (14), (15) and (16) respectively can be employed to evaluate the integrals (19) to (21) asserted in Theorems 3.2 to 3.4. We however, prefer to omit the details.

3.1. Special cases

In this section, we shall mention several known results.

(i) In (18), if we take $e = b$ and $f = c$, we get a known result due to Awad et al. [3].

(ii) In (19), if we take $f = a$ and $e = b$, we get a known result due to Awad et al. [3].

(iii) In (20), if we take $e = b$, we get a known result due to Awad et al. [3].

(iv) In (21), if we take $e = a$ and $f = b$, we get a known result due to Awad et al. [3].

Similarly, other results can be obtained.
We conclude this section by remarking that the integrals (18) to (21) asserted in Theorems 3.1 to 3.4 are of a fairly general nature because of the presence of $m \in \mathbb{N}$. So by assigning values to m, we can obtain a large number of integrals, which may be potentially useful.

4. Laplace-type single integrals

In this section, we shall establish new class of four Laplace-type integrals involving generalized hypergeometric functions asserted in the following theorems.

Theorem 4.1. *For $m \in \mathbb{N}$, $Re(s) > 0$, $Re(e) > 0$, the following result holds true.*

$$\int_0^{\infty} e^{-st} t^{e-1} {}_4F_4\left[\begin{array}{c} a,\ b,\ d+1,\ 1 \\ e,\ c+1,\ d,\ m \end{array};st\right] dt = \Gamma(e) s^{-e} \Omega_1, \tag{22}$$

where Ω_1 is the same as given in (13).

Theorem 4.2. *For $m \in \mathbb{N}$,$Re(s) > 0$,$Re(c) > 0$,the following result holds true.*

$$\int_0^{\infty} e^{-st} t^{c-1} {}_4F_4\left[\begin{array}{c} a,\ b,\ d+1,\ 1 \\ \frac{1}{2}(a+b+3),\ c,\ d,\ m \end{array};\frac{st}{2}\right] dt = \Gamma(c) s^{-c} \Omega_2, \tag{23}$$

where Ω_2 is the same as given in (14).

Theorem 4.3. *For $m \in \mathbb{N}$,$Re(s) > 0$ and $Re(e) > 0$,the following result holds true.*

$$\int_0^{\infty} e^{-st} t^{e-1} {}_4F_4\left[\begin{array}{c} a,\ b,\ d+1,\ 1 \\ 1+a-b+m,\ e,\ d,\ m \end{array};-st\right] dt = \Gamma(e) s^{-e} \Omega_3, \tag{24}$$

where Ω_3 is the same as given in (15).

Theorem 4.4. *For $m \in \mathbb{N}$,$Re(s) > 0$ and $Re(c) > 0$,the following result holds true.*

$$\int_0^\infty e^{-st} t^{c-1} {}_4F_4 \left[\begin{matrix} a,\ 2m-a-1,\ d+1,\ 1 \\ b+1,\ c,\ d,\ m \end{matrix} ; \frac{st}{2} \right] dt = \Gamma(c) s^{-c} \Omega_4, \tag{25}$$

where Ω_4 is the same as given in (16).

Proof. The derivations of the four Laplace-type integrals asserted in the above mentioned theorems are quite straight forward. Therefore, in order to evaluate the integral (22) asserted in Theorem 4.1, we proceed as follows. Denoting the left-hand side of (22) by I, we have,

$$I = \int_0^\infty e^{-st} t^{e-1} {}_4F_4 \left[\begin{matrix} a,\ b,\ d+1,\ 1 \\ e,\ c+1,\ d,\ m \end{matrix} ; st \right] dt,$$

Now express ${}_4F_4$ as a series, change the order of integration and summation which is justified due to the uniform convergence of the series, we have

$$I = \sum_{n=0}^{\infty} \frac{(a)_n (b)_n (d+1)_n (1)_n s^n}{(e)_n (c+1)_n (d)_n (m)_n n!} \int_0^\infty e^{-st} t^{n+e-1} dt,$$

Evaluating the Gamma integral and using the result (2) we have,

$$I = \Gamma(e) s^{-e} \sum_{n=0}^{\infty} \frac{(a)_n (b)_n (d+1)_n (1)_n}{(c+1)_n (d)_n (m)_n n!}$$

Summing up the series, we have,

$$I = \Gamma(e) s^{-e} {}_4F_3 \left[\begin{matrix} a,\ b,\ d+1,\ 1 \\ c+1,\ d,\ m \end{matrix} ; 1 \right],$$

Finally using summation theorem (13), we easily arrive at the right-hand side of (22). □

This completes the proof of (22).

In exactly the same manner, the integrals (23) to (25) asserted in Theorems 4.2 to 4.4 can be evaluated with the help of the summation Theorems (14), (15) and (16) respectively.

4.1. Special cases

In this section, we shall mention some known results.

(i) In (22), if we take $e = b$, we get a known result due to Awad et al. [3].

(ii) In (22), if we take $e = b$ and $d = c$, we get a known result due to Koepf et al. [9].

(iii) In (23), if we take $c = a$, we get a known result due to Awad et al. [3].

(iv) In (23), if we take $c = a$ and $d = \frac{1}{2}(a+b+1)$, we get a known result due to Koepf et al. [9].

(v) In (24), if we take $e = b$, we get a known result due to Awad et al. [3].

(vi) In (24), if we take $e = b$ and $d = a - b + m$, we get a known result due to Koepf et al. [9].

(vii) In (25), if we take $c = a$, we get a known result due to Awad et al. [3].

(viii) In (25), if we take $c = a$ and $d = b$, we get a known result due to Koepf et al. [9].

We conclude this section by remarking that the integrals (22) to (25) asserted in Theorems 4.1 to 4.4 are of very general nature because of the presence of $m \in \mathbb{N}$. So by giving values to $m \in \mathbb{N}$, we can obtain a large number of integrals, which may be potentially useful.

5. Edwards-type double integrals

In this section, we shall establish eight new class of Edwards-type double integrals involving generalized hypergeometric functions asserted in the following theorems. Derivations of these theorems are exactly similar to the derivations of (18) to (21) with the help of Edwards's Integral (17). Hence we prefer to omit the proof.

Theorem 5.1. *For $m \in \mathbb{N}$, $Re(\alpha) > 0$,$Re(\beta) > 0$, $Re(c-a-b+m) > 1$, the following result holds true.*

$$\int_0^1\int_0^1 y^{\alpha}(1-x)^{\alpha-1}(1-y)^{\beta-1}(1-xy)^{1-\alpha-\beta}\,{}_5F_4\left[\begin{matrix}a,\ b,\ d+1,\ \alpha+\beta,\ 1\\ c+1,\ d,\ \alpha,\ m\end{matrix};\frac{y(1-x)}{1-xy}\right]dxdy = \\ = \frac{\Gamma(\alpha)\Gamma(\beta)}{\Gamma(\alpha+\beta)}\Omega_1, \tag{26}$$

where Ω_1 is the same as given in (13).

Theorem 5.2. *For $m \in \mathbb{N}$, $Re(\alpha) > 0$,$Re(\beta) > 0$, the following result holds true.*

$$\int_0^1\int_0^1 y^{\alpha}(1-x)^{\alpha-1}(1-y)^{\beta-1}(1-xy)^{1-\alpha-\beta}\times \\ \times\,{}_5F_4\left[\begin{matrix}a,\ b,\ d+1,\ \alpha+\beta,\ 1\\ \frac{1}{2}(a+b+3),\ d,\ \alpha,\ m\end{matrix};\frac{y(1-x)}{2(1-xy)}\right]dxdy = \\ = \frac{\Gamma(\alpha)\Gamma(\beta)}{\Gamma(\alpha+\beta)}\Omega_2, \tag{27}$$

where Ω_2 is the same as given in (14).

Theorem 5.3. *For $m \in \mathbb{N}$, $Re(\alpha) > 0$,$Re(\beta) > 0$, the following result holds true.*

$$\int_0^1\int_0^1 y^{\alpha}(1-x)^{\alpha-1}(1-y)^{\beta-1}(1-xy)^{1-\alpha-\beta}\times \\ \times\,{}_5F_4\left[\begin{matrix}a,\ b,\ d+1,\ \alpha+\beta,\ 1\\ 1+a-b+m,\ d,\ \alpha,\ m\end{matrix};\frac{-y(1-x)}{1-xy}\right]dxdy = \\ = \frac{\Gamma(\alpha)\Gamma(\beta)}{\Gamma(\alpha+\beta)}\Omega_3, \tag{28}$$

where Ω_3 is the same as given in (15).

Theorem 5.4. *For $m \in \mathbb{N}$, $Re(\alpha) > 0$, $Re(\beta) > 0$, the following result holds true.*

$$\int_0^1\int_0^1 y^{\alpha}(1-x)^{\alpha-1}(1-y)^{\beta-1}(1-xy)^{1-\alpha-\beta}\times \\ \times\,{}_5F_4\left[\begin{matrix}a,\ 2m-a-1,\ d+1,\ \alpha+\beta,\ 1\\ b+1,\ d,\ \alpha,\ m\end{matrix};\frac{y(1-x)}{2(1-xy)}\right]dxdy = \\ = \frac{\Gamma(\alpha)\Gamma(\beta)}{\Gamma(\alpha+\beta)}\Omega_4, \tag{29}$$

where Ω_4 is the same as given in (16).

Theorem 5.5. *For $m \in \mathbb{N}$, $Re(\alpha) > 0$, $Re(\beta) > 0$, the following result holds true.*

$$\int_0^1 \int_0^1 y^{\alpha}(1-x)^{\alpha-1}(1-y)^{\beta-1}(1-xy)^{1-\alpha-\beta}\, {}_5F_4\left[\begin{matrix} a,\ b,\ d+1,\ \alpha+\beta,\ 1 \\ c+1,\ d,\ \beta,\ m \end{matrix}; \frac{(1-y)}{1-xy}\right] dxdy = \\ = \frac{\Gamma(\alpha)\Gamma(\beta)}{\Gamma(\alpha+\beta)}\Omega_1, \tag{30}$$

where Ω_1 is the same as given in (13).

Theorem 5.6. *For $m \in \mathbb{N}$, $Re(\alpha) > 0$, $Re(\beta) > 0$, the following result holds true.*

$$\int_0^1 \int_0^1 y^{\alpha}(1-x)^{\alpha-1}(1-y)^{\beta-1}(1-xy)^{1-\alpha-\beta} \times {}_5F_4\left[\begin{matrix} a,\ b,\ d+1,\ \alpha+\beta,\ 1 \\ \frac{1}{2}(a+b+3),\ d,\ \beta,\ m \end{matrix}; \frac{(1-y)}{2(1-xy)}\right] dxdy = \\ = \frac{\Gamma(\alpha)\Gamma(\beta)}{\Gamma(\alpha+\beta)}\Omega_2, \tag{31}$$

where Ω_2 is the same as given in (14).

Theorem 5.7. *For $m \in \mathbb{N}$, $Re(\alpha) > 0$, $Re(\beta) > 0$, the following result holds true.*

$$\int_0^1 \int_0^1 y^{\alpha}(1-x)^{\alpha-1}(1-y)^{\beta-1}(1-xy)^{1-\alpha-\beta} \times {}_5F_4\left[\begin{matrix} a,\ b,\ d+1,\ \alpha+\beta,\ 1 \\ 1+a-b+m,\ d,\ \beta,\ m \end{matrix}; \frac{-(1-y)}{(1-xy)}\right] dxdy = \\ = \frac{\Gamma(\alpha)\Gamma(\beta)}{\Gamma(\alpha+\beta)}\Omega_3, \tag{32}$$

where Ω_3 is the same as given in (15).

Theorem 5.8. *For $m \in \mathbb{N}$, $Re(\alpha) > 0$, $Re(\beta) > 0$, the following result holds true.*

$$\int_0^1 \int_0^1 y^{\alpha}(1-x)^{\alpha-1}(1-y)^{\beta-1}(1-xy)^{1-\alpha-\beta} \times \\ \times {}_5F_4\left[\begin{matrix} a,\ 2m-a-1,\ d+1,\ \alpha+\beta,\ 1 \\ b+1,\ d,\ \beta,\ m \end{matrix}; \frac{(1-y)}{2(1-xy)}\right] dxdy = \\ = \frac{\Gamma(\alpha)\Gamma(\beta)}{\Gamma(\alpha+\beta)}\Omega_4, \tag{33}$$

where Ω_4 is the same as given in (16).

5.1. Special cases

In this section, we shall mention several known results.

(i) In (26), by taking $\alpha = b$, $\beta = c - b$ and replacing c by d, we get a known result due to Kim et al. [7].

(ii) In (27), by taking $\alpha = b$, $\beta = \frac{1}{2}(a-b+1)$ and replacing d by $\frac{1}{2}(a+b+1)$, we get a known result due to Kim et al. [7].

(iii) In (28), by taking $\alpha = b$, $\beta = a - 2b + m$ and replacing d by $a - b + m$, we get a known result due to Kim et al. [7].

(iv) In (29), by taking $\alpha = a$, $\beta = b - a$ and replacing d by b, we get a known result due to Kim et al. [7].

(v) In (30), by taking $\alpha = c - b$, $\beta = b$ and replacing d by c, we get a known result due to Kim et al. [7].

(vi) In (31), by taking $\alpha = \frac{1}{2}(a - b + 1)$, $\beta = b$ and replacing d by $\frac{1}{2}(a + b + 1)$, we get a known result due to Kim et al. [7].

(vii) In (32), by taking $\alpha = a - 2b + m$, $\beta = b$ and replacing d by $a - b + m$, we get a known result due to Kim et al. [7].

(viii) In (33), by taking $\alpha = b - a$, $\beta = a$ and replacing d by b, we get a known result due to Kim et al. [7].

Concluding remark

In this paper, an effort has been made to provide a list of new Eulerian-type integrals involving generalised hypergeometric functions ${}_pF_q$ for $p = 5$ and $q = 4$, a list of new Laplace-type integrals involving generalised hypergeometric functions, ${}_pF_p$ for $p = 4$, in their most general forms and a list of Edwards-type integrals involving generalized hypergeometric functions ${}_pF_q$ for $p = 5$ and $q = 4$. These are obtained with the help of the summation theorems obtained very recently by Awad, et al. [3]. Several known results have also been obtained as special cases of our main findings. The results established in this paper are simple to accomplish, interesting, easily established and may be potentially useful.

As a final note to conclude this section, we would like to point out that, further applications of the Masjed–Jamei and Koepf extended summation theorems are currently being investigated and will be discussed in a part of the subsequent paper in this direction.

References

[1] G.E.Andrews, R.Askey, R.Roy, Special Functions. *Encyclopedia of Mathematics and Its Applications*, Volume 71, Cambridge University Press, Cambridge, UK, 1999.

[2] G.Arfken, Mathematical Methods for Physicists, Academic Press, New York, NY, USA, 1985.

[3] M.M.Awad, W.Koepf, A.O.Mohammed, M.A.Rakha, A.K.Rathie, A study of extensions of classical summation theorems for the series ${}_3F_2$ and ${}_4F_3$ with applications, *Results in Mathematics*, **76**(2021), no. 65. DOI: 10.1007/s00025-021-01367-9

[4] W.N.Bailey, Generalized Hypergeometric Series, Cambridge Tracts in Mathematics and Mathematical Physics, No. 32, Stechert-Hafner, New York, NY, USA, 1964.

[5] J.A.Edwards, Treaties on the Integral Calculus with Applications, Examples and Problems, Vol. II, Chelsea Publishing Campany, New York, (1954).

[6] S.Jun, I.Kim, A.K.Rathie, On a new class of Eulerian's-type integrals involving generalized hypergeometric functions, *The Aust. J. Math. Anal. Appl.*, **16**(2019), no. 1, 1–15.

[7] I.Kim, A.K.Rathie, M.M.Jamei, *On a new class of double type integrals involving generalized hypergeometric functions* (submitted for publication).

[8] W.Koepf, Hypergeometric Summation: An Algorithmic Approach to Summation and Special Functions Identities, 2nd edn. Springer, London, 2014.

[9] W.Koepf, I.Kim, A.K.Rathie, On a new class of Laplace-type integrals involving generalized hypergeometric functions, *Axioms*, **8**(2019), 87. DOI: 10.3390/axioms8030087

[10] Y.S.Kim, M.A.Rakha, A.K.Rathie, Extensions of certain classical summation theorems for the series ${}_2F_1$, ${}_3F_2$ and ${}_4F_3$ with applications in Ramanujan's summations, *Int. J. Math., Math. Sci.*, **2010**(2010), Article ID 209503. DOI: 10.1155/2010/309503

[11] A.P.Prudnikov, Yu.A.Brychkov, O.I.Marichev, Integrals and Series, vol. 3, Science Publications, Amsterdam, 1990.

[12] M.M.Jamei. W Koepf, Some Summation Theorems for Generalized Hypergeometric Functions, *Axioms*, **38**(2018), no. 7. DOI: 10.3390/axioms7020038

[13] A.M.Mathai, R.K.Saxena, Generalized Hypergeometric Functions with Applications in Statistics and Physical Sciences, Lecture Note in Mathematics, Springer: Berlin/Heidelberg, Germany; New York, NY, USA, Volume 348, 1973.

[14] A.F.Nikiforov, V.B.Uvarov, Special Functions of Mathematical Physics. A Unified Introduction with Applications, Birkhauser: Basel, Switzerland, 1988.

[15] E.D.Rainville, Special Functions, Macmillan Company, New York, 1960; Reprinted by Chelsea Publishing Company, Bronx, New York, 1971.

[16] M.A.Rakha, A.K.Rathie, Generalizations of classical summation theorems for the series ${}_2F_1$ and ${}_3F_2$ with applications, *Integral Transforms Spec. Fun.*, **22**(2011), no. 11, 823–840. DOI: 10.1080/10652469.2010.549487

[17] L.J.Slater, Confluent Hypergeometric Functions, Cambridge University Press, Cambridge, UK, 1960.

[18] L.J.Slater, Generalized Hypergeometric Functions, Cambridge University Press, Cambridge, UK, 1966.

О некоторых новых интегралах типа Эйлера, Лапласа и Эдвардса, содержащих обобщенные гипергеометрические функции

Амбика Нараяна
AJ Институт инженерии и технологий
Висвесварайский технологический университет (ВТУ), Белагави
Мангалуру-575006, Карнатака, Индия
Шанта Кумари Курумуджи
Технологический институт NMAM, Нитте (считается университетом)
Нитте, 574110, Карнатака, Индия

Аннотация. В 2018 году Masjed–Jamei & Koepf [12] установили некоторые теоремы суммирования для обобщенных гипергеометрических функций. В 2021 году Awad et al. [3] исследовали расширения этих классических теорем суммирования для рядов ${}_3F_2$ и ${}_4F_3$ с приложениями в интегралах типа Эйлера и Лапласа. В этом исследовании устанавливаются новые интегралы типа Эйлера, Лапласа и Эдвардса с использованием расширений классических теорем суммирования, предоставленных Awad et al. [3]. В качестве особых примеров наших основных результатов также продемонстрированы результаты предыдущих исследований Авада и др. [3], Кёпфа и др. [9] и Кима и др. [7].

Ключевые слова: обобщенная гипергеометрическая функция, классические теоремы суммирования, интеграл типа Эйлера, интеграл типа Лапласа, интеграл типа Эдвардса.